8-13-2019

Footprint of Calcium on Regulation of Extracellular Calcium-Sensing Receptor and Connexin26

Rakshya Gorkhali

FOOTPRINT OF CALCIUM ON REGULATION OF

EXTRACELLULAR CALCIUM-SENSING RECEPTOR AND CONNEXIN26

by

RAKSHYA GORKHALI

Under the Direction of Jenny Yang, Ph.D.

ABSTRACT

Calcium (Ca^{2+}) functions as a primary and secondary messenger regulating crucial cellular processes. We study two central membrane proteins, extracellular calcium-sensing receptor (CaSR) and connexin26 (Cx26) gap junction (GJ) channel, that are regulated by Ca^{2+} and play critical roles in regulating Ca^{2+} homeostasis and communication between the intra- and extra-cellular milieu. Mutations in CaSR are associated with abnormal Ca^{2+} homeostasis, hypoparathyroidism, myocardial infarction and cancers. Similarly, mutations in Cx26 are implicated in many hereditary deafness and dermatological disorders. The role of Ca^{2+} in CaSR biosynthesis, CaSR mediated intracellular Ca^{2+} signaling, Cx26 regulation and tuning of their regulators in biological and pathological is reported, however, the knowledge of exact molecular mechanism is obscure due to challenges associated with membrane proteins.

In this dissertation, we first report the discovery of 98 novel putative CaSR interactors using co-immunoprecipitation, mass-spectrometry and confocal imaging. Our findings suggest that extracellular Ca^{2+} dependent CaSR mediated intracellular signaling facilitates ER quality control and trafficking by upregulating the interaction with proteins affiliated with ubiquitination, chaperoning and glycosylation. Next, the cooperative activation of CaSR by Ca^{2+}, Mg^{2+} and aromatic amino acids is validated in wild type CaSR in HEK293 cells. CaSR mutations at conserved metal binding sites reduce Ca^{2+}/Mg^{2+} evoked intracellular Ca^{2+} mobilization and Ca^{2+} oscillation. This work further uses single cell imaging, immunoassay and sequencing to report tissue specific expression and differential capabilities of cations and drugs to tune CaSR mediated signaling in prostate (PCa) and thyroid cancer cells. We report a presence of wild type CaSR in PCa cell using RT-PCR. Additionally, proteomics and gene ontology show differential proteostasis between prostate cancer and HEK293 cells. Finally, this study endeavored at expressing and purifying a challenging protein, Cx26, and established binding affinity for Tb^{3+} and Ca^{2+} as 1.8 µM and 37 mM, respectively. The N-terminal lobe of CaM was found to bind Ca^{2+} tighter by 2.5-folds greater than C-lobe in the presence of $Cx26p_{1-21}$. Our study on role of Ca^{2+} on regulation of CaSR and Cx26 allows for greater understanding of their function and provides avenue for potential therapeutic targets.

INDEX WORDS: Calcium (Ca^{2+}), Magnesium (Mg^{2+}), Calcium-sensing receptor (CaSR), Gap Junction (GJ), Connexin26 (Cx26), Calmodulin (CaM), Interactome, Ca^{2+} signaling, Proteomics, Gene ontology, Trafficking, RT-PCR, Fluorescence, Drugs

FOOTPRINT OF CALCIUM ON REGULATION OF EXTRACELLULAR CALCIUM -SENSING RECEPTOR AND CONNEXIN26

by

RAKSHYA GORKHALI

A Dissertation Submitted in Partial Fulfillment of the Requirements for the Degree of

Doctor of Philosophy

in the College of Arts and Sciences

Georgia State University

2019

FOOTPRINT OF CALCIUM ON REGULATION OF

EXTRACELLULAR CALCIUM -SENSING RECEPTOR AND CONNEXIN26

by

RAKSHYA GORKHALI

Committee Chair: Jenny J. Yang

Committee: Zhi-Ren Liu

Ming Luo

Donald Hamelberg

Electronic Version Approved:

Office of Graduate Studies

College of Arts and Sciences

Georgia State University

July 2019

DEDICATION

I would like to dedicate this work to my family, my father, Mr. Ratna Lal Shrestha, my mother, Mrs. Manika Shrestha, my brother, Saswat Gorkhali and my husband, Vinish Shrestha. Without their love, encouragement, care and endless support, I would not be able to drive myself through the ups and downs during this journey. I will never forget the sacrifices my parents made to ensure my bright future and I thank them for the values of hard-work, honesty and appreciation for education they inculcated in me from a young age. I thank my younger brother for always being there whenever I needed someone to fall to and whenever I felt short of drive and determination. I will always cherish your presence in my life as my friend and guardian. I met my husband towards the fourth year of my program. Being a researcher himself, he rekindled my initial drive and motivation for research, especially during the times of failures. I am utterly thankful for the positivity, friendship and love he has bestowed in my life. I thank them all for being patient with me during my phases of positivity and negativity, and for being supportive of this venture. I would also like to remember all my extended family members and friends who have supported me through this time.

ACKNOWLEDGEMENTS

I would like to thank my advisor and mentor, Dr. Jenny Yang from the bottom of my heart. She has been a pillar and a guardian angel throughout my journey of the master's and PhD program. I am ever grateful to her for giving me an opportunity to be a part of her prolific research group and for allowing me a chance to learn and grow so much. She has guided me during the entire time towards becoming a true researcher and a scholar. I appreciate her continuous faith in me and for teaching me to never giving up. I am grateful for the understanding and care she has shown for my successful career as well as for my personal life. Her drive and hard work for science and discovery are highly contagious and have been encouraging during the high and low times of the research I have faced. As a woman, it is great to have such as great role model who is dedicated, intelligent and caring. I believe I have become a stronger individual with greater confidence and drive as well as valuable skills that will stay with me forever and will help me in my career.

I would also like to thank our previous group member, Dr. Juan Zou, Dr. Chen Zhang, Dr. Jie Feng, Dr. Shenghui Xue and Dr. Florence Reddish for being great mentors. I appreciate the amount of time and effort you put into mentoring me for valuable laboratory skills. Dr. Zou taught me expression and purification of protein, cell-culture and molecular biology techniques such as cloning, BRET assay, fluorimetry and immuno-assays. I will always remember the times of challenges we faced together with gap-junction project. I thank her for guiding me and having patience during the initial stages of my graduate life. I am greatly thankful to Dr. Zhang for teaching me fluorescence microscopy for monitoring Ca^{2+} signaling, immune-assays and imparting most of her skills when she left us. These techniques were pivotal for the projects where I studied CaSR mediated signaling. I thank her for the opportunity to be a part of the important paper on CaSR and for being available and guiding me, even from California. I inherited the

CaSR/prostate cancer metastasis project from Dr. Feng. I thank her for educating me about the interesting aspects of cancer cells and for instructing me on techniques such as invasion and migration assays and gene knockdown. I will remember the times we went to Clark Atlanta University together to optimize our mass spectrometry sampling. I would like to extend my gratitude to Dr. Xue for imparting his expertise on image and calcium binding site analysis. It was a great breakthrough for me in order to make sense of my raw data. I thank Dr. Florence Reddish for introducing me to calcium sensor project.

I would also like to thank Dr. Jin Zou (a Yang lab alumnus) from Clark Atlanta University for his patient help during the initial optimization of mass spectrometry studies. I thank him for his valuable suggestions throughout the process. I cannot forget to thank Dr. Xiaojuan Tan (previous Yang Lab research assistant) and Dr. Yu Li (CDC). I couldn't have progressed with the RT-PCR study of CaSR without your expertise and valuable guidance. I would like to thank Pritha Bagchi and Duc Duong from Emory University for all the time they put into patiently educating me the basics of mass spectrometry analysis and gene ontology studies. Without them I could not have completed the CaSR interactome project.

My acknowledgement wouldn't be complete without thanking all members of the Yang lab, Shanshan Tan, Mani Salarian, Cassandra Miller, Xiaonan Deng, Jingjuan Qiao, Oluwatosin Odubade, and Anvi Patel for their friendship and support during this venture. I have learnt a lot from them professionally and personally.

I would like to thank all the collaborators for their help with the projects. I thank Dr. Daqing Wu (Augusta University) for his consistent valuable support and guidance for the cancer project, Dr. Edward Brown (Harvard University) for his expert suggestions and Dr. Nick Seyfried for his

expertise on mass spectrometry. I thank Dr. Jun Yin and Li Zhou for their expertise in ubiquitination studies.

Last but not the least, I would like to thank all my committee members, Dr. Zhi-Ren Liu, Dr. Ming Luo and Dr. Donald Hamelberg for being a part of my PhD committee. I thank them for their valuable input towards the success of my research.

TABLE OF CONTENTS

LIST OF TABLES

LIST OF FIGURES

LIST OF ABBREVIATIONS

- Ca^{2+}: Calcium
- Mg^{2+}: Magnesium
- CaSR: Calcium-sensing receptor
- GJ: Gap Junction
- Cx26: Connexin26:
- $[Ca^{2+}]_o$: Extracellular calcium concentration
- $[Ca^{2+}]_i$: Intracellular calcium concentration
- $[Ca^{2+}_{cyt}]$: Cytosolic calcium concentration
- ER: Endoplasmic reticulum
- $[Ca^{2+}_{ER}]$: Endoplasmic reticulum calcium concentration
- WB: Western Blot
- ICC: Immuno-cyto chemistry
- IB: Immuno-blot
- IF: Immuno-fluorescence
- PCa: Prostate cancer
- PC3: Prostate cancer cell
- TT: Human thyroid cancer cell
- 6-23: Rat thyroid cancer cell
- MTC: Medullary thyroid carcinoma
- BSA: Bovine Serum Albumin
- Ab: Antibody
- P/S: Penicillin/Streptomycin

- DMEM: Dulbecco's modified Eagle Medium
- K_d: Dissociation constant
- OD: Optical density
- PCR: Polymerase chain reaction
- IHC: Immuno-histo chemistry
- PMSF: Phenylmethylsulfonyl fluoride
- IPTG: Isopropyl β-D-1-thiogalactopyranoside
- SDS-PAGE: Sodium dodecyl sulfate polyacrylamide gel electrophoresis
- WT: Wild type
- TBST: Tris-buffered saline with Tween 20
- TBST: Tris-buffered saline
- FRET: Förster resonance energy transfer
- FPLC: Fast protein liquid chromatography
- EGTA: Ethylene glycol tetra-acetic acid
- EDTA: Ethylenediaminetetraacetic acid
- EC_{50}: Half maximal concentration
- ECD: Extracellular domain
- ICD: Intracellular domain
- TMD: Transmembrane domain
- IL: Intracellular loop
- GPCR: G-protein coupled receptor
- PTH: Parathyroid hormone
- CT: Calcitonin

- FHH: Familial hypocalciuric hypercalcemia
- ADH: Autosomal dominant hypocalcemia
- NSHPT: Neonatal Severe Primary Hyperparathyroidism
- PTHrP: Parathyroid hormone-related peptide
- $InsP_3R$: Inositol (1,4,5) tri-phosphate receptor
- IP_3: Inositol-1,4,5-trisphosphate
- DAG: Diacylglycerol
- IP_1: Inositol mono-phosphate
- ERQC: Endoplasmic reticulum quality control
- ERAD: Endoplasmic reticulum associated degradation
- CICR: Ca^{2+} induced Ca^{2+} release
- CRAC: Ca^{2+} release-activated Ca^{2+} (channel)
- RyR: Ryanodine receptors
- PMCA: Plasma membrane Ca^{2+}-ATPase
- SERCA: Sarcoplasmic/endoplasmic reticulum Ca^{2+}-ATPase
- SPCA: Secretory pathway Ca^{2+}-ATPase
- NCX: Na^{+}/Ca^{2+} exchanger
- CCT: Cinacalcet
- LC-MS/MS: Liquid chromatography tandem mass spectrometry
- PSM: Peptide spectrum match
- LFQ: Label free quantitation

1. CHAPTER I: INTRODUCTION`

1.1 Calcium

1.1.1 Calcium distribution

Calcium (Ca^{2+}) is an integral part of life and impacts almost every aspect of life. It exists as the fifth most abundant element in the human body [17] and plays a crucial role in skeletal mineralization and Ca^{2+} signaling. ~ 99 % of the Ca^{2+} is primarily present as calcium-phosphate complexes, mostly as hydroxyapatite, in bones [19]. The rest of the 1 % of total body calcium (~ 10 g in an adult) [17] is used for a broad range of functions, including extra- and intracellular signaling, nerve impulse transmission, and muscle contraction [20, 21]. The existence of various forms of Ca^{2+} are as follows: free ions (~ 51%), protein-bound complexes (~ 40%), and ionic complexes (~ 9%) [22]. The physiologic range of serum ionized calcium is tightly maintained within a concentration of 1.10 to 1.35 mM [17] (**Figure 1.3)** in the form of calcium- phosphates, carbonates, and oxalates. There are many Ca^{2+} pools and Ca^{2+} buffer proteins in the cells that allow for the rapid and constant exchange of Ca^{2+} (**Figure 1.3)**.

1.1.2 Physical properties of Ca^{2+}

Evolution of cells is accompanied by complexity but is refined the spatial and temporal compartmentalization of specific mineral such as Ca^{2+}. Ca^{2+} is able to modulate protein in two ways, namely, by binding to a protein and changing its conformation and/or charge [23]. To carry out a defined function, Ca^{2+} is compartmentalized in specialized pools, sequestered by buffers proteins or extruded by channels (**Figure 1.3)**. Furthermore, the binding affinity of Ca^{2+} for various proteins is broad, ranging from nM to mM [23]. This property is established due to its special physical properties. Ca^{2+} ions can bind 4-12 oxygen atoms in their primary coordination sphere

(Figure 1.1). Proteins bind to Ca^{2+} using their oxygen atoms of carboxyl and carbonyl groups (and sometimes water). The usual coordination geometry that Ca^{2+} attains is pentagonal bipyramid with 6-7 oxygen atoms binding Ca^{2+} at ~2.5Å [24] **(Figure 1.1).**

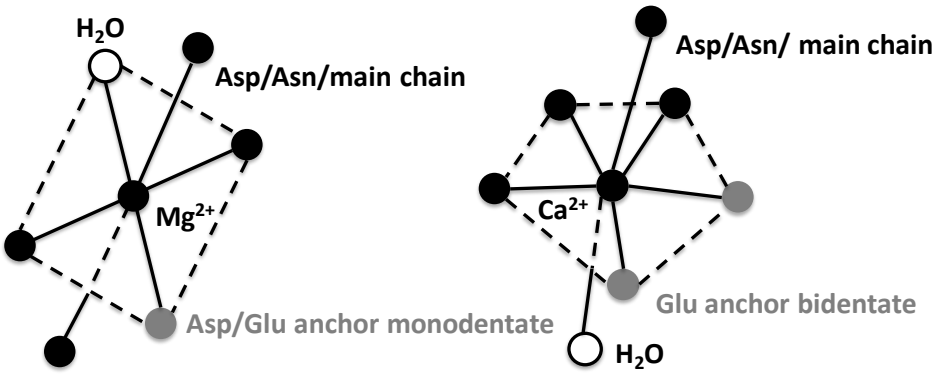

Figure 1.1 Coordination properties of Ca^{2+} and Mg^{2+}

Ca^{2+} ions have special physical properties where Ca^{2+}can bind 4-12 oxygen atoms in its primary coordination sphere with a coordination geometry of pentagonal bipyramid with 6-7 oxygen atoms binding Ca^{2+} at ~2.5Å. Mg^{2+}, on the other hand, favors six-fold, octahedral coordination with six ligands. Proteins bind to cation using their oxygen atoms of carboxyl and carbonyl groups (and sometimes water).

Table 1.1 Physical properties of Ca^{2+} and Mg^{2+}

Properties	Ca^{2+}	Mg^{2+}
Ionic radius A	0.99	0.65
Ligands	O	O
Coordinating residues	Asp, Glu	Asp, Glu
Metal-Oxygen distance	2.3-2.6	2.00−2.15
H_2O molcule/per metal site	1.5	2.2
Molecular geometry	Pentagonal bipyramidal	Octahedral
Coordination number	6-8	6
Interaction	electrostatic	electrostatic
Intracellular concentration	0.1-1uM	0.25-1mM

1.1.3 Comparison of Ca^{2+} with Magnesium (Mg^{2+}) cations

Mg^{2+} is the fourth most abundant ion in the body and second most abundant intracellularly [25]. Mg^{2+} acts as a competitive ion to Ca^{2+}, either inhibiting or modifying the function. Both Mg^{2+} and Ca^{2+} are small, closed-shell, spherical cations that prefer the formation of ionic bonds as compared to covalent bonds **(Figure 1.1)**. Mg^{2+} favors six-fold, octahedral coordination, whereas Ca^{2+} prefers seven to eight ligands [26]. Both are hard ions and prefers hard ligands with low polarizability like oxygen [27]. The Mg^{2+} ligands to primarily to Asp/Gln carboxylic side chains, followed by Asn/Gln side chains or peptide backbone of carbonyl groups [28]. Rest of the coordination is complemented by water ligand. The bond distance between Ca^{2+} and the ligand is usually 2.3-2.6 Å [26]. On the other hand, Mg^{2+} and ligand bond distance is usually 2.0-2.1 Å. Mg^{2+} has 1000-fold lower desolvation rate than Ca^{2+} [29].

1.2 Background on CaSR

The calcium-sensing receptor (CaSR) belongs to one of the largest cell surface receptor family, the C family, G-protein-coupled receptor (cGPCR). Other members of the cGPCR comprise of the two heterodimeric-aminobutyric acid B ($GABA_B$) receptors, eight metabotropic glutamate (mGlu1-8) receptors, three taste (T1R) receptors, one L-amino acid receptor (GPRC6A), and five orphan receptors [8]. CaSR was first cloned by Dr. Edward M. Brown in 1993 from the bovine parathyroid gland [30]. This receptor is present in a wide range of tissues and organs for systemic Ca^{2+} homeostasis such as parathyroid, thyroid, gastrointestinal tract, kidney and bone (osteoclasts, osteoblasts, and osteocytes) **(Figure 1.2)**. In addition, CaSR is also expressed in renal tubule, liver, lung, breast, placenta, vasculature, chondrocytes, lens epithelial cells, pancreas, neurons and glia in the CNS, exocrine cells in the pituitary, peripheral perivascular sensory nerves, keratinocytes and prostate [31]. Furthermore, the detection of CaSR in multiple cardiovascular

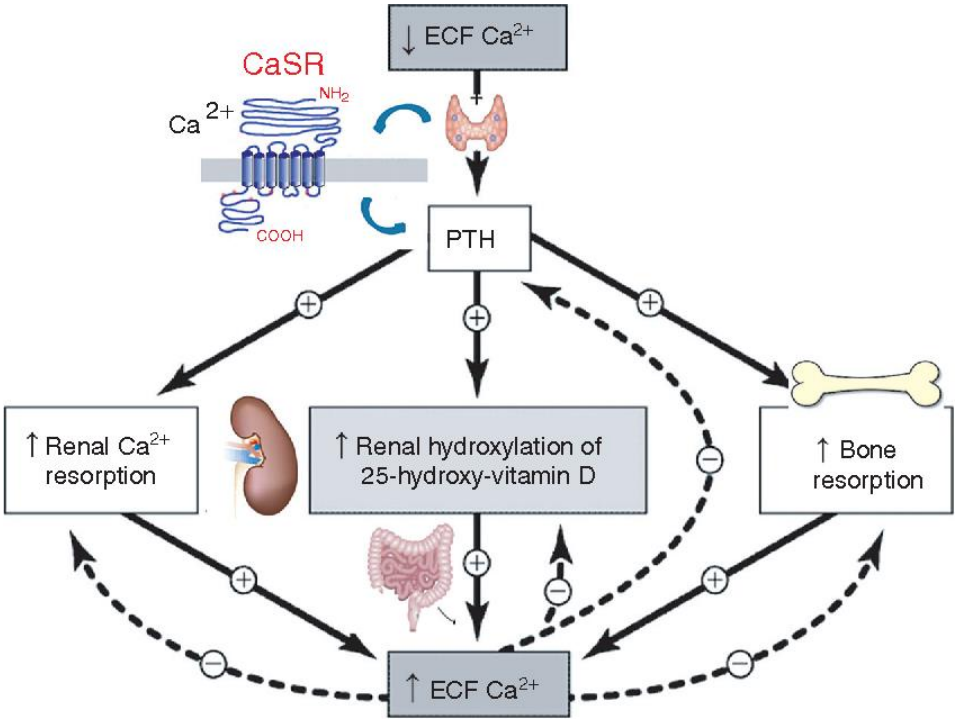

Figure 1.2 Systemic regulation of calcium homeostasis by CaSR [1]

The systemic balance is an integrated regulation by serum ionized calcium and the calcium-sensing receptor (CaSR), parathyroid hormone (PTH) and the PTH receptor (PTHR) and 1,25-dihydroxyvitamin D [1,25(OH)$_2$D] and the vitamin D receptor (VDR. CaSR regulates parathyroid hormone (PTH) secretion from parathyroid glands and calcitonin secretion from thyroidal C-cells upon sensing the alteration of the $Ca^{2+}{}_o$ concentration. A decrease in serum calcium inactivates the CaSR in the parathyroid glands to increase PTH secretion, which acts on the PTHR in the kidney to increase tubular calcium reabsorption, and in the bone to increase net bone resorption[17]. The increased PTH also stimulates the kidney to increase secretion of 1,25(OH)$_2$D, which activates the VDR in gut to increase calcium absorption, in the parathyroid glands to decrease PTH secretion, and in bone to increase resorption. The decrease in serum calcium probably also inactivates the CaSR in the kidney to increase calcium reabsorption and potentiate the effect of PTH. This integrated hormonal response restores serum calcium and closes the negative feedback loop.

cells and tissue types, such as vascular smooth muscle cells (VSMCs), human aortic smooth muscle cells (HAoSMC), cardiac myocytes, myocardial microvasculature, cardiac fibroblasts, the atria and ventricle of the rat heart, human aortic endothelial cells (HAECs), etc implicates the importance of CaSR function in cardiovascular system [32]. In addition to the diverse expression of CaSR in many tissues and organs, CaSR activation and mechanism is also complicated with

numerous types of agonists and co-agonists that can cooperatively mediate CaSR signaling. Furthermore, the sensitivity of CaSR to extracellular [Ca^{2+}] can vary in different cells and tissues. For example, in bone, the local extracellular [Ca^{2+}] can reach 40 mM but in skin, the extracellular [Ca^{2+}] range from 0.03 mM to > 0.5 mM [33]. Moreover, numerous mutations related to CaSR diseases and CaSR associated cancer along with diversified expressions of CaSR with altered signaling is prevalent. It is vital to explore the varied tissue- and species-specific genetic information of CaSR and its disease related mutations in order to understand the versatile function of CaSR in broad microenvironments at genetic and molecular levels.

1.2.1 Calcium Homeostasis

Calcium (Ca^{2+}) homeostasis is an indispensable process where a 10,000 fold electrochemical gradient is maintained between the extracellular (1.10~1.35 mM) and intracellular (10−7 to 10−8 M) of the cell [20] (**Figure 1.3).** Ca^{2+} controls crucial processes such as apoptosis, fertilization, exocytosis, contraction, proliferation, transcription, and metabolism. Ca^{2+} was the first intracellular signal messenger discovered [34] and was established as an extracellular first messenger in 1993 by Brown et al. [30]. Calcium metabolism is regulated by three main mechanisms: intestinal absorption, renal reabsorption, and bone turnover [17] **(Figure 1.2)**. This systemic balance is an integrated regulation by serum ionized calcium and the calcium-sensing receptor (CaSR), parathyroid hormone (PTH) and the PTH receptor (PTHR) [35] and 1,25-dihydroxyvitamin D [$1,25(OH)_2D$] and the vitamin D receptor (VDR) [36]. CaSR regulates parathyroid hormone (PTH) secretion from parathyroid glands and calcitonin secretion from thyroidal C-cells upon sensing the alteration of the $Ca^{2+}{}_o$ concentration [8]. A decrease in serum calcium inactivates the CaSR in the parathyroid glands to increase PTH secretion, which acts on

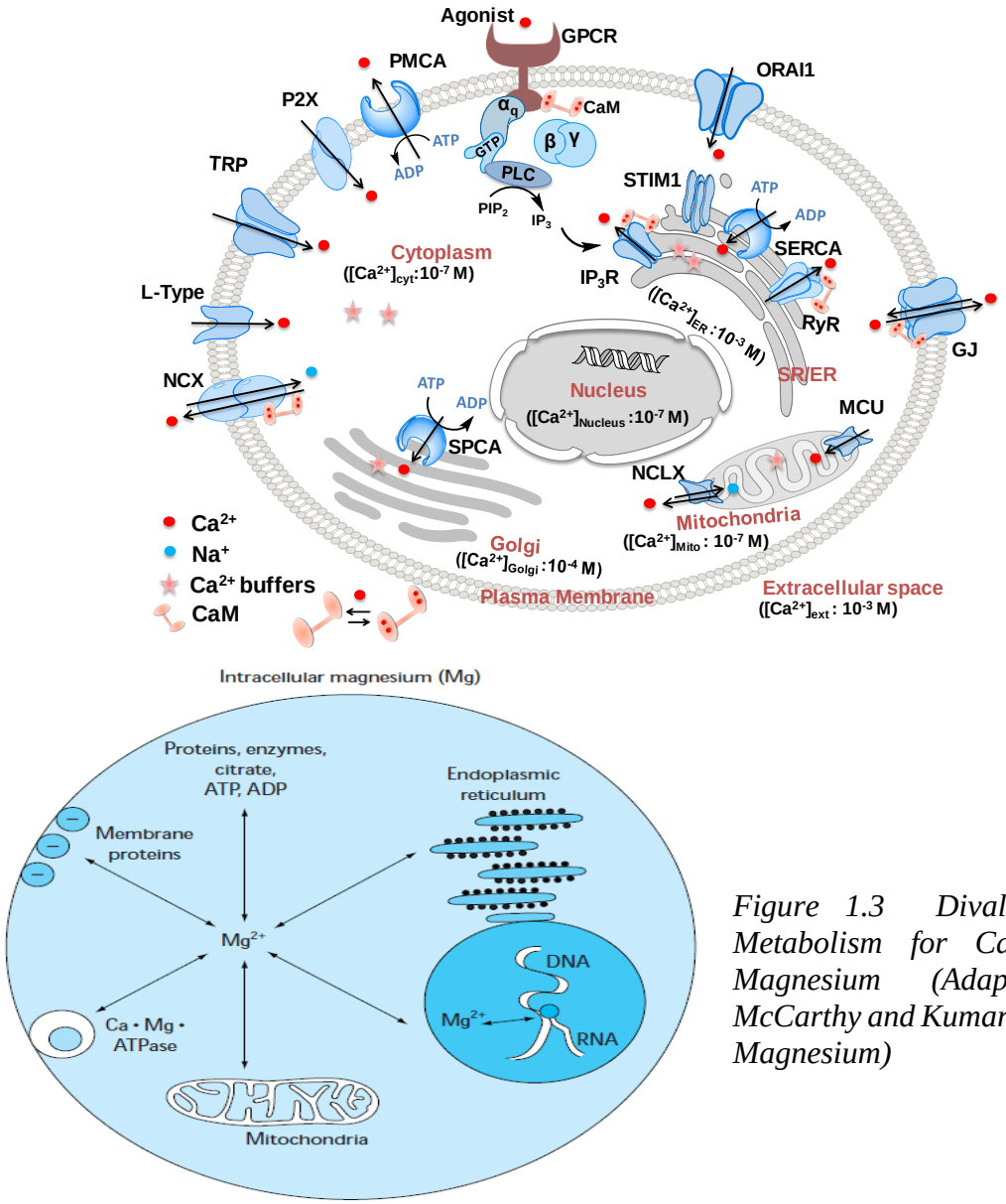

Figure 1.3 Divalent Cation Metabolism for Calcium and Magnesium (Adapted from McCarthy and Kumar Chapter on Magnesium)

A. The physiologic range of serum ionized calcium is tightly maintained within a concentration of 1.10 to 2.2 mM and cytosolic Ca^{2+}at about 10,000-fold lower gradient. Apart from GPCR such as CaSR, many Ca^{2+} and Na^{+} channels, ORAI, TRPC and gap junctions allows for Ca^{2+} sensing and influx/efflux on plasma membrane. The intracellular compartmental channels like Ryanodine receptor (RyR), inositol-triphosphate receptor (IP_3R) and sarco/endoplasmic reticulum Ca^{2+} ATPase (SERCA) in the ER and uniporters in mitochondria allows for cytoplasmic Ca^{2+} control as ER and mitochondria act as Ca^{2+} stores.B. Mg^{2+} functions as a versatile cofactor to more than 300 enzymes, regulator in replication, protein synthesis, glycolysis GPCR signaling, muscle contraction, potassium transport, calcium channels, and neuronal conduction.

the PTHR in the kidney to increase tubular calcium reabsorption, and in the bone to increase net bone resorption [17] **(Figure 1.2)**. The up regulation in PTH further stimulates the increase in the

secretion of $1,25(OH)_2D$ in the kidney. These results in the increase in calcium absorption in the gut, decrease in PTH secretion in the parathyroid glands and an increase in resorption in the bone by activating the VDR. The decrease in serum calcium may inactivate the CaSR in the kidney to increase calcium reabsorption and potentiate the effect of PTH. This integrated hormonal response restores serum calcium and closes the negative feedback loop. With a rise in serum calcium, these actions are reversed, and the integrated hormonal response reduces serum calcium. Together, these negative feedback mechanisms help to maintain total serum calcium levels in healthy individuals within a relatively narrow physiologic range of ~ 10 % [17].

1.2.2 Comparison of Ca^{2+} with Mg^{2+} in cellular function

Both Ca^{2+} and Mg^{2+} are ubiquitously present cations that are essential for cellular function and shares parathyroid hormone (PTH) and vitamin D during their regulatory roles. Mg^{2+} functions as a versatile cofactor to more than 300 enzymes for the enzyme by not only complexing with ATP but also acting as an allosteric activator [25]. Mg^{2+} functions as a regulator in oxidative phosphorylation, replication, protein synthesis, and glycolysis [25] **(Figure 1.3)**. It also is essential for GPCR signaling, muscle contraction, potassium transport, calcium channels, and neuronal conduction. Therefore, Mg^{2+} has both catalytic and structural roles. Out of the total Mg^{2+}, 0.5-5.0% are free. The serum contains 0.66-1.07 mM Mg^{2+} [25]. Disorders in Mg^{2+} lead to hypo- or hypermagnesemia.

1.2.3 Activation and regulation of CaSR

The architecture of CaSR consists of an extracellular domain (ECD) with the first 612 amino-acids, the seven transmembrane domains (TMDs) which comprise residues 613 to 862, and the intracellular domain (ICD), which comprises residues 863 to 1068 [8] (**Figure 1.4)**. The ECD domain is important for the dynamic co-translational processing, receptor dimerization, binding

ligands, and transmitting activation signals. The principal agonist of CaSR is known to be the extracellular Ca^{2+} (Ca^{2+}_o) that binds to the CaSR is a highly cooperative process (the hill coefficient of ~3) [37]. CaSR can distinguish small (~200 μM) fluctuations in the extracellular [Ca^{2+}] [38]. The functional diversity of CaSR results from its ability to activate multiple downstream signaling pathways through $G_{q/11}$, $G_{i/o}$, $G_{12/13}$ and G_s proteins when a ligand binds to the CaSR ECD [39] **(Figure 1.5)**. In addition to Ca^{2+}, CaSR is also regulated through several orthosteric agonists such as cations, polyamines, cationic polypeptides and endogenous allosteric modulators such as the extracellular pH [40] and ionic strength [41]. Cooperative activation of CaSR is carried out by divalent and trivalent metals such as La^{3+}, Gd^{3+}, Ba^{2+}, Cd^{2+}, Co^{2+}, Fe^{2+}, Ni^{2+} and Pb^{2+} (but not Fe^{3+} or Hg^{2+}) [42] with varying efficacies. Al^{3+} is considered a weak CaSR agonist since it can activate CaSR at mM concentrations [43]. Pb^{2+} is a potent CaSR activator with an EC_{50} of ~100 μM and therefore, can cause the toxicity by its ability to replace other cations [43, 44]. The potency of CaSR agonists can vary in various cells types. For example, in parathyroid, Mg^{2+} and Ca^{2+} have similar potency, but in sheep parafollicular cells of the thyroid, the potency is ranked as $Gd^{3+}>Ba^{2+}>Ca^{2+}>>Mg^{2+}$ [45].

Polycations and molecules with a high positive-charge density, such as polylysine (EC_{50} < 1 μM) [46], are more potent agonists than those with a lower charge density, such as Mg^{2+}, which, with its larger hydration radius that 'dilutes' its positive charge, requires concentrations twofold to three-fold higher than Ca^{2+} to be effective. Endogenous polyamines, such as spermine, spermidine and putrescine, are also CaSR agonists [37]. With four positive charges, spermine is the most potent of these compounds (the EC_{50} is ~500 μM in the presence of 0.5 mM Ca^{2+}). Polyamines are produced endogenously by bacteria in the gut and by many cell types in the body. Antibiotic such as neomycin [47, 48], G418, gentamycin and tobramycin [49] are polycationic

compounds and act as antagonists. It is of note that, at concentrations that are typically added to cell-culture growth media, streptomycin can significantly activate the CaSR, as can G4ll [50], which is often used as a selection agent for mammalian cells. Furthermore, aromatic and aliphatic L-amino acids such as L-Phe and L-Trp is known to increase the sensitivity of CaSR for Ca^{2+} and are considered as positive allosteric modulators of the receptor [41]. Synthetic positive allosteric modulators such as calcimimetics are known to left-shift, whereas the negative allosteric modulators, known as calcilytics, right-shift the concentration-response curve of Ca^{2+} [30]. Recent work by Zhang et al. has reported a novel Tryptophan derivative as a co-agonist for CaSR's activation [8].

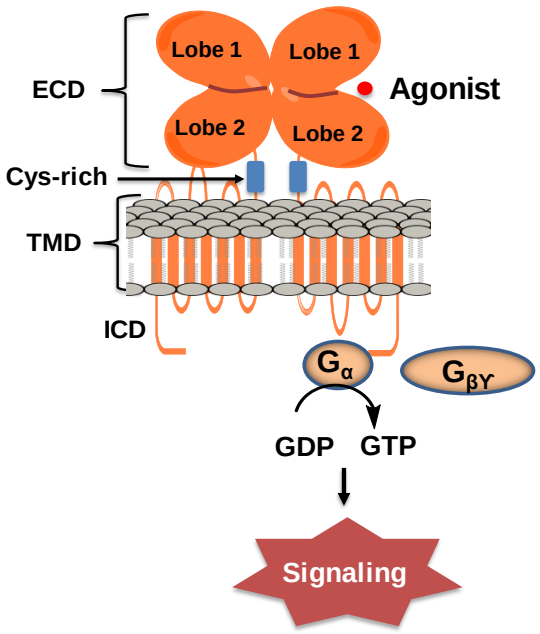

Figure 1.4 Architecture and general G-protein mediated signaling in GPCRs

The architecture of a homodimeric GPCR consists of an extracellular domain (ECD) consisting of lobe 1 and 2 (comprising of the first 612 amino acids in CaSR), the 7 transmembrane domains (TMDs) (comprises of residues 613 to 862 in CaSR), and the intracellular domain (ICD) (comprises of residues 863 to 1068 in CaSR). A conserved nine Cys residue-rich domain connects the ECD with TMD. The signaling is resulted by activation of GPCR and consequent dissociation of trimeric G-proteins.

1.2.3.1 Non-essential metal Pb^{2+} interferes with Ca^{2+} dependent functions

The cGPCRs are potential targets for Pb^{2+} due to their direct activation by binding to Ca^{2+}, or indirect modulation by interactions with other CABPs modulators, as seen in the case of calmodulin (CaM) [44]. Consequently, Pb^{2+} can interfere with downstream Ca^{2+} signaling pathways through the displacement of Ca^{2+}, or through opportunistic binding of Pb^{2+} to regions besides the Ca^{2+} binding sites [44]. The interactions between Pb^{2+} and CaBPs or proteins involved in Ca^{2+}-signaling pathways are based on three potential modes of Pb^{2+} activity as follows: (i). Pb^{2+} may occupy Ca^{2+}-binding sites, altering the structure of the protein and inhibiting the activity of the protein. (ii). Pb^{2+} may occupy Ca^{2+}-binding sites and mimic Ca^{2+}, thereby falsely activating the protein and perturbing downstream activities. (iii). Pb^{2+} may bind with proteins in sites other than Ca^{2+}-binding sites, thereby altering the conformation and function of the protein. Pb^{2+} is known to activate Ca^{2+} associated neuronal proteins at low concentrations and deactivate at higher concentrations, as characterized by a bell curve. Pieces of evidence also suggest that Pb^{2+} interacts with CaM, either through ionic displacement or through opportunistic binding, which likely disrupts a wide range of downstream activities [44].

1.2.4 Ca^{2+} signaling mediated by CaSR

CaSR mediates diverse downstream signaling pathways which regulate critical cellular processes including secretion, apoptosis, chemotactic responses, cell proliferation, cytoskeletal rearrangements, ion channel activity, the control of gene expression and cell differentiation [51, 52]. $Ca^{2+}{}_o$ can trigger CaSR-mediated intracellular signaling pathways, including activation of phospholipases C, A_2, and D, and various mitogen-activated protein kinases (MAPKs), as well as inhibition of cAMP production [53-58]. CaSRs have been reported to be present not only in the

key tissues involved in Ca^{2+}_o homeostasis (e.g., parathyroid gland, kidneys, bone) but also in other, non-homeostatic tissues (e.g., brain, skin) [38, 53, 59-71].

During the 'on' reactions, stimuli induce both the entry of external Ca^{2+} and the formation of second messengers that release internal Ca^{2+} that is stored within the endoplasmic/sarcoplasmic reticulum (ER/SR) (**Figure 1.3)**. Most of this Ca^{2+} is bound to buffers, whereas a small proportion binds to the effectors that activate various cellular processes. During the 'off' reactions, Ca^{2+} leaves the effectors and buffers and is removed from the cell by various exchangers and pumps. The Na^+/Ca^{2+} exchanger (NCX) and the plasma membrane Ca^{2+}-ATPase (PMCA) extrude Ca^{2+} to the outside, whereas the sarco(endo)plasmic reticulum Ca^{2+}-ATPase (SERCA) pumps Ca^{2+} back into the ER [23] (**Figure 1.3)**. Mitochondria, on the other hand, sequester Ca^{2+} rapidly through a uniporter, and this is then released more slowly back into the cytosol to be dealt with by the SERCA and the PMCA. Ins(1,4,5)P_3R, inositol-1,4,5-trisphosphate receptor and ryanodine receptor control the extruding of calcium from ER while SERCA replenishes the calcium store. The on and off reaction allows for a unique Ca^{2+}_i oscillation that can be used to detect the CaSR activation.

GPCRs are known to activate Gα proteins such as $G\alpha_i$ $G\alpha_q$ and $G\alpha_{12/13}$ to carry out different signaling and biological effects in various regions of a cell and in different cells **(Figure 1.5)**. CaSR inhibits adenylyl cyclase and activates extracellular signal-regulated kinase (ERK) through $G\alpha_i$ and phospholipase C is activated through Gαq, therefore, increasing intracellular Ca^{2+} (Ca^{2+}_i), diacylglycerol (DAG) levels and activating phospholipase A2 **(Figure 1.5)**. Finally, $G\alpha_{12/13}$ activates Rho-dependent phospho-lipase D and L-amino acid-induced Ca^{2+} mobilization [55, 72] **(Figure 1.5)**.

Approximately 30% of therapeutic drugs used clinically directly target GPCRs; therefore, it is of paramount importance to understand the mechanisms by which GPCRs are regulated [73]. Functional cooperativity of CaSR (i.e., based on biological activity determined using functional assays rather than a direct binding assay), particularly the functional positive homotropic cooperative response to Ca^{2+}_o, is essential for the receptor's ability to respond over a narrow physiological range of Ca^{2+}_o (1.1-1.3 mM) [54]. CaSR has an estimated hill coefficient of 3-4 for its regulation of biological processes such as activating intracellular Ca^{2+} signaling and inhibiting PTH release. CaSR has been shown to be cooperatively regulated by aromatic amino acids such as L-Phe and L-Trp [74].

1.2.5 Evolution of CaSR

CaSR is found in a variety of vertebrate species, including mammal, bird, reptile, amphibian, and fish. CaSR-like proteins are found in sea urchin, fruit fly, round-worm and tunicates [75]. Among the CaSR nucleotide sequences of 42 vertebrate species available from public databases, all vertebrate CaSRs (tetrapod and fishes) are grouped together and share the most recent common ancestor with the CaSR-like proteins of chordate (urochordates and cephalochordates) [76]. According to the detailed sub-group phylogenetic tree of CaSR and CaSR-like protein sequences, a distinctive indel in the ECD and noticeable variation in ICD length were observed **(Figure 1.6, Figure 1.7)**. Among different species, the 7TM domain is the most conserved region with 85-91% identity, and ECD shows the identity of 70-77% [75]. The ICD is the least conserved with variable length **(Figure 1.6, Figure 1.7)**.

Of the 1059 amino acid residues of the matured human CaSR, 44% sites are completely conservative during the evolution including the nine cysteine residues in cysteine rich (CR) domain and the predicted calcium-binding site 1 (S147, S170, D190, Y218, E297) [77] **(Figure 1.7)**. Most of these conserved sites are buried inside the protein in 3D structure, which might be necessary for the maintenance of protein structure and function (**Figure 1.7)**. The calcium binding site 1 overlap with the L-Trp binding site determined in CaSR crystal structure which is located in the cleft

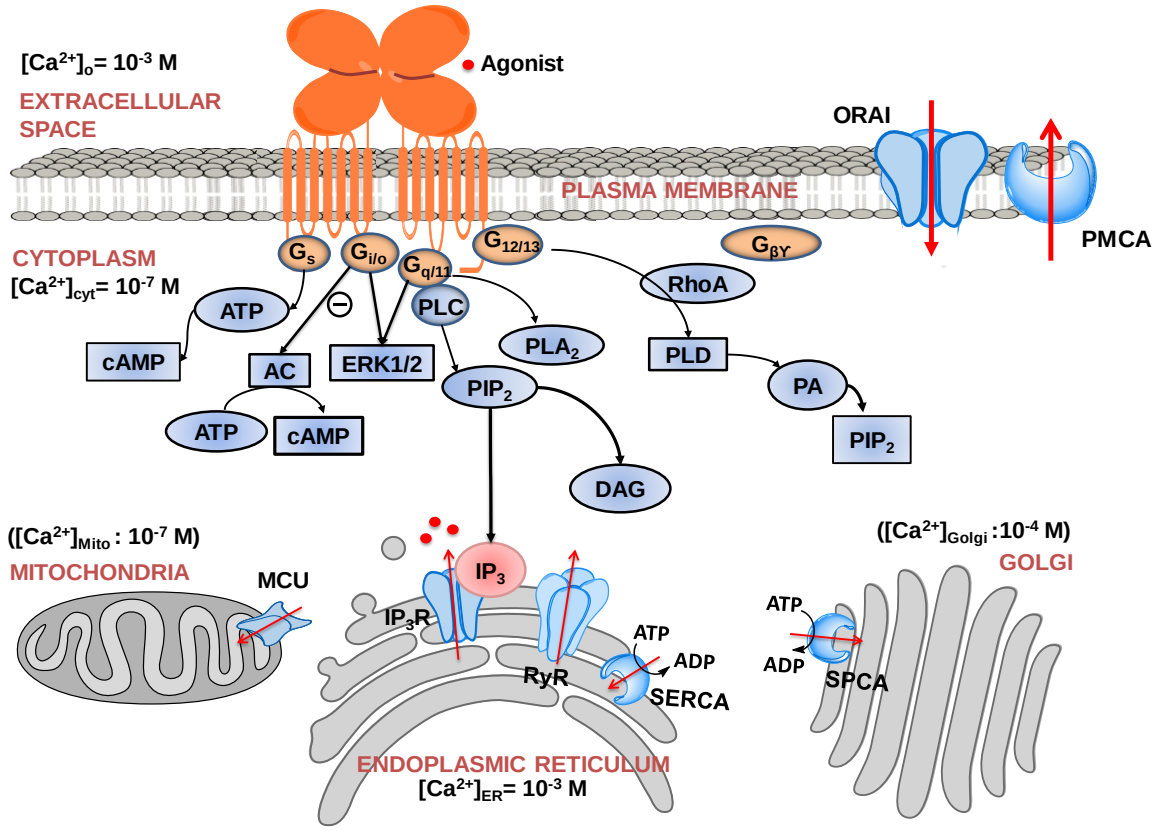

Figure 1.5 CaSR mediated signaling through G-proteins

GPCRs are known to activate Gα proteins such as $G\alpha_i$ $G\alpha_q$ and $G\alpha_{12/13}$ to carry out different signaling and biological effects in various regions of a cell and in different cell. CaSR inhibits adenylyl cyclase and activates extracellular signal-regulated kinase (ERK) through $G\alpha_i$ and phospholipase C is activated through Gαq, therefore, increasing intracellular Ca^{2+} ($Ca^{2+}{}_i$), diacyl glycerol (DAG) levels and activating phospholipase A2. Finally, $G\alpha_{12/13}$ activates Rho dependent phospho-lipase D and L-amino acid-induced Ca^{2+} mobilization. Channels in the ER such as the IP3R, RyR and SERCA allows for the Ca^{2+} homeostasis through mobilization Ca^{2+} from the ER store.

between the two lobes of VF [78] **(Figure 1.7)**. The other metal-binding sites determined by CaSR crystallization or predicted by computational approach are relatively conserved but with slight heterogeneity, which might be related to the alteration of habitat during evolution.

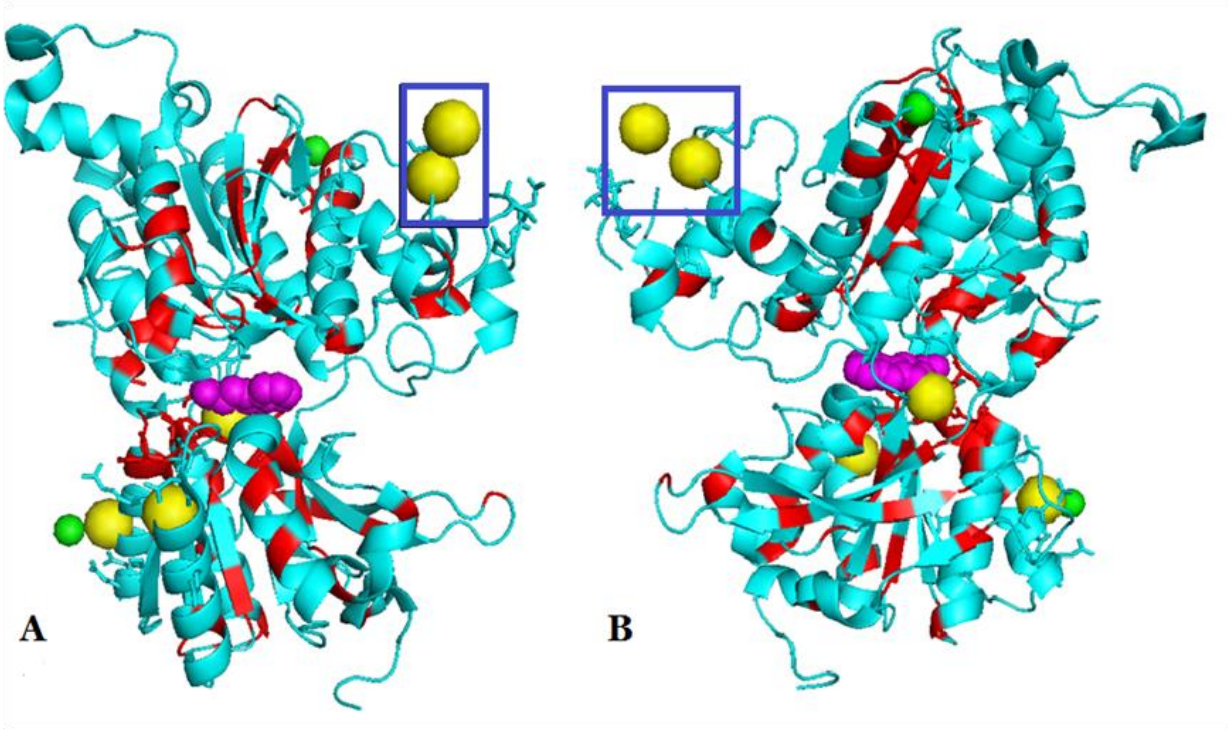

Figure 1.6 Conservative amino acid sites of vertebrate CaSR (in red) displayed in hCaSR-ECD (PDB ID: 5FBK), (A) the front view and (B) the back view. The predicted Ca^{2+} binding sites by Huang et al. are shown as yellow spheres. [4]

Figure 1.7 The alignment of deduced amino acid sequence of the CaSR from different species.

The underlined sequence is signal peptide. The black boxes indicate the indel spot in ECD and ICD individually. "-", gaps in alignment. [4]

1.2.6 CaSR gene

As shown in **Figure 1.8,** CaSR gene (CASR) encodes for calcium-sensing receptor and is a ~100-kb spanning single-copy gene that maps to human 3q13.3-21. Out of the eight exons, exons 2 to 7 encode the CaSR protein of 1068 amino acids **(Figure 1.8)**. Exons 1A and 1B are able to encode for two alternative 5′- untranslated region (UTR) that may splice to a common segment encoded by exon 2 [31]. Exon 2 contains 242 nucleotides of the 5′-UTR upstream of the ATG translation initiation codon [31].

1.2.7 Alternative Transcripts

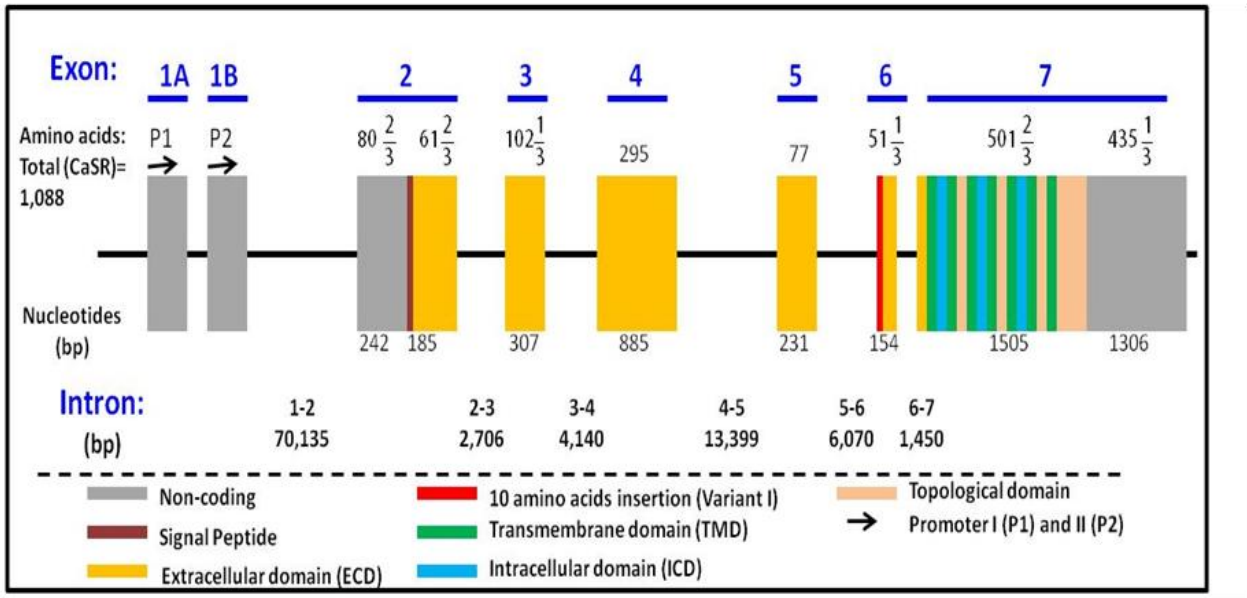

Figure 1.8 Genetic make-up of CaSR.
It is a ~100-kb spanning single copy gene that maps to human 3q13.3-21. Exons 2 to 7 encode the CaSR protein of 1068 aa. [4]

CASR is expressed in multiple tissues and organs at various levels. The variation of expression of CASR gene as multiple alternative transcripts in multiple tissues/organs hint at the ability to diversify its functions and regulations. In addition to the wild type variant II CASR, low abundant variant I exists which contains additional 10 amino acid inserted after amino acid 536 in

the CaSR (GenBank #U20760). This variant I is known to function similarly to variant II [31]. While, in human kidney, both the 5.4-kb transcript and the 10-kb transcript are similarly predominant [31]. The use and presence of the two promoters in CaSR gene allow for variation in the transcription of alternative 5′ UTR exons (1A and 1B) [31]. The real-time PCR (qPCR) analysis has shown that exon 1B-transcripts in human parathyroid cells were significantly more expressed than exon 1A-containing transcripts. The 5.4 and 10-kb transcripts in human parathyroid adenomas and normal glands use exon 1A exclusively as shown by northern blot analysis, while the 4.2-kb transcripts are either derived from 1A or 1B [31]. 5.4 and 4.2-kb sized transcripts are derived from the use of the two alternative polyadenylation sites in the 3′ UTR tract [31].

An exon 3-deleted CASR transcript has been reported in thyroid TT cells, placental cytotrophoblast, and in parathyroid, thyroid, and kidney [31]. This protein is poorly expressed and does not traffic to the cell surface. Another alternative transcript of CaSR exists in human keratinocytes where exon 5 is deleted (with a 77-amino acid in-frame deletion in the exodomain). The relative amounts of full-length is lowered during keratinocyte differentiation and the alternatively spliced variant is shown to cause the full-length protein to be less responsive to Ca^{2+}. This variant of CaSR is also known to be upregulated in skin and kidney in the knockout mice and is shown to compensate for the absence of the full-length CaSR in bone and cartilage [31].

1.2.8 CaSR monomer and dimer

CaSR has been detected as a monomer at various molecular weight depending upon the amount of glycosylation. 100-120 kDa are known as the unglycosylated form of CaSR, 130-140 kDa are an immature form of CaSR that are glycosylated with mannose forms of carbohydrates and 150-160 kDa are mature forms of CaSR glycosylated with complex carbohydrates [51, 79]. These mature forms are expressed at the cell surface [80]and the immature ones are proteolyzed.

A functional CaSR is expressed as a homodimer at greater than 200 kDa which may represent a dimer or an oligomer.

1.2.9 Disorder of Ca^{2+} homeostasis and CaSR

Over 225 mutations in the Ca^{2+}-sensing receptor result in hypercalcemic or hypocalcemic disorders, such as familial hypocalciuric hypercalcemia, neonatal severe primary hyperparathyroidism, and autosomal dominant hypocalcemic hypercalciuria **(Figure 1.9).** Abnormal function of CaSR is associated with Ca^{2+} homeostatic disorders. Loss-of-function mutations in CaSR lead to potentially fatal neonatal severe primary hyperparathyroidism, while gain-of-function mutations cause autosomal dominant hypocalcemia [81, 82]. However, not all the mutations detected from patients are disease related, and some nucleotide diversity can be a rare allele of single nucleotide polymorphism. For example, a CaSR variant (Glu250Lys) identified in FHH and ADHH probands were demonstrated to be a functionally neutral polymorphism [83].

1.2.10 Cancer and CaSR

CaSR is a master regulator of Ca^{2+} homeostasis, and additionally, it affects the cellular fate through control over proliferation, differentiation, apoptosis and chemotaxis [66]. Therefore, CaSR has a pivotal role in the regulation of cancer expression. There are many single nucleotide polymorphisms (SNPs) in CaSR that are associated with cancer. Three common nonsynonymous SNPs (rs1801725, rs1042636, and rs1801726) have been the primary research targets for cancer risk, but inconsistent results have been reported in MEDLINE, EMBASE, Web of Science, Scopus, and the HuGE databases [84]. rs1801725 (A986S, 2956G.T) is where T allele is associated with higher levels of serum calcium, colorectal adenoma, whereas rs1042636 (R990G, 2968A.G) mostly present in Asians, induces a gain-of-function mutation associated with primary hyperparathyroidism and calcium stone formation [84]. It is shown to be lower in colorectal

adenoma. On the other hand, rs1801726 (Q1101E, 3403C.G) is a common polymorphism in African ethnicity and is less carried in prostate cancer patients. Patients with this SNP have increased risk of colorectal adenoma. Another polymorphism called rs17251221 (1378–1412A.G) is an SNP in introns. rs1801725 induces a gain-of-function mutation associated with total serum

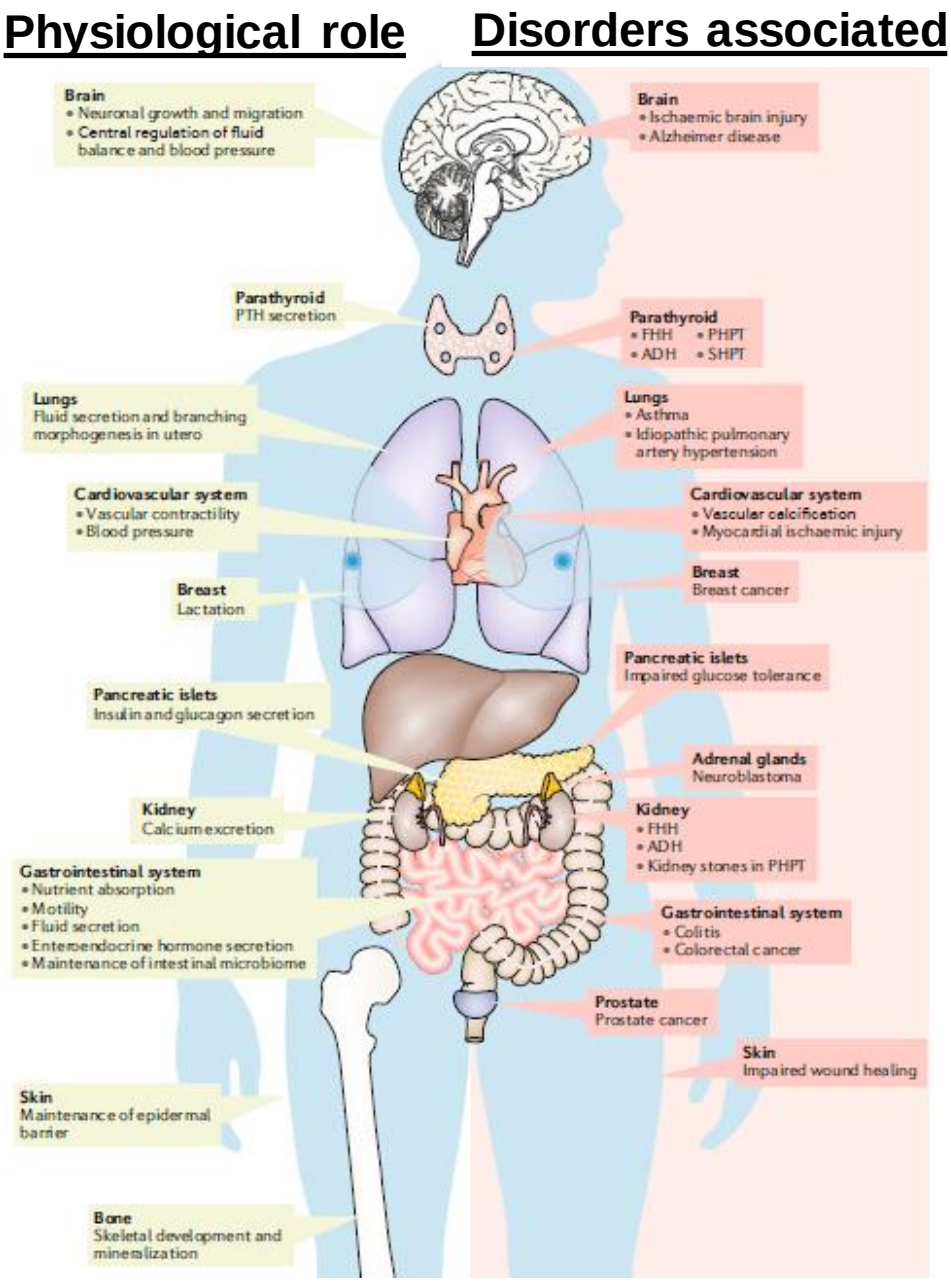

Figure 1.9 Physiological role and clinical relevance of CaSR. Adapted from [5]

calcium concentration, and stone multiplicity in patients with nephrolithiasis, noticeable association with prostate and breast cancer increased risk [84].

CaSR expression and mechanism are highly dubious in various cancer cells. In prostate, testicular, ovarian, and breast cancer, CaSR promotes proliferation and inhibition of apoptosis, thus, acting as an oncogene [2] **(Figure 1.10).** In parathyroid, colorectal cancer and neuroblastomas, CaSR expression is reduced and thus, CaSR functions as a tumor suppressor [2] **(Figure 1.10)**. CaSR may act as the mediator of the anti-tumorigenic effect of calcium in these cancers. Loss of expression of CaSR in neuroblastomas and colorectal cancer is epigenetic. However, in parathyroid cancer, CaSR expression is not affected by epigenetic or genetic mechanisms [2]. For example, in colon cancer, 69% CaSR gene showed methylation and showed an inverse correlation with the degree of differentiation. The methylation was significantly correlated with reduced mRNA and protein expression of CaSR. The study showed a significant role of epigenetic silencing of CASR in colorectal carcinogenesis [85]. Besides, meta-analysis studies investigating association of CASR polymorphisms with cancer risks have presented many inconclusive results. The role of CASR polymorphisms as a tumor suppressor or an oncogene is known to differ by cancer site and environmental condition. High calcium intake is shown to reduce the risk of colorectal cancer development as E-cadherin stimulated by CaSR is known to interact with β-catenin, an important proto-oncogene [84]. The increased expression of CaSR by high calcium levels is known to promote MCF-7 breast cancer cells and PC3 and C4-2B prostate cancer cells that are known to metastasize to the bone. These cancer cell proliferation process is linked to extracellular signal-regulated kinases 1 and 2 (ERK 1/2) phosphorylation [84].

The role of CaSR in cancer is directly related to its role at the regulation of synthesis of the parathyroid hormone-related peptide (PTHrP) (81). PTHrP, a peptide growth factor, binds to the

binding region of PTH. It is able to increase the expression of receptor activator of nuclear factor κ B ligand (RANKL), a tumor necrosis factor cytokine family. This, in turn, stimulates the osteoclastic bone resorption [86]. PTHrP is associated with osteolytic bone destruction and releasing of bone-derived growth factors [2]. PTHrP causes humoral hypercalcemia of malignancy (HHM) which is a common complication found in breast, prostate, lung, kidney cancer and myelomas [87]. Several studies implicate the role of $Ca^{2+}{}_o$ and CaSR in cancer bone metastasis of breast, prostate, lung, and kidney with an incidence of 65-40% [88]. Stephen Paget's theory on "seed and soil" postulates the importance of the microenvironment (soil), in the secondary site in organ-specific metastasis [89]. The blood plasma Ca^{2+} concentration is ~2.2-2.6 mM whereas, the bone plasma is around 10 mM and 20 mM in extracellular space of bone tissue [22]. High Ca^{2+} could act as a favorable microenvironment for the metastasized cells. Feng et al also showed CaSR expression to be higher in the bone metastasis than in the primary prostate tissues [90]. Furthermore, Liao et al showed a higher proliferation of skeletal metastatic cells, PC3, in increased Ca^{2+} condition as compared to LNCaP cells that metastasize to lymph nodes, and this mechanism is mediated by CaSR as shown by the decrease in proliferation when CaSR is knocked-down [91]. In addition to prostate cancer, CaSR has been shown to be highly expressed in patients with primary renal cell tumors with bone metastasis in comparison to lung metastases or no metastases. Further, the proliferation and migration induced by Ca^{2+} treatment in RCC cells obtained from patients with bone metastasis, was inhibited by CaSR inhibitor NPS2143 [92].

Various pathways have been implicated in promoting tumor by CaSR activation. However, the exact mechanism is obscure. In malignant or normal ovarian epithelial cells, the CaSR activation induces proliferation by activation of the ERK1/2 pathway [93, 94]. The osteoblastic metastases in prostate cancer is caused by CaSR mediated stimulation through PTHrP. PTHrP is

higher in prostate tumors as compared to healthy prostate epithelial cells, and PTHrP associated proliferation has been accounted for in PC3 cells and not LNCaP cells [95]. The PTHrP could

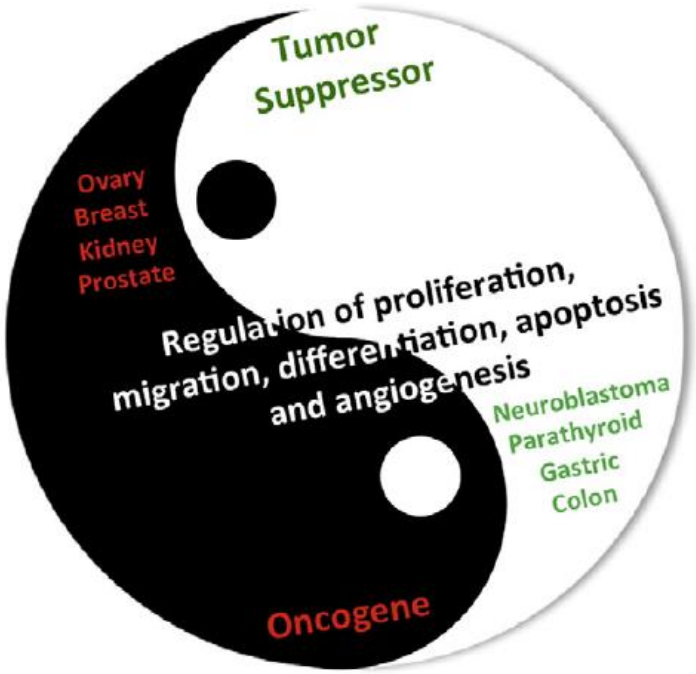

Figure 1.10 The role of CaSR as oncogene or suppressor in cancer [2]

CaSR expression and mechanism are highly dubious in various cancer cells. In prostate, testicular, ovarian, and breast cancer, CaSR promotes proliferation and inhibition of apoptosis, thus, acting as an oncogene. In parathyroid, colorectal cancer and neuroblastomas, CaSR expression is reduced and thus, CaSR functions as a tumor suppressor

mediate the transactivation of epithelial growth factor receptor (EGFR) and ERK1/2 [96]. It has been shown that knockdown of PTHrP in PC3 cells inhibits epithelial-to-mesenchymal transition (EMT) and tumor progression [97]. Further, CaSR mediated Akt [91] and Rho [98] signaling pathway is also associated with tumor proliferation.

1.3 Challenges faced in studying CaSR

There are many challenges to studying CaSR. First, it is a large membrane protein with 1068 amino acids. Therefore, it is difficult to separate it from the cells due to their hydrophobic transmembrane domain. Further, a large amount of aggregation of the 7TM region occurs due to

the heating process and thus reduce the solubility of the protein. Second, CaSR is highly cooperative with high hill coefficient (~ 3); therefore, when we study the mechanism, we are looking at multiple binding sites. Third, it is highly heterogeneous with many variants and isoforms with varying functional capabilities depending on the tissue-type. Fourth, CaSR is a dynamic receptor and undergoes a multitude of actions involving folding, glycosylation, dimerization, trafficking, and endocytosis. CaSR has multiple binding partners involved in a wide range of downstream signaling. These partners are known to bind not only various transmembrane or intracellular loop exposed to cytosol but are known to bind differentially spatially depending on which part of life-cycle CaSR is present in. Last but not the least, studying CaSR in cancer is complicated as it is found to be low in endogenous expression, for example, 7-8 folds lower in PC3 cells as compared to wild type. In addition, studying Ca^{2+} is challenging as it binds with low binding affinity and cannot be measured directly with fluorescence. Ca^{2+} signaling is further complicated as Ca^{2+} not only acts as a primary messenger but also the secondary messenger.

Using techniques such as RT-PCR and mass-spectrometry is highly dependent on the amount of expression of the transcript or proteins or their kinetics. For example, in co-immunoprecipitation and mass spectrometry may not be able to provide a complete snapshot of the putative CaSR interactome. They have obvious limitations with likely detection of partners with only high binding affinity and slow dissociation constants. This results in less prospect of detection of transient interactions, as well as likely detection of interaction of more abundant partner as compared to lower abundant ones. Due to the absence of the native state of CaSR as the lysis destroys the plasma membrane and cannot provide accurate and adequate membrane environment with detergent, the binding can be perturbed. Also, there is the possibility of interactors being washed out during the Co-IP process and un-specific binding and detection due

to general enrichment in the cell. This can result in the incomplete recruitment of protein complexes and the absence in the detection of some of the known CaSR partners in our experiment. The mass-spectrometry utilized in our study is incapable of separating the divergent forms of CaSR with various post-translational modifications, which can indirectly impact the interactors over its lifecycle. The LC-MS has a typical dynamic range of detection at 4-6 orders of magnitude which is much lower as compared to the protein concentration range in biological samples at 12 orders of magnitude [99]. Also, using an online database for annotations have limitations since the known knowledge is not complete. The generation of complicated networks of inter-related and similar terms can be overwhelming and can produce convoluted results.

1.4 Background on Gap Junction

Gap junctions (GJ) are integral membrane proteins which assist in communication and coordination between cells through processes including, exchange of metabolites and electrical signal **(Figure 1.3)**. In humans, GJs are expressed in all tissues except differentiated skeletal muscle, erythrocytes, and mature sperm cells **(Figure 1.11)** [100]. GJ proteins consist of intercellular aqueous channels between adjacent cells that permit the exchange of hydrophilic molecules such as ions, and metabolites (ATP, NAD^+, small peptides and nucleotides), and secondary messengers (Ca^{2+}, cAMP, IP_3) of less than 1kDa [100]. They are known to modulate wide range of functions such as immune response, inflammation, memory, apoptosis, water channels, metabolism and muscle contraction [100].

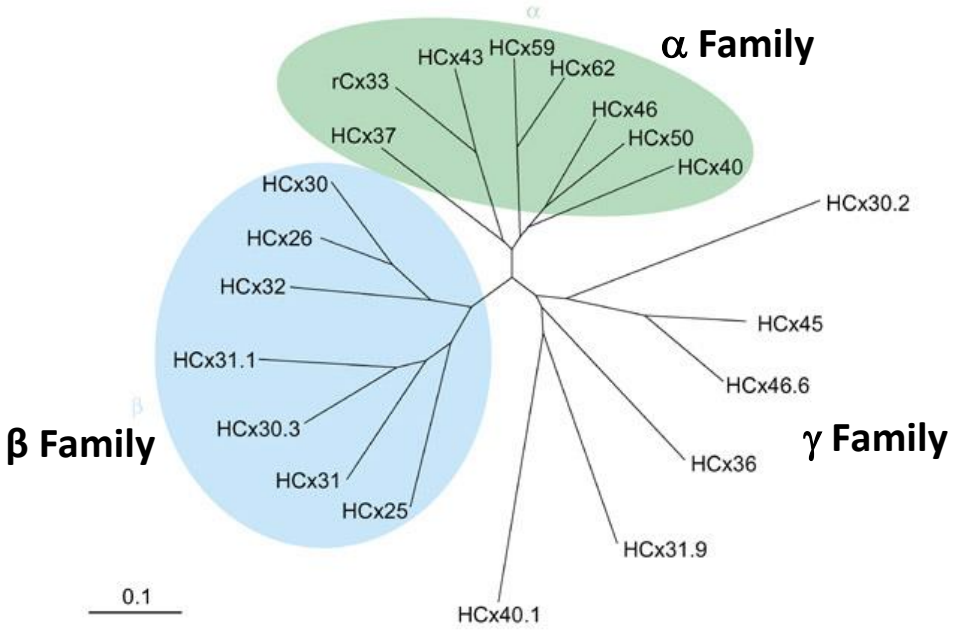

Figure 1.11 Connexins are divided into three major families (α, β and ϒ)

Around 21 connexin genes have been identified in humans categorized as a α, β, γ, δ or ε isoform based on their sequence homology and length of the CL. Each of the isoforms have distinct physiological properties and regulation responses. Therefore, the unique properties of GJ function and regulation such as their selectivity for small molecules, voltage dependent gating, and response to Ca^{2+}, pH and phosphorylation is determined by its connexin composition.

Table 1.2 Various families of gap junction and their expression patterns

Name	Family	Expression Patterns
Cx26	β	Cochlea, skin, liver, placenta, breast
Cx43	α	Heart, lens, brain, adrenal gland
Cx45	γ	Heart and brain
Cx46	α	Lens
Cx50	α	Lens

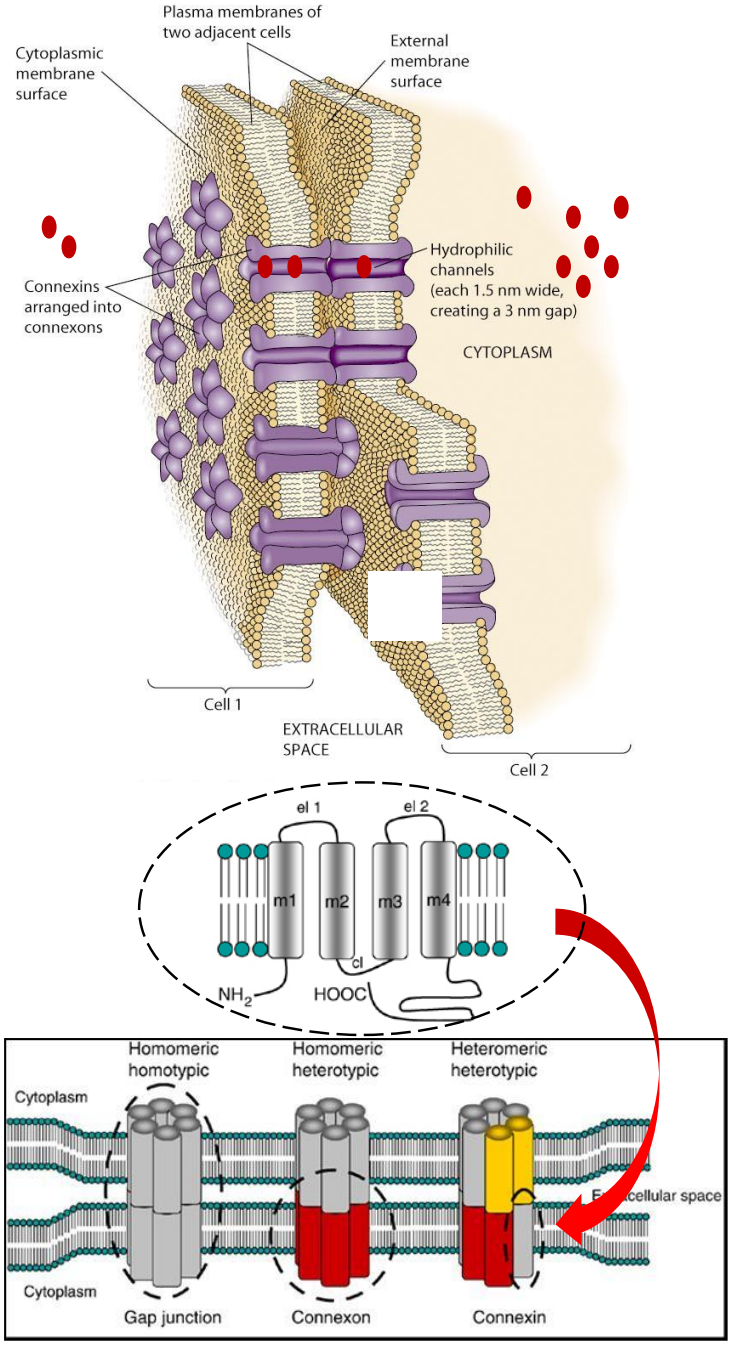

Figure 1.12 Structure of Gap Junction

A. Gap Junction forms a channel with head-head docking of the two hemichannels (connexons). The hydrophobic interactions at the extracellular domains drive hemichannels to redock into dodecameric channels B. Connexins are formed by four transmembrane domains connected by extracellular loops and a cytosolic loop. [11] exchange of hydrophilic molecules such as ions, and metabolites (ATP, NAD^+, small peptides and nucleotides), and secondary messengers (Ca^{2+}, cAMP, IP_3) of less than 1kDa

1.4.1 Structure of Gap Junction

Docking of head to head of two hexameric connexins form GJ proteins in vertebrates whereas, in non-vertebrates, they are formed by innexins [101]. The hydrophobic interactions at the extracellular domains drive hemichannels to redock into dodecameric channels [102]. Proteins with sequence homology to innexins in vertebrates are called pannexins which can form intercellular channels [101]. Each connexin consists of four α-helical transmembranes (TM) domains connected by two extracellular loops (EL) and a cytoplasmic loop (CL) with both N-and C-terminus facing the cytosol [103]. Intermolecular interactions between two adjoining connexons involve both EL1 and EL2 domains. EL1 and EL2 are connected via intra-connexin disulfide bonds between six highly conserved Cys residues, three in each loop. The channel interior, that connects between adjacent cells, is tightly isolated due to to the presence of numerous hydrogen bonds and salt bridges [100]. The TM domains and the EL's are highly conserved among the connexin families. N-terminus is relatively conserved, whereas, the CL and C-terminus vary significantly between the isoforms. Currently, around 21 connexin genes have been identified in humans categorized as a α, β, γ, δ or ε isoform based on their sequence homology and length of the CL **(Figure 1.11**Figure 1.11**)** [103]. Each of the isoforms has distinct physiological properties and regulation responses. Therefore, the unique properties of GJ function and regulation such as their selectivity for small molecules, voltage-dependent gating, and response to Ca^{2+}, pH, and phosphorylation is determined by its connexin composition [103].

1.4.2 Connexin26 and related disorders

Connexin26 (Cx26) is the second smallest, and one of the most ubiquitous members of the GJ protein β-family distributed in cochlea, skin, liver, placenta, brain, and breast **(Figure 1.11)** [104]. Hereditary mutations in human Cx26 is associated with skin disorders and non-syndromic-

and syndromic- deafness **(Figure 1.13)** [104]. Cx26 are also implicated in cancers where Cx26 had an inverse relation with cancer into human breast tumor cell line, for example, in breast cancer

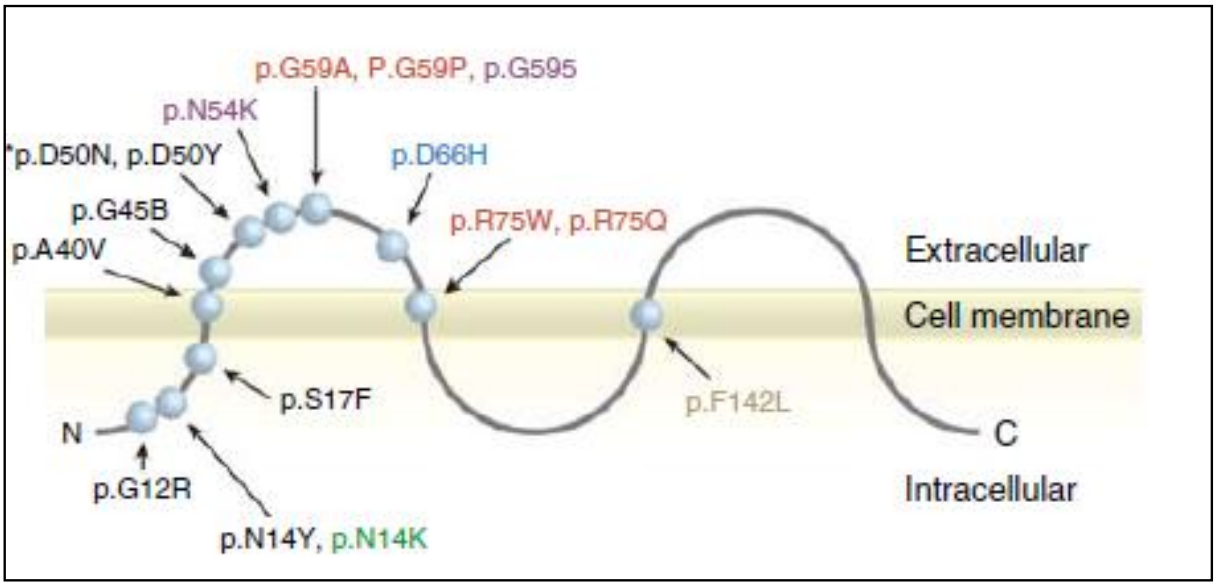

Figure 1.13 Various disease related mutations are present in Cx26 [15].

Keratitis Ichthyosis Deafness (KID) syndrome (black), Palmoplantar keratoderma with deafness (red), Vohwinkel's syndrome (blue) and Bart Pumphrey Syndrome (BPS) (purple)

[105] and bladder cancer [106]. Therefore, understanding the gating mechanism of Cx26 or any GJ's can be exploited for the therapeutic target of numerous disorders. Connexin26 is the only GJ protein with an x-ray crystal structure and this was made possible due to its short CT as compared with other connexins. The flexibility of the cytoplasmic domains has been a challenge for the crystal structure. [102, 107]. The N-domain serves as the plug as demonstrated by Oshima et al. where its deletion mutation resulted in no electrical activity in paired Xenopus oocytes and reduced dye transferring capability in Hela cells [102]. This was also supported by Maeda et al through a 3.5 A^o crystal structure [108].

1.5 Challenges faced in studying Cx26

Connexins are large membrane proteins which prefer the state of oligomerization. This makes it difficult to express and purify due to low solubility. The expression especially in *E.coli.* and insect cells is challenging due to the fact that bacteria lack a proper mechanism for eukaryotic protein folding, translocating, trafficking, disulfide bond formation, and post-translational modifications. Also, the phospholipid composition in bacteria and insects varies from that of eukaryotic cells. These may result in improper surface expression of membrane proteins such as connexins. Understanding their mechanism is limited due to the unavailability of their dynamic structures. This again is resulted due to the heavy glycosylation, dynamic structures, high instability, oligomerization and large molecular size. For example, the closed-form structure is unavailable. Additionally, understanding the calcium modulation is a challenge due to its weak binding and that Ca^{2+} binding has high on- and off- rate. Furthermore, calcium is silent spectroscopically, which makes the study a challenge.

1.6 Overview of the dissertation, and major question to be addressed

In this dissertation, in order to understand the regulatory role of Ca^{2+} on important membrane proteins such as CaSR and Cx26, we addressed many challenges and carried out several approaches to tackle them.

CHAPTER I is an overview of the background of Ca^{2+} homeostasis, Ca^{2+} signaling, calcium-sensing receptor and connexin26. CaSR is a versatile receptor that allows control of serum Ca^{2+} concentration at the microscopic level and is known to be modulated by divalent cations and amino acids. It's expression and function are highly diverse in various tissues and pathological conditions. Cx26 is a gap junction protein that allows for intra- and extra- cellular communication.

Both CaSR and Cx26 are integral membrane proteins that regulated the normal functioning of a cell.

The recent advancement in its study such as the crystal structure obtained in 2016 has expanded our knowledge on the function of CaSR at a molecular level to some degree, highlighting its modulation through divalent cations such as Ca^{2+} and Mg^{2+}, and Trp-derivative ligand as co-agonist. However, the agility of this receptor as a multifunctional receptor comes from many factors such as (i) diversity in transcripts and expression levels in various tissues, organs and species, (ii) various modes of regulation such as multitude of agonists and co-agonists, (iii) disease-mutations that affect its signaling and expression and (iv) wide range of spatially and temporally modulated downstream signaling molecules attributing to diverse intricate control. An in-depth understanding of differential molecular function, genomic organization, expression and interaction with its microenvironments is necessary in order to help us design and develop organ- or tissue-specific therapeutics and targeting methods against CaSR related maladies.

CHAPTER II describes the project on understanding the global effect of Ca^{2+}_{o} on protein-protein interaction network of CaSR. We attempt at establishing the first CaSR interactome. Co-immunoprecipitation using recombinant FLAG-CaSR and anti-FLAG antibody, and proteomics were utilized to quantify the difference in downstream signaling pathways. This was further studied using gene ontology and statistics to obtain information on function, location and pathways associated with the enriched proteins. We address question such as:

a) How do we optimize co-immunoprecipitation to achieve the optimal enrichment of CaSR and its interactors?
b) What are CaSR interactors during its cellular biosynthesis and trafficking?

c) Will prolonged exposure to Ca^{2+}_o or deprivation of Ca^{2+}_o using EGTA affect the biosynthesis of other interactors and regulators of CaSR?

d) Can CaSR regulate its biosynthesis due to prolonged signaling?

e) Does CaSR act as a communicator between the intra- and extra- cellular Ca^{2+} signaling?

f) What is the implication of enrichment of some proteins with the treatment of Ca^{2+}_o?

g) What are biological pathways most affected with Ca^{2+}_o?

CHAPTER III is a project investigating the CaSR mediated signaling in HEK293 cells and endogenous CaSR mediated signaling in thyroid cancer cells. This chapter attempts at characterizing the Gαq mediated signaling and examining the molecular difference in the CaSR to explain the differences. The biostatistical methodology was employed for precise measurement of the Ca^{2+} oscillation pattern and further immunoassays and calcium sensor such as FURA-2 AM were used to monitor intracellular signaling mediated by CaSR. Effect of various CaSR-related drugs was monitored to understanding Ca^{2+} signaling mediated by CaSR in different cell types. The questions addressed in this chapter are:

h) How do Ca^{2+}, Mg^{2+} and amino acids modulate the mechanism of WT CaSR?

i) How does CaSR mediated signaling differ in thyroid cancer cells?

j) How species- and tissue-specific is the expression and signaling of CaSR?

k) Do the CaSR-related drugs carry similar potency in all cell types?

l) Can we use bio-statistics to quantitate the difference?

m) Is the differential signaling due to expression?

n) Is the cause of the differential CaSR mediated signaling splice variants?

CHAPTER IV is a project on the molecular investigation of CaSR in the prostate cancer cell, PC3. We examine the CaSR from RNA to DNA level and study the signaling as compared to the

WT in HEK293 cells. This chapter probes the $G\alpha_q$ mediated signaling mediated by CaSR by employing calcium sensors such as FURA-2 AM and CaSR related drugs. We also delve into the difference in global proteomics difference between the Ca^{2+} and EGTA treatment conditions as well as cell types. The questions addressed in this chapter are:

o) Does PC3 express WT CaSR?

p) Do CaSR in PC3 have similar signaling as WT?

q) If not, what is the reason behind it?

r) Is the differential signaling due to the presence of splice variant?

s) Is the differential signaling due to proteomics difference?

t) How does Ca^{2+}_o affect the global proteomics in HEK293 cells and PC3 cells?

u) Do the CaSR-related drugs carry similar potency in all cell types?

CHAPTER V is a project on gap junction, Cx26. We aimed at optimizing expression and purification of this challenging membrane protein using a bacterial system. We also characterized the protein stability and used it for biophysical assays to understand the gating through Ca^{2+}_o and CaM. We address questions such as:

v) What parameters can optimize the expression of hCx26?

w) What detergents and strategies are optimal for purification of hCx26?

x) What are the biophysical characteristics/stability of the purified protein?

y) What is the stoichiometry, metal binding affinity and metal selectivity of the hCx26?

z) How does Ca^{2+} induce conformational changes, stability, and assembly?

aa) What is the major mechanism of interacts between CaM/Ca^{2+} and Cx26?

2 CHAPTER II: GLOBAL EFFECT OF EXTRACELLULAR CALCIUM ION ON CALCIUM-SENSING RECEPTOR INTERACTOME INVOLVED IN RECEPTOR MATURATION AND TRAFFICKING

2.1 Abstract

The calcium-sensing receptor (CaSR) maintains systemic calcium (Ca^{2+}) homeostasis by integrating Ca^{2+}-signaling from changes in extracellular Ca^{2+} concentrations to intracellular signaling networks which is critical for many (patho)physiological processes in multiple organs including parathyroid, kidney, bone, brain, and skin. Agonist-driven insertional signaling results in the mobilization of the intracellular pool of nascent CaSR to its functional form at the plasma membrane in the chronic presence of extracellular calcium. Little is known on the CaSR interactomes associated with regulators of calcium ion (Ca^{2+}) storage and transport during its biosynthesis and trafficking, and the effect of Ca^{2+}_o perturbation on these interactomes. To identify CaSR interacting partners, the recombinant FLAG-tagged CaSR (transfected in HEK293 cells) was immunoprecipitated and subjected to high-resolution mass spectrometry and extensive bioinformatics analysis. Two different reagents —(i) 4 mM Ca^{2+}_o and (ii) 2 mM EGTA—were used to perturb the Ca^{2+}_o concentration and the results were compared. Combining the results from both treatments, 106 proteins were identified as putative CaSR interactors with ≥ two-fold enrichment over the negative control (transfection with empty pcDNA3.1). Markedly, 65% of these 106 proteins had higher abundance with 2-43 folds in samples treated with Ca^{2+} as compared to EGTA. Gene ontology analysis revealed that these CaSR-interactors are most significantly enriched in the endoplasmic reticulum (ER) with predominant molecular functions of GTPase activity, GTP binding, cadherin binding involved in cell-cell adhesion, and unfolded protein binding. The KEGG pathways enriched was the protein processing in the ER which was supported

by the biological processes enriched such as the protein folding in the ER. On the contrary, 31% of the 106 proteins were upregulated with < 1.5-fold change irrespective of the presence of added Ca^{2+} or EGTA. These interactors are enriched in the extracellular matrix, focal adhesion, ribosome, and mitochondrial inner membrane and are involved in RNA binding, structural constituent of ribosome, heat shock protein binding, and ATPase activities. Interestingly, this study identified 98 novel CaSR interactors (e.g., Rab18, Rab5C, Rab6, heat-shock proteins, Dnaj, vesicle-associated membrane protein-associated protein A/B, 14-3-3 γ, SERCA, E3 ubiquitin ligases (CHIP, RanBP2 and AMFR), tubulins, and voltage-dependent anion-selective channel protein 2) that were earlier reported in the literature as GPCR interactors. This indicates an overlapping signaling cascades and trafficking between the protein and other members of the GPCR family. Eight previously known CaSR interactors, namely $G\alpha_{i,}$ $G\beta_2$, 14-3-3 θ, 14-3-3 ζ, 14-3-3 ε, 14-3-3 γ, calnexin and p24 were also revalidated in this study. Moreover, 98 novel putative CaSR interactors were detected. With literature mining, we find that these novel CaSR interactors may regulate co-translational translocation (SRP complex, Sec61, GRP78, palmitoyl-transferase, oligosaccharyl-transferases, glucosidases, glycosyltransferase), calnexin cycle (calnexin, protein disulfide isomerase, glucosyltransferase), ER/Golgi trafficking (Rab6, VAMP-associated proteins), endocytosis (Rab18, Rab5c, clathrin heavy chain), degradation pathway (E3 ubiquitin ligase STUB1, RanBP2 and heat shock proteins) and Ca^{2+} handling (SERCA, TMCO1, VDAC2, TIMM50). Taken together, our findings surmise the role of $Ca^{2+}{}_o$ in CaSR-mediated modulation of the proteostasis and CaSR-interactome through a series of events—differential signal transduction mediated by activation of CaSR via $Ca^{2+}{}_o$ perturbation, modifications in regulatory proteins maintaining Ca^{2+} homeostasis, stimulation of cellular activities such as the biosynthesis and trafficking or changes in the binding affinity of interactors to CaSR due to alteration of the $Ca^{2+}{}_o$ concentration. Taken

together, our findings largely extend the repertoire of CaSR biosynthesis and trafficking revealing previously unknown major players and potential mechanism for the mobilization of nascent CaSR from the ER that is induced by extracellular Ca^{2+} mediated CaSR signaling. Our findings may serve as potential therapeutic targets for pathologies resulting in hypercalcemia and hypocalcemia in the overall G-protein coupled receptor family that CaSR belongs to.

2.2 Introduction

2.2.1 Calcium-sensing receptor and its mediated signaling

Calcium-sensing receptor (CaSR) is a class-C, G-protein coupled receptor (GPCR) that maintains a tight cellular Ca^{2+} homeostasis with a 10,000 fold electrochemical gradient between the extracellular (1.1 to 1.4 X 10^{-3} M) and cytosolic (10^{-7} to 10^{-8} M) Ca^{2+} concentrations in the cell [20]. Ca^{2+}_o, acting as an extracellular first messenger [30], activates CaSR at a half-maximal concentration of 3-4 mM as mentioned in chapter I. Henceforth, CaSR mediated intracellular signaling is induced through the association of CaSR-intracellular loops with heterotrimeric G proteins, $G_{q/11}$, $G_{i/o}$, $G_{12/13}$, and G_s. [39] **(Figure 1.5).** Through $G_{q/11}$, the CaSR activates phospholipase C, increases cytosolic Ca^{2+} (Ca^{2+}_{cyt}) and DAG (diacylglycerol) levels, and activates phospholipase A2. Through $G_{i/o}$, the CaSR inhibits adenylyl cyclase, decreases cAMP production, and activates extracellular signal-regulated kinase (ERK). Through $G_{12/13}$, it activates Rho-dependent phospholipase D and amino acid-induced Ca^{2+} mobilization [69, 72]. This functional diversity allows CaSR to regulate Ca^{2+}_i concentrations in various cellular compartments, including, the cytosol (Ca^{2+}_{cyt}), ER (Ca^{2+}_{ER}) and mitochondrial (Ca^{2+}_{mito}). These perturbations of Ca^{2+} concentrations act as intracellular signal messenger [34] and in turn controls the critical cellular processes including secretion, apoptosis, chemotactic responses, cell proliferation,

cytoskeletal rearrangements, ion channel activity, the control of gene expression, and cell differentiation [51, 52].

2.2.2 CaSR mediated intracellular Ca^{2+} mobilization

Stimulation of CaSR elicits Ca^{2+} mobilization from intracellular stores such as the ER [54], which causes acute increase in the Ca^{2+}_{cyt} [109]. The decrease in Ca^{2+}internal stores results in the store-operated channel (SOC) mediated Ca^{2+} influx followed by an increase in Ca^{2+}_{cyt} [110].This further activates the influx through the plasma membrane channels, therefore, resulting in a sustained rise in [Ca^{2+}_{cyt}]. Extended increase in [Ca^{2+}_{cyt}] can cause overstimulation of the cellular responses and cytotoxicity, and therefore, needs tight control by Ca^{2+}-binding proteins, pumps, and channels in the plasma membrane, ER and Golgi [109].

2.2.3 Unique features of CaSR sensitization, desensitization and ADIS

CaSR is an exceptional receptor with minimal functional desensitization in the chronic presence of agonist [111-113], and it can distinguish as small as ~200 μM fluctuations in [Ca^{2+}_{o}]. These unique properties are integrative effects of its highly cooperative activation with Ca^{2+}_{o} with Hill coefficient of 3 [38, 66, 114] and its distinctive intracellular Ca^{2+} signaling and trafficking machinery involving various regulators [115]. Agonist driven insertional signaling (ADIS) is a phenomenon where the agonist such as the Ca^{2+} in case of CaSR, augment the plasma membrane insertion of the receptor [116]. It has been implied that ADIS regulates the two unique features of CaSR, the signal cooperativity as well as the time course and extent of signal desensitization [116]. This finding suggests that CaSR trafficking and signaling is directly associated with each other. Few proteins have been identified as regulators for CaSR trafficking, but much information is largely missing.

2.2.4 CaSR life cycle and known regulators in trafficking

The regulation of the abundance of CaSR can occur at various stages of its life-cycle such as modulation of transcription, the stability of mRNA, translation efficiency, ER quality control (ERQC) and degradation at proteasome or lysosome [116]. CaSR undergoes a dynamic life-cycle with anterograde transport of nascent receptors from the ER, Golgi and ER-Golgi intermediate compartments (ERGIC) to the plasma membrane, and with subsequent retrograde transport to lysosome or proteasome for degradation [115] [8] **(Figure 2.1)**. Prolonged exposure to Ca^{2+}_o induces ADIS which mobilizes the intracellular pool of CaSR to enhance anterograde trafficking [115]. First, the CaSR undergoes the ERQC during the co-translational and immediate post-translational period. To date, the known proteins involved in this process are small GTP binding proteins (Rabs, Sar1, and ARFs), cargo/chaperones (p24A, RAMPs) and interacting proteins (14-3-3 proteins, CaM). Second, CaSR endocytosis is facilitated by G protein receptor kinases (GRKs), protein kinase C and β-arrestins. Finally, CaSR is degraded by proteasome or lysosome by ubiquitination by E3 ubiquitin ligase, dorfin [117] (**Figure 2.1, Table 2.1**).

It is critical to further determine the rest of the CaSR interactors and to understand the effects of Ca^{2+}_o perturbation on CaSR mediated proteostasis. Not only is CaSR exposed to its primary agonist, Ca^{2+} in the plasma membrane but also in the ER, therefore, $[Ca^{2+}_{ER}]$ plays a major role to induce its active conformation and dictate the life of CaSR[116]. CaSR acts as a mediator and induces intricate crosstalk between the Ca^{2+}_o and intracellular Ca^{2+} signaling, which is modulated through CaSR interactomes and regulators associated with Ca^{2+} handling and trafficking throughout various stages of the dynamic life cycle of CaSR. To address this and to illustrate the first comprehensive protein-protein interaction network for CaSR, we employed treatments of 4 mM Ca^{2+}_o and 2 mM EGTA on HEK293 cells transfected with either recombinant

Table 2.1 List of known CaSR interactors. Adapted from [8]

Times	Assay Used	Function	CaSR domain	Ref.
AMSH	Y2H, GST	Trafficking/ de Ub enzyme	C-terminal	(Herrera-Vigenor et al., 2006)
β-Arrestin	Functional	Trafficking/signaling	Unknown	(Lorenz et al., 2007)
Caveolin	Co-IP	Structural/scaffolding/ Trafficking/signaling	Intracellular loop 1 and 3	(Kifor et al., 1998; Kifor et al., 2003; Sun and Murphy, 2010; Breitwieser, 2013)
E3 Ub ligase	Y2H, IP, Functional	Trafficking	C-terminal	(Huang et al., 2006)
Filamin	Y2H, Co-IP, GST, Functional	Structural/scaffolding/trafficking	C-terminal	(Awata et al., 2001; Hjalm et al., 2001; Pi et al., 2002)
GRK-2	Functional	Signaling	Intracellular domain	(Lorenz et al., 2007)
GRK-4	Functional	Signaling	Intracellular domain	(Lorenz et al., 2007)
Kir4.1	Y2H, Co-IP, Functional	K channel	C-terminal	(Huang et al., 2007a)
Kir4.2	Y2H, Co-IP, Functional	K channel	C-terminal	(Huang et al., 2007a)
PI-4-Kinase	Co-IP,	Signaling	Unknown	(Huang et al., 2002)
PKC	Functional	Signaling	C-terminal	(Lorenz et al., 2007)
RAMP1	Co-IP, Functional	Structural/trafficking	ECD and TM	(Bouschet et al., 2005)
RAMP3	Co-IP, Functional	Structural/trafficking	ECD and TM	(Bouschet et al., 2005)
RGS proteins	Functional	Signaling	Unknown	(Huang et al., 2002; Huang et al., 2004)
Rho	Co-IP	Signallling	Unknown	(Huang et al., 2002)
14-3-3	Yeast two-hybrid screen, CaR tail pull-down studies, Co-IP	Trafficking, , expression, signaling	Proximal membane region, CaSR tail	(Grant et al., 2011; Arulpragasam et al., 2012)
CaM	GST, Co-IP, Functional	Signaling/Stabilize	C-terminal	(Huang et al., 2010)
P24A	Co-IP	Stabilize/ trafficking	C-terminal	(Stepanchick and Breitwieser, 2010)
Sar1	Functional	Trafficking	ECD	(Zhuang et al., 2010)
Rab1, Rab7, Rab 11a	Functional, RNAi	Trafficking/signaling	possible ECD	(Zerial and McBride, 2001; Grosshans et al., 2006)
Dorfin	Co-IP, Functional	Trafficking	Intracellular loop, C-terminal	(Huang et al., 2006)
Integrins	Co-IP, Proteomic analysis, co-localization, (functional?)	Cell migration and adhesion in cancer cells (trafficking??), Signaling	Unknown	(Tharmalingam et al., 2011)

FLAG-tagged CaSR pcDNA3.1 or empty pcDNA3.1 (negative control) and subjected them to co-immunoprecipitation with anti-FLAG antibody and liquid chromatography coupled to tandem mass spectrometry (LC-MS/MS). The proteome identified were further analyzed using extensive bioinformatics tools to understand the gene ontology of the CaSR-mediated pathways and functions. The identified molecules suggest a major role of chronic exposure of $Ca^{2+}{}_o$ in amplifying anterograde trafficking of CaSR and possibly a bias towards Gαi signaling pathway. Our study re-

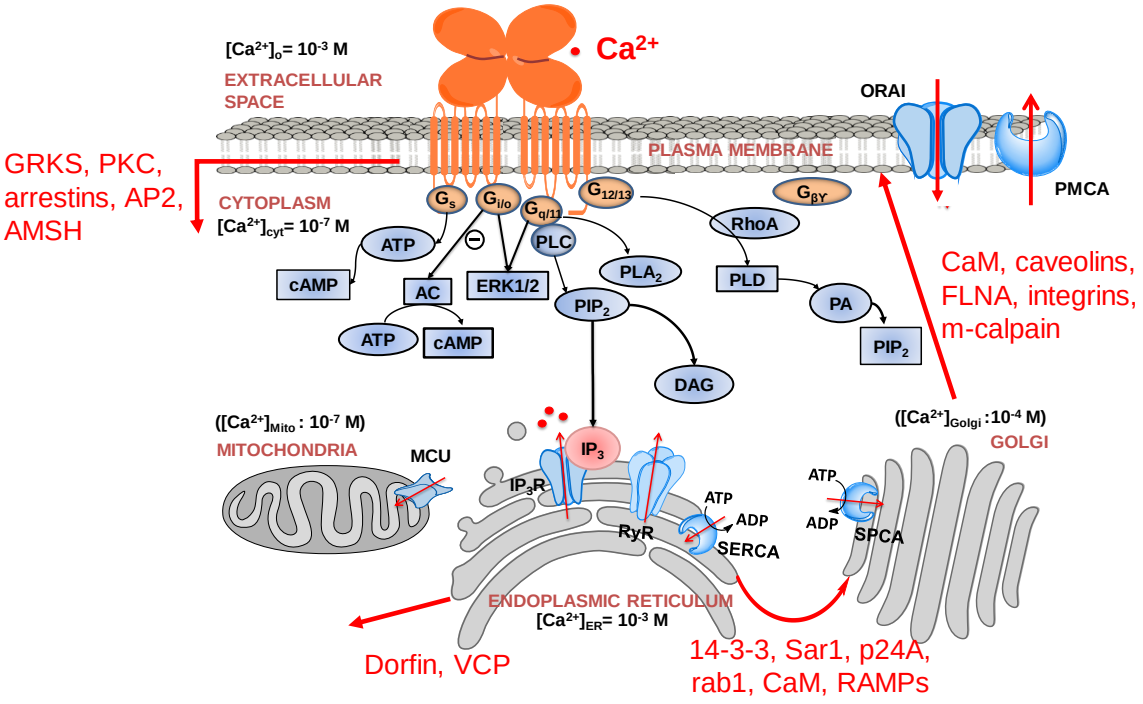

Figure 2.1 Known CaSR interacting proteins through its life-cycle (Adapted from [14])

CaSR undergoes a dynamic lifecycle with anterograde transport of nascent receptors from the ER, Golgi and ER-Golgi intermediate compartments (ERGIC) to the plasma membrane, and with subsequent retrograde transport to lysosome or proteasome for degradation. Prolonged exposure to $Ca^{2+}{}_o$ induces ADIS which mobilizes the intracellular pool of CaSR to enhance anterograde trafficking. First, the CaSR undergoes the ERQC during the co-translational and immediate post-translational period regulated by small GTP binding proteins (Rabs, Sar1 and ARFs), cargo/chaperones (p24A, RAMPs) and interacting proteins (14-3-3 proteins, CaM). Second, CaSR endocytosis is facilitated by G protein receptor kinases (GRKs), protein kinase C and β-arrestins. Finally, CaSR is degraded by proteasome or lysosome by ubiquitination by E3 ubiquitin ligase, dorfin.

enforces the concept by Brown and MacLeod that CaSR senses Ca^{2+} not only in the plasma membrane but also within the intracellular stores [66].

Table 2.2 List and details of previous attempt on mass spectrometry optimization

Experiment	Sample Processed By	Date	Number of PC3 Dishes	Number of HEK dishes	Antibody	Notes on Experiment	Results
Co-IP with no spin column. Sent as in gel digestion	Dr. Chen Ma (GSU)	~Jan 2015	40 dishes of PC-3		1:1000 dilution of ADD CaSR antibody		No CaSR Found
Co-IP, spin column, and no control beads. Sent as in gel digestion	Dr. Wu (Gtech)	~March 2015	40 dishes PC-3	10 each for HEK5001 and HEK293	1:1000 dilution of ADD CaSR antibody	HEK293 + CaSR lost during IP (sample spilled) // 3ml lysis buffer in 40 dishes of PC-3 and 1ml lysis buffer in 10 dishes of 5001	5001 (4 unique peptides, band a) and Hek 293 (12 unique peptides, band b)
Co-IP, spin column, and no control beads. Sent in-solution.	Dr. Wu (Gtech)	4/15/2015	40 dishes PC-3	10 dishes HEK5001	1:1000 dilution of ADD CaSR antibody	SDS sample buffer for elution	No CaSR Found, number of proteins detected decreased
Co-IP, spin column, and with control agarose beads wash. Sent as in-gel, binding and elution buffer from Thermon kit.	Dr. Wu (Gtech)	5/2015	40 dishes PC-3	10 dishes HEK5001	1:1000 dilution of ADD CaSR antibody	3ml lysis buffer + 3ul ADD antibody to 40 plates and 1ml + 1ul of Ab to 10 dishes	5001; 4 unique peptides (band 5 from gel B)
Membrane/cytosol protein extraction kit & UFLC/ in solution	Dr. Jin Zou (Clark Atlanta) Then sent	11/2015	4 dishes PC-3	2 dishes HEK5001			5001 (10 unique peptides)
Co-IP & membrane/cytosol protein extraction kit, in solution	Dr. Jin Zou (Clark Atlanta) Then sent out for processing	2/2016	4 dishes of PC-3	2 dishes HEK5001	15ul of ADD antibody to 2 plates		No CaSR Found
Classic Co-IP & membrane/cytosol protein extraction kit/ in gel	Dr. Chen Ma (GSU)	Jun-16	4 dishes of 5001 for each conditions	4 dishes of 5001 for each conditions	2 or 10 ug of ADD antibody per 10,000 ug protein		CaSR detected in all samples expect for one cytoplasmic fraction

2.2.5 Hypercalcemia and hypocalcemia

Higher serum Ca^{2+} is termed as hypercalcemia. Hypercalcemia is ranked as mild (2.60-2.97 mM or 10.5-11.9 mg/dL), moderate (3.0-3.47 mM or 12-13.9 mg/dL) and severe (> 3.5mM

or 14 mg/dL) [118]. This condition occurs during irregular Ca^{2+} homeostasis and is known to be caused due to malignancy or hyperparathyroidism in 90% of the cases. It occurs in almost 30% of patients with malignancy, including commonly in lung cancer, multiple myeloma, renal cell carcinoma, breast cancer, and colorectal cancer [119, 120]. 80% of these malignancies associated hypercalcemia is contributed to an increased parathyroid hormone-related peptide (PTHrP) [119].

On the other hand, total blood calcium below 8.5 mg/dL or ionized blood calcium below 4.6 mg/dL is referred to as hypocalcemia[121, 122]. This condition has been shown to occur in about 30% of patients with advanced prostate cancer [123]. Both conditions are closely associated with CaSR. Our experiment may contribute to the examination of the differential CaSR interactome involved in ADIS-mobilization mediated by hypercalcemic condition at 4 mM Ca^{2+}_o and hypocalcemia condition at 2 mM EGTA in pathologies such as cancers and secondary hyperparathyroidism.

2.3 Challenges and previous attempts

. As mentioned in chapter I, several obvious limitations exist in the method involving co-immunoprecipitation and mass spectrometry, including, likely detection of partners with only high binding affinity and slow dissociation constants which can result in less prospect of detection of transient interactions. Likely detection of interaction of more abundant partner as compared to lower abundant ones and the CaSR is not being in native state as the lysis destroys plasma membrane and thereby, cannot provide accurate and adequate membrane environment with detergent. There is also possibility of interactors being washed out during the Co-IP process, and incorrect detection due to un-specific binding and general enrichment in the cell. The mass-spectrometry utilized in our study is incapable of separating the divergent forms of CaSR with various post-translational modifications, which can indirectly impact the interactors over its life-

cycle. The LC-MS has a typical dynamic range of detection at 4-6 orders of magnitude which is much lower as compared to the protein concentration range in biological samples at 12 orders of magnitude [99]. Also, using an online database for annotations have limitations since the known knowledge is not complete. The generation of complicated networks of inter-related and similar terms can be overwhelming and can produce convoluted results.

Previous attempts were made by Dr. Jie Feng and some in collaboration with me for the Co-IP and mass spectrometry (**Table 2.2)**. The number of unique peptides for CaSR detected were limited to 12 with Dr. Wu in Georgia Tech and 10 with Dr. Zhou from Clark Atlanta University. Anti-ADD CaSR antibody for endogenous CaSR in 5001 was used.

2.4 Major questions addressed in this chapter

a) How do we optimize co-immunoprecipitation to achieve the optimal enrichment of CaSR and its interactors?

b) What are CaSR interactors during its cellular biosynthesis and trafficking?

c) Will prolonged exposure to Ca^{2+}_o or deprivation of Ca^{2+}_o using EGTA affect the biosynthesis of other interactors and regulators of CaSR?

d) Can CaSR regulate its biosynthesis due to prolonged signaling?

e) Does CaSR act as a communicator between the intra- and extra- cellular Ca^{2+} signaling?

f) What is the implication of enrichment of some proteins with the treatment of Ca^{2+}_o?

g) What are the biological pathways most affected with Ca^{2+}_o?

2.5 Materials and Methods:

2.5.1 Plasmids and reagents

6-8 µg of empty pcDNA3.1 and human CaSR with FLAG-tag (between Asp^{371} and Thr^{372}) in pcDNA3.1 were used for transfection in 100 mm dish for negative and positive controls, respectively. The purified plasmids were prepared using the Mini-Prep Kit (Qiagen, Toronto, Canada).

2.5.2 Cell culture

Monolayer culture of HEK293 cells were purchased from American Type Culture Collection (ATCC CRL-1573) and cultured with high glucose (4.5 g/L) Dulbecco's Modified Eagle Medium (DMEM) (Invitrogen, Carlsbad, California) supplemented with 10 % fetal bovine serum (Atlanta Biologicals) in a humidified environment at 37 °C with 5 % CO_2. Transient transfection was performed using lipofectamine 3000 in the same medium following the manufacturer's protocol (Invitrogen, Carlsbad, California). 48 hours post-transfection, the cells were washed with Hank's Balanced Salt Solution (HBSS) (Sigma-Aldrich, Canada) at 37 °C, incubated in starving medium-low glucose DMEM, 0 mM Ca^{2+} with 0.1 % BSA for 30 minutes and finally treated with 4 mM Ca^{2+} or 2 mM EGTA for 2 hours. For ubiquitination assay, HEK293 cells with stably CHIP knocked down were provided by Li Zhou from Dr. Jun Yin's lab (GSU). These cells were cultured in DMEM with 10% FBS.

2.5.3 Antibodies

Anti-FLAG antibody, mouse (Sigma-Aldrich, Canada) was used to precipitate the CaSR/interactor complex. Anti-CaSR C0493, mouse (Abcam, Cambridge, MA, USA) and Anti-GAPDH mouse (Abcam, Cambridge, MA, USA) were used for western blot. Anti-GRP78 rabbit (Abcam, Cambridge, MA, USA), anti-CHIP mouse (Santa Cruz), anti-ubiquitin mouse (Santa

Cruz) anti-VAPA rabbit (Thermo fisher) and anti-14-3-3 eta rabbit (Abcam, Cambridge, MA, USA) antibodies were used in the western blot and immunostaining experiments. Goat anti-mouse Alexa Fluor 488, Alexa fluor 647, or Alexa fluor 550–conjugated secondary antibodies (Invitrogen) were used in immunostaining.

2.5.4 Total protein extracts

Transfected HEK293 cells from 90-100 % confluent 100 mm dishes were harvested after the treatment with 4 mM Ca^{2+} or 2 mM EGTA. They were washed with ice cold Phosphate-buffered saline (PBS) with 0 mM Ca^{2+} 3 times. 600 µL of 10 mM Sodium β-glycerophosphate, 50 mM Tris-Cl (pH 7.4), 150 mM NaCl, 1 mM EDTA (pH 8.0), 1% Triton X-100, 2 mM Na_3VO_4, 50 mM NaF, 10 mM sodium pyrophosphate supplied with proteinase inhibitor cocktail (Roche, Basel, Switzerland) was used to lyse cells for 30 min in ice with frequent vortex and subsequently centrifuged to pellet cell debris. Cleared cell lysates were subjected to anti-FLAG immunoprecipitation prior to immunoblotting

2.5.5 Coimmunoprecipitation

For each condition, a total of 1.0 mg of total protein was used as measured by Bradford assay. Anti-FLAG antibody (10ug) and 50 µL Protein G Dynabeads (Thermo Fisher) were incubated for 30 minutes at room temperature in 200ul PBS and 0.01% Tween20 and washed once with lysis buffer. Antigen was added and incubated for 10 hours at 4°C. Next day, the beads were washed two times with lysis buffer and two times with PBS. 10% beads were suspended in 30 ul of 2X sample buffer with 5% β-mercaptonol and heated for 10 min at 100 degrees. Rest of the 90 % bead was used for LC-MS/MS.

2.5.6 LC-MS/MS (Co-IP bead)

This work was supported by Georgia Institute of Technology's Parker H. Petit Institute for Bioengineering and Bioscience including the Systems Mass Spectrometry Core Facility. Peptides were analyzed with Nano-High Pressure Liquid Chromatography-Tandem Mass Spectrometry (nano-LC-MS/MS). Briefly, the peptides were loaded onto an in-house packed column (40 cm long X 75 µm ID X 360 OD, Dr. Maisch GmbH ReproSil-Pur 120 C18-AQ 3.0 µm beads) analytical column (Thermo Scientific) using a Dionex nanoLC system (Thermo Scientific). A flow rate of 0.300 µL/min with a linear acetonitrile gradient from 8 to 27% in 0.1% formic acid for 120 min was used. The column output was connected to a Q Exactive Plus mass spectrometer (Thermo Scientific) through a nanoelectrospray ion source. The mass spectrometer was controlled by Xcalibur software (Thermo, 4.0.27.19) and operated in the data-dependent mode in which the initial MS scan recorded the mass-to-charge ratios (m/z) of ions over the range of 350–1750 at a resolution of 70 000 with a target value of 1×10^6 ions and a maximum injection time of 100 ms. The 10 most abundant ions were automatically selected for subsequent higher-energy collision dissociation (HCD) with the energy set at 28 NCE. The MS/MS settings included a resolution of 35 000, a target value of 5×10^5 ions, a maximum integration time of 108 ms, and an isolation window was set at 3.0 m/z. Ions with undetermined charge, z = 1, 8, and z > 8 were excluded.

2.5.7 Cell preparation for mass spectrometry (MS)

The cell pellet was collected from HEK293 cells (transfected with CaSR pcDNA3.1 and empty pcDNA3.1) and PC3 cells after treating with 4mM Ca^{2+} and 2 mM EGTA. The following sample prep and analysis was carried out by Emory Integrated Proteomics Core [124, 125]. They were vortexed in urea lysis buffer (8 M urea, 100 mM NaH_2PO4, pH 8.5), including HALT protease

and phosphatase inhibitor cocktail (Pierce). Protein supernatants were transferred to 1.5-ml Eppendorf tubes, subjected to centrifugation at 14,000 rpm for 1 min and sonicated (Sonic Dismembrator, Fisher Scientific) 3 times for 5 s with 15-s intervals of rest at 30% amplitude to disrupt nucleic acids. Samples were subsequently vortexed. Protein concentrations were determined by the bicinchoninic acid (BCA) method, and samples frozen in aliquots at 80 °C. Protein homogenates (100 mg) were then treated with 1 mM dithiothreitol (DTT) at 25°C for 30 min, followed by 5 mM iodoacetimide (IAA) at 25°C for 30 min in the dark. Protein was digested with 1:100 (w/w) lysyl endopeptidase (Wako) at 25°C overnight. Samples were then diluted with 50 mM NH_4HCO_3 to a final concentration of less than 2 M urea and further digested overnight with 1:50 (w/w) trypsin (Promega) at 25°C. Resulting peptides were desalted with a Sep-Pak C18 column (Waters) and dried under vacuum.

2.5.8 LC-MS/MS (cell pellet)

This work was supported by Georgia Institute of Technology's Parker H. Petit Institute for Bioengineering and Bioscience including the Systems Mass Spectrometry Core Facility. Each sample was analyzed by nano LC-MS/MS with a Waters NanoAcquity HPLC system interfaced to a ThermoFisher Q Exactive. Peptides were loaded on a trapping column and eluted over a 75μm analytical column at 350nL/min; both columns were packed with Luna C18 resin (Phenomenex). The mass spectrometer was operated in the data-dependent mode in which the initial MS scan recorded the mass-to-charge ratios (m/z) of ions over the range of 300–1600 at a resolution of 70 000 with a target value of 3×10^6 ions and a maximum injection time of 120 ms. The 15 most abundant ions were automatically selected for subsequent higher-energy collision dissociation (HCD) with the energy set at 25 NCE. The MS/MS settings included a resolution of 17,500, a

target value of 1×10^5 ions, a maximum integration time of 120 ms, and an isolation window was set at 1.5 m/z. Ions with undetermined charge, z = 1, and z > 8 were excluded.

2.5.9 MaxQuant for Label-Free Proteome Quantification

Data files for the samples were analyzed using MaxQuant v1.5.2.8 with Thermo Foundation 2.0 for RAW file reading capability. The search engine Andromeda was used to build and search a concatenated target-decoy UniProt Knowledgebase (UniProtKB) containing both Swiss-Prot and TrEMBL human reference protein sequences (90,411 target sequences downloaded April 21, 2015), plus 245 contaminant proteins included as a parameter for Andromeda search within MaxQuant [126]. Methionine oxidation (+15.9949 Da), asparagine and glutamine deamidation (+0.9840 Da), and protein N-terminal acetylation (+42.0106 Da) were variable modifications (up to 5 allowed per peptide); cysteine was assigned a fixed carbamidomethyl modification (+57.0215 Da). Only fully tryptic peptides were considered with up to 2 mis-cleavages in the database search. A precursor mass tolerance of ± 20 ppm was applied prior to mass accuracy calibration and ± 4.5 ppm after internal MaxQuant calibration. Other search settings included a maximum peptide mass of 6,000 Da, a minimum peptide length of 6 residues, 0.05 Da tolerance for high resolution MS/MS scans. The false discovery rate (FDR) for peptide spectral matches, proteins, and site decoy fraction were all set to 1 percent. Quantification settings were as follows: re-quantify with a second peak finding attempt after protein identification has completed; match full MS1 peaks between runs; a 0.7 min retention time match window was used after an alignment function was found with a 20 min retention time search space. The label free quantitation (LFQ) algorithm in MaxQuant [126, 127]was used for protein quantitation. The quantitation method only considered razor and unique peptides for protein level quantitation. The total summed protein intensity was also used to assess overall signal drift across samples prior to LFQ normalization. Retention time internal

standards were identified by searching against a small database containing the isotopic peptide standard sequences, keratins, and brain specific spectrins with fixed modification of +8.014 Da (Lys) and +10.008 Da (Arg) using Proteome Discoverer 1.4. Briefly, precursor mass tolerance was ± 10 ppm, fragment ion tolerance was 0.05 Da, and FDR was enforced by Percolator [128] at 1%, enabling identification of MS/MS spectra for 14 of the 15 standard peptides. Thermo .MSF files were imported as peptide searches into Skyline 3.1 [129] with chromatograms within 2 min of a MS/MS match to one of the standard peptides. Identified peak boundaries were visually checked and adjusted as necessary, and precursor (M, M+1, and M+2) isotopic peak areas were exported. These areas were summed, and each peak area was divided by the average area of the corresponding peak across all runs to calculate aggregate signal responsiveness within the run.

2.5.10 Immunoblotting

A total input protein of 50 µg and 30 µl of the 10 % bead samples were loaded in 8.5 % acrylamide gels and subjected to sodium dodecyl sulfate-polyacrylamide gel electrophoresis (SDs-PAGE) to separate proteins, then transferred to nitrocellulose membranes. The membranes were blocked with 3 % nonfat milk (w/v) in TBS for 2 hours at room-temperature with constant shaking. The antibodies of interest were diluted in 3 % non-fat milk (w/v) and 0.2% Tween-20 in TBS (TBST). Anti-CaSR C0493, mouse (Abcam, Cambridge, MA, USA) was used at 1:700 dilution and HRP-conjugated mouse secondary antibody was used (Sigma-Aldrich, United States) at 1:3000 dilution to probe CaSR. For, GAPDH, anti-GAPDH mouse (Abcam, Cambridge, MA, USA) was used at 1:3000 dilution and HRP-conjugated mouse secondary antibody was used (Sigma-Aldrich, United States) at 1:10,000 dilution. For CHIP, anti-CHIP mouse (Santa Cruz) was used at 1:100 or 500 dilution and HRP-conjugated mouse secondary antibody was used at 1:2000 dilution. For GRP78, anti-GRP78 rabbit antibody (Abcam) was used at 1 µg/mL and HRP-

conjugated rabbit was used at 1:2000 dilution. Similarly, anti 14-3-3 eta rabbit antibody (Abcam) was used at 1:1000 dilutions and HRP-conjugated rabbit was used at 1:2000 dilution. For ubiquitin, anti-ubiquitin mouse antibody (Santa Cruz) was used at 1:100 or 500 dilutions were used and and HRP-conjugated mouse was used at 1:2000 dilution. Membranes were incubated with the primary and secondary antibodies for 1 hour at room-temperature with constant shaking, and finally washed with TBST. Secondary antibody was visualized using ECL detection reagents (GE healthcare, Little Chalfont, UK) developed on X-OMAT^{TM} imaging film (Kodak, Rochester, NY).

2.5.11 Immunostaining

HEK293 cells were grown on 20 × 20 mm coverslips placed in 6-well plates one day before the transfection. Cells were subjected to transfection and after 48 h were treated for immunostaining. Cells were washed with ice cold PBS and fixed with 3.7 % formaldehyde for 15 min at room temperature, followed by wash with PBS three times. Cells were permeabilized using 0.2 % Triton X in PBS for 10 min at room temperature. Mouse anti-FLAG monoclonal antibody was diluted 1000 times and incubated with cells overnight at 4°C or 1 h at room temperature to stain the CaSR. Similarly, 2.5 µg/mL anti-GRP78 (rabbit). 1:100 anti-CHIP (mouse), 2 µg/mL anti-VAPA (rabbit) and 1:200 anti-14-3-3 eta (rabbit) antibodies were used in the respective experiments. The cells were subsequently washed with PBS and stained with goat anti-mouse Alexa fluor 488, alexa fluor 647, or alexa fluor 550 –conjugated secondary antibodies at 5 µg/mL for 1 hour at room temperature. Nuclei were stained with 4′,6-diamidino-2-phenylindole. Fluorescence was visualized using a Zeiss LSM700 confocal microscope.

2.5.12 Quantitation of immunostaining

The images were processed using Image J and zen lite. The stain of interest were in RGB or given pseudo RGB in zen lite. Henceforth, the stains were split in image J, given RGB for two

stains of interest and analyzed using surface plot. The 2D peaks in the plot represent the position and intensity of the stain and is compared. Further, plugin coloc2 is used to obtain Pearson's coefficient after deducting the background.

2.5.13 Ca^{2+} and CaM binding site prediction

For Ca^{2+} binding site prediction, CaPS (Calcium Pattern Search) was used. This algorithm developed by Dr. Shenghui Xue identified Ca^{2+} binding motifs in proteins based on unique patterns that are known in various proteins. Calmodulin target database (http://calcium.uhnres.utoronto.ca/ctdb/ctdb/home.html) was used to predict the CaM binding sites. This website provides various motif classes using sequence homology analyses available in the database.

2.5.14 Protein identification, label-free quantitation and statistical analysis

LC-MS/MS Q-Extractive Orbitrap was used. Raw data files were analyzed using MaxQuant version 1.6.3.3 with Thermo Foundation 2.0 for RAW file reading capability. Intensity of each protein for each treatment condition was averaged from three negative control IP samples and three CaSR IP samples. The missing values were imputed as previously described using Perseus [130]. Enrichment of proteins was considered significant if the intensities had at least two-fold difference, i.e., $\log_2$(HEK293 + CaSR-FLAG pcDNA / Hek293 + pcDNA3.1) $\geq$ 1.00. *P*-values were calculated using a two-sided Student's t test of a null hypothesis that there is no difference in protein relative abundance between the two groups. For robust stringency, we employed a $P < 0.05$, a requirement of minimum PSM of 2 for no less than two replicates and identification with at least one unique peptide.

2.5.15 Functional annotation of identified protein partners

Protein-protein interaction was performed using Search Tool for the Retrieval of Interacting Genes/Proteins (STRING) version 10.0. Interaction network view was used to identify and visualize the degrees of interaction amongst the 106 putative CaSR interactors (*homo sapiens*). STRING uses evidence from experimental and knowledge-based databases to provide the confidence in functional associations or interaction through the Edge Confidence. Size of colored nodes represent evidence of known or predicted 3-dimensitional protein structure.

The Database for Annotation, Visualization, and Integrated Discovery (DAVID), version 6.8, was used for the functional annotation and analysis of enrichment of 106 proteins determined as putative CaSR interactors. The set of total proteins identified and quantified (n = 625) was used as the background. The numbers of 106 proteins of interest and background lists are compared in each functional cluster. A two-tailed modified fisher's exact test (EASE score of 1) with classification stringency at "medium" were employed to generate statistically significant enrichment annotations and to categorize them under annotation terms: cellular compartments, biological processes, molecular function and KEGG pathways. Correction for multiple hypothesis testing was carried out using standard false discovery rate control methods. A Bonferroni-corrected $P \geq 0.05$ and an enrichment ≥ 1.3 were used as a cut-off [131].

2.5.16 Rich club analysis for understanding presence of significant rich hubs in network

This was carried out in collaboration with Shrikant Pawar from the Department of Biology. Proteins and its interactions with confidence values from String 9.1 were inputted in Cytoscape to construct an interactome. A degree centrality measure was applied and 6 sub-interactomes (Figure 1: A, B, C, D, E and F) were constructed with degree measures varying between 1-5, 6-10, 11-15, 16-20, 21-25 and >25. Power-law distribution analysis was performed on each of the sub-

interactomes to generate pearsons correlation coefficient values (Figure 1: Ai, Bi, Ci, Di, Ei and Fi) between number of nodes and betweeness centrality measure. Further, a rich-club coefficient values were generated for each of these sub-interactomes. The rich-club coefficient is the ratio, for every degree k, of the number of actual to the number of potential edges for nodes with degree greater than k.

$$\phi(k) = \frac{2E_{>k}}{N_{>k}(N_{>k} - 1)}$$ *Equation 2. 1*

Where, E is the number of edges between the nodes of degree greater than or equal to k, and N is the number of nodes with degree greater than or equal to k. The rich-club coefficient was calculated by Python library, NetworkX.

2.6 Results

2.6.1 Identification of potential CaSR interactors

CaSR interactome was studied using HEK293 cells transfected with a FLAG-tagged CaSR pcDNA3.1 (positive control) or an empty pcDNA3.1 (negative control). Cells were treated with 4 mM Ca^{2+} (based on previously reported half maximal CaSR-activating Ca^{2+}_o concentration) or 2 mM EGTA (to chelate Ca^{2+}_o), followed by immunoprecipitation with anti-FLAG antibody, LC-MS/MS, and gene ontology analysis (**Figure 2.2**). All experiments were run in triplicate. When cells were transfected with CaSR, an equivalent amount of total CaSR (input) (**Figure 2.3A**. upper panel, duplicate shown, third in **Figure 2.3B)** and immunoprecipitated CaSR (output) **(Figure 2.3**, lower panel, duplicate shown) were detected for both treatment conditions, Ca^{2+} and EGTA. CaSR was observed at > 250 kDa molecular weight as opposed to its monomer at 120-160 kDa (depending on its level of glycosylation maturation); this could have resulted due to formation of a complex or oligomerization. Similarly, the MS intensity (averaged over three replicates) detected

for CaSR output was 9.43 ± 0.833 X 10^9 in the presence of Ca^{2+} as compared to 7.67 ± 0.751 X 10^9 in EGTA. Although CaSR was not identified in the negative control, comparable GAPDH blots for total input was observed (**Figure 2.3**, middle panel, duplicate shown). Immunostaining show proper transfection of HEK293 cells and presence of CaSR throughout the cells after the treatment with 4 mM Ca^{2+} (**Figure 2.3**). Immunostaining result for EGTA treatment was not possible due to cells not attaching to the coverslip.

A total of 625 proteins detected by LC-MS/MS were sorted and 106 were identified as reliable CaSR interactors. For this, we employed successive stringencies to ensure robust upregulation, reproducibility, and detection**:** (i) the treatments and IP for the positive and negative controls were performed in triplicates, (ii) identified proteins were at least two-fold enriched in the CaSR transfected samples over the negative controls, (iii) a two tailed t-test with $P \leq 0.05$ between the groups being compared was considered statistically significant, (iv) proteins had a minimum peptide spectrum matches (PSMs) of two for at least two replicates, and (v) proteins were identified with at least one unique peptide.

In **Figure 2.4A and B**, the volcano plots depict significantly enriched ($\log_2$ intensity (CaSR/pcDNA3.1) ≥ 1, -log10(P) ≥ 1.3) potential CaSR interactors in the presence of Ca^{2+} (**Figure 2.4A**, red dots) and EGTA (**Figure 2.4B**, green dots). 88% of these proteins were highly enriched by ≥ three-fold. CaSR had the highest $\log_2$ intensity (fold change) in both samples treated with either 4 mM Ca^{2+} [$\log_2$ intensity (CaSR/pcDNA3.1) = 11.61 ± 1.07, -$\log_{10}$(P) = 3.05] or 2 mM EGTA [$\log_2$ intensity (CaSR/pcDNA3.1) = 14.32 ± 0.76, -$\log_{10}$(P) = 3.85]. Out of 106 CaSR interacting partners, 46 were exclusively identified in the presence of Ca^{2+}, 13 exclusively in the presence of EGTA, and 48 were found common in both conditions (**Figure 2.4C**).

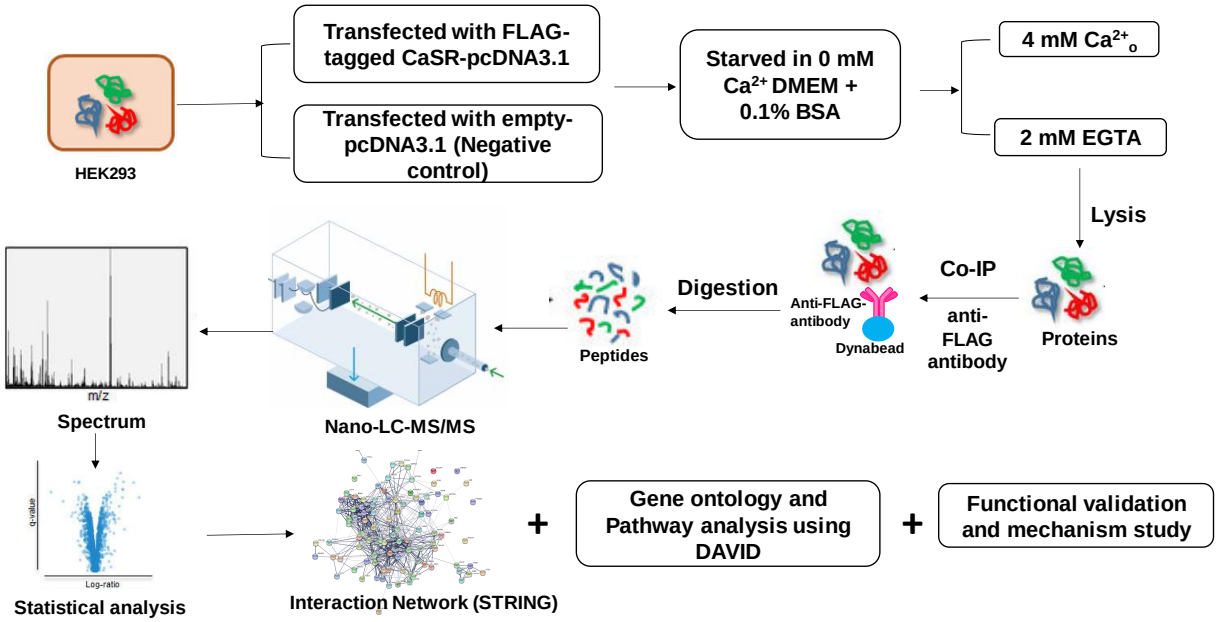

Figure 2.2 The overview of the experimental workflow.

CaSR interacting proteins characterized using co-immunoprecipitation and MS detection. HEK293 cells transfected with FLAG-tagged CaSR pcDNA3.1 (positive control) or empty pcDNA3.1 (negative control) were subjected with 4mM $Ca^{2+}{}_o$ and 2mM EGTA. The proteins identified using LC-MS/MS that were highly enriched in positive control by ≥ 2 folds were assessed as putative CaSR interacting proteins. For functional enrichment study, the complete list of CaSR interacting proteins were analyzed using the DAVID database. Further, the interaction between each protein was obtained using STRING PPI database search.

2.6.2 Analysis of differentially expressed proteins due to presence of 4 mM Ca^{2+}

The 106 proteins identified as putative CaSR interactors with high confidence were further evaluated for their differential expression levels between Ca^{2+} and EGTA treatments **(Figure 2.5A)**. Remarkably, in the presence of Ca^{2+}, 65 % of these proteins were significantly up-regulated at varying degrees from ≥ eight-fold [$\log_2$ intensity (Ca^{2+}/EGTA) = ≥ 3] to 1.5 folds [$\log_2$ intensity (Ca^{2+}/EGTA) = 0.58] (**Figure 2.5C, Table 2.9**). 12 proteins were up-regulated by ≥ 8-fold [$\log_2$ intensity (fold change) = ≥ 4] (red open circles), 9 between 4-8-fold [$\log_2$ intensity (fold change) = < 4 ≥ 2] (magenta open circles), 21 between 2-4-fold [$\log_2$ intensity (fold change) < 2 ≥ 1.5] (orange open circles) and 26 between 1.5-2 fold [$\log_2$ intensity (fold change) < 1.5 ≥ 0.58] (green

open circles). Only 5 that were up-regulated in the presence of EGTA by ≥ 1.5 folds [log_2 intensity (fold change) = ≤ - 0.58] (left quadrant, blue open circles). 31% were detected with less than 1.5-fold change in abundance in the two conditions [log_2 intensity (Ca^{2+}/EGTA) = < 0.58 and > -0.58] (grey closed circles). The size of the circles represents the degree of up-regulation. This group of proteins comprised of important transducer of Ca^{2+} signaling in the cytosol, regulators of Ca^{2+} in the ER and mitochondria, and chaperones and ubiquitin proteins implicated in trafficking and protein recycling (Table 1). Conversely, there were only 5 that were up-regulated in the presence of EGTA by ≥ 1.5-fold [log_2 intensity (Ca^{2+}/EGTA) = ≤ - 0.58]. These proteins included 14-3-3 -θ (YWHAQ), -ζ (YWHAZ), -ε (YWHAE), Tubulin α-1C (TUBA1C) and THO complex subunit 4 (ALYREF) (**Figure 2.5A, Table 2.9**). Interestingly, 31 % proteins were detected with less than 1.5-fold change in abundance [log_2 intensity (Ca^{2+}/EGTA) = < 0.58 and > -0.58]; irrespective of the presence of $Ca^{2+}{}_o$ or EGTA, comprising primarily of ribosomal proteins (e.g., RPS20, RPL22, RPL23 and RPS3), tubulins (e.g., TUB-A1B, A4A, B, B4A and B8) and heat shock proteins (e.g., HSP-A1A, A6, A7, A8 and 90AB1) The function of these proteins must have less correlation with $Ca^{2+}{}_o$.

In order to test whether the interactions we observed were true and not due to overall increase in the abundance of the proteins in cell due to treatments, LC-MS/MS was carried out on the total lysate of cells after respective treatments with $Ca^{2+}{}_o$ and EGTA. The 106 proteins of interest did not show significant change in the abundance (**Figure 2.5B**). Similarly, bioinformatic tool, Calcium Pattern Search (CaPS) was utilized to search any existing Ca^{2+} binding sites on the 106 putative interactors in order to verify if the CaSR interactions were dependent on Ca^{2+} binding. Only 10 proteins consisting of heat shock proteins, Dnaj and DNA dependent protein kinase contained some form of Ca^{2+} binding sites (**Table 2.3)** using calcium pattern search.

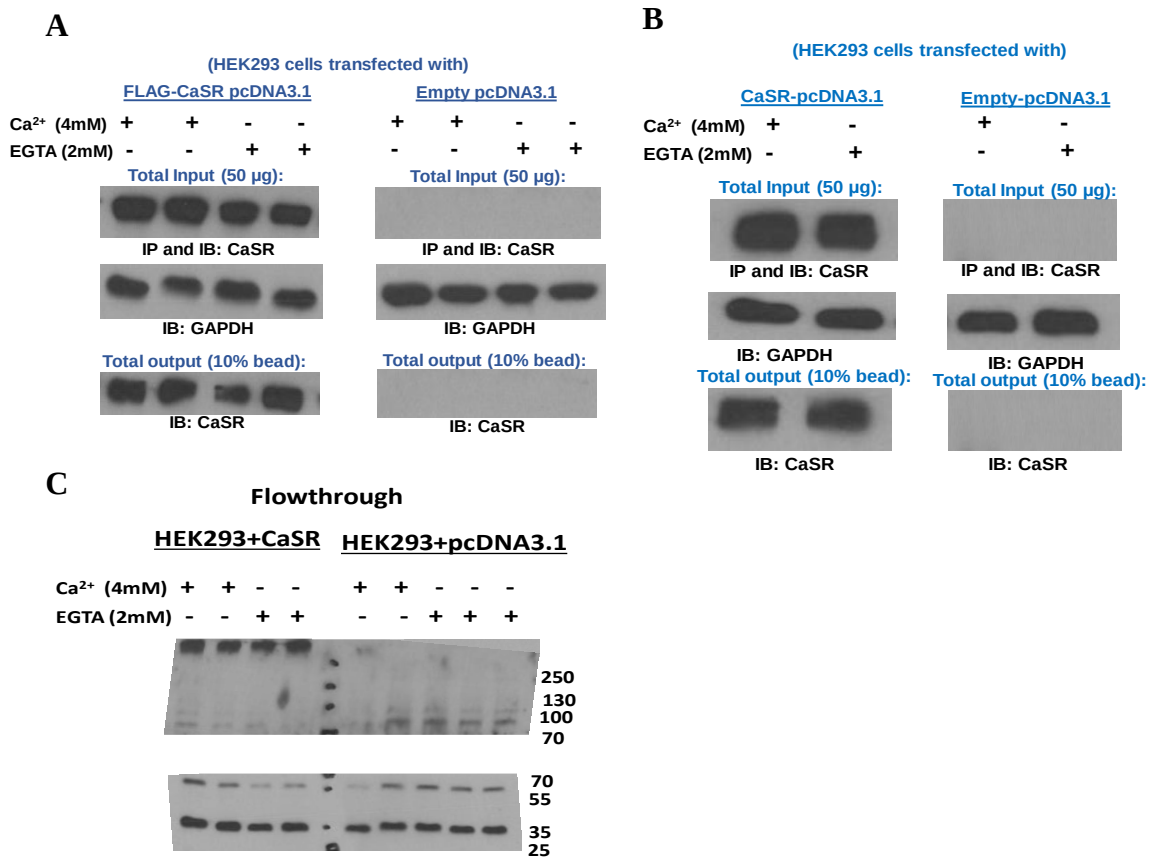

Figure 2.3. Co-immunoprecipitation experiments verified by western blot

A.Co-immunoprecipitation experiments using anti-FLAG antibody on total cell extracts from HEK293 followed by western blot analysis with anti-CaSR antibody and anti-GAPDH (as control) was carried out in triplicates (duplicate representative blot is shown.). Western blot result indicates an equivalent amount of CaSR input (B, upper panel) in positive control for both Ca^{2+} and EGTA treatments and equivalent total protein input (middle panel, GAPDH, 50 µg total) in all conditions. Output CaSR is presented in positive control (C, lower panel) in both Ca^{2+} and EGTA treatments. Majority CaSR was observed at >250KDa molecular weight which could have resulted due to it formation of a complex or due to oligomerization. B. *Third replicate for Co-IP experiments using anti-FLAG antibody on total cell extracts (50 µg) from HEK293 followed by western blot analysis with anti-CaSR antibody and anti-GAPDH (as control) was carried out in triplicates (only single replicate shown). Flowthrough for CO-IP experiment. It shows that there was a loss of some CaSR during the process of IP. However, since we used same amount of antibody and bead, the result from MS*

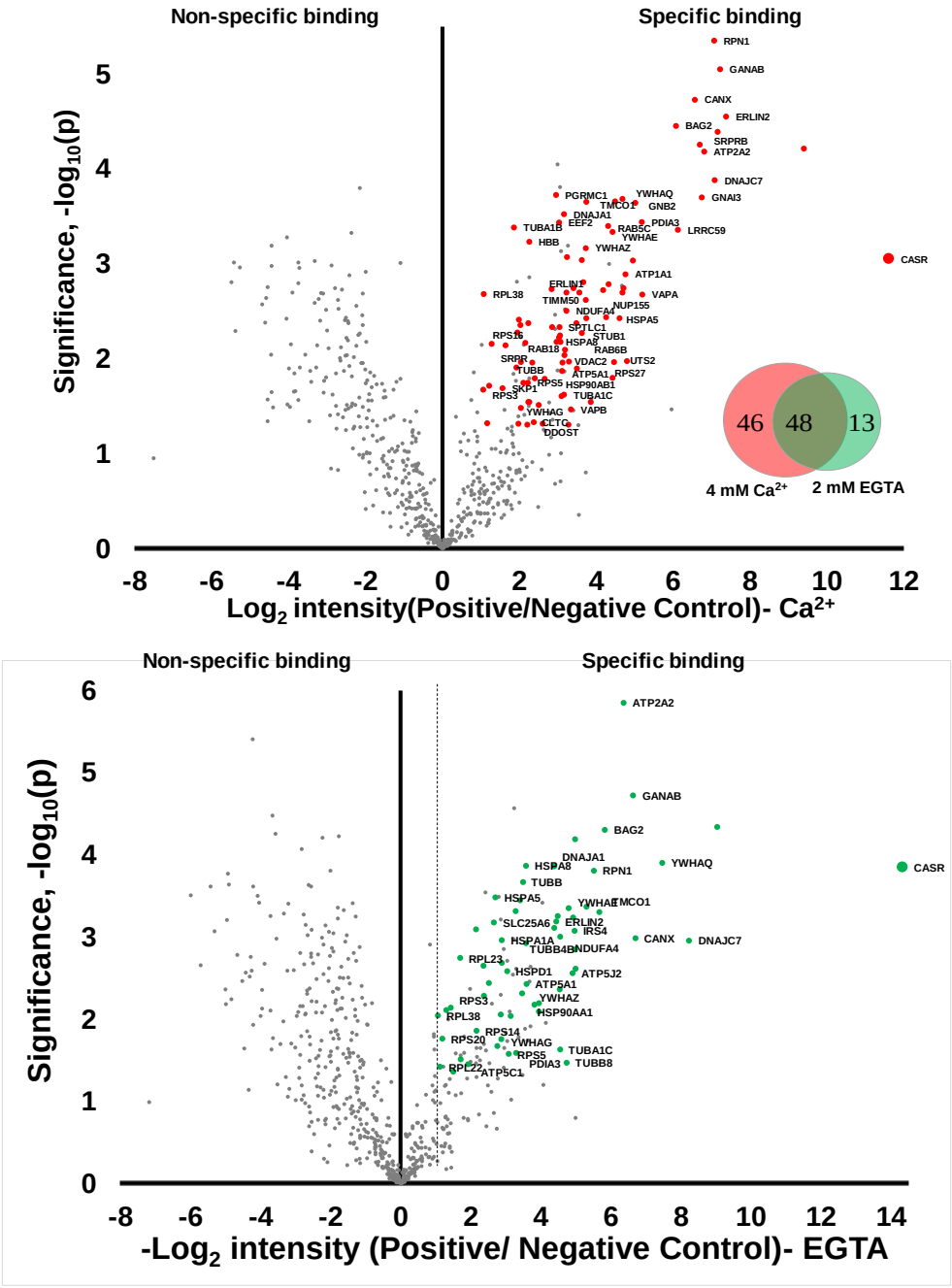

Figure 2.4 106 CaSR interactors are enriched by ≥ 2 folds

Insert: Venn diagram represents the number of proteins detected in each of the conditions. Volcano plot of CaSR interactors (n=3) enriched in 4 mM Ca^{2+} (A, red dots) and 2 mM EGTA perturbation (B, green dots) in pairwise experiments versus negative control (n=3). Total of 625 proteins are plotted ***(A and B).*** *106 specific interactors of CaSR were determined to be significantly enriched with $p \leq 0.05$ and at least 2 folds over the average of the negative control. 94 were determined in the presence of 4 mM Ca^{2+} (A, red dots), 61 in the presence of 2 mM EGTA (B, green dots) and out of which 48 were common in both the conditions. 88 % out of the 106 proteins were highly upregulated by ≥ 3 folds. CaSR was most enriched.*

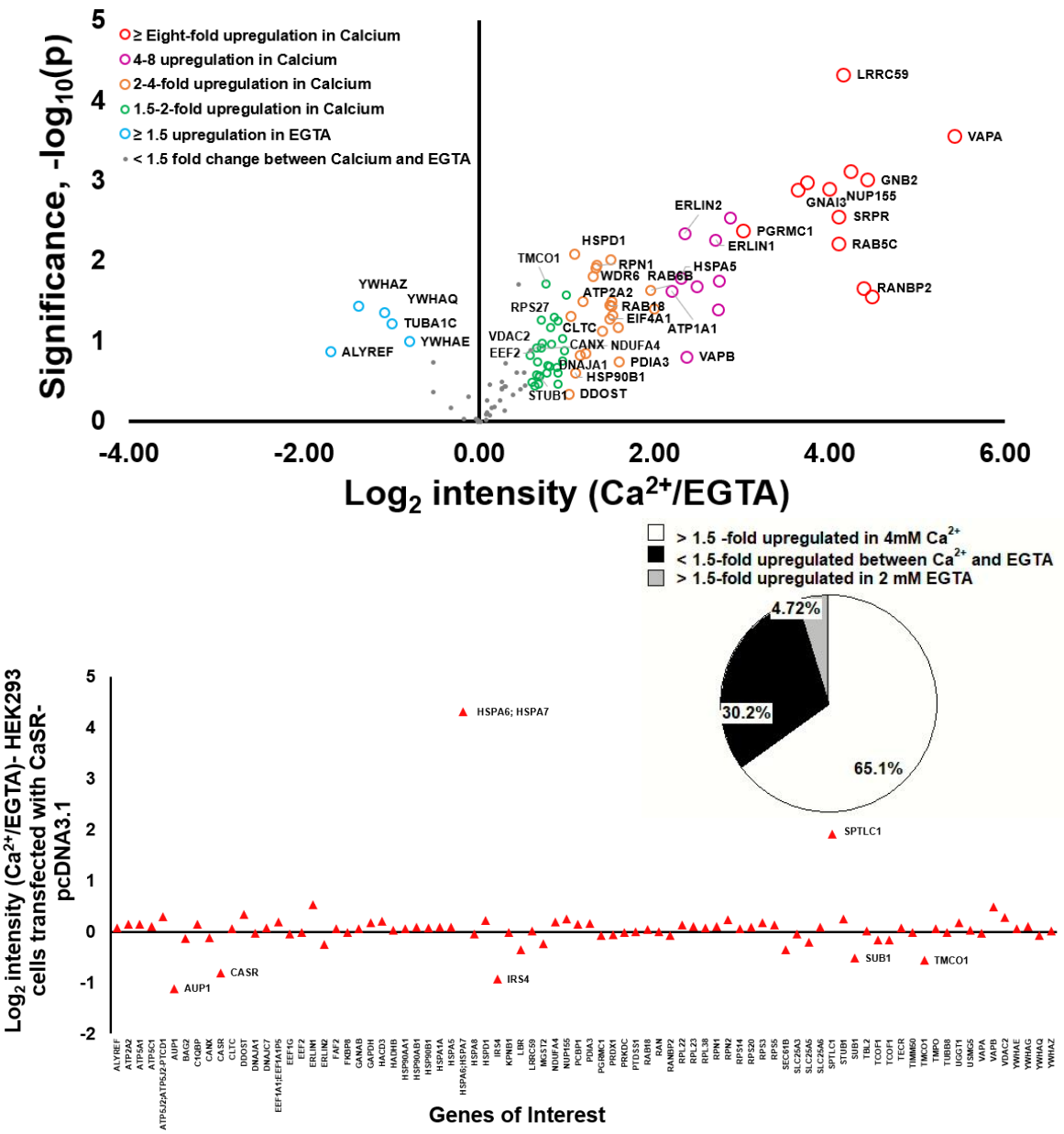

Figure 2.5 A. Volcano plot of CaSR interactors (n=3) differentially enriched at various degrees in the presence of 4 mM $[Ca^{2+}]_o$ or 2 mM EGTA.

A total of 106 potential interactors of CaSR are plotted in volcano plot where the x-axis is log_2 intensity (Ca^{2+}/EGTA) and y-axis is -log_{10}(p-value). A significant differential expression was observed between the treatment conditions. 65 % were significantly up-regulated by ≥ 1.5 folds in the presence of extracellular Ca^{2+}. Out of these, 12 proteins were up-regulated by ≥ 8 folds [log_2 intensity (fold change) = ≥ 4] (red open circles), 9 between 4-8 folds [log_2 intensity (fold change) = < 4 ≥ 2] (magenta open circles), 21 between 2-4 folds [log_2 intensity (fold change) < 2 ≥ 1.5] (orange open circles) and 26 between 1.5-2

folds [log_2 intensity (fold change) < 1.5 ≥ 0.58] (green open circles). Only 5 that were up-regulated in the presence of EGTA by ≥ 1.5 folds [log_2 intensity (fold change) = ≤ - 0.58] (left quadrant, blue open circles). 31% were detected with less than 1.5 folds change in abundance in the two conditions [log_2 intensity (Ca^{2+}/EGTA) = < 0.58 and > -0.58] (grey closed circles). The size of the circles represents the degree of up-regulation. B. Log_2 intensity(Ca^{2+}/EGTA) for total cell lysate after the treatments. Minimal change observed between the treatment groups. C Venn diagram of the distribution of proteins differentially up-regulated in Ca^{2+}.

2.6.3 Gene ontology study of potential CaSR binding partners

Gene ontology enrichment analysis was carried out using the Database for Annotation, Visualization, and Integrated Discovery (DAVID) 6.8 version. A two-tailed modified Fisher Exact test (EASE score threshold of 1) with classification stringency at "medium" were employed to generate statistically significant enrichment annotations. Correction for multiple hypothesis testing was carried out using standard false discovery rate control methods. A Bonferroni-corrected $P \leq 0.05$ and an enrichment ≥ 1.3 were used as a cut-off [131]. The functional annotation cluster was generated separately for the 65% and 31% potential CaSR interactors out of the 106 derived from log_2 intensity (Ca^{2+}/EGTA) ≥ 0.58 and log_2 intensity (Ca^{2+}/EGTA) < 0.58 and > 0.58, respectively and compared. A Bonferroni-corrected $P \leq 0.05$ and an enrichment ≥ 1.3 were used as a cut-off. The numbers on top of each bars represent the number of genes involved. A. represents the enrichment annotation for cellular compartment, B. represents biological processes, C. represent molecular function and D. represents pathway. Presence of $Ca^{2+}{}_o$ revealed a contrasting effect on the enrichment classifications, namely, cellular compartment, molecular function and biological process. The up-regulated gene clusters were most significantly enriched in the ER membrane and cell-cell adherens junction in the presence of $Ca^{2+}{}_o$ (**Figure 2.7A, Table 2.5)**. Concomitantly, the biological processes such as the protein folding in the ER, ER unfolded protein response and cell-cell adhesion were enriched in the presence of $Ca^{2+}{}_o$ (**Figure 2.7B, Table 2.4).** Molecular function analysis for these proteins revealed significant enrichment in GTP binding, GTPase activity and

cadherin binding in the presence of Ca^{2+}_o (**Figure 2.7C, Table 2.6**Error! Reference source not found.**)**. The most significant KEGG pathway was protein processing in the ER **(Figure 2.7D**). This may suggest that Ca^{2+}_o augments the CaSR trafficking and its interactions with regulators involved in Ca^{2+} handling and trafficking in the ER.

Table 2.3 10 proteins out of 106 that contained Ca^{2+} binding site using Ca^{2+} Pattern Search (CaPS)

Accession	Protein	Type	Ca^{2+} binding sequence
Q14739.2	Integral nuclear envelope inner membrane protein	Pseudo	VYDFFIGRELNPRIGTFDLK
Q15311.3	Ral-interacting protein; AltName: Full=Dinitrophenyl S-glutathione ATPase	Pseudo	NYLLISWLIVHMDHVIAKELE
Q9Y5M8.3	Signal recognition particle receptor subunit beta	loop	NNNRGNSLTLID
P78527.3	DNA-dependent protein kinase catalytic subunit	loop	DGDPSDRMEVQE
P08107.5	Heat shock 70 kDa protein 1A/1B	EF_hand_like	DIDANGILNVTATD
P11142.1	Heat shock cognate 71 kDa protein	EF_hand_like	DIDANGILNVSAVD
Q9Y4P3.1	Transducin beta-like protein 2	EF_hand_like	DFSSNGKYLATCAD
P10809.2	60 kDa heat shock protein, mitochondrial	loop	NTSKGQKCEFQD
Q99615.2	DnaJ homolog subfamily C member 7	EF_hand_like	DLDEEGMNMGDFD
P17066.2	Heat shock 70 kDa protein 6	EF_hand_like	DIDANGILSVTATD

The 31% proteins that were < 1.5 fold upregulated between the Ca^{2+}_o and EGTA treatment conditions had marked significant enrichment in extracellular matrix, ribosome, ribosomal subunit and focal adhesion (**Figure 2.7C, Table 2.5)**. In parallel, biological process attributed to ribosome such as translation, rRNA processing and SRP-dependent cotranslational protein targeting to membrane were enriched for this group (**Figure 2.7B, Table 2.6)**. On the other hand, molecular functions: ATPase activity, structural constituent of ribosome and heat shock protein binding were

enriched (**Figure 2.7C, Table 2.5)**. The most significant KEGG pathway was ribosome-related (**Figure 2.7B, Table 2.4)**. Therefore, we can deduce that these processes are ubiquitous and possibly not affected by the Ca^{2+}_{o}.

Table 2.4 Genes involved in the biological process enrichment analysis between 94 and 61 proteins enriched in Ca^{2+} and EGTA treatment condition, respectively.

Biological Process	Gene In Liganded condition	Gene In Un-Liganded condition
cell-cell adhesion	HSP90AB1, YWHAZ, VAPA, RAN, VAPB, EEF2, HSPA1A, YWHAE, PCBP1, LRRC59, EEF1G, HSPA5, TMPO, PTPN1, HSPA8	HSP90AB1, YWHAZ, PCBP1, HSPA1A, HSPA5, TMPO, YWHAE, PRDX1, HSPA8
translation	RPS27, RPS16, RPL23, SLC25A5, SLC25A6, SLC25A3, RPS27L, SLC25A1, RPL38, RPS5, RPS3	SLC25A5, SLC25A6, RPS27L, RPL38, RPS5, RPS3, RPS27, RPL23, RPS17, RPL22, RPS14, SLC25A3, SLC25A1, RPS20
SRP-dependent cotranslational protein targeting to membrane	RPS27, RPS16, RPL23, SRPRB, RPL38, RPS5, RPS3	RPS27, RPL23, RPS17, RPL22, RPS14, RPL38, RPS20, RPS5, RPS3
response to unfolded protein	HSP90AB1, HSP90AA1, HSPA6, DNAJA1, FAF2, HSPD1, HSPA8	HSP90AB1, HSP90AA1, HSPA6, DNAJA1, HSPD1, HSPA8
microtubule-based process	TUBB, TUBB8, TUBA1B, TUBA1C, TUBB4B	TUBB, TUBB8, TUBA1B, TUBA1C, TUBB4B
protein refolding	HSP90AA1, HSPA6, HSPA1A, HSPD1, HSPA8	HSP90AA1, HSPA6, HSPA1A, HSPD1, HSPA8
protein folding in endoplasmic reticulum	HSP90B1, PDIA3, VAPA, HSPA5, CANX	
rRNA processing		RPS27, RPL23, RPS17, RPL22, RPS14, RPS27L, RPL38, RPS20, RPS5, RPS3
protein folding		HSP90AB1, HSP90AA1, GANAB, PDIA3, BAG2, DNAJC7, DNAJA1, CANX, HSPA8
ribosomal small subunit assembly		RPS27, RPS17, RPS14, RPS27L, RPS5

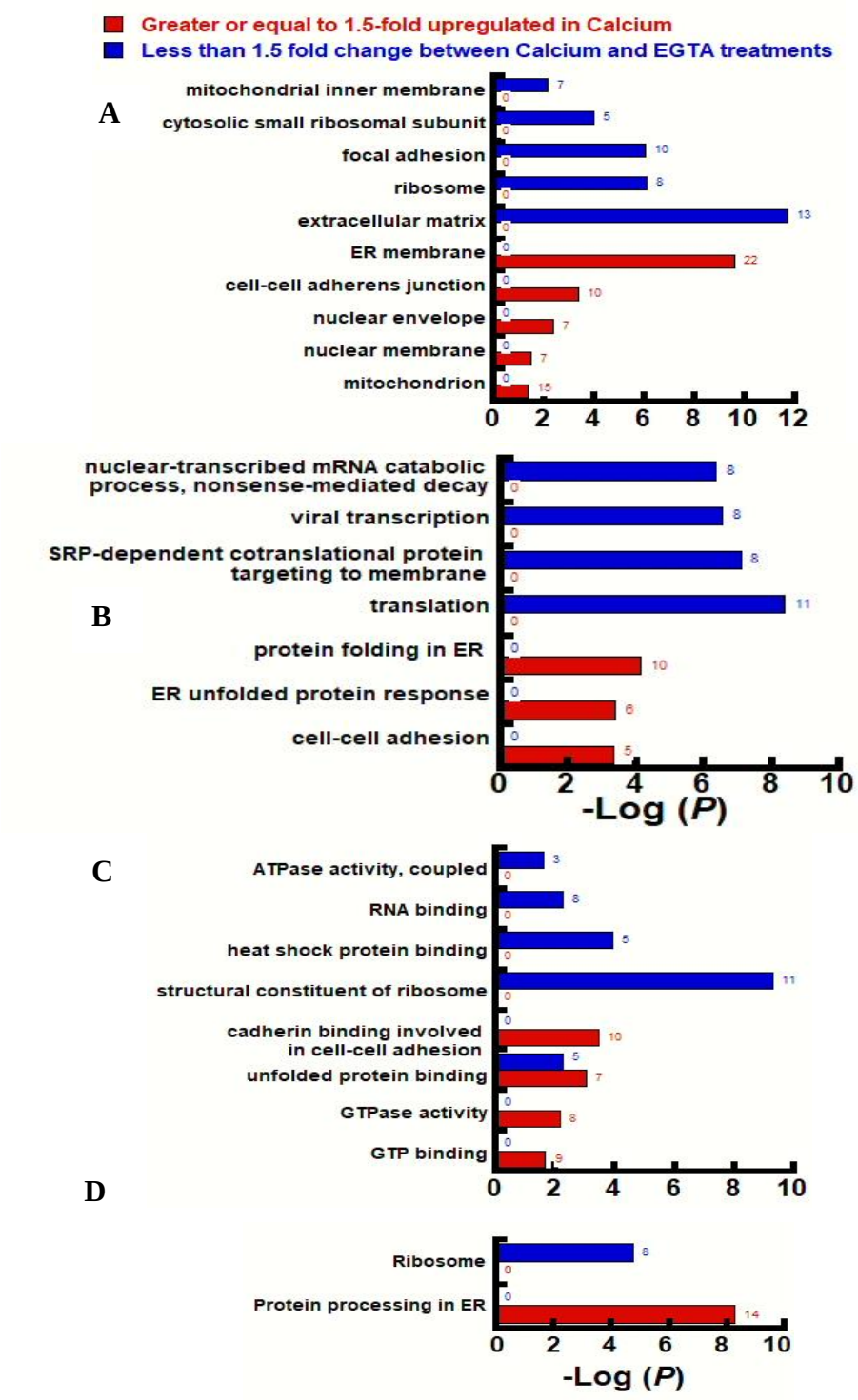

Figure 2.6 Overrepresented gene-ontologies among the 65% CaSR interactors upregulated by ≥ 1.5 folds in presence of 4 mM Ca^{2+}

Overrepresented gene-ontologies among the 65% CaSR interactors upregulated by ≥ 1.5 folds in presence of 4 mM Ca^{2+}, (Red bars) as compared to EGTA and 31% CaSR interactors upregulated by < 1.5 folds between Ca^{2+} and EGTA treatment (Blue bars) were examined with DAVID to obtain annotation enrichments. A Bonferroni-corrected $P \leq 0.05$ and an enrichment ≥ 1.3 were used as a cut-off. The numbers on top of each bars represent the number of genes involved. Representation of the enrichment annotation for cellular compartment (A), biological processes (B), molecular function (C) and pathway (D) are shown.

Table 2.5 Genes involved in the cellular compartment enrichment analysis between 94 and 61 proteins enriched in Ca^{2+} and EGTA treatment condition, respectively

Cellular Compartments	Gene In Liganded condition	Gene In Un-Liganded condition
endoplasmic reticulum membrane	**FKBP8, SPTLC1, VAPA, VAPB, ERLIN2, ERLIN1, SRPRB, CANX, TECR, HSP90B1, SEC61B, RAB18, ATP2A2, PGRMC1, LRRC59, RPN1, RPN2, HSPA5, TMPO, PTDSS1, DDOST, MGST2**	
cell-cell adherens junction	HSP90AB1, YWHAZ, **VAPA**, **RAN, VAPB, EEF2**, HSPA1A, YWHAE, PCBP1, **LRRC59, EEF1G,** HSPA5, TMPO, **PTPN1,** HSPA8	HSP90AB1, YWHAZ, PCBP1, HSPA1A, HSPA5, TMPO, YWHAE, PRDX1, HSPA8
mitochondrial inner membrane	NDUFA4, SLC25A5, SLC25A6, SLC25A3, SLC25A1, **TIMM50**, ATP5A1, HSPD1, **VDAC2**, RPS3, **HADHB**	NDUFA4, ATP5J2, SLC25A5, SLC25A6, SLC25A3, ATP5C1, SLC25A1, ATP5A1, HSPD1, RPS3
ribosome	RPS27, RPS16, RPL23, RPS27L, RPL38, CANX, RPS3	RPS27, RPL23, **RPS17, RPL22, RPS14,** RPS27L, RPL38, **RPS20**, **CANX**, RPS3
cytosolic small ribosomal subunit	RPS27, RPS16, RPS27L, RPS5, RPS3	RPS27, RPS17, RPS14, RPS27L, RPS20, RPS5, RPS3
intracellular ribonucleoprotein complex		RPL22, PCBP1, RPS5, GAPDH, HSPA8, RPS3
melanosome		HSP90AB1, YWHAZ, HSP90AA1, GANAB, PDIA3, RPN1, HSPA5, YWHAE, PRDX1, CANX, HSPA8

Table 2.6 Genes involved in the molecular function enrichment analysis between 94 and 61 proteins enriched in Ca^{2+} and EGTA treatment condition, respectively

Molecular Function	Gene In Liganded condition	Gene In Un-Liganded condition
GTP binding	HSP90AB1, EEF1A1, GNAI3, HSP90AA1, RAB5C, RAN, EEF2, SRPRB, TUBB, RAB18, RAB6B, TUBB8, TUBA1B, TUBA1C, TUBB4B	
GTPase activity	EEF1A1, TUBB, GNAI3, RAB18, GNB2, RAB5C, RAN, EEF2, RAB6B, TUBB8, TUBA1B, TUBA1C, TUBB4B	
G-protein coupled receptor binding	GNAI3, DNAJA1, HSPA1A, STUB1, HSPA8	
C3HC4-type RING finger domain binding		DNAJA1, HSPA1A, HSPA8
MHC class II protein complex binding	HSP90AB1, HSP90AA1, YWHAE, HSPA8	HSP90AB1, HSP90AA1, YWHAE, HSPA8
heat shock protein binding	HSP90AB1, DNAJC7, HSPA6, HSPA1A, HSPA8	HSP90AB1, DNAJC7, HSPA6, HSPA1A, HSPA8
protein domain specific binding	TUBB, YWHAZ, YWHAG, GNAI3, VAPA, YWHAQ, ATP1A1, HSPA5, YWHAE	TUBB, YWHAZ, YWHAG, YWHAQ, HSPA5, KPNB1, YWHAE
ATPase activity		ATP5J2, HSP90AA1, ATP5C1, HSPA1A, ATP5A1, HSPD1, HSPA5, HSPA8
cadherin binding involved in cell-cell adhesion	HSP90AB1, YWHAZ, VAPA, RAN, VAPB, EEF2, HSPA1A, YWHAE, PCBP1, LRRC59, EEF1G, HSPA5, TMPO, PTPN1, HSPA8	HSP90AB1, YWHAZ, PCBP1, HSPA1A, HSPA5, TMPO, YWHAE, PRDX1, HSPA8
unfolded protein binding	HSP90AB1, HSP90B1, HSP90AA1, HSPA6, DNAJA1, HSPA1A, HSPD1, HSPA5, UGGT1, CANX, HSPA8, TUBB4B	HSP90AB1, HSP90AA1, HSPA6, DNAJA1, HSPA1A, HSPD1, HSPA5, CANX, HSPA8, TUBB4B
enzyme binding	HACD3, ATP2A2, VAPB, HSPA6, HSPA1A, PTPN1, HSPA5, YWHAE, STUB1, HSPA8, RPS3	HACD3, ATP2A2, HSPA6, PRKDC, HSPA1A, HSPA5, KPNB1, YWHAE, HSPA8, RPS3
structural constituent of ribosome	RPS27, RPS16, RPL23, SLC25A5, SLC25A6, SLC25A3, RPS27L, SLC25A1, RPL38, RPS5, RPS3	SLC25A5, SLC25A6, RPS27L, RPL38, RPS5, RPS3, RPS27, RPL23, RPS17, RPL22, RPS14, SLC25A3, SLC25A1, RPS20

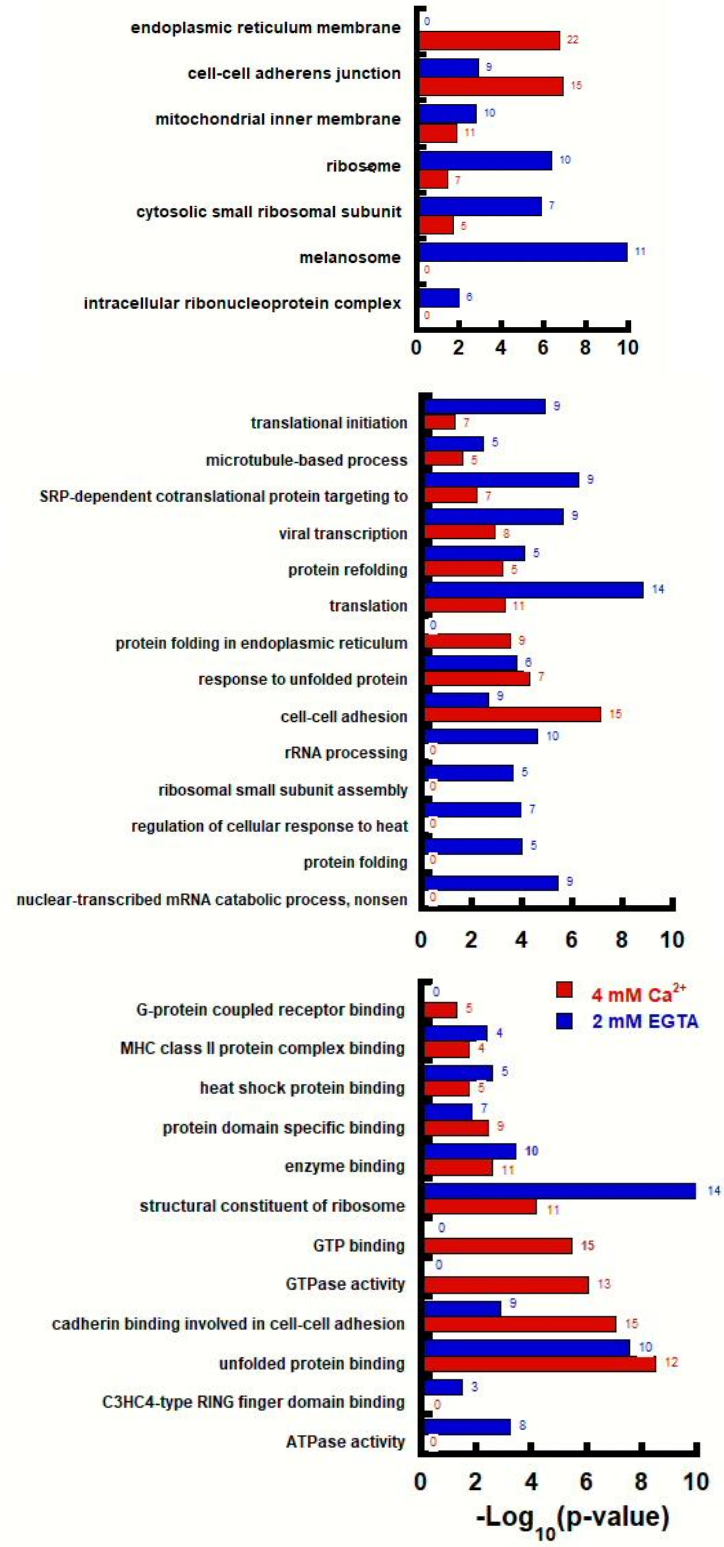

Figure 2.7 Overrepresented gene ontologies among the 91 CaSR interactors upregulated by ≥ 2 fold in presence of 4 mM Ca^{2+}o, (red bars) and 61 in presence of 2 mM EGTA (blue bar) over the negative control were examined with DAVID

2.6.4 STRING analysis for interaction networks

A visual representation of protein-protein interaction for putative 106 CaSR interactors was generated using Search Tool for the Retrieval of Interacting Genes/Proteins (STRING**) (Figure 2.8)**. Spheres or nodes of different colors represent proteins. Large nodes represent proteins with known 3D structure while small nodes represent proteins with unknown structure. The thickness of lines between the nodes denotes "edges" and represents the confidence score for a true interaction based on available evidence. The thicker and darker the edge is, the confidence score for a true interaction based on available evidence is higher. The network edge confidence is ranked between 0 and 1, 1 being the most confident score. The strength of connecting nodes is not represented by the length or the location of the nodes. 106 proteins scored a medium local clustering coefficient of 0.551 with 633 edges and a PPI enrichment P < 1.00E-16 (Table S 5). The106 putative CaSR interactors scored a medium local clustering coefficient of 0.551 with 633 edges and a PPI enrichment *P* < 1.00E-16 (Table S 5). Differentially enriched protein groups were input separately into STRING tool to test their PPI. There was no particular trend, however, all groups had medium to high network edge confidence of 0.714, 0.481, 0.356 and 0.498 for ≥ eight-fold, 4-8 fold, 2-4 fold and 1.5-2 fold enriched groups [$\log_2$ intensity (Ca^{2+}/EGTA)], respectively **(Figure 2.10)**. The edge confidence for 31 % of the proteins that were < 1.5 fold enriched [$\log_2$ intensity (Ca^{2+}/EGTA) < 0.58 and > -0.58] was 0.637 (**Figure 2.9)** and that for 65 % protein group highly enriched ≥ 1.5 fold in the presence of $Ca^{2+}{}_o$ was 0.496 **(Figure 2.10).**

2.6.5 Re-validation of known CaSR interactors

Six previously known CaSR interactors involved in signaling and trafficking were re-validated, namely, $G\alpha_i$ [132-134], $G\beta_2$ [132-134], 14-3-3 θ [135], 14-3-3 ζ [135], 14-3-3 ε [135], 14-3-3 γ [135], p24 [136] and calnexin [14] (**Table 2.1**). G-proteins, $G\alpha_i$, and $G\beta_2$ were detected

exclusively in the presence of Ca^{2+}_o. Heterotrimeric G-proteins are known GPCR interactors [132-134] and activated GPCRs transduce downstream signaling through GTP-bound Gα and Gβγ dissociation. $G\alpha_i$ mediates inhibition of the cAMP dependent pathway through inhibition of adenylate cyclase [137]. On the other hand, $G\beta_2$ is a part of Gβϒ complex that is widely expressed in cytoplasm, nucleus and cytoplasmic surface of the plasma membrane [138]. It modulates activity of effectors and regulators, including enzymes and several forms of potassium and calcium ion channels [139]. $G\beta_2$ is closely associated with microtubule assembly and plays potential role in regulation of cell proliferation, and microtubule and mitotic spindle organization in mammalian cells [140]. Zha *et. al.* reported a non-canonical role of G_β—as a substrate recognition factor to recruit a specific substrate to a cullin-RING E3 ubiquitin ligase for GPCR regulation [141]. 14-3-3 θ and 14-3-3 ζ belong to ubiquitously expressed chaperones family, 14-3-3, known to play important role in regulation of cell signaling events and cellular trafficking [142, 143]. 14-3-3 θ is a known GPCR-interactor, including, melatonin receptor 1B [133] and glucagon receptor [132]. 14-3-3 θ and 14-3-3 ζ were detected in both the presence and absence of Ca^{2+}_o but were significantly down regulated in the presence of Ca^{2+}_o. Arulpragasam *et. al.* characterized their negative roles in CaSR dependent SRE activation through CaSR tail binding and distinctive function of 14-3-3 ζ in lowering CaSR membrane expression [135]. p24 family is a type 1 transmembrane protein which interacts with cargo and COPI or COPII coatomers and have been shown to interact with CaSR as a limiting factor in CaSR trafficking in the early secretory pathway and suggested to assist in transportation to and from the ERGIC [136].

2.6.6 Novel CaSR interactors validated by other GPCR study

The major significance of our study is the identification of several novel CaSR interactors (Table 1). This knowledge can provide new opportunities for understanding the function and

regulation of CaSR as well as provide insight on the crosstalk between signaling pathways within an interactome. Some of these novel interactors have been validated for other families of GPCR, which adds to the significance of our work, indicating them as functionally relevant. Most of these interactors were up-regulated in the presence of Ca^{2+}_o by varying degrees and were shown to be enriched in the ER, cell-cell adherens junction or mitochondrial inner membrane and associated with ER quality control, trafficking and Ca^{2+} homeostasis. Vesicle-associated membrane protein-associated protein-A and -B (VAPA and VAPB) was enriched solely in the presence of Ca^{2+}_o by > 3 folds. VAPA is known to be involved in androgen receptor intracellular trafficking [144] and also oxysterol-binding protein related protein 3 is known to bind to VAPA to modify export from the ER [144]. Similarly, in the previous study, VAPB was identified as glucagon [132] and melatonin receptor type 1A [133] interactor. Ras-related proteins, Rab- 1, 7 and 11a are known CaSR interactors [145, 146]. We detected three other Rab isoforms (5C, 6 and 18) upregulated by > 2.5 folds in the presence of Ca^{2+}_o. Different isoforms of Rab proteins have been found as GPCR interactors including Rap-1A and Rab-10 [132, 133]. Another scaffolding and chaperone protein, calnexin is spotted in both the conditions, but upregulated in the presence of Ca^{2+}_o by > 1.5 folds. It is a known melatonin receptor interactor 1A and 1B [133]. In our experiment, E3 ubiquitin ligases (CHIP, RanBP2 and AMFR) were detected which could be a binding partner for the $G\beta_2$. Further, E3 ubiquitin ligases are known CaSR interactors and have been demonstrated with Co-IP and functional assays to regulate ubiquitination and degradation of CaSR through ERAD pathway [117].

We also observe an upregulation of pumps that maintains the Ca^{2+} concentration of the ER. Sodium/potassium-transporting ATPase (ATP1A1/ ATP1A3/ ATP1A2) and Sarcoplasmic/endoplasmic reticulum calcium ATPase 2 (ATP2A2), a glucagon receptor interactor

[132], was also detected in our experiment in both the conditions, but are highly abundant by > 2.5 and > 2 folds, respectively, in the presence of Ca^{2+}_o. These proteins are involved in cellular signaling and molecular transport. A different isoform of voltage-dependent anion-selective channel protein (VDAC-2), interactor of glucagon receptor [132], was detected in both in the presence and absence of Ca^{2+}_o, but was found to be more abundant in the presence of Ca^{2+}_o by 1.5 folds.

Membrane-associated progesterone receptor component 1 (PGRMC1) is also upregulated by > 2.5 folds in the presence of Ca^{2+}_o and is a known glucagon [132] and melatonin receptor [133] interactor. Insulin receptor substrate 4 (IRS4) is also a known melatonin receptor 1B interactor and is found to be equivalently upregulated in the presence and absence of Ca^{2+}_o. Elongation factor 1-gamma (EEF1G) is also a melatonin interactor (1A) [133] and is upregulated in the presence of Ca^{2+}_o by 2-2.5 folds. Heat shock proteins (HSPA6, HSPA7, HSPA8, HSP90AB, HSPA1A) were detected in equivalently in both the conditions and therefore, must be ubiquitously present irrespective of the Ca^{2+}_o. HSPs are known cell surface receptor regulator including the GPCRs: α_{2c} adrenergic, CB2 cannabinoid and PAR-1 protease-activated receptors [147]. Leucine-rich repeat-containing protein 59 (LRRC59) is a known melatonin receptor type 1A interactor as shown by Daulat *et. al.* [133]. This protein is detected in both presence and absence of Ca^{2+}_o, however, is found to be > 2.5-fold more abundant in the 4 mM Ca^{2+}_o **(Table 2.9).** Only 5 out of the 106 interactors were up-regulated in the absence of Ca^{2+}_o. 14-3-3- θ, ζ, and ε are detected in both the conditions but were up-regulated in the absence of Ca^{2+}_o by ≥ 1.5 folds. On the other hand, 14-3-3 γ is found in equivalent abundance in both the conditions. Potentially, in the absence of Ca^{2+}_o, 14-3-3 acts to downregulate the trafficking of CaSR from the ER.

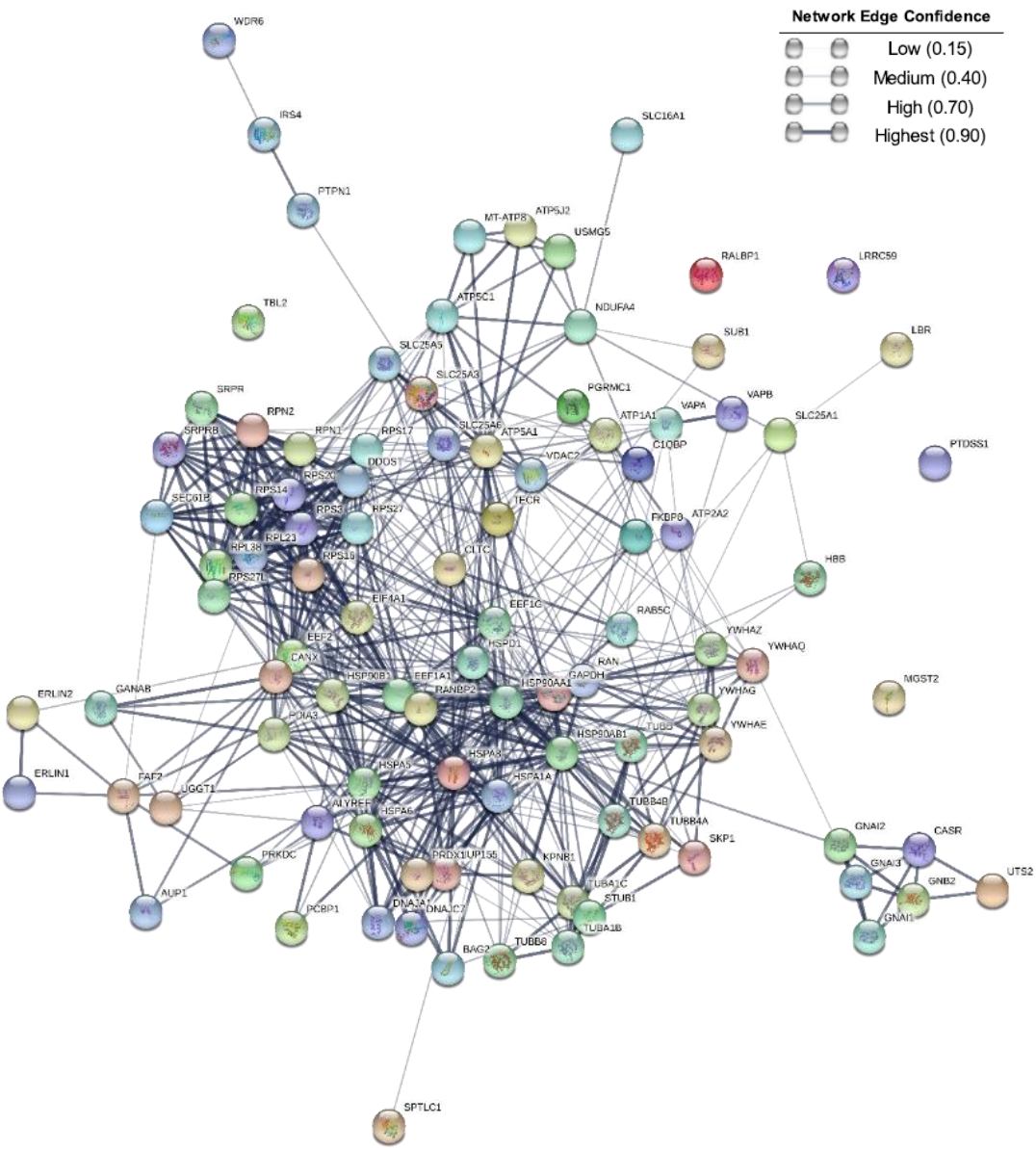

Figure 2.8 A visual representation of protein-protein interaction for putative 106 CaSR interactors generated using STRING.

A visual representation of protein-protein interaction for putative 106 CaSR interactors generated using STRING. Spheres or nodes of different colors represent proteins. Large nodes represent proteins with known 3D structure while small nodes represent proteins with unknown structure. The lines between the nodes represent "edges". The thicker and darker the edge is, the confidence score for a true interaction based on available evidence is higher. The network edge confidence is ranked between 0 and 1, 1 being the most confident score. The strength of connecting nodes is not represented by the length or the location of the nodes. 106 proteins scored a medium local clustering coefficient of 0.551 with 633 edges and a PPI enrichment P < 1.00E-16.

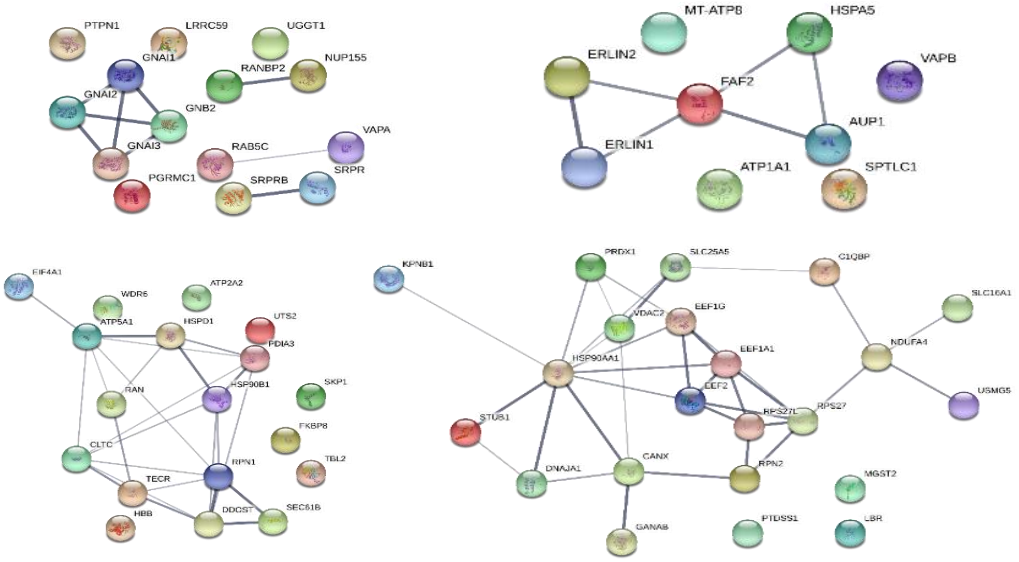

Figure 2.10 A visual representation of protein-protein interaction for putative CaSR interactors upregulated at various degree in the presence of $Ca^{2+}{}_o$ generated using STRING. A. ≥ four folds. B. 3-4 folds. C. 2-3 folds. D. 1.5-2 folds.

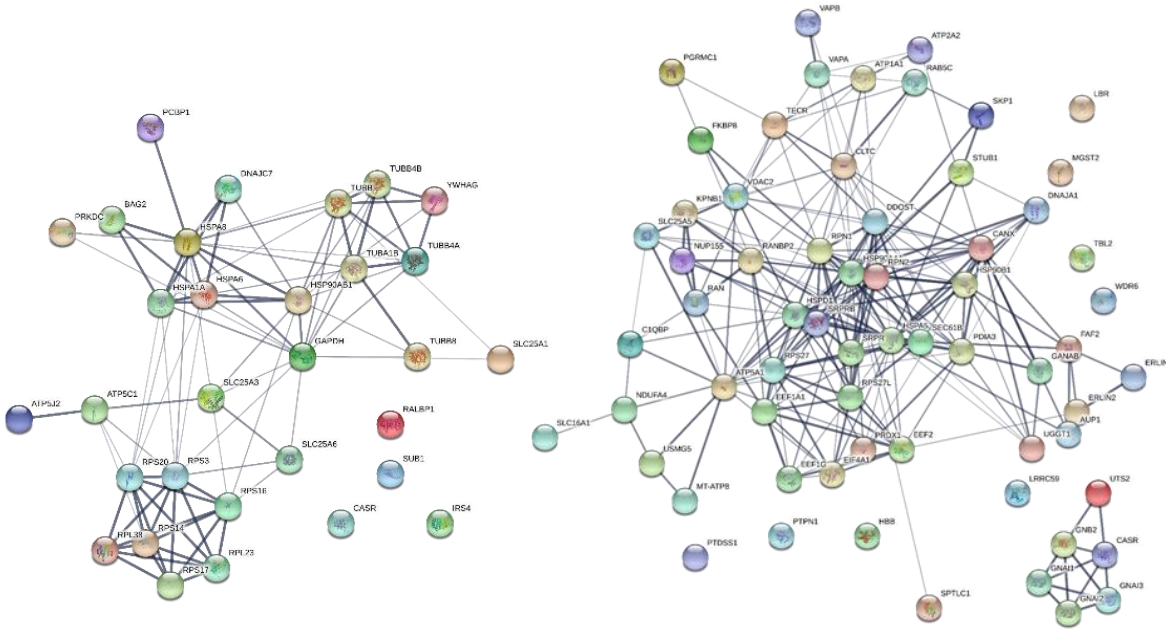

Figure 2.9 A. A visual representation of protein-protein interaction for putative 33 CaSR interactors not affected by Ca^{2+}

[-log2 (Ca^{2+}/EGTA <0.58 and > -0.58] generated using STRING had an average local clustering coefficient of 0.617 with 90 edges and a PPI enrichment P < 7.86E-14. (Table S 5). B. STRING visualization for 61 CaSR interactors found highly abundant in Ca^{2+} [-log2 (Ca^{2+}/EGTA ≥ 0.58] with local clustering coefficient of 0.496 with 90 edges and a PPI enrichment P < 1.00E-16. (Table S 5).

Table 2.7 Network statistic available from STRING for various groups of putative CaSR interactors.

STRING Network Statistics	All putative CaSR interactors	CaSR interactors eriched in Ca^{2+}_o by ≥ 1.5 folds	CaSR interactors enriched by < 1.5 folds in Ca^{2+}_o and EGTA	CaSR interactors enriched by ≥ four folds in Ca^{2+}_o	CaSR interactors enriched by ≥ 3 and < 4 folds in Ca^{2+}_o	CaSR interactors enriched by ≥ 2 and < 3 folds in Ca^{2+}_o	CaSR interactors enriched by ≥ 1.5 and < 2 folds in Ca^{2+}_o
Reference to Figure	Figure 2.8	Figure 2.9	Figure 2.10	Figure 2.9A	Figure 2.9B	Figure 2.9C	Figure 2.9D
Number of interacting nodes	99	63	30	14	9	18	22
Number of edges	633	215	90	9	6	24	34
Average local clustering coefficient	0.551	0.489	0.637	0.714	0.481	0.356	0.498
Enrichment p-value	< 1.0E-16	< 1.0E-16	1.33E-15	0.0786	3.67E-06	1.19E-06	1.10E-06

Table 2.8 Groups of proteins with various stringencies

Groups	Stringency used	Number of proteins
Group A	log_2 intensity (Positive/negative control)-Ca2+ ≥ 1	94
Group B	log_2 intensity (Positive/negative control)-EGTA ≥ 2	61
Group C	log_2 intensity (Ca2+/EGTA)≥ 0.58	69
Group D	log_2 intensity (Ca2+/EGTA) ≥ - 0.58	5
Group E	log_2 intensity (Ca2+/EGTA) < 0.58 and > -0.58	33
Group F	log_2 intensity (Ca2+/EGTA)≥ 4	12
Group G	log_2 intensity (Ca2+/EGTA) <4 and ≥ 2	9
Group H	log_2 intensity (Ca2+/EGTA) <2 and ≥ 1	21
Group I	log_2 intensity (Ca2+/EGTA) <1 and ≥ 0.58	26

Table 2.9 Relevant upregulated proteins from 106 putative CaSR interactors with ≥ 2 folds enrichment as compared to negative control

			Average PSM				Relative expression Log_2 (intensity ratio) between				
			Positive control		Negative control						
Protein names	Gene names	Unique peptides	Ca^{2+}	EGTA	Ca^{2+}	EGTA	WT and Neg control in Ca^{2+}	WT and Neg conrol in EGTA	Ca^{2+} and EGTA (WT)	Reference	GPCR binding partner
Vesicle-associated membrane protein-associated protein A	VAPA	3.00	4.33	0.00	0.00	0.00	5.19	-0.53	5.42	2015, Han et al (VAPB), 2007 Daulat	Glucagon receptor, Melatonin receptor type 1A (MT1)
UDP-glucose:glycoprotein glucosyltransferase 1	UGGT1	15.00	8.00	0.00	0.00	0.00	4.79	0.20	4.48		
Guanine nucleotide-binding protein G(I)/G(S)/G(T) subunit beta-2	GNB2	4.00	4.33	0.00	0.00	0.00	5.02	1.00	4.43	2015, Han et al; Enz et al, 2006	Glucagon receptor; mGluR
E3 SUMO-protein ligase RanBP2	RANBP2	8.00	5.33	0.00	0.33	0.00	3.86	0.39	4.39		
Tyrosine-protein phosphatase non-receptor type 1	PTPN1	2.00	2.00	0.00	0.00	0.00	3.03	-2.00	4.24		
Leucine-rich repeat-containing protein 59	LRRC59	5.00	4.00	0.00	0.00	0.00	6.14	2.80	4.16	2007 Daulat et al	Melatonin receptor type 1A (MT1)
Signal recognition particle receptor subunit alpha	SRPR	3.00	3.00	0.00	0.00	0.00	3.29	-0.41	4.11		
Ras-related protein Rab-5C	RAB5C	5.00	5.33	0.00	0.00	0.00	4.31	1.18	4.10	2001, Groohane 2006(Rab 1, 7, 11a)	CaSR
Nuclear pore complex protein Nup155	NUP155	5.00	3.67	0.00	0.00	0.00	4.71	0.36	4.00		
Signal recognition particle receptor subunit beta	SRPRB	8.00	13.67	0.67	0.00	0.00	6.69	2.84	3.74		
Guanine nucleotide-binding protein G(k) subunit alpha; G(i) subunit alpha-1; G(i) subunit alpha-2; G(o) subunit alpha	GNAI3;GNAI1;GNAI2;GNAO1	5.00	8.00	0.67	0.00	0.00	6.75	1.04	3.64	2015, Han et al, 2007 Daulat et al (Giα3, Giα1,	Glucagon receptor, Melatonin receptor type 1A and 1B
Membrane-associated progesterone receptor component 1	PGRMC1	2.00	1.33	0.00	0.00	0.00	2.95	0.59	3.02	2015, Han et al, 2007 Daulat	Glucagon receptor, MT1
Ancient ubiquitous protein 1	AUP1	3.00	5.00	0.33	0.00	0.00	3.67	1.27	2.87		
Serine palmitoyltransferase 1	SPTLC1	3.00	2.00	0.00	0.00	0.00	3.04	0.59	2.74	et al (SPTLC2)	Glucagon receptor
ATP synthase protein 8	MT-ATP8	1.00	3.00	2.00	0.00	0.00	2.66	1.16	2.73		
Erlin-1	ERLIN1	1.00	2.33	1.00	0.00	0.00	2.84	0.22	2.70		
FAS-associated factor 2	FAF2	6.00	4.00	1.00	0.00	0.00	4.61	1.89	2.48		
Vesicle-associated membrane protein-associated protein B/C	VAPB	3.00	2.00	0.00	0.00	0.00	3.34	1.00	2.37	et al (VAPB),	receptor, Melatonin
Erlin-2	ERLIN2	9.00	13.33	3.33	0.00	0.00	7.38	4.43	2.35		
78 kDa glucose-regulated protein	HSPA5	22.00	60.67	21.33	4.67	3.00	4.25	2.69	2.30	2007 Daulat et	Melatonin receptor type
ATPase subunit alpha-1;alpha-3;alpha-2	ATP1A1;ATP1A3;ATP1A2	4.00	3.67	1.33	0.33	0.00	4.76	1.81	2.20	2015, Han et al	Glucagon receptor
S-phase kinase-associated protein 1	SKP1	1.00	2.33	2.00	0.33	0.00	1.56	0.46	2.00		
Ras-related protein Rab-6A;6B;39A	RAB6B;RAB6A;RAB39A	1.00	2.67	1.33	0.00	0.00	3.19	1.26	1.96	Zerial, 2001,	CaSR
Protein disulfide-isomerase A3	PDIA3	8.00	6.00	1.33	0.00	0.00	5.19	3.28	1.60		
Urotensin-2	UTS2	1.00	2.67	0.67	0.00	0.00	4.46	3.10	1.58		
GTP-binding nuclear protein Ran	RAN	5.00	5.67	1.33	1.00	1.00	3.07	2.23	1.52		
Lamina-associated polypeptide 2, isoforms beta/gamma;isoform alpha;Thymopoietin;Thymopentin	TMPO	8.00	10.00	3.00	0.33	0.00	3.17	3.40	1.51		

Ras-related protein Rab-18	RAB18	2.00	2.00	0.33	0.00	0.00	2.15	1.70	1.51	2015, Han et al, 2007 Daulat	Glucagon receptor, MT1
Peptidyl-prolyl cis-trans isomerase FKBP8;Peptidyl-prolyl cis-trans isomerase	FKBP8	3.00	2.00	0.00	0.00	0.00	4.32	3.22	1.50		
Very-long-chain enoyl-CoA reductase	TECR	2.00	4.33	3.33	0.00	0.00	3.63	2.51	1.49		
Eukaryotic initiation factor 4A-I; 4A-II; 4A-II, N-terminally processed	EIF4A1;EIF4A2	3.00	4.67	0.67	0.00	0.00	2.26	1.80	1.49		
ATP synthase subunit alpha, mitochondrial	ATP5A1	5.00	5.00	1.33	0.33	0.00	3.12	3.58	1.41		
Dolichyl-diphosphooligosaccharide-protein glycosyltransferase subunit	RPN1	13.00	14.67	5.67	0.00	0.00	7.07	5.51	1.35		
Protein transport protein Sec61 subunit beta	SEC61B	1.00	2.00	1.00	0.00	0.00	3.40	2.18	1.33		
WD repeat-containing protein 6	WDR6	14.00	17.00	5.00	0.67	0.00	3.53	3.46	1.30		
Hemoglobin subunit beta;LVV-hemorphin-7;Spinorphin	HBB	2.00	2.33	0.67	0.00	1.33	2.26	-0.37	1.22		
Sarcoplasmic/endoplasmic reticulum calcium ATPase 2	ATP2A2	12.00	11.33	4.33	0.00	0.00	6.81	6.36	1.18	2015, Han et al	Glucagon receptor
Transducin beta-like protein 2	TBL2	4.00	3.00	1.33	0.00	0.00	3.73	3.29	1.15		
Endoplasmin	HSP90B1	3.00	2.67	1.00	0.00	0.00	4.18	2.93	1.10		
60 kDa heat shock protein, mitochondrial	HSPD1	6.00	4.00	1.67	0.00	0.00	3.27	3.03	1.09		
heavy chain 1	CLTC	12.00	5.67	1.33	0.67	0.33	2.37	1.92	1.05		
Dolichyl-diphosphooligosaccharide-protein glycosyltransferase 48 kDa subunit	DDOST	5.00	2.67	1.00	0.00	0.00	2.21	1.93	1.02		
Phosphatidylserine synthase 1	PTDSS1	2.00	1.67	0.33	0.00	0.00	2.41	1.99	1.00		
Complement component 1 Q subcomponent-binding protein, mitochondrial	C1QBP	4.00	6.00	3.33	2.67	0.67	0.66	1.70	0.98		
Elongation factor 1-gamma	EEF1G	4.00	2.67	0.67	0.00	0.00	3.56	3.69	0.95	2007	Melatonin
Elongation factor 2	EEF2	4.00	1.67	0.33	0.00	0.00	3.03	2.98	0.95		
40S ribosomal protein S5;40S ribosomal protein S5, N-terminally	RPS5	4.00	4.33	4.33	1.33	0.33	2.22	3.08	0.90		
40S ribosomal protein S27	RPS27	2.00	8.00	6.67	2.00	0.33	3.49	3.93	0.90		
Elongation factor 1-alpha 1;Putative elongation factor 1-alpha-like 3	EEF1A1;EEF1A1P5	11.00	18.00	13.67	8.67	5.67	1.95	1.39	0.90		
Trifunctional enzyme subunit beta, mitochondrial;3-ketoacyl-CoA thiolase	HADHB	1.00	1.67	0.67	0.67	0.33	1.16	1.79	0.89		
DnaJ homolog subfamily A member 1	DNAJA1	2.00	3.67	2.33	0.00	0.00	3.16	4.37	0.86		
40S ribosomal protein S27;40S ribosomal protein S27-like	RPS27L	1.00	2.00	1.67	0.00	0.00	3.73	2.87	0.82		
Microsomal glutathione S-transferase 2	MGST2	1.00	2.67	1.00	0.00	0.00	3.74	3.70	0.81		
Lamin-B receptor	LBR	3.00	3.67	0.33	0.00	0.00	3.48	3.21	0.81		
Importin subunit beta-1	KPNB1	7.00	4.67	2.67	1.00	0.00	2.08	3.94	0.79		
E3 ubiquitin-protein ligase CHIP	STUB1	5.00	3.33	1.67	0.00	0.00	3.06	2.43	0.78	al, 2006	CaSR
Neutral alpha-glucosidase AB	GANAB	19.00	18.00	6.00	0.00	0.00	7.22	6.63	0.76		
Very-long-chain (3R)-3-hydroxyacyl-CoA dehydratase 3	HACD3	3.00	5.67	5.00	0.67	0.00	4.42	4.97	0.72		
Calnexin	CANX	10.00	8.00	5.67	0.00	0.00	6.57	6.69	0.71	Daulat et	receptor type
Peroxiredoxin-1	PRDX1	4.00	5.00	3.67	2.67	1.67	0.89	1.30	0.71		
Heat shock protein HSP 90-alpha	HSP90AA1	4.00	3.00	2.33	0.00	0.00	3.24	2.84	0.69		
Up-regulated during skeletal muscle growth protein 5	USMG5	2.00	2.33	0.00	0.00	0.00	3.09	1.57	0.68		
Dolichyl-diphosphooligosaccharide-protein glycosyltransferase subunit	RPN2	8.00	3.00	2.33	0.00	0.00	4.68	4.79	0.68		
Monocarboxylate transporter 1	SLC16A1	2.00	2.67	2.67	0.00	0.00	4.95	4.48	0.66		
Cytochrome c oxidase subunit NDUFA4	NDUFA4	2.00	3.67	4.33	0.00	0.00	3.22	4.54	0.66		
Voltage-dependent anion-selective channel protein 2	VDAC2	4.00	4.33	1.00	0.33	0.00	3.11	3.03	0.66	2015, Han et al	Glucagon receptor
Proteasome subunit alpha type; type-4; beta type	PSMA4	2.00	1.67	1.33	0.00	0.00	2.24	2.53	0.63		

ADP/ATP translocase 2;ADP/ATP translocase 2, N-terminally processed	SLC25A5	6.00	9.33	6.67	2.33	1.00	2.11	2.35	0.60		
Transmembrane and coiled-coil domain-containing protein 1	TMCO1	2.00	3.67	3.00	0.00	0.00	4.49	5.66	0.58		
40S ribosomal protein S14	RPS14	7.00	10.33	11.00	7.00	1.33	0.81	2.16	0.58		
Phosphate carrier protein, mitochondrial	SLC25A3	7.00	11.33	9.33	3.00	2.00	3.63	4.38	0.52		
translocase 3, N-terminally processed	SLC25A6	5.00	28.67	22.00	11.33	5.67	2.03	2.65	0.51		
40S ribosomal protein S20	RPS20	3.00	7.33	5.33	4.00	2.00	0.75	1.18	0.47		
Poly(rC)-binding protein 1	PCBP1	3.00	8.00	7.00	3.00	1.67	1.99	2.14	0.44		
Heat shock cognate 71 kDa protein	HSPA8	22.00	85.33	70.00	13.00	7.00	2.96	3.57	0.43		
DnaJ homolog subfamily C member 7	DNAJC7	18.00	20.00	22.00	0.00	0.00	7.08	8.23	0.38		
Extracellular calcium-sensing receptor	CASR	52.00	496.00	427.33	4.33	0.00	11.61	14.32	0.30		
Insulin receptor substrate 4	IRS4	25.00	41.33	31.00	6.00	2.00	2.85	4.96	0.30		receptor type
40S ribosomal protein S3	RPS3	12.00	29.33	30.33	16.67	11.33	1.06	1.43	0.29		
ATP synthase subunit gamma, mitochondrial	ATP5C1	3.00	2.00	2.67	1.00	1.00	1.07	1.92	0.28		
Heat shock protein HSP 90-beta	HSP90AB1	7.00	21.33	19.00	4.33	1.33	2.34	3.81	0.26		
Heat shock 70 kDa protein 1A	HSPA1A	12.00	56.33	49.33	22.67	12.67	2.03	2.88	0.26		
40S ribosomal protein S16	0	9.00	18.00	15.67	8.67	7.33	1.28	0.93	0.26		
60S ribosomal protein L22	RPL22	2.00	3.67	3.33	2.67	1.33	0.63	1.11	0.24		
BAG family molecular chaperone regulator 2	BAG2	10.00	35.00	32.00	0.00	1.33	6.08	5.83	0.17		
DNA-dependent protein kinase catalytic subunit	PRKDC	13.00	7.67	8.33	2.00	0.33	1.53	4.98	0.13		
membrane translocase subunit TIM50	TIMM50	3.00	3.33	1.00	0.00	0.00	3.23	2.37	0.13		
Glyceraldehyde-3-phosphate dehydrogenase	GAPDH	4.00	3.67	2.33	0.67	0.33	2.23	2.38	0.12		
60S ribosomal protein L38	RPL38	5.00	12.33	13.33	5.33	3.67	1.07	1.05	0.11		
60S ribosomal protein L23	RPL23	4.00	12.33	9.00	6.33	5.67	1.21	1.69	0.09		
Tubulin beta-4B chain;Tubulin beta-4A chain	TUBB4B;TUBB4A	3.00	12.33	12.67	6.33	2.00	1.64	3.57	0.09		
RalA-binding protein 1	RALBP1	1.00	2.00	1.33	0.00	2.33	7.16	-0.21	0.08		
GPALPP motifs-containing protein 1	GPALPP1	1.00	4.00	3.33	0.00	0.00	9.40	9.03	0.07		
Tubulin beta chain;Tubulin beta-2B chain;Tubulin beta-2A chain	TUBB;TUBB2B;TUBB2A	4.00	53.00	56.33	25.00	9.00	1.92	3.48	0.01		
6;Putative heat shock 70 kDa protein 7	HSPA6;HSPA7	1.00	2.67	2.00	0.00	0.00	1.97	2.88	-0.02		
Tubulin beta-8 chain	TUBB8	2.00	2.33	2.33	0.33	0.33	2.61	4.73	-0.02		
14-3-3 protein gamma;14-3-3 protein gamma, N-terminally processed	YWHAG	1.00	1.67	2.00	0.00	0.00	2.04	2.75	-0.04		
Tubulin alpha-1B chain;Tubulin alpha-4A chain	TUBA1B;TUBA4A	1.00	56.00	61.33	23.00	14.00	1.85	3.28	-0.12		
ATP synthase subunit f, mitochondrial	ATP5J2;ATP5J2-PTCD1	3.00	3.33	2.67	0.00	0.00	3.08	4.90	-0.18		
Tricarboxylate transport protein, mitochondrial	SLC25A1	3.00	3.67	5.00	0.00	0.00	2.51	5.30	-0.33		
40S ribosomal protein S17-like;40S ribosomal protein S17	RPS17;RPS17L	4.00	3.33	2.33	0.33	0.00	0.03	4.97	-0.53		
Activated RNA polymerase II transcriptional coactivator p15	SUB1	2.00	1.67	2.67	1.33	0.00	1.53	3.13	-0.53		
14-3-3 protein epsilon	YWHAE	11.00	14.00	23.33	0.00	0.00	4.42	4.91	-0.80	Arulpraga	Glucagon
Tubulin alpha-1C chain	TUBA1C;TUBA1B	2.00	2.33	3.00	0.33	0.00	3.16	4.54	-0.99		
14-3-3 protein theta	YWHAQ	8.00	15.67	21.67	2.33	0.00	4.68	7.46	-1.08	2012, Arulpraga	CaSR, Glucagon
14-3-3 protein zeta/delta 14-3-3 ζ	YWHAZ	4.00	4.00	8.33	0.00	0.33	3.72	4.54	-1.38		
THO complex subunit 4	ALYREF	6.00	2.33	9.00	2.67	1.00	-0.94	1.49	-1.69		

2.6.7 Rich Hub study

A rich club is a set of high-degree nodes that are more densely interconnected than predicted by the node degrees alone [148]. The rich-club nodes may form a hub that is used by the other components in the network to influence each other. A Power-law distribution curve of the constructed 6 networks shows a strong positive correlation between the number of nodes (y axis) and the node-specific degree (x axis), Pearson correlation coefficient values ranging from 0.7-0.9. As the networks get sparse, correlation is improved suggesting that the frequency of nodes negatively correlates with the connection degree indicating a few number of nodes have the majority of the interactions in the network and therefore may form a connection hub. To investigate the significance of the discovered rich-club, the rich-club coefficient of the interactome networks was compared to that of randomly generated networks with similar degree distribution. The rich-club coefficient of all the six networks ranged from 0.3-0.4, while that of random network was recorded to be 0.07, the rich-club coefficient reveals the presence of significant rich hubs in sub-interactomes.

Four proteins, HSPA8, HSPA5, HSP90AB1, and HSP90AA1 were seen to be part of most enriched hub **(*Figure 2.11*)**. HSPA8 functions as a chaperone and binds to nascent polypeptides to facilitate correct folding. It also functions as an ATPase in the disassembly of clathrin-coated vesicles during transport of membrane components through the cell [149]. HSPA5 is involved in the correct folding of proteins and degradation of misfolded proteins via its interaction with DNAJC10/ERdj5, probably to facilitate the release of DNAJC10/ERdj5 from its substrate and acts as a key repressor of the ERN1/IRE1-mediated unfolded protein response [150]. HSP90AB1 and HSP90AA1 are molecular chaperones that promotes the maturation, structural maintenance and proper regulation of specific target proteins involved for instance in cell cycle control and signal

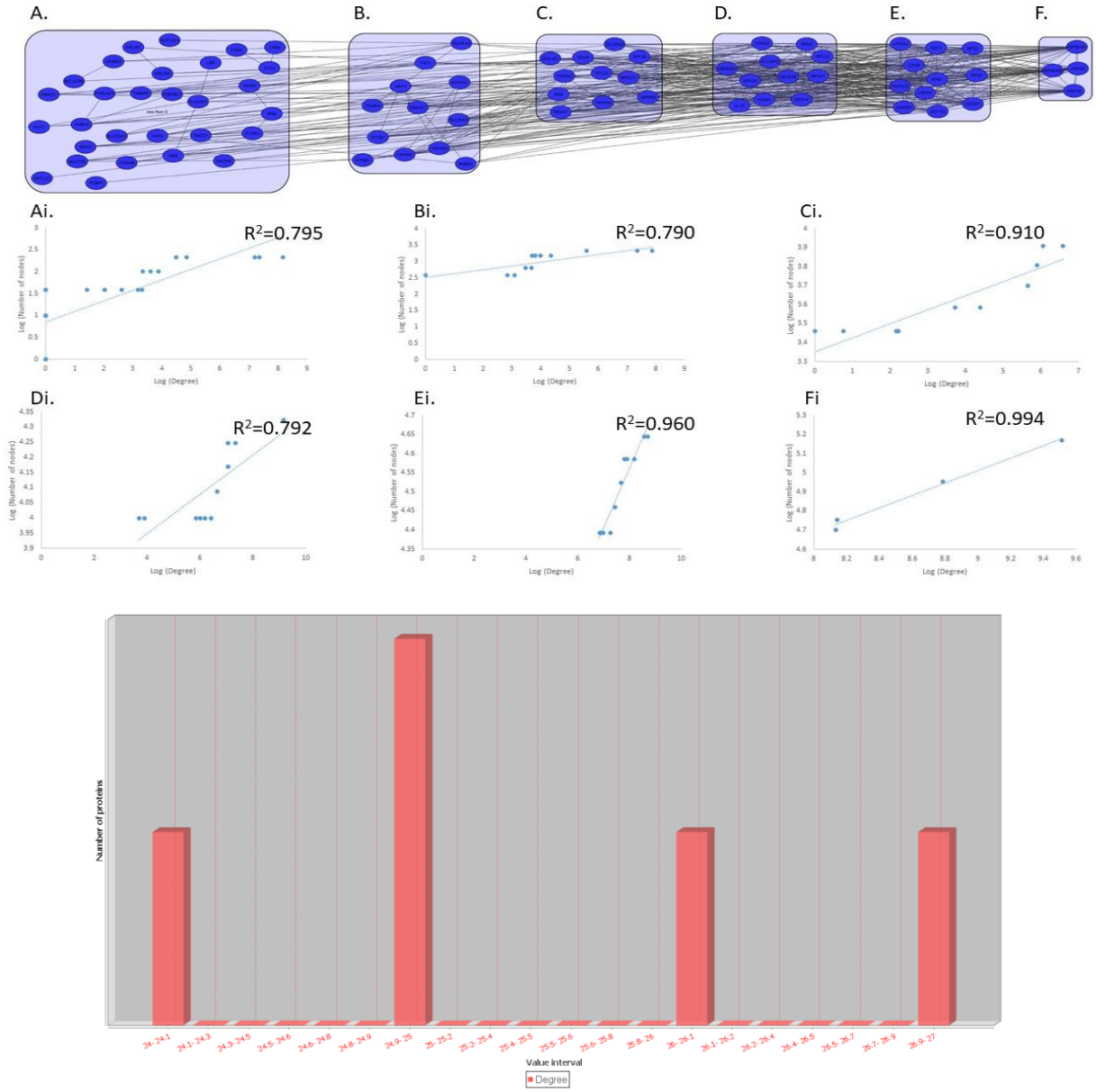

Figure 2.11 Rich hub analysis for CaSR interactome and degree centrality distribution of String interacted proteins .

A degree centrality measure was applied and 6 sub-interactomes (Figure 1: A, B, C, D, E and F) were constructed with degree measures varying between 1-5, 6-10, 11-15, 16-20, 21-25 and >25. Power-law distribution analysis was performed on each of the sub-interactomes to generate Pearson's correlation coefficient values (Figure 1: Ai, Bi, Ci, Di, Ei and Fi) between number of nodes and betweenness centrality measure. *Degree centrality distribution of all the String interacted proteins.*

transduction. It undergoes a functional cycle that is linked to its ATPase activity. This cycle probably induces conformational changes in the client proteins, thereby causing their activation.

They interact dynamically with various co-chaperones that modulate its substrate recognition, ATPase cycle and chaperone function [151].

2.6.8 Validation of some of the detected proteins

2.6.8.1 Coimmunoprecipitation and Western blot

We selected few novel putative CaSR interactors which are involved in trafficking, quality control or signaling to re-validate with western blot of the co-immunoprecipitated product. HEK293 cells transfected with 6 µg of FLAG-CaSR or empty pcDNA3.1 was treated with either Ca^{2+} or EGTA and lysed. The 1.5 mg lysate was subjected with co-immunoprecipitation using 10 µg of FLAG-antibody overnight in 50 µL of dyna bead solution. SDS-Page gel was run for 50 µg of total lysate. 30 µL 2X SDS-sample buffer was used to elute the bound proteins after washing and 25 µL of the eluate was used for SDS-Page gel for each treatment conditions.

30 kDa blot for 14-3-3 ε if any in the immunoprecipitation is concealed by overpowering 25 kD antibody light chain blot **(Figure 2.12)**. The 14-3-3 ε blot at much higher molecular weight where we saw CaSR blots, so could be a complex. GRP78 is present in both the positive controls in Ca^{2+} and EGTA treatment but band is not quantitative **(Figure 2.12)**. The GRP78 blot at much higher molecular weight where we saw CaSR blots, so could be a complex. CHIP is present in both the positive controls in Ca^{2+} and EGTA treatment but band is not quantitative **(Figure 2.13)**. But we saw the CHIP blot at much higher molecular weight where we saw CaSR blots, so could be a complex. IP_3R is present in both the positive controls in Ca^{2+} and EGTA treatment but band is not quantitative **(Figure 2.13**).

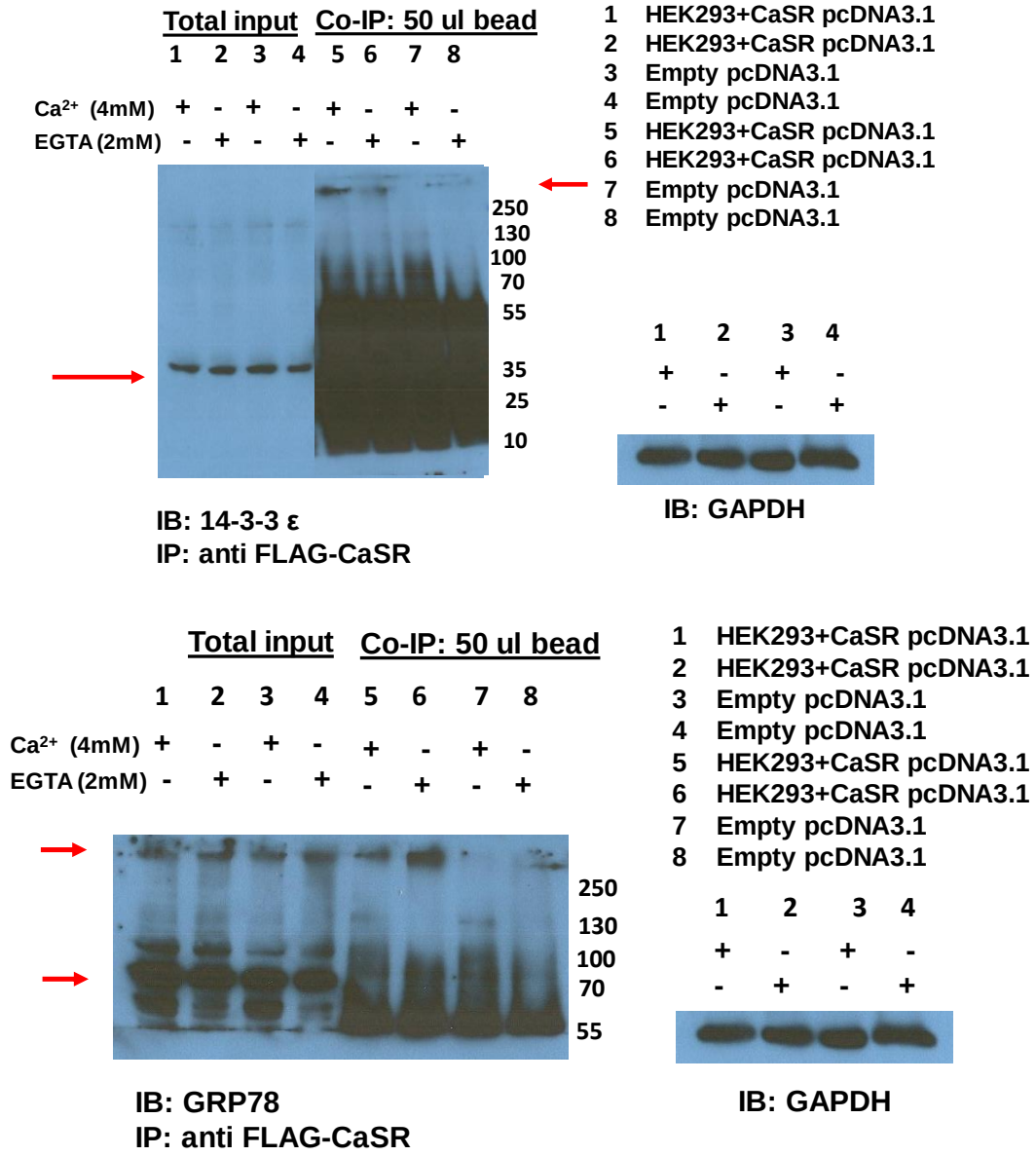

Figure 2.12 Validation for 14-3-3 ε and GRP78

HEK293 cells transfected with 6 µg of FLAG-CaSR or empty pcDNA3.1 was treated with either Ca^{2+} or EGTA and lysed. The 1.5 mg lysate was subjected with co-immunoprecipitation using 10 µg of FLAG-antibody overnight in 50 µL of dyna bead solution. SDS-gel was run for 50 µg of total lysate. 30 µL 2X SDS-sample buffer was used to elute the bound proteins after washing and 25 µL of the eluate was used for SDS-gel for each treatment conditions. Western blot was analyzed using 14-3-3 3 ε at 1:1000 dilution and GRP78 at 1µg/mL antibodies.

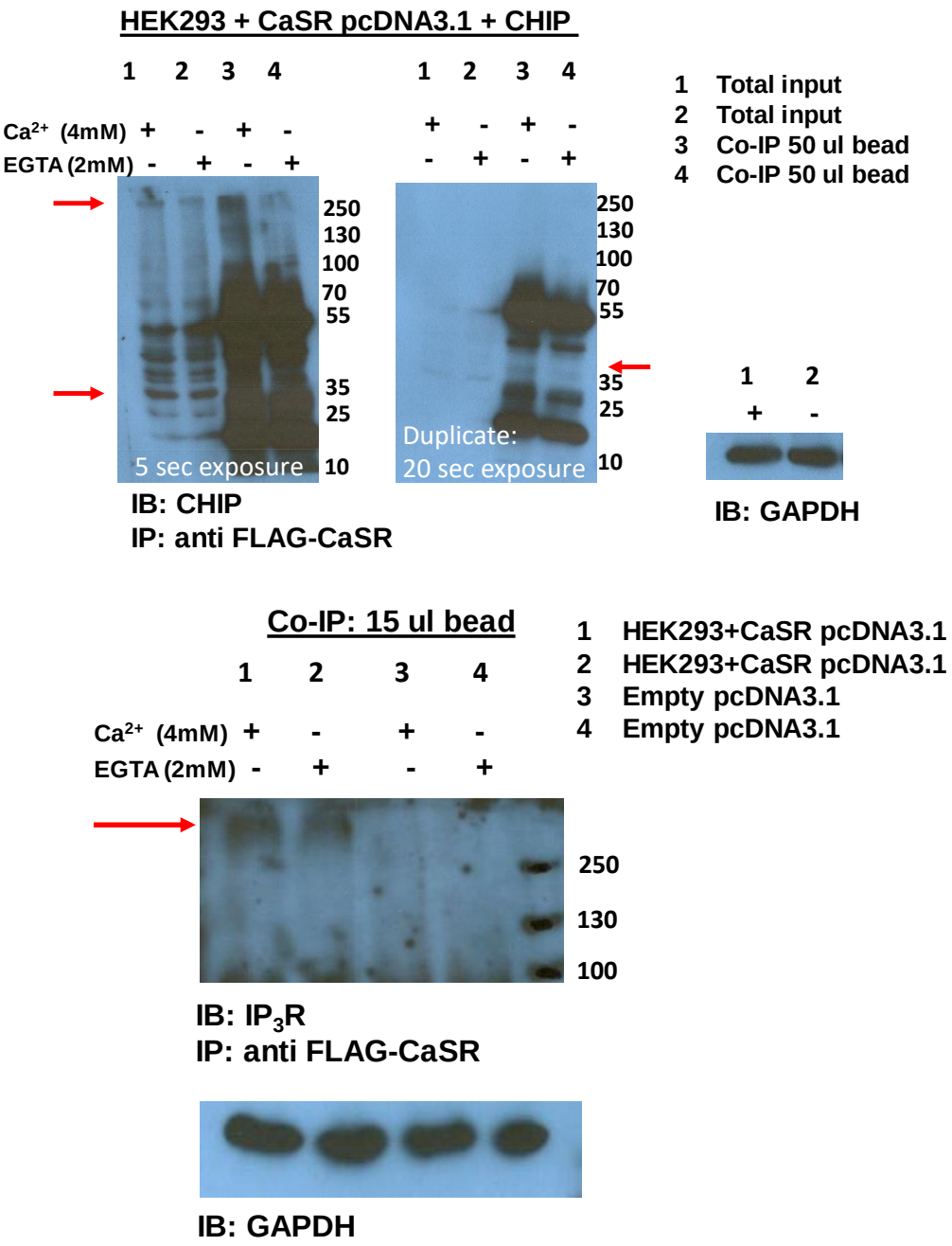

Figure 2.13 validation for CHIP and IP3R

HEK293 cells transfected with 6 µg of FLAG-CaSR or empty pcDNA3.1 was treated with either Ca^{2+} or EGTA and lysed. The 1.5 mg lysate was subjected with co-immunoprecipitation using 10 µg of FLAG-antibody overnight in 50 µL of dyna bead solution. SDS-gel was run for 50 µg of total lysate. 30 µL 2X SDS-sample buffer was used to elute the bound proteins after washing and 25 µL of the eluate was used for SDS-gel for each treatment conditions. Western blot was analyzed using CHIP at 1:500 dilution and IP_3R at 1:1000 antibodies.

2.6.8.2 Immuno-staining

HEK293 cells transfected with 2.5 µg of FLAG-CaSR or empty pcDNA3.1 in 20 × 20 mm coverslips was starved and then treated with Ca^{2+}. The cells were subjected to immunostaining using mouse anti FLAG-antibody at 1:1500 dilution and rabbit anti GRP7/Bip8 at 2 µg/mL. Secondary goat anti mouse Alexa fluor 488 at 4 µg/mL and secondary goat anti rabbit Alexa fluor

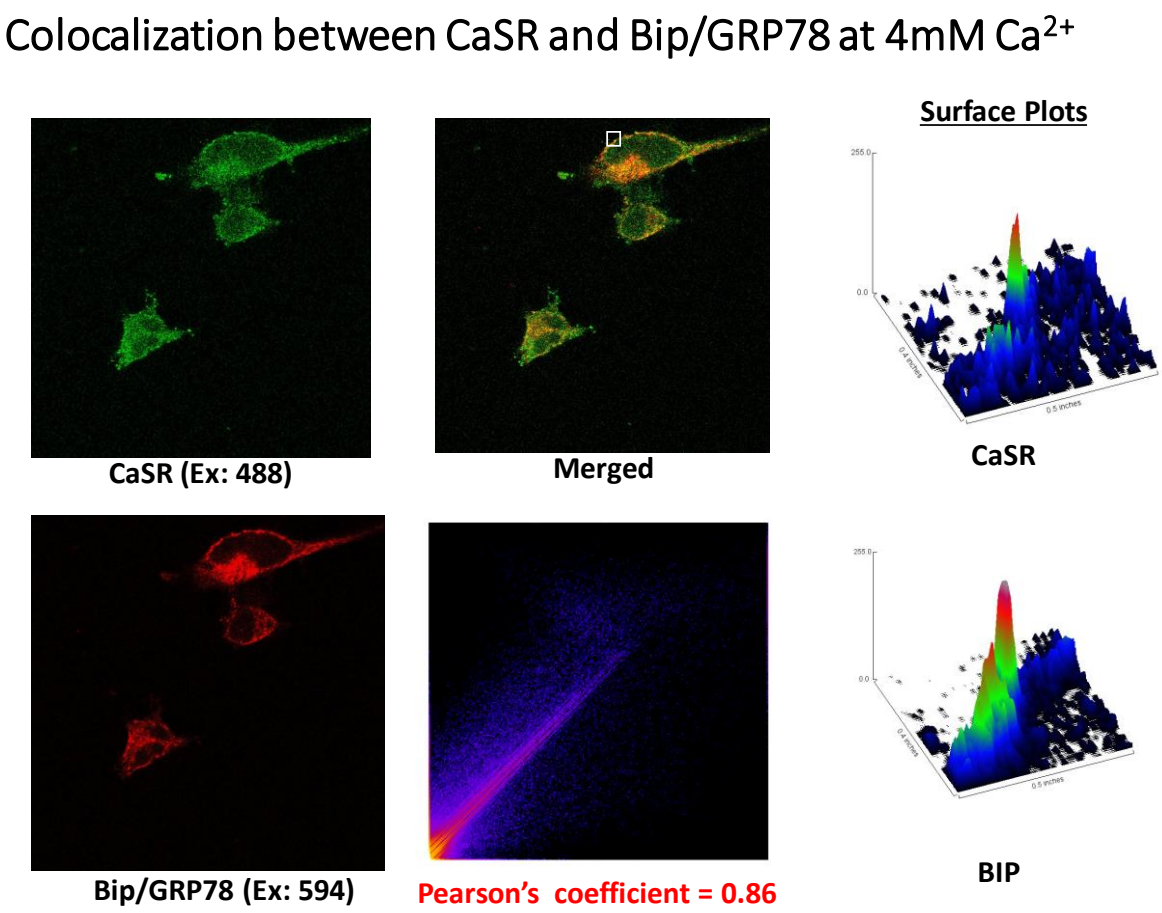

Figure 2.14 *A. Co-localization of FLAG-CaSR and endogenous GRP78*

HEK293 cells transfected with 2.5 µg of FLAG-CaSR or empty pcDNA3.1 in 20 × 20 mm coverslips was treated with Ca^{2+}. The cells were subjected to immunostaining using mouse anti FLAG-antibody at 1:1500 dilution and rabbit anti GRP78 at 2 µg/mL. Secondary goat anti mouse Alexa fluor 488 at 4 µg/mL and secondary goat anti rabbit Alexa fluor 647 at 4 µg/mL were used. Image-J was used to process the co-localization. Yellow represents co-localization. Surface plot of pixel intensities from confocal images of the area marked in grey square of HEK293 cells expressing FLAG-CaSR and endogenous GRP78 after 4mM Ca^{2+} treatment show similar corresponding peaks. Co-localization is observed on the membrane as well as interior of cell.

647 at 4 µg/mL were used. Image-J was used to process the co-localization. Yellow represents co-localization. To further observe the co-localization at the microscopic level, surface plot of pixel

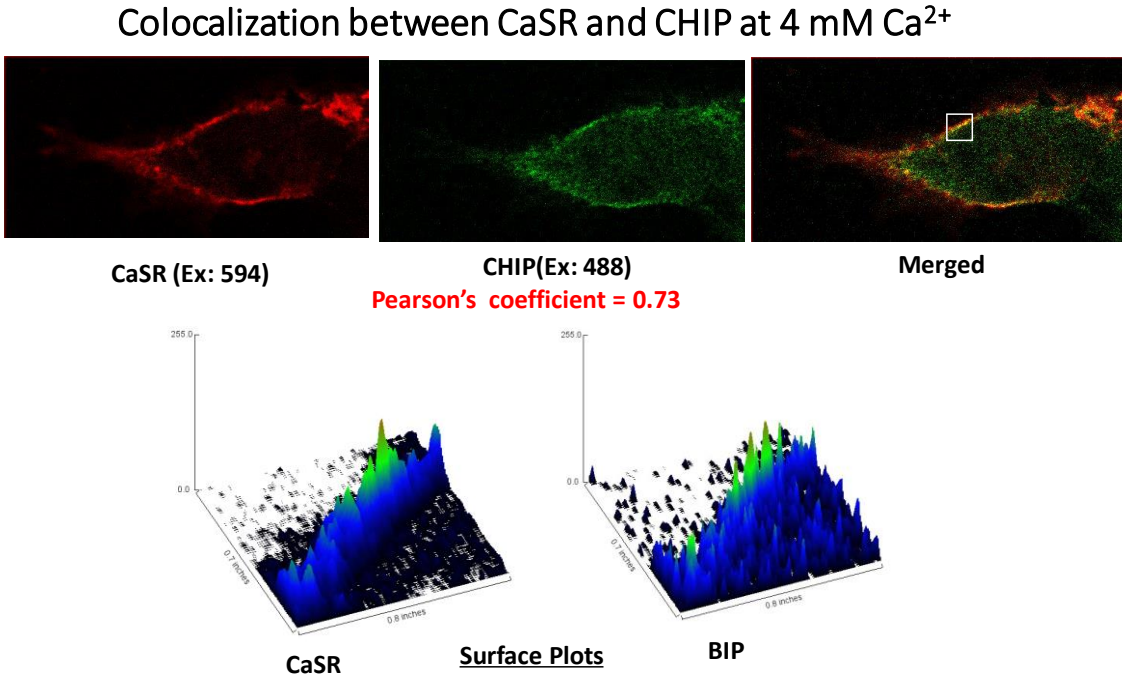

Figure 2.15 Membrane *CaSR co-localized with endogenous STUB1 (CHIP)*

HEK293 cells transfected with 2.5 µg of FLAG-CaSR or empty pcDNA3.1 in 20 × 20 mm coverslips was treated with Ca^{2+}. The cells were subjected to immunostaining using rabbit anti CaSR-antibody (ab137408) at 1:100 dilution and mouse anti CHIP antibody at 1:200 dilution. Secondary goat anti mouse Alexa fluor 488 at 4 µg/mL and secondary goat anti rabbit Alexa fluor 647 at 4 µg/mL were used. Image-J was used to process the co-localization. Yellow represents co-localization. Surface plot of pixel intensities from confocal images of the area marked in grey square of HEK293 cells expressing FLAG-CaSR and endogenous CHIP after 4mM Ca^{2+} treatment show similar corresponding peaks. Co-localization is observed on the membrane.

intensities from confocal images of the area marked in grey square of HEK293 cells was plotted. The cells expressing FLAG-CaSR and endogenous GRP78 after 4mM Ca^{2+} treatment show similar corresponding peaks **(Figure 2.14)**. Co-localization is observed on the membrane as well as interior of cell. Similarly, CHIP after 4mM Ca^{2+} treatment show similar corresponding peaks in surface plot as well as show significant yellow in the merged image suggesting high degree of

colocalization of CHIP with CaSR. In order to figure out where the co-localization is taking place, we carried out the study with ER and CaSR. Surface plot of pixel intensities from confocal images of the area marked in grey square of HEK293 cells expressing FLAG-CaSR and ER after 4mM Ca^{2+} treatment show similar corresponding peaks. Co-localization is observed on the interior of cell. Not only is the ER and CaSR localized, but for the same cells, ER and Bip is also observed.

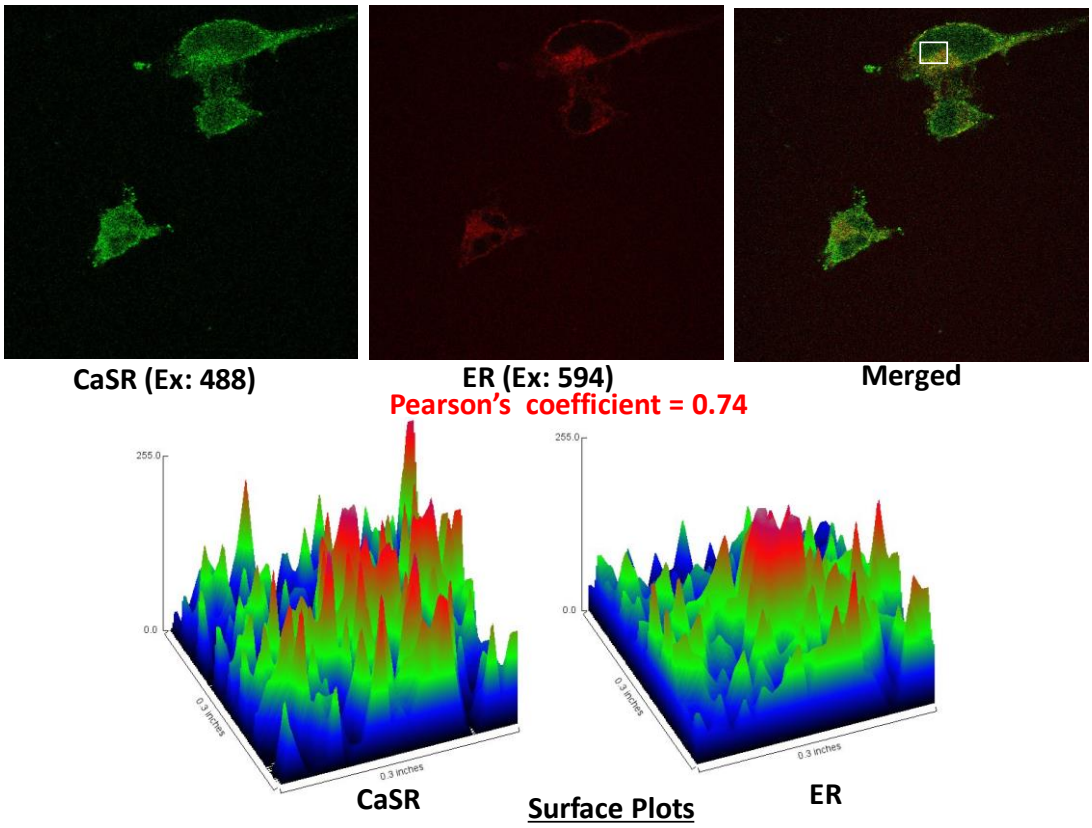

Figure 2.16 *CaSR co-localized with ER.*

HEK293 cells transfected with 2.5 µg of FLAG-CaSR or empty pcDNA3.1 in 20 × 20 mm coverslips was treated with Ca^{2+}. The cells were subjected to immunostaining using mouse anti FLAG-antibody at 1:1500 dilution and ER tracker dye at 1 µM. Secondary goat anti mouse Alexa fluor 488 at 4 µg/mL was used. Image-J was used to process the co-localization. Yellow represents co-localization. Surface plot of pixel intensities from confocal images of the area marked in grey square of HEK293 cells expressing FLAG-CaSR and ER after 4mM Ca^{2+} treatment show similar corresponding peaks. Co-localization is observed on the interior of cell.

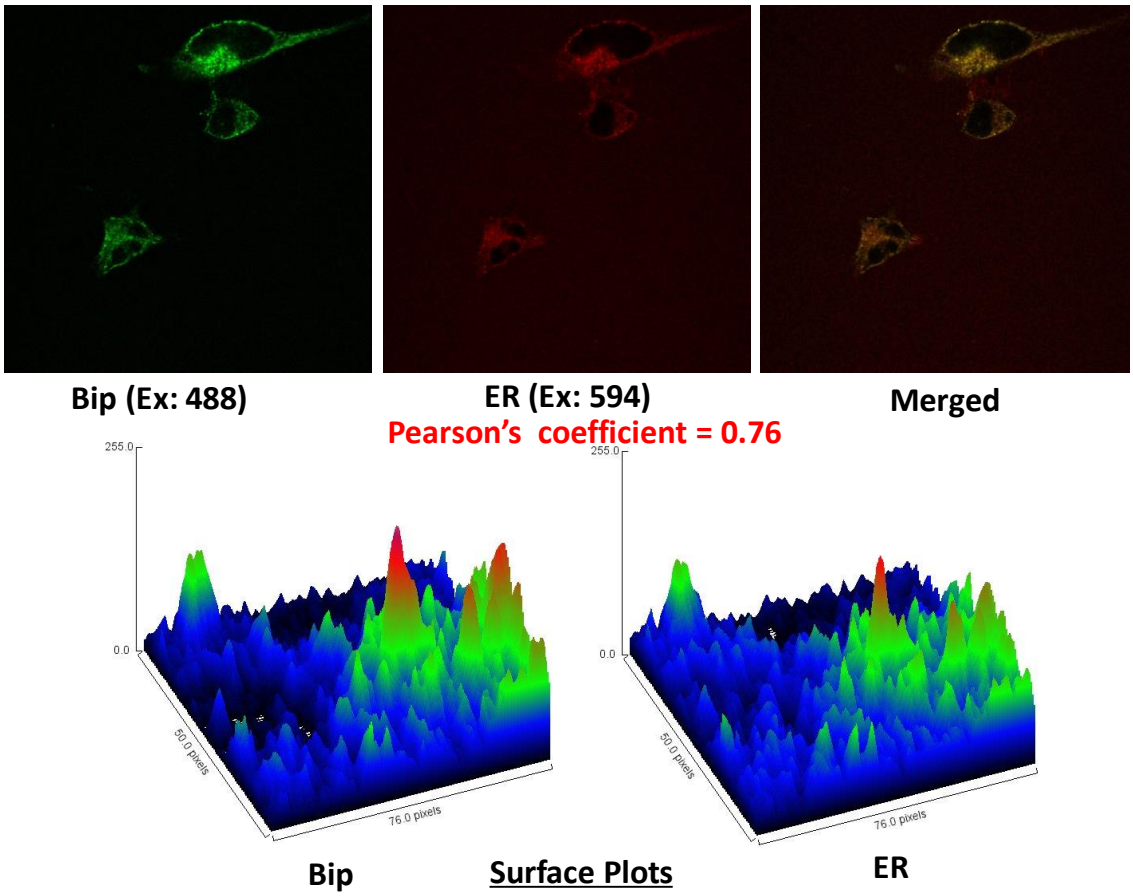

Figure 2.17 Colocalization of Bip and ER at 4mM Ca^{2+}

HEK293 cells transfected with 2.5 µg of FLAG-CaSR or empty pcDNA3.1 in 20 × 20 mm coverslips was treated with Ca^{2+}. The cells were subjected to immunostaining using mouse anti FLAG-antibody at 1:1500 dilution and ER tracker dye at 1 µM. Secondary goat anti mouse Alexa fluor 694 at 4 µg/mL was used and pseudo color red was given for image-J processing. Image-J was used to process the co-localization. Yellow represents co-localization. Surface plot of pixel intensities from confocal images of the area marked in grey square of HEK293 cells expressing Bip and ER after 4mM Ca^{2+} treatment show similar corresponding peaks. Co-localization is observed on the interior of cell.

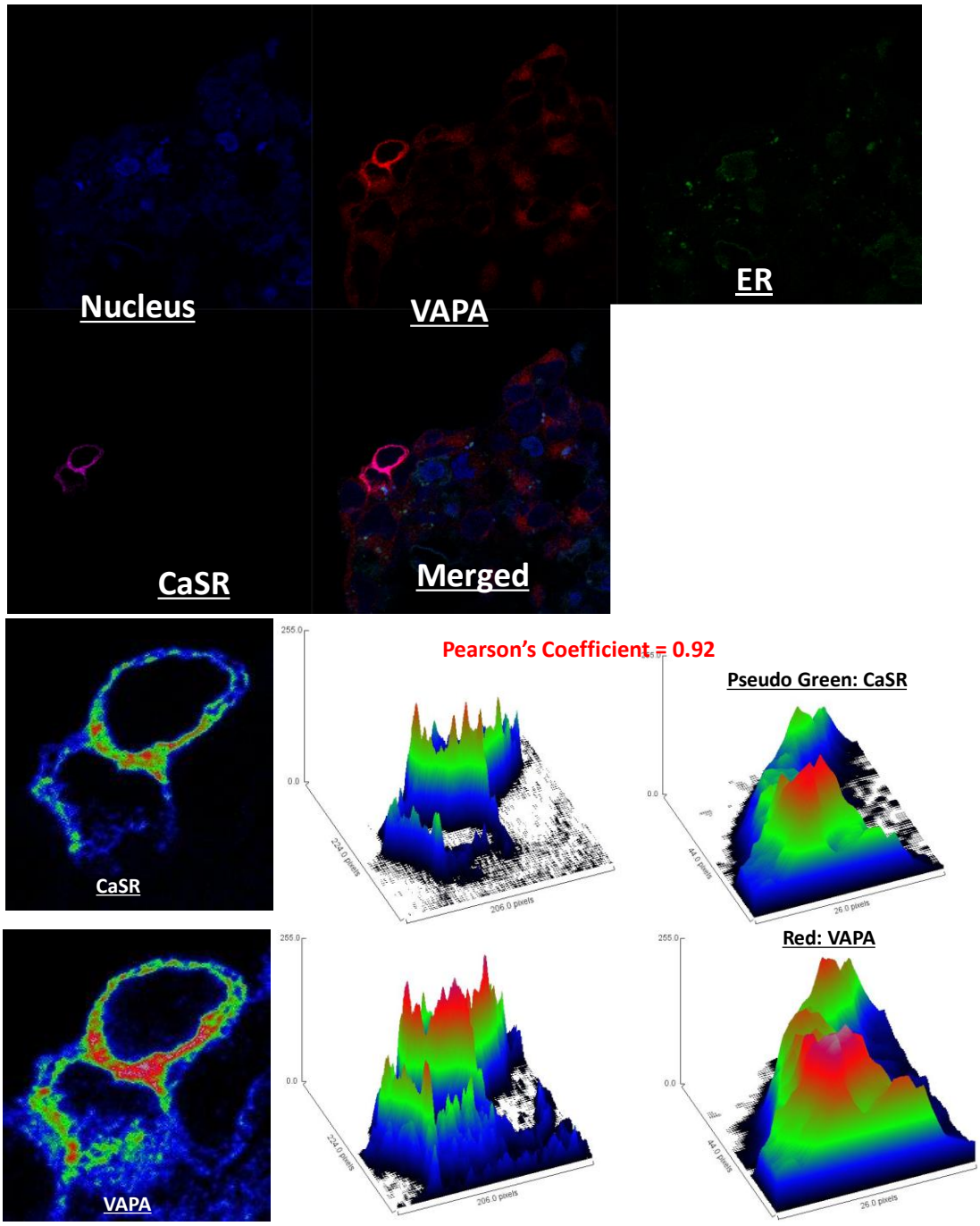

Figure 2.18 Colocalization of VAPA and CaSR at 4mM Ca^{2+}

HEK293 cells transfected with 1.5 µg of FLAG-CaSR or empty pcDNA3.1 in 20 × 20 mm coverslips was treated with Ca^{2+}. The cells were subjected to immunostaining using mouse anti FLAG-antibody at 1:1500 dilution and anti VAPA antibody at 2µg/mL. Secondary goat anti mouse Alexa fluor 647 and anti-rabbit Alexa fluor 550 at 4 µg/mL were used. Surface plot of pixel intensities from confocal images of the area marked in grey square of HEK293 cells expressing VAPA and CaSR after 4mM Ca^{2+} treatment show similar corresponding peaks.

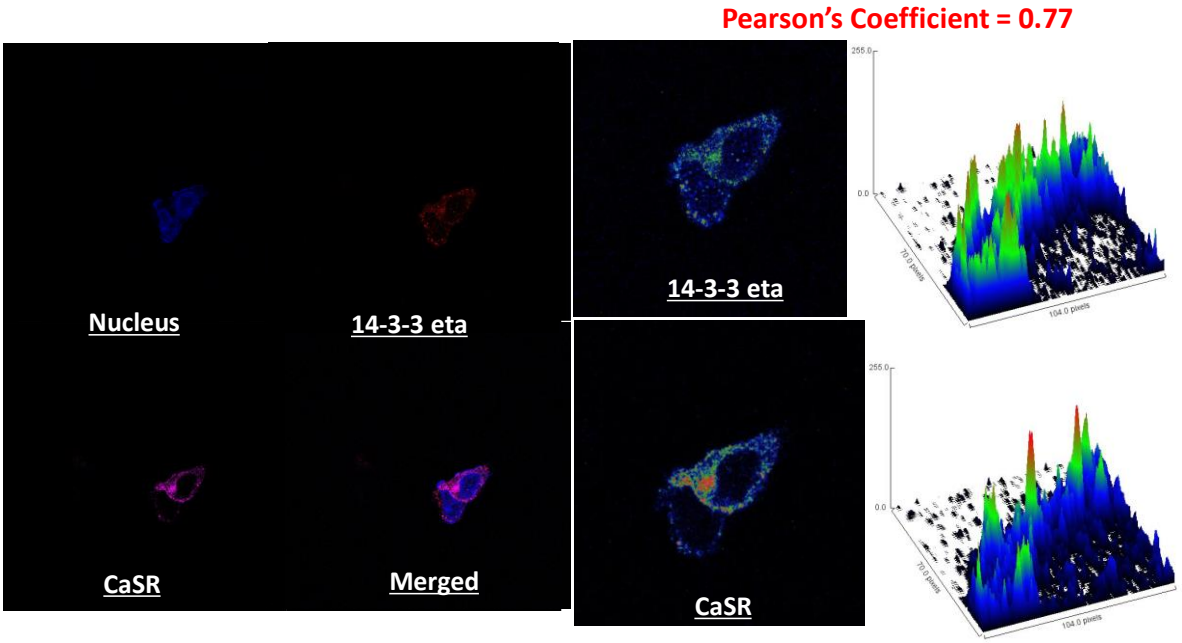

Figure 2.19 Colocalization of 14-3-3 eta and FLAG-CaSR at 4mM Ca^{2+}

2.6.9 ER oscillation mediated by CaSR

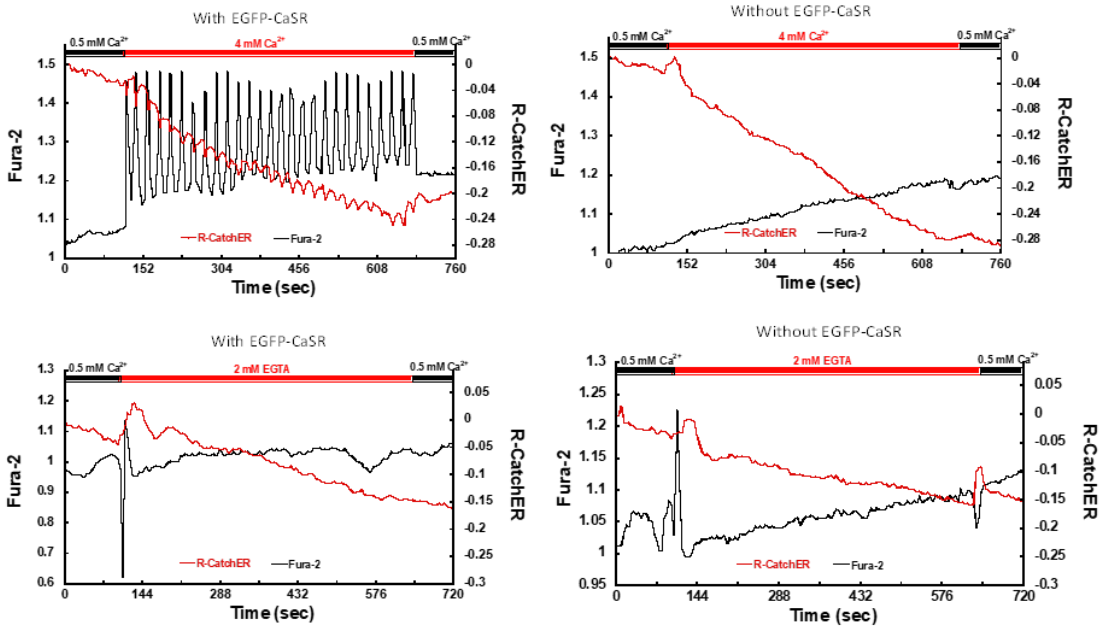

Figure 2.20 ER oscillation is triggered by the extracellular Ca^{2+} perturbation at 4 mM Ca^{2+} ((as observed by a recombinant red sensor which is not yet published)

This oscillation coordinates with the intracellular Ca^{2+} oscillation mediated by CaSR. This ER oscillation mediated by CaSR activation must code for cellular processes involved in biosynthesis, ER quality control and trafficking of CaSR.

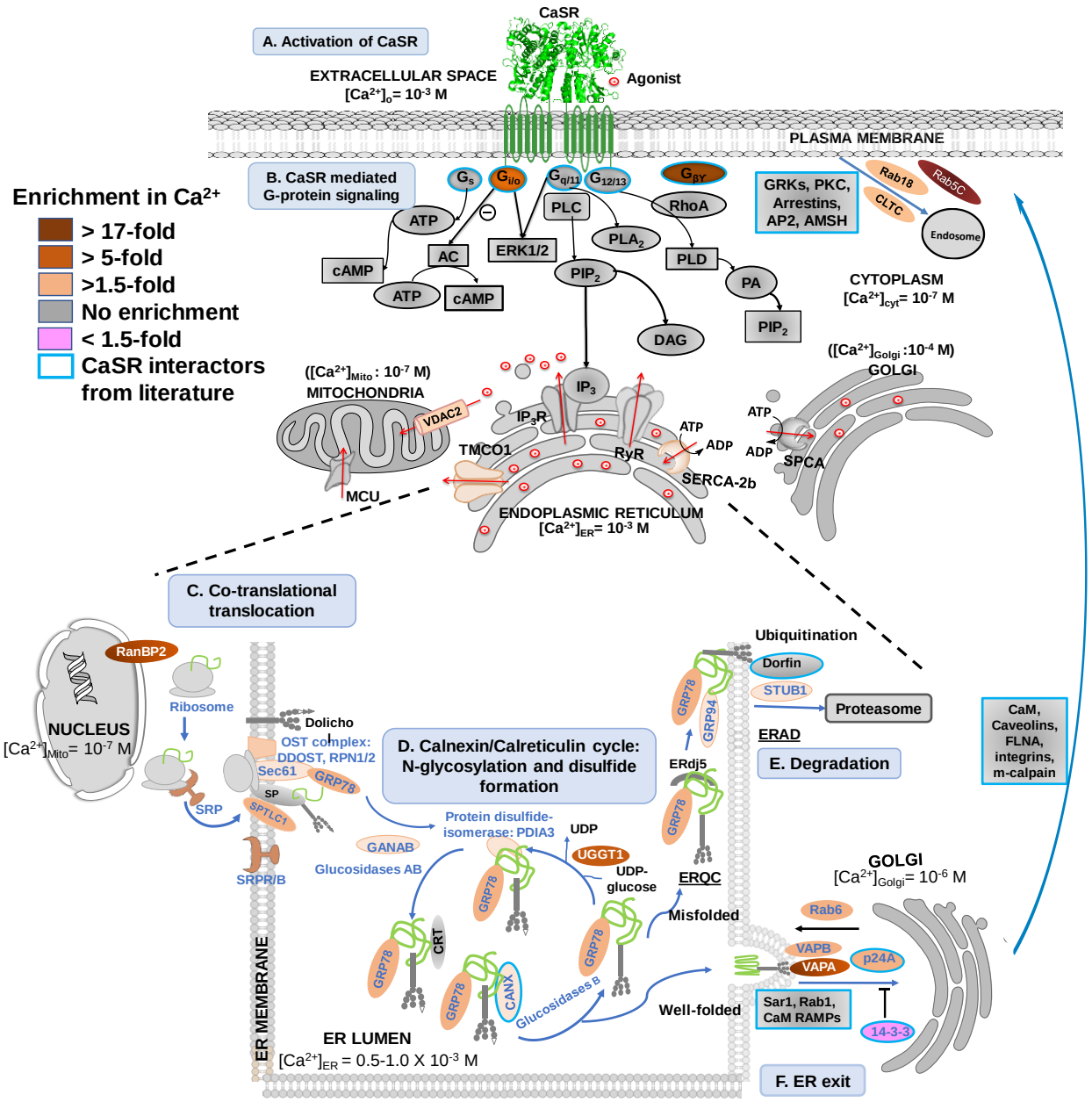

Figure 2.21 The schematic model of CaSR mediated signaling, ER quality control and ADIS of CaSR invoked through extracellular Ca^{2+} perturbation.

Identified proteins from the experiment are colored; dark brown representing ≥ 17 folds, brown representing ≥ 5 and < 17 folds and light brown representing ≥ 1.5 and < 5 folds enrichment ($log_2(Ca^{2+}$/EGTA)-positive controls). Treatment of 4 mM Ca^{2+} influenced the CaSR interactome involved in biosynthesis, trafficking and Ca^{2+} handling. A.CaSR is activated with 4 mM extracellular Ca^{2+}. B. CaSR mediated G-protein signaling: Ca^{2+}induces CaSR mediated phospho-lipase C(PLC) activation and subsequently, IP_3 invoked release of Ca^{2+} from the ER. Additionally, Ca^{2+} dependent $G\alpha_i$ invoked inhibition of acetyl cyclase is induced. Ca^{2+} handling proteins (SERCA-2b, TMCO1, VDAC2, TIMM50) are enriched in the presence of Ca^{2+}.

Alteration in $Ca^{2+}{}_{ER}$ induce amplification of CaSR biosynthesis in the ER. C. Co-translational translocation: The newly synthesized polypeptide bound to the signal recognition particle (SRP) is directed to the ER membrane to the Sec complex by the SRP receptor. Release of SRP and SRP receptor allows translocation.After processing of signal sequence by signal peptidase (SP) complex, the oligosaccharyl transferases (OST: DDOST and RPN1/2) and palmitoyl-transferase-SPTLC1 catalyzes the transfer of oligosaccharides. GRP78 chaperones CaSR polypeptide to ER lumen. Glucosidases GANAB allows for the removal of outermost glucose residues. D. Calnexin cycle: Lectin chaperones calnexin (CNX) and/or calreticulin (CLTC) along with GRP78 promotes proper folding by preventing aggregation and premature export from the ER. PDIA3, a protein disulfide isomerase catalyzes the disulfide formation. Next, innermost glucose is cleaved by glucosidase and the CaSR is released from the cycle. UGGT, a glucosyl transferase acts as a check- point where improperly folded CaSR is re-glucosylated. E. Degradation pathway: Terminally misfolded CaSR undergo ERAD and are ubiquitinated through E3 ligases STUB1 and RanBP2, or, CaSR from the plasma membrane can be endocytosed assisted by Rab5, Rab18 and clathrin heavy chain-CLTC. F. ER-exit: Properly folded CaSR anterograde trafficking from the ER to the Golgi assisted by VAPA and VAPB as well as chaperone proteins p24A. Rab6 assist in retrograde trafficking from Golgi to the ER. Similarly, 14-3-3 allows the CaSR to retain in the ER in the absence of Ca^{2+}.

Heterotrimeric G-proteins are known GPCR interactors [132-134] and activated GPCRs transduce downstream signaling through GTP-bound Gα and Gβγ dissociation. G-proteins, $G\alpha_i$, and $G\beta_2$ are detected exclusively in the presence of Ca^{2+}, up-regulated at 12.5- and 22-folds, respectively. $G\alpha_i$ mediates inhibition of the cAMP dependent pathway through inhibition of adenylate cyclase [137]. On the other hand, $G\beta_2$ is a part of GβϒComplex that modulates activity of effectors and regulators, including enzymes and several forms of potassium and calcium ion channTable 2. 2 The heat map of proteins involved in the working modelels [139] and Gβϒ inhibitor, gallein is shown to block the signaling induced anterograde trafficking [14]. $G\beta_2$ is closely associated with microtubule assembly [140] and substrate recognition to recruit a specific substrate to a cullin-RING E3 ubiquitin ligase for GPCR regulation [141]. We know that Gq/11 activates phospholipase C, which in turn transduce the inositol triphosphate (IP_3) induced $Ca^{2+}{}_{ER}$ release causing increase in the $Ca^{2+}{}_{cyt}$. Physiologically, ER lumen Ca^{2+} concentration is maintained within the 100–500 µM range, whereas, the cytosolic at 5-50 nM [152] through a large number of Ca^{2+} binding proteins that act as chaperones and buffers [153]. Many of the channels and pumps involved in sustaining the Ca^{2+} concentration at the ER and cytoplasm such as SERCA, TMCO1 and VDAC are enriched in the presence of Ca^{2+}. This must be a compensatory mechanism to maintain the Ca^{2+} homeostasis. One of the most ubiquitous isoforms of SERCA with highest Ca^{2+} affinity, namely, ATP2A2 (SERCA-2b) [154] is found to be enriched at 2.3 folds. SERCA is a known class B, GPCR (glucagon receptor) interactor [132]. Modulation of SERCA activity and expression level maintains the resting $Ca^{2+}{}_{cyt}$ concentration by rapid re-uptake of Ca^{2+} into the ER once the ER/SR Ca^{2+} is released into the cytoplasm [154]. In gain of function mutation of CaSR, SERCA expression is known to increase [155]. Additionally, our result show a 1.5-folds enrichment of an ER transmembrane channel, TMCO1, which is known to respond to the ER luminal Ca^{2+} overloading by homo-tetramerization and by functioning as Ca^{2+} load-activated Ca^{2+} (CLAC) release channel maintaining ER Ca^{2+} homeostasis [156]. Therefore, TMCO1 and SERCA may work opposing to each other to maintain the Ca^{2+} concentration in the ER and cytosol. We propose that the CaSR mediated G-protein signaling is directly linked with CaSR ER quality control (ERQC) through the above crosstalk with ER Ca^{2+} signaling.

Table 2.10 The heat map of proteins involved in the working model

Protein names	Gene names	Log_2 [positive/negative control] - Ca^{2+}	Log_2 [positive/negative control] - EGTA	Log_2 (Ca^{2+}/EGTA)-Positive control
Vesicle-associated membrane protein-associated protein A	VAPA	5.19	-0.53	5.42
UDP-glucose:glycoprotein glucosyltransferase 1	UGGT1	4.79	0.20	4.48
Guanine nucleotide-binding protein G(I)/G(S)/G(T) subunit beta-2	GNB2	5.02	1.00	4.43
E3 SUMO-protein ligase RanBP2	RANBP2	3.86	0.39	4.39
Signal recognition particle receptor subunit alpha	SRPR	3.29	-0.41	4.11
Ras-related protein Rab-5C	RAB5C	4.31	1.18	4.10
Signal recognition particle receptor subunit beta	SRPRB	6.69	2.84	3.74
Guanine nucleotide-binding protein subunits G(k); G(i) alpha-1; G(i) alpha-2; G(o) alpha	GNAI3	6.75	1.04	3.64
Serine palmitoyltransferase 1	SPTLC1	3.04	0.59	2.74
Vesicle-associated membrane protein-associated protein B/C	VAPB	3.34	1.00	2.37
78 kDa glucose-regulated protein	HSPA5	4.25	2.69	2.30
Sodium/potassium-transporting ATPase subunit alpha-1; alpha-3; alpha-2	ATP1A1	4.76	1.81	2.20
Ras-related protein Rab-6A;Ras-related protein Rab-6B;Ras-related protein Rab-39A	RAB6B	3.19	1.26	1.96
Protein disulfide-isomerase A3	PDIA3	5.19	3.28	1.60
Ras-related protein Rab-18	RAB18	2.15	1.70	1.51
Dolichyl-diphosphooligosaccharide--protein glycosyltransferase subunit 1	RPN1	7.07	5.51	1.35
Protein transport protein Sec61 subunit beta	SEC61B	3.40	2.18	1.33
Sarcoplasmic/endoplasmic reticulum calcium ATPase 2	ATP2A2	6.81	6.36	1.18
Endoplasmin	HSP90B1	4.18	2.93	1.10
Clathrin heavy chain;Clathrin heavy chain 1	CLTC	2.37	1.92	1.05
Dolichyl-diphosphooligosaccharide--protein glycosyltransferase 48 kDa subunit	DDOST	2.21	1.93	1.02
40S ribosomal protein S27	RPS27	3.49	3.93	0.90
DnaJ homolog subfamily A member 1	DNAJA1	3.16	4.37	0.86
E3 ubiquitin-protein ligase CHIP	STUB1	3.06	2.43	0.78
Neutral alpha-glucosidase AB	GANAB	7.22	6.63	0.76
Calnexin	CANX	6.57	6.69	0.71
Heat shock protein HSP 90-alpha	HSP90AA1	3.24	2.84	0.69
Dolichyl-diphosphooligosaccharide--protein glycosyltransferase subunit 2	RPN2	4.68	4.79	0.68
Voltage-dependent anion-selective channel protein 2	VDAC2	3.11	3.03	0.66
Extracellular calcium-sensing receptor	CASR	11.61	14.32	0.30
Heat shock 70 kDa protein 1A	HSPA1A	2.03	2.88	0.26
60S ribosomal protein L22	RPL22	0.63	1.11	0.24
BAG family molecular chaperone regulator 2	BAG2	6.08	5.83	0.17
14-3-3 protein gamma;14-3-3 protein gamma, N-terminally processed	YWHAG	2.04	2.75	-0.04
14-3-3 protein epsilon	YWHAE	4.42	4.91	-0.80
14-3-3 protein theta	YWHAQ	4.68	7.46	-1.08
14-3-3 protein zeta/delta	YWHAZ	3.72	4.54	-1.38

2.6.10 CHIP ubiquitination of CaSR

CHIP (carboxyl terminus of Hsc70-interacting protein) or STUB1 is a E3 ubiquitin ligase targeting the misfolded chaperone substrates which direct them towards proteasomal degradation.

It is a U-box type E3 ligase that carried out a function of a chaperone [157]. CHIP is known to attenuate ATP hydrolysis and inhibit the cycle of Hsc70/Hsp70 [157]. Additionally, it is a known target for Hsp90 and Hsp70 for 26S proteasomal degradation [157]. Only dorfin has been identified as a degradation enzyme related with CaSR. We identified an upregulation of CHIP interaction with CaSR in the presence of Ca^{2+} suggesting a new proteasomal degradation pathway possibly dependent on Ca^{2+}. We collaborated with Dr. Jun Yin and Li Zhou where we obtained the CHIP knocked down HEK293 cells. We expect to observe a change in the level of ubiquitination which appears as a smear for various degree of ubiquitination on CaSR. Unfortunately, our experiments still require optimization. We did not observe obvious changes between the CHIP knocked down HEK293 cells and the normal HEK293 cells. Additionally, we did not detect any distinct change in the smear due to Ca^{2+} **(Figure 2.22, Figure 2.23**).

For future, we will have to optimize the presence of the oligomer CaSR as it acts as a limit for the observation of a clear smear for ubiquitination. Also, the western blot has to be optimized to obtain a clear band. Furthermore, it is important to obtain the knock in of CHIP in the experiment which for some reason has not been able to achieve especially in the shCHIP knocked down HEK293 cells. The negative control for HEK293 cells without CaSR transient transfection does not provide a good result as well. Therefore, the Co-IP has to be improved, possibly with more stringent washing or using anti-CHIP antibody to pull out CaSR.

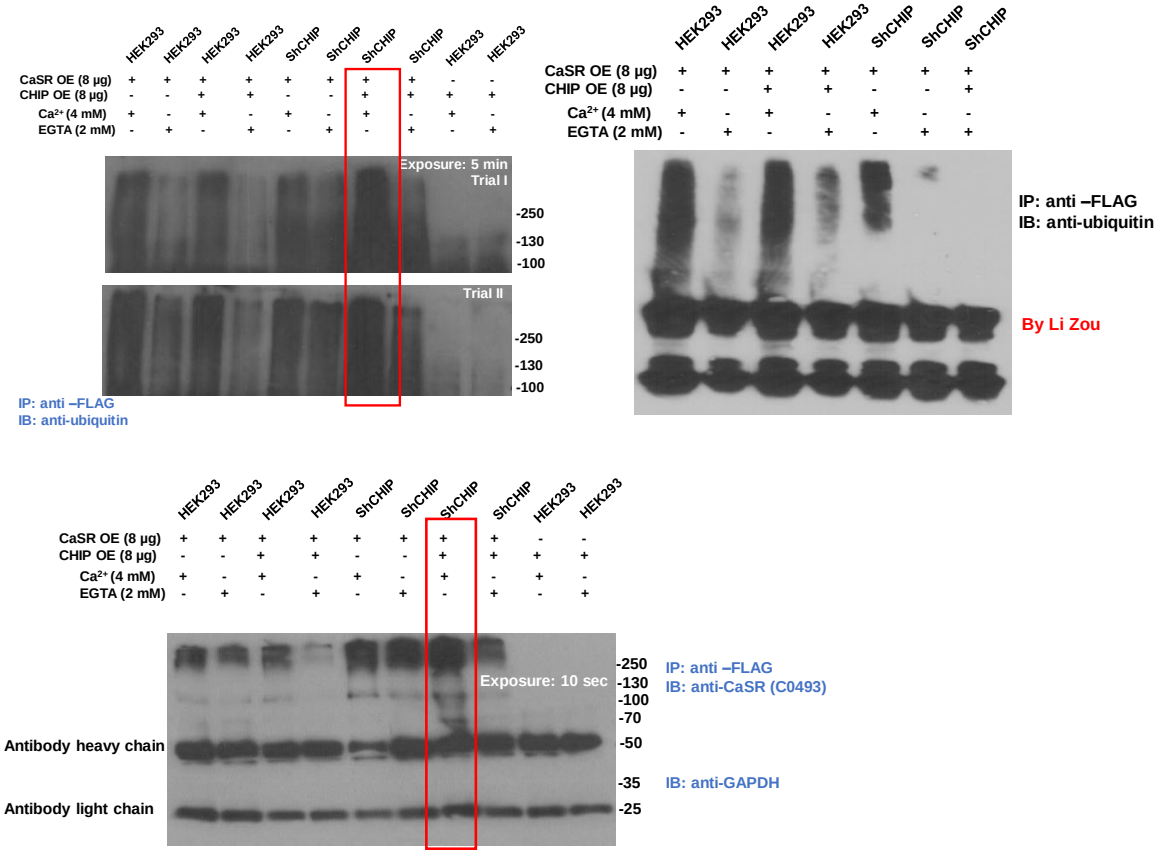

Figure 2.22 Ubiquitination of CaSR by CHIP assay trial I.

Ubiquitination of CaSR is evidently higher in the presence of 4 mM Ca^{2+} as compared to 2 mM EGTA in HEK293 cells and ShCHIP HEK293 cells. OE of CHIP in HEK293 cells and CHIP KD HEK293 cells do not have apparent change in ubiquitination, respectively. Therefore, these results do not support our hypothesis of CHIP ubiquitination of CaSR. OE of both CaSR and CHIP in ShCHIP HEK293 cells in the presence of 4 mM Ca^{2+}, which supports our hypothesis. Results from Li matched my results but his OE of CaSR and CHIP in ShCHIP HEK293 cell data is missing for confirmation

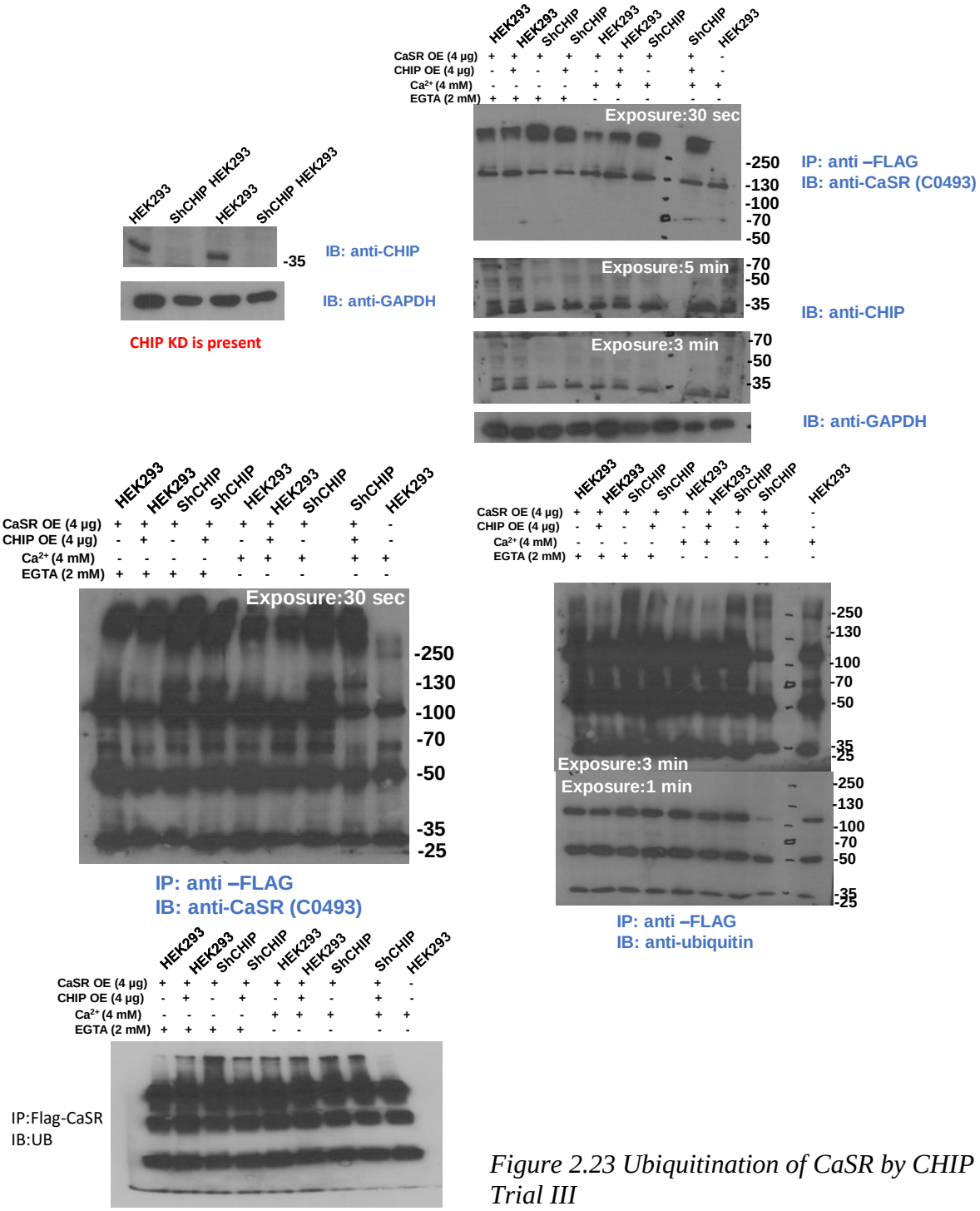

Figure 2.23 Ubiquitination of CaSR by CHIP Trial III

ShCHIP HEK293 has good KD of CaSR. CaSR total is seen but disproportionate in total input for some reason. Not sure what 130-150 kDa species is as it is present throughout the negative control and IB of CaSR, Ub in total. CaSR IP is present in all samples but not same throughout. Negative control is clean but 100 kDa blot is seen meaning it is not CaSR. Ubiquitin does not have any trend between Ca2+ and EGTA. Also, no trend between CHIP KD or control

2.6.11 Ca^{2+} and CaM binding sites prediction on CHIP and GRP78

(PDB: 2C2L)

2559 4854 9497 9500 (related four ligand oxygen atom IDs in the file: 2c2l.pdb)
ASN57B ASN57C SO41305B SO41305B (related four residue type and IDs in the file: 2c2l.pdb)
-27.481 8.422 24.124(psdCa coordinates)
2.212 (psdCa-O)

4039 4054 4063 4175 (related four ligand oxygen atom IDs in the file: 2c2l.pdb)
SER237B GLU239B LEU240B ASP254B (related four residue type and IDs in the file: 2c2l.pdb)
21.530 6.261 27.633(psdCa coordinates)
2.392 (psdCa-O)

8629 8644 8653 8765 (related four ligand oxygen atom IDs in the file: 2c2l.pdb)
SER237D GLU239D LEU240D ASP254D (related four residue type and IDs in the file: 2c2l.pdb)
-16.417 -55.688 44.579(psdCa coordinates)
2.397 (psdCa-O)

3583 3611 3648 3649 (related four ligand oxygen atom IDs in the file: 2c2l.pdb)
GLN182B HIS185B GLU189B GLU189B (related four residue type and IDs in the file: 2c2l.pdb)
32.962 18.472 93.141(psdCa coordinates)
2.491 (psdCa-O)

8173 8201 8238 8239 (related four ligand oxygen atom IDs in the file: 2c2l.pdb)
GLN182D HIS185D GLU189D GLU189D (related four residue type and IDs in the file: 2c2l.pdb)
-4.234 -68.020 -20.756(psdCa coordinates)
2.497 (psdCa-O)

1744 1759 1768 1880 (related four ligand oxygen atom IDs in the file: 2c2l.pdb)
SER237A GLU239A LEU240A ASP254A (related four residue type and IDs in the file: 2c2l.pdb)
27.025 -18.768 37.034(psdCa coordinates)
2.748 (psdCa-O)

6334 6349 6358 6470 (related four ligand oxygen atom IDs in the file: 2c2l.pdb)
SER237C GLU239C LEU240C ASP254C (related four residue type and IDs in the file: 2c2l.pdb)
-10.912 -30.655 35.097(psdCa coordinates)
2.755 (psdCa-O)

8552 8553 8557 8576 (related four ligand oxygen atom IDs in the file: 2c2l.pdb)
ASP227D ASP227D ILE228D ASP230D (related four residue type and IDs in the file: 2c2l.pdb)
-6.642 -57.204 36.758(psdCa coordinates)
2.800 (psdCa-O)

3962 3963 3967 3986 (related four ligand oxygen atom IDs in the file: 2c2l.pdb)
ASP227B ASP227B ILE228B ASP230B (related four residue type and IDs in the file: 2c2l.pdb)
31.236 7.755 35.593(psdCa coordinates)
2.803 (psdCa-O)

5872 5878 5882 5943 (related four ligand oxygen atom IDs in the file: 2c2l.pdb)
CYS181C GLN182C GLN182C GLU189C (related four residue type and IDs in the file: 2c2l.pdb)
-35.300 -61.654 -10.270(psdCa coordinates)
2.909 (psdCa-O)

1282 1288 1292 1353 (related four ligand oxygen atom IDs in the file: 2c2l.pdb)
CYS181A GLN182A GLN182A GLU189A (related four residue type and IDs in the file: 2c2l.pdb)
2.006 12.051 82.207(psdCa coordinates)
2.910 (psdCa-O)

264 9482 9483 9484 (related four ligand oxygen atom IDs in the file: 2c2l.pdb)
ASN57A SO41305A SO41305A SO41305A (related four residue type and IDs in the file: 2c2l.pdb)
11.288 -59.966 47.495(psdCa coordinates)
2.953 (psdCa-O)

Figure 2.24 Ca^{2+} binding sites predicted for CHIP (2C2L) using GG

PDB: 5o4p

7514 7516 7807 7809 (related four ligand oxygen atom IDs in the file: 5o4p.pdb)
THR485B THR485B THR525B THR525B (related four residue type and IDs in the file: 5o4p.pdb)
47.691 21.207 34.662(psdCa coordinates)
2.019 (psdCa-O)

4046 4064 4078 4252 (related four ligand oxygen atom IDs in the file: 5o4p.pdb)
GLY36B TYR39B SER40B SER64B (related four residue type and IDs in the file: 5o4p.pdb)
86.368 26.244 42.612(psdCa coordinates)
2.184 (psdCa-O)

44 49 1105 1335 (related four ligand oxygen atom IDs in the file: 5o4p.pdb)
ASP34A LEU35A THR171A GLU201A (related four residue type and IDs in the file: 5o4p.pdb)
69.713 -5.626 -0.123(psdCa coordinates)
2.491 (psdCa-O)

4033 4038 5088 5318 (related four ligand oxygen atom IDs in the file: 5o4p.pdb)
ASP34B LEU35B THR171B GLU201B (related four residue type and IDs in the file: 5o4p.pdb)
83.367 20.948 42.197(psdCa coordinates)
2.491 (psdCa-O)

5317 5492 5493 8040 (related four ligand oxygen atom IDs in the file: 5o4p.pdb)
GLU201B ASP224B ASP224B SO4603B (related four residue type and IDs in the file: 5o4p.pdb)
84.122 18.045 48.175(psdCa coordinates)
2.842 (psdCa-O)

7738 7755 7769 7785 (related four ligand oxygen atom IDs in the file: 5o4p.pdb)
ASP515B GLY517B ASN520B ASN522B (related four residue type and IDs in the file: 5o4p.pdb)
43.090 10.177 29.432(psdCa coordinates)
2.843 (psdCa-O)

1500 1504 1528 1548 (related four ligand oxygen atom IDs in the file: 5o4p.pdb)
ASP224A ASP224A ALA229A ASP231A (related four residue type and IDs in the file: 5o4p.pdb)
69.990 -0.853 -6.204(psdCa coordinates)
2.887 (psdCa-O)

Figure 2.25 Ca^{2+} binding sites predicted for GRP78 (5O4P) using GG

7369 7373 7375 7379 (related four ligand oxygen atom IDs in the file: 2c63.pdb)
SEP4P SEP4P SEP4P LEU5P (related four residue type and IDs in the file: 2c63.pdb)
5.951 -5.648 16.816(psdCa coordinates)
2.334 (psdCa-O)

4969 4983 5313 5315 (related four ligand oxygen atom IDs in the file: 2c63.pdb)
GLN166C THR168C THR210C THR210C (related four residue type and IDs in the file: 2c63.pdb)
20.287 51.024 -2.087(psdCa coordinates)
2.438 (psdCa-O)

Figure 2.26 No Ca^{2+} binding sites was predicted for 14-3-3 eta using GG.

Calcium pattern search, on online search engine designed by Dr. Xue was used to find the putative Ca^{2+} binding sites. GG (Graph theory and Geometry) uses the graph theory and geometric parameters to identify oxygen clusters on Ca^{2+} sites [158] using the crystal structure provided. We show that a Ca^{2+} binding site was predicted in CHIP and GRP78. But, 14-3-3 eta does not have any sites **(Figure 2.24, Figure 2.25, Figure 2.26).** This could explain to an extent and suggests that change in extracellular Ca^{2+} resulted in intracellular and ER Ca^{2+} which further allowed these proteins to be activated.

CaM binding database was used to predict the CaM binding domains. This search engine uses sequence homology to tabulate the putative CaM binding sites on protein of interest. We found multiple CaM binding domains with high score in CHIP (**Figure 2.27**). Again, this suggests that with the CaSR mediated extracellular Ca2+ perturbation, the CaM which is a Ca^{2+} dependent protein, activates CHIP for its cellular function of ubiquitinating CaSR.

Figure 2.27 Motif score for putative CaM binding sites in E3 Ubiquitin Ligase CHIP

2.6.12 Mass spectrometry analysis for intra-cellular Ca^{2+} pertubation

These experiments were first batches of optimization for Co-IP. A trial was conducted for co-immunoprecipitation of FLAG-CaSR after treatment of extracellular 2 mM Ca^{2+} and 2 mM EGTA, and subsequently same treatments for intracellular after lysis of cells. The trail was repeated on different month and Orbitrap XL was used to generate the LC MS/MS for both on different days. Three stringencies were applied to obtain proteins upregulated in Ca^{2+} condition: (i) $\log_2$ intensity (Ca^{2+}/EGTA) > 0.584, (ii) $\log_2$ intensity (positive/negative controls)-Ca^{2+} > 0.584, and (iii) PSM (Ca^{2+}) > 10. Unfortunately, the resulting proteins between the two trials were only four out of the total 128 and 127 obtained, respectively. These four proteins were cytoplasmic dynein 1 heavy chain 1, translation initiation factor 5B, Myosin-9 and phosphatase. This result implies that our experiment was not reliable.

A second trial consisted of an additional 10 mM Ca^{2+} treatment apart from the 2 mM Ca^{2+} and 2 mM EGTA. Interestingly, even if the PSM of CaSR was lower by 3-fold in 10 mM Ca^{2+} as compared to other two treatments, there were number of proteins such as the 14-3-3 family (ζ, ε and θ) and CaM that were increased by greater than 3-fold when the extra- and intra- cellular Ca^{2+} was perturbed to 10 mM (**Figure 2.28, Table 2.11**). Higher Ca^{2+} is known to be used for greater IP of CaSR in previous literature. But this contradicted our result, thereby, suggesting a direct correlation of Ca^{2+} with the interaction.

Table 2.11 Analysis of CaSR and CaM with extra- and intra- cellular Ca^{2+} perturbation

Samples	Coverage of CaSR	CaSR PSM	CaSR Area	CaM PSM	CaM Area
HEK293 negative control	0	0	0.00E+00	1	4.86E+05
HEK293 + CaSR/2 mM EGTA	48.33024	123	2.50E+08	1	1.33E+05
HEK293 + CaSR/ 2 mM Ca^{2+}	45.36178	135	2.85E+08	0	0.00E+00
HEK293 + CaSR/10 mM Ca^{2+}	20.40441	40	4.94E+07	3	1.09E+07

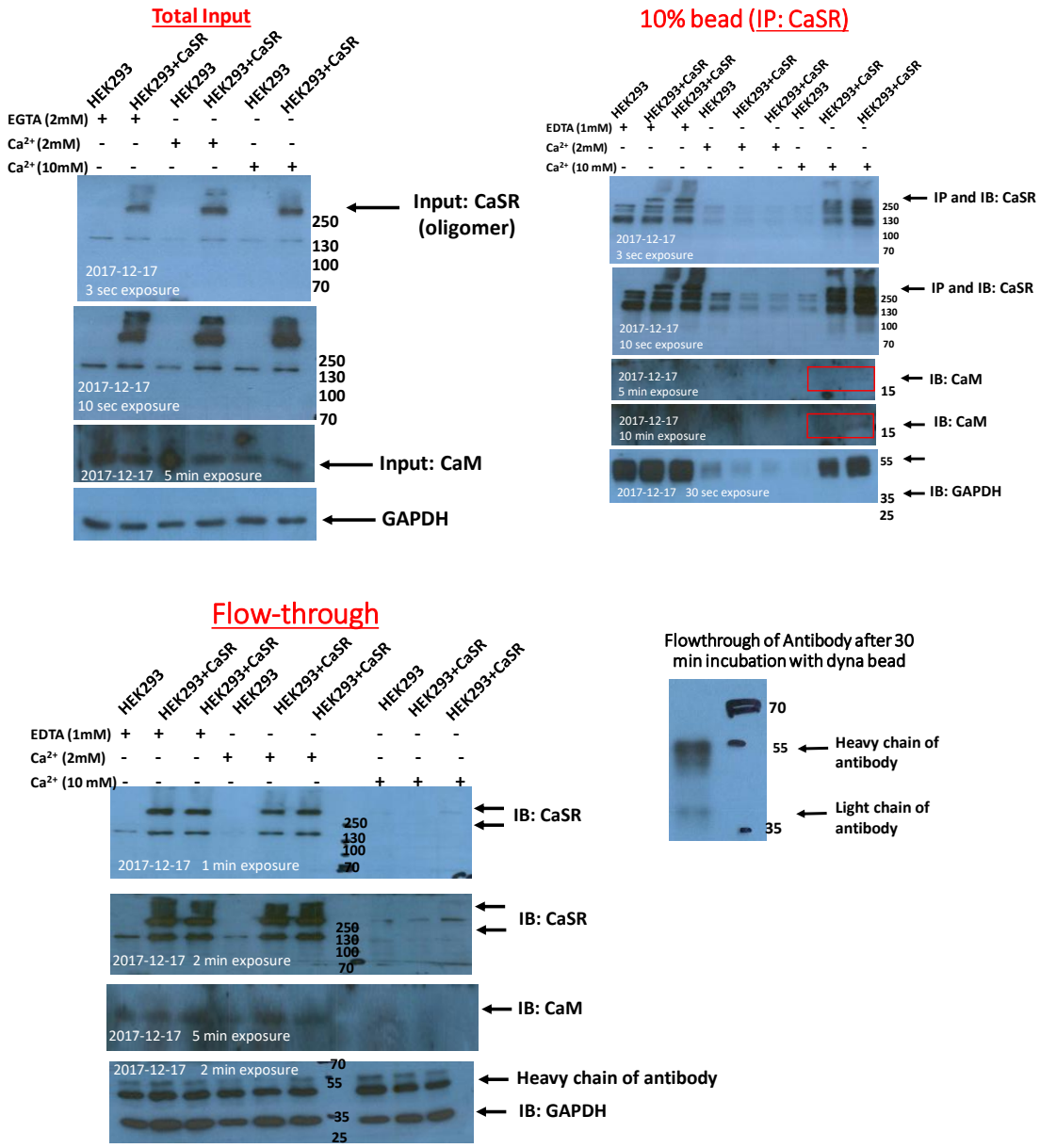

Figure 2.28 IP of CaSR and Co-IP of CaM in Trial II with intra- and extra-0cellular Ca^{2+} perturbation

Two plates for each condition were lysed for 30 min. 1.2 mg protein were used for IP using 10 µg of anti-FLAG antibody. The antibody was first incubated with dyna bead for 30 min at RT and subsequently, washed with lysis buffer. Antigen was added and incubated overnight at 4 degrees. The beads were washed and heated in sample buffer for 10 min at 70 degrees. All the samples were added with 10 mM DTT and 40 mM IAA and incubated in dark and RT for few hours.

Equivalent amount of total input of CaSR and CaM were observed (**Figure 2.28**). IP of CaSR for 10% bead produced multiple bands with the use of DTT and IAA. Ignoring the common bands in negative control HEK293, the major CaSR oligomer is absent in 2mM Ca^{2+} condition, possibly an error in western blot. Also, 10mM has similar amount of CaSR oligomer as the 2 mM EGTA condition which contradicts the MS result.

2.7 Discussion

To the best of our knowledge, this is the first comprehensive proteomics study examining the role of Ca^{2+} on CaSR interactome. During the experimental design and analysis, we employed rigorous and careful considerations to identify putative interactors of CaSR. All experiments were conducted in triplicates, appropriate negative controls were used to identify and avoid background signals, magnetic beads were used as they give a low background of the contaminant proteins [159], a very stringent statistical analysis was employed, and a total lysate MS/MS was conducted to circumvent the un-specific binding due to general enrichment in the cell. In our study, we employed co-immunoprecipitation, LC-MS/MS and gene ontology to report novel CaSR interactors, study the influence of chronic exposure of extracellular Ca^{2+} and provide a putative relative quantitative measure of the interactions. The major significance of our study is the identification of 100 novel CaSR interactors, many of which have been validated for other members of GPCR family. This adds to the significance of our work, indicating them as functionally relevant. Additionally, eight previously known CaSR interactors involved in signaling and trafficking were re-validated, namely, $G\alpha_i$ [132-134], $G\beta_2$ [132-134], 14-3-3 θ [135], 14-3-3 ζ [135], 14-3-3 ε [135], 14-3-3 γ [135], p24 [136] and calnexin [14]. Most importantly, we observe an enrichment ranging from 2- 43 folds in 65% of the 106 total proteins in the presence of extracellular Ca^{2+}. These proteomes are affiliated with (i) the signal transduction, (iii) regulatory

intracellular proteins maintaining Ca^{2+} handling and (iii) quality control of the maturation of CaSR in the ER and trafficking to the plasma membrane.

ERQC is a surveillance system which monitors proper folding of membrane protein and its trafficking to the membrane or facilitation of degradation of misfolded proteins. CaSR trafficking is dynamic and it undergoes ADIS where the intracellular pool of CaSR is mobilized to the plasma membrane due to exposure to Ca^{2+} [115, 116]. ER chaperones and regulators are dependent on the optimal Ca^{2+}_{ER} concentration for proper post-translational processing, folding and export of proteins [160] [161], and Ca^{2+}_{ER} concentration depletion is known to inhibit the proteins involved in folding and maturation. The gene ontology study showed that Ca^{2+} enriched the protein processing in the ER pertaining to protein folding and ER unfolded protein response. In keeping with our results, we propose that the treatment of Ca^{2+} as compared to EGTA manifests in the enrichment in proteins involved in the co-translational translocation and calnexin cycle in the ER, anterograde and retrograde trafficking in the ERGICs and degradation pathways in the cytosol [162]. Signal recognition particle (SRP) receptor is enriched by 17 folds and it may direct nascent CaSR polypeptides to the Sec complex (enriched by 2.5 folds) on the ER membrane. After the release of SRP and SRP receptor, the polypeptide signal sequence is known to be processed by signal peptidase (SP) complex. Oligosaccharyl transferases (OSTs: DDOST and RPN1/2, enriched by 2-4 folds)) and palmitoyl-transferase (SPTLC1, enriched by 7 folds) which catalyzes the transfer of oligosaccharides are identified as CaSR interactors. Glycosylation blocker, tunicamycin has been shown to impede the anterograde trafficking as well [14]. We can concur that enrichment of SPTLC1 interaction with CaSR could be a result of overall upregulation of its expression as observed in total cell lysate. HSPA5/GRP78 is a major ER chaperone and its expression level has direct impact on compensatory activities of mitochondrial and ER [163]. In this study GRP78 is

enriched by 5 folds and may direct CaSR polypeptide to ER lumen where glucosidases (GANAB, enriched by 1.7 folds) catalyzes the removal of outermost glucose residues. Next, polypeptides undergo calnexin cycle where lectin chaperones, calnexin (CANX, enriched by 1.6 folds) and/or calreticulin (CLTC) along with GRP78 which can promote proper folding by preventing aggregation and premature export from the ER. Calnexin is known to have high Ca^{2+} binding affinity [164] and is known to interact transiently with varieties of soluble non-native conformers of glycoproteins. Calnexin cycle also contain PDIA3. It is a protein disulfide isomerase which catalyze the disulfide formation [165] and is enriched by 3 folds in the presence of Ca^{2+}. This step follows the cleavage of the innermost glucose by glucosidase and release of the CaSR from the calnexin-cycle. UGGT, a glucosyl transferase acts as a checkpoint where improperly folded CaSR is re-glucosylated and this enzyme is enriched by 22 folds in the presence of Ca^{2+}.

The properly folded CaSR exits the ER through anterograde trafficking to the Golgi assisted by VAP family proteins, VAPA (enriched by 43 folds) and VAPB (enriched by 5 folds) and by chaperone protein, p24A (enriched by 7 folds). p24 family is a type 1 transmembrane protein which interacts with cargo and COPI or COPII coatomers and have been shown to interact with CaSR as a limiting factor in CaSR trafficking in the early secretory pathway and suggested to assist in transportation to and from the ERGIC [136]. p24A is not presented in the 106-list due to low PSM of 1. VAP-A/B are involved in vesicle trafficking, membrane fusion, protein complex assembly, and cell motility [166]. VAPA is known to be involved in androgen receptor and oxysterol-binding protein related protein 3 trafficking from the ER [144]. Similarly, in the previous study, VAPB was identified as interactors of glucagon [132] and melatonin receptor type 1A [133]. Rabs are ubiquitously expressed, largest monomeric small GTPases and are involved in vesicle mediated transport including targeting, tethering and fusion of transport vesicles with acceptor membrane

[167]. Rab- 1, 7 and 11a are known CaSR interactors [145, 146]. Rab6 is associated with retrograde translocation from the Golgi to the ER and intra-Golgi transport [168] and are enriched by 4 folds in the presence of Ca^{2+}. Another protein involved with CaSR trafficking through ERGIC is 14-3-3 proteins. 14-3-3 family are known to play important role in regulation of cell signaling events and cellular trafficking [142, 143]. They have negative roles in CaSR dependent SRE activation through CaSR tail binding and 14-3-3 ζ has distinct function in lowering CaSR membrane expression [116, 135, 169]. Interestingly presence of extracellular Ca^{2+} decreased 14-3-3 proteins interaction with CaSR. We show that 14-3-3 (ζ, θ and ε) binds CaSR in Ca^{2+} dependent manner and may retains CaSR to ER in the absence of Ca^{2+} by disruption of the contact.

Finally, terminally misfolded CaSR proteins may undergo ER associated degradation by ubiquitination through E3 ligases. GPCRs are known to undergo agonist-induced ubiquitination leading to internalization and lysosomal degradation [170]. E3 ubiquitin ligases, STUB1/ CHIP and RanBP2 were found to be enriched by 1.7 and 21 folds, respectively. Several GPCRs including, adenosine, dopamine-, P2Y, PAR1, glucagon, GABA, mGluRs and CaSR receptor are known to interact with various ubiquitin [170]. Recent work by Mukherjee et al. has reviewed the Ca^{2+} dependent regulation of ubiquitin and role of calcium binding protein such as CaM in its regulation [171]. Our result complements their list by adding Ca^{2+} dependent interaction of RanBP2 and STUB1 to CaSR. The desensitization of CaSR occurs through endocytosis from the plasma membrane by Ras-related proteins and clathrin heavy chain (CLTC). In this study, we show an enrichment of Ca^{2+} dependent regulators of endocytosis: Rab5, Rab18 and CLTC by 17, 3 and 2 folds, respectively. Rab5 is known to be involved in modulation of half-life of clathrin-coated pits on plasma membrane forming the vesicle [172]. Additionally, Rab5 also regulates the

attachment of early endosomes to and the motility along the microtubules [173]. Rab18 is also involved in apical endocytosis/recycling during early endosome [174].

Our study identifies several HSPs as CaSR interactors such as Hsp-A1A, A6/7, A8, 90AA1and 90AB1. Heat shock proteins (HSPs) are a family of molecular chaperones that bind transiently and assist in folding, stabilization, translocation and degradation of target proteins [175]. In previous studies, increased expression of Hsp70 is shown to reduce agonist but not antagonist binding to the alpha2A adrenergic receptor (α2A-R), therefore, providing an evidence for uncoupling of GPCR from G-proteins during cellular stress [147]. In our experiment, Hsp may act as a switch to suppress the prolonged activation of CaSR to promote survival of the cells. Proteins involved in the Ca^{2+} handling and in early events in apoptosis in the mitochondria/ER including, VDAC, TIMM50, PGRMC1 and NDUFA4 were enriched in our experiment in the presence of Ca^{2+} [176, 177]. These results infer that CaSR mediated Ca^{2+} signaling may allow for the intracellular CaSR to associate directly or indirectly with modulators of Ca^{2+} handling in the ER and mitochondrial membrane.

The proteins we have identified fall into the categories of proteins associated with functions mentioned in the review by Wu et. al. where it points out several distinguishing characteristics of GPCR trafficking to the plasma membrane. Cell surface targeting is involved with (1) proteins such as RAMPs, ER chaperones and accessory proteins which assist in stabilizing receptor conformation, facilitating maturation and promoting delivery to the surface [178-180], (2) post-translational modifications, such as N-liked glycosylation, are known to be associated with GPCR delivery to the plasma membrane [181]. (3) GPCR cell surface targeting is associated with microtubule networks [182] and that GPCR interact with tubulin for cell-surface movement [183]. (4) GPCR folding/assembly as well as its ability to pass through the ER quality-control system

may be influenced by dimerization [7]. (5) Specific motifs embedded within the receptors direct the exit of GPCRs from the ER [178, 184, 185].

Some other proteins known as GPCR binding proteins are PGRMC1 and IRS4 which are directly or indirectly associated with various cellular pathways. IRS4 belongs to insulin receptor substrate (IRS) family [186] and is localized in the cytoplasm. It is known to recruit and activate various adapter molecules or enzymes, such as phosphoinositide 3-kinase (PI3K) and mitogen-activated protein kinase (MAPK) to facilitate glucose uptake [187, 188], lipid metabolism [189] and cell proliferation [190] upon insulin stimulation. It also binds to ubiquitin-specific protease 18 (USP18) in nucleus to diminish the blunting effect of USP18 on IFN-a-induced Jak/STAT signaling [191]. LRRC59 facilitates transport of cytosolic fibroblast growth factor 1 (FGF1) through nuclear pores by interaction with Kpns and movement of LRRC59 along the ER and NE membranes [192].

The Co-IP assay developed and used for generation of the putative CaSR interactors is an improvement as compared to the previous attempts made till 2017. There was a marked increase in the number of unique peptides for CaSR detected from 12 with Dr. Wu in Georgia Tech and 10 with Dr. Zhou from Clark Atlanta University to 52 with Dr. Seyfried in Emory. A crucial aspect to note is that the antibody used in the latter case was anti-FLAG antibody as compared to anti-ADD CaSR antibody for endogenous CaSR in 5001 in previous cases. This increased IP points out that the specificity of an antibody plays the most crucial role in the success of IP as well as Co-IP. In order to study the endogenous CaSR, especially in the pathological cells, it would require additional optimization with anti-CaSR antibody. A new CaSR antibody is being developed currently in rabbit using CaSR ECD protein that will have greater affinity than the anti-ADD CaSR antibody. Steps such as amount of antibody, amount of antigen, time of incubation and stringent

washing steps need to be considered for optimization. The optimization I have attained improved not only is the detection but also decreased the amount of cells and the number of plates used from initial ten to one plate per treatment. This has cut the cost of the experiment as well as manual labor. Additionally, prevention of loss of sample was optimized. In gel digestion, using Thermon kit, membrane/cytosol extraction kit, UFLC separation, or cross-linking proved to decrease the detection, most possibly due to sample loss during the dilutions resulted by extensive steps.

We can say that with all the strategies applied, our experimental approach is not a complete snapshot of the putative CaSR interactome. Several limitations exist which may explain the incomplete recruitment of protein complexes and the absence in the detection of some of the known CaSR partners in our experiment such as some of the g-proteins. Our whole cell lysate MS/MS result validate that G-proteins including Gq/11, Gi_1, Gi_3, Gs, $G\gamma_{12}$ and $G\gamma_5$ are expressed at low abundance in cells with an average PSM count of less than 1 and the Gi_2, $G\beta_2$, and $G\beta_2$-like-1 proteins have higher average PSM counts of 3-27, therefore, resulting in robust detection. It is known in previous studies that it is a challenge for the G-protein detection and have been observed in natural membrane environment with intact receptors using tandem affinity purification [133]. Further, our result supports earlier study of CaM interaction with CaSR in intracellular Ca^{2+} dependent manner which was missing in our study [3]. Similarly, filamin A and B were detected; filamin A with more robust PSM between (6-46) and was enriched in the presence of 4 mM Ca^{2+}. However, there was no significant change between the positive and negative controls, implying an un-specific enrichment of abundant filamin (total lysate MS/MS had high average PSM count of 80). CaM is known to bind to the same binding region as the filamin-A or Gβγ -subunits within the mGluR7a C terminus [193]. This could be the reason why we only detected Gβγ -subunits. Additionally, we observe incomplete immunoprecipitation of total CaSR (Figure S3) which may

result in the incomplete picture. Also, the enrichment we observe are relative quantification and may be affected by binding affinities and may not directly co-relate with the function. Further, we can also not negate the fact that the putative CaSR binding partners detected may be due to direct or indirect interactions. Further studies and validation are warranted to examine the mechanism of each interactors individually.

For future work, it is necessary to obtain CaSR monomer in order to achieve a distinct detection of the IP and Co-IP and for detection of ubiquitination. Also, assay needs to be developed for avoiding heavy and light chain of antibody in order to prevent overlap between them and the protein of interests. This initial information attained on putative CaSR interactors provides multitude of novel pathways that CaSR is biologically involved in such as the CHIP ubiqitination, role of VAPA trafficking, sumolyation of CaSR by RanBP2, endocytosis by Rab5C, etc. The immuno-fluorescence and western blot of the Co-IP results suggest the co-localization and interactions of CaSR with interactors such as CHIP, GRP78 and 14-3-3 eta proteins. However, the role of extracellular Ca^{2+} on these interactions are not apparent. Additionally, the location of the interactors has to be analyzed and we hypothesize that these would be present in ER/Golgi region at higher Ca^{2+}. Secondly, the trafficking mechanism needs to be deciphered by focusing on the role of Ca^{2+} on the interaction of specific proteins in ER vs those in ER/Golgi for anterograde and retrograde trafficking.

2.8 Major conclusion

Sustained Ca^{2+} increase in cytosol can induce mitochondrial meditated apoptosis via protein such as calcineurin or by mitochondrial Ca^{2+} overload [194]. Therefore, protein homeostasis is directly altered due to [Ca^{2+}] regulation in the ER and cytosol. This is presented

during several diseases including diabetes mellitus, vascular and neurological diseases [195], and therefore, regulators for Ca^{2+} handling and trafficking can be used as novel therapeutics target. In this study we have been able to provide the first protein-protein interaction network for CaSR at a larger scale. Our work surmises the role of $Ca^{2+}{}_o$ and CaSR in modulating the proteome expression levels which may have manifested due to differential signal transduction mediated by activation of CaSR via $Ca^{2+}{}_o$, changes in regulatory proteins maintaining Ca^{2+} homeostasis and stimulation of cellular activities such as the trafficking of CaSR itself to various compartments. Known CaSR and GPCR interactors novel for CaSR re-validates our work and indicates overlapping signaling cascade and trafficking. 98 novel putative CaSR interactors were identified. The results recognized distinct effect of $Ca^{2+}{}_o$ on CaSR interactions with 65% enriched by $Ca^{2+}{}_o$ involved in processing in the ER. Whereas, 31% $Ca^{2+}{}_o$ independent interactors were involved in ribosomal pathway. The results demonstrated that the 14-3-3 proteins interaction with CaSR is negatively correlated with $Ca^{2+}{}_o$. The first protein-protein interaction (PPI) network obtained had strong confidence of 0.551 and a PPI enrichment $P < 1.00E\text{-}16$. Additionally, the identified novel regulators and pathways for CaSR that are extracellular Ca^{2+} signaling dependent were co-translational translocation (SRP, Sec61, GRP78), ubiquitination (CHIP), calnexin cycle, glycosylation, trafficking, endocytosis and calcium handling. Taken together, this study offers an insight into the interconnection of GPCR function, intracellular trafficking, and potential targets for Ca^{2+} homeostasis related pathogenesis of diseases. Additionally, this study may offer an insight into the overall GPCR function, intracellular trafficking, and potential targets for Ca^{2+} homeostasis related pathogenesis of diseases.

3 CHAPTER III: CHARACTERIZATION OF CALCIUM-SENSING RECEPTOR MEDIATED SIGNALING IN HEK293 AND THYROID CANCER CELLS

3.1 Abstract

CaSR a class C, G-protein coupled receptors (GPCR) regulates Ca^{2+} and Mg^{2+} homeostasis which are indispensable processes that regulate multitude processes in cells for normal functioning. More than 400 mutations in CaSR are associated with abnormal metal homeostasis, including familial hypocalciuric hypercalcemia (FHH), neonatal severe hyperparathyroidism (NSHPT), and autosomal dominant hypocalcemia (ADH). Moreover, CaSR is intimately associated with various cancers. The systemic Ca^{2+} homeostasis through CaSR is mediated by three hormones, namely, calcitonin (CT), parathyroid hormone (PTH) and 1,25-dihydroxyvitamin D_3 (1,25-$(OH)_2D_3$). In this work, we first study intracellular Ca^{2+} response facilitated by CaSR activation via extracellular Ca^{2+}, Mg^{2+} and tryptophan derivative (l-1,2,3,4-tetrahydronorharman-3-carboxylic acid, TNCA) in HEK293 cells with transfected wild type (human parathyroid) CaSR. EC_{50} of CaSR for Ca^{2+} was 4 mM with a Hill number of 3 and for Mg^{2+} EC_{50} was 13 mM and Hill number of 2.9. Presence of 0.5 mM and 1.5 mM Ca^{2+} was able to influence the potency of Mg^{2+} by decreasing EC_{50} for Mg^{2+} to 7.5 and 5.9 mM respectively, which proved the cooperative nature between Ca^{2+} and Mg^{2+}. Moreover, TNCA was able to act as a co-agonist and reduce the EC_{50} for both Ca^{2+} and Mg^{2+}, but more significantly for Mg^{2+} by 2.5 folds. Oscillation study with site-directed mutations at the highly conserved Mg^{2+} binding sites derived from CaSR crystal structure, which overlap the ADH related residues, E228I and E229I, resulted in impediment of the Ca^{2+}/Mg^{2+} CaSR sensing as well as CaSR mediated Mg^{2+} evoked $Ca^{2+}{}_i$ mobilization and Ca^{2+} oscillation.

Coupling and regulation between extra- and intra- cellular Ca^{2+} sensing and calcitonin is imperative in endocrine cells such as the C cells. Calcitonin maintains the systemic Ca^{2+} homeostasis by inhibiting the function of bone-resorbing osteoclasts, increasing Ca^{2+} excretion by kidneys and stimulation of calcitriol (1,25-$(OH)_2D_3$) production. Ca^{2+} sensing through voltage gated channel have been extensively studied in C-cells, including rat and human medullary thyroid cancer cells (6-23, TT, respectively) but contradictory and little information is known about CaSR mediated $Ca^{2+}{}_i$ response due to extracellular Ca^{2+}. Cell lines derived from tumors represent a critical tool to understand the oncogenic mechanism as well as preclinical tool to understand to study efficacy of new therapies in vitro and in vivo. We report an altered CaSR expression level with four-fold lower expression in both 6-23 and TT cells as compared to wild type CaSR stably transfected in HEK293 cells (5001) or transiently transfected in HEK293 cells. Moreover, CaSR in 6-23 displays oligomer and lacks monomers even in reducing condition unlike CaSR in TT and the wild type. CaSR surface expression of CaSR in both C cells is low relative to the cytosolic CaSR or membrane expression in 5001 and transiently transfected wild type CaSR in HEK293 cells. We examined the endogenous CaSR mediated intracellular Ca^{2+} response pattern at various extracellular Ca^{2+} concentrations and monitored the changes with the use of CaSR allosteric agonist (cinacalcet) and antagonist (NPS-2143). We further investigated the role of calmodulin (CaM), a CaSR regulating protein, by monitoring the intracellular Ca^{2+} response pattern with CaM inhibitor, W7, treatment. TT cells demonstrated CaSR mediated transient peaks at 5 and/or 7.5 mM extracellular Ca^{2+} by < 30 % of the cells (n=23). Whereas, addition of 10 µM cinacalcet evoked the transients at 2 mM Ca^{2+} in 88% of the cells and resulting in 40% increase in the amplitude as compared to other treatments (n=24). NPS2143 was able to inhibit the Ca^{2+} response at 7.5 mM and preincubation with 50 µM W7 was able to impede the agonistic behavior of

cinacalcet, clarifying the case that cinacalcet and W7 have additive effect on one mechanism, the CaSR mediated signaling.

A highly non-synchronous CaSR mediated oscillatory behavior was revealed in 6-23 cells. These cells contained a mixture of CaSR with variable activity, some with low EC_{50} for Ca^{2+} at 0.5 mM and a lower Hill number of 1.5 and some that were un-responsive to Ca^{2+}. Using R-programming, $Ca^{2+}{}_i$ were quantitated. We report that cinacalcet can up-regulate the $Ca^{2+}{}_i$ response, percentage of cells responding and increase oscillation frequency. Pre-incubation with W7 is able to down-regulate the effects of cinacalcet. NPS-2143 was unable to completely inhibit $Ca^{2+}{}_i$ response, suggesting an alternative Ca^{2+} sensing mechanism. Interestingly, CaSR in both the C cells were selective to Ca^{2+} and not to Mg^{2+} implying biased signaling. These results (1) validates the oscillation and transient peaks were partially but to a greater extent CaSR mediated in C- cells and (2) establishes role of calmodulin in CaSR mediated signaling. Our findings provide an important insight into potential differential modes of modulation of intracellular Ca^{2+} signaling and thereby, control of calcitonin, through regulation of endogenous CaSR activation in pathologies related to dysregulation of Ca^{2+} homeostasis.

3.2 Introduction

3.2.1 CaSR mediated signaling and oscillation

Various Gα proteins, such as $G\alpha_i$, $G\alpha_{q/11}$ and $G\alpha_{12/13}$, associated with CaSR intracellular loops carry out diverse signaling and biological effects in cells. CaSR inhibits adenylyl cyclase and activates extracellular signal-regulated kinase (ERK) through $G\alpha_i$ and phospholipase C is activated through $G\alpha_q$, therefore, increasing intracellular Ca^{2+}, diacyl glycerol (DAG) levels and activating phospholipase A2. Finally, $G\alpha_{12/13}$ activated Rho and phospholipase D [55]. CaSR mediated $Ca^{2+}{}_i$ oscillation is presented as sequential regenerative increase of $Ca^{2+}{}_i$ concentration.

This results from the Ca^{2+} release from ER which is triggered by GPCR mediated phospholipase-C derived inositol 1,4,5-triphosphate (IP_3) [196] and Ca^{2+} entry through the store operated channels in cell membrane [197]. IP_3 is generated by cleavage of phosphatidylinositol 4,5-bisphosphate and it binds to IP_3 receptors (IP_3Rs) on the membrane of the ER/SR which allow for a rapid flow of Ca^{2+} out of the ER/SR, and a consequent rise in cytosolic [$Ca^{2+}{}_{cyt}$]. Cytosolic Ca^{2+} concentrations ([Ca^{2+}]$_{cyt}$) in resting cells are maintained at levels ranging from 1,000-10,000 times lower than extracellular concentrations. This gradient across the plasma membrane required to maintain $Ca^{2+}{}_i$ homeostasis and regulate Ca^{2+} signaling involves influx of Ca^{2+} from the extracellular medium via Ca^{2+} channels. The release or sequestration of internal Ca^{2+} levels within internal Ca^{2+} stores (ER or SR) is mediated by the IP_3 receptors (IP_3R) and the ryanodine receptors (RyR), and cytosolic Ca^{2+} homeostasis is further maintained by the actions of proteins, including the plasma membrane Ca^{2+}-ATPase (PMCA), the sarcoplasmic/endoplasmic reticulum Ca^{2+}-ATPase (SERCA), the secretory pathway Ca^{2+}-ATPase (SPCA), and the Na^+/Ca^{2+} exchanger (NCX), among others. Therefore, the two major mechanisms namely, Ca^{2+} induced Ca^{2+} release (CICR) from ER/SR and Ca^{2+} release induced Ca^{2+} entry from plasma membrane regulate the oscillation. This characteristic oscillation is known to be varied depending on the cell type and conditions.

3.2.2 Thyroid cancer

Thyroid cancer is more common in women than in men (3 out of 4 cases) and occurs between the age of 25 and 65 years old (https://www.cancer.org/cancer/thyroid-cancer/about/key-statistics.html) . About 2% of thyroid cancers occur in children and teens. About 52,070 new cases of thyroid cancer (14,260 in men and 37,810 in women) and about 2170 deaths from thyroid cancer (1020 men and 1150 women) were estimated in United States for 2019. Medullary carcinoma of the thyroid comprises of around 4% to 10% of all thyroid cancers in the United States [198].

3.2.3 History of calcium-sensing mechanism in medullary thyroid cancer cells

Medullary thyroid cancer (MTC) is derived from parafollicular thyroid C-cells. C-cells from thyroid gland is one of the most prominent CaSR expressing homeostatic tissues. ~ 75% to 95% patients with medullary thyroid cancer show a thyroid nodule in the upper portion of the gland where C cells are located [198]. ~ 70% will have cervical lymphadenopathy and few patients will show symptoms of dysphagia, hoarseness, or respiratory difficulty [198]. These cancers do not respond to radioactive iodine (RAI; as they do not express sodium-iodine symporter) [199], conventional chemotherapy or suppressant to thyroid stimulating hormone (TSH, as C cells do not contain the receptor) [198]. The management of this cancer is through total thyroidectomy [198] or the metastatic and progressive MTC is managed by FDA approved kinase inhibitors with significant side effects [200, 201]. This ailment results in hyperparathyroidism and hypercalcemia. Imaging modalities such as magnetic resonance imaging, ultrasound and computed monography are not sensitive enough to determine [199]. Therefore, further understanding of its biological mechanism of the pathology in C-cells is warranted in order to develop better treatment conditions.

The C-cells produce a hormone called calcitonin (CT) which is a biochemical marker for MTCs [199]. CT along with parathyroid hormone (PTH) and 1,25-dihydroxyvitamin D_3 (1,25-$(OH)_2D_3$) are three hormones that regulates cellular Ca^{2+} homeostasis. CT works opposing to PTH. PTH increases the serum calcium by enhancing bone resorption and absorption of calcium from the gut and reducing renal calcium excretion [202], on the other hand, CT reduces serum Ca^{2+} by inhibiting the function of bone-resorbing osteoclasts, increasing Ca^{2+} excretion by kidneys and stimulation 1,25-$(OH)_2D_3$ production [203-205]. CT is the only hormone known to decrease serum Ca^{2+} in humans [6]. It is found that patients with MTCs have high serum calcitonin level due to the consequence of the disease. Massively elevated levels of serum CT is found in MTCs and no

detectable hypocalcemia or influence on bone-mineral density is found [6, 206]. CaSR in C cell mediates Ca^{2+}_o evoked stimulation of this hypocalcemic hormone, CT [207]. It is also known that CT hypocalcemic action is species specific where the action is greater in rodents than humans [207]. Apart from CaSR, L-type calcium channel is known to sense Ca^{2+} in C cells [6]. There have been many contradicting studies conducted on two established MTC cell lines, namely, with human medullary thyroid carcinoma cell line TT and rat medullary thyroid carcinoma cell line 6-23 [208]to understand the Ca^{2+} sensing and CaSR mediated intracellular responses.

3.2.3.1 TT cells

The TT cells resemble parafollicular C cells and calcitonin secretion is shown to be present [209]. In a study by Haller-Brem et al. in 1987 show that TT cells are Ca^{2+} insensitive where neither Ca^{2+}_i nor CT is affected by extracellular Ca^{2+}. In TT, the rise of Ca^{2+} from 0.5 to 3 mM does not affect the Ca^{2+}_i, CT and calcitonin gene-related peptide (CGRP) **(Figure 3.1**) [13]. On the contrary, CT and CGRP release were shown to be dose-dependent on Ca^{2+}_i in TT only when electropermeabilized or when ionomycin was used [13]. Ionomycin is able to mobilize Ca^{2+} from intracellular stores. This indicates a defect in the Ca^{2+} signal transduction in the TT cell line, lack of extracellular Ca^{2+} sensitivity resulting in defective Ca^{2+}_i release, but not the intracellular Ca^{2+} sensitivity. TT cells were shown to lack voltage-dependent L-type calcium channels and DHP-sensitive voltage-dependent Ca^{2+} channel **(Figure 3.2)** [6, 210]. It has been shown that TT cells display DHP-insensitive, voltage-dependent Ca2+ channel with low activation threshold and fast inactivation kinetics [211]. These depolarization-induced voltage-dependent Ca^{2+} currents are quickly inactivated unlike that in 6-23 cells. Also, no conductivity is observed through the T-type Ca^{2+} channels [6]. A physiological level of Ca^{2+} cannot elicit any action potential and/or depolarize TT cells [211]. Only in 1996, Freichel et al showed the involvement of CaSR in Ca^{2+} sensing in

TT where a truncated CaSR variant, CaSRb with 5.4 kilobase mRNA was identified [212]. Contrary to earlier mentioned studies, this study showed Ca^{2+}_i transients and/or oscillation to 3 mM Ca^{2+}_o and CaSR agonists including, Gd^{3+}, La^{3+} and neomycin as monitored by Fura-2 [212]. Additionally, calcitonin increase was observed with 3 mM Ca^{2+}_o with an added time course and with La^{3+} and Gd^{3+} in dose-dependent manner. Moreover, recent work by Desai et al in 2014 showed that healthy TT cells displayed higher intracellular Ca^{2+} to 1.5 mM Ca^{2+} in the presence of cinacalcet and neomycin (CaSR agonist) than the TT cells with siRNA knockdown of RAMP (receptor activity modifying protein), a CaSR regulator [16] as monitored using Fluo-4AM (**Figure 3.3)**. Ca^{2+} sensing at higher Ca^{2+}_o concentration is missing in these studies.

3.2.3.2 Rat MTC cells

6-23 cells respond to rise in Ca^{2+} from 0.5 to 3 mM with a transient intracellular Ca^{2+} peak [13] and an increase in CT and calcitonin gene-related peptide (CGRP) **(Figure 3.1**). Another study by Eckert et al in 1989 showed that pre-incubation of 6-23 cells with 1 µM glucagon or 1 mM 8-bromo-cAMP caused intracellular calcium oscillation when Ca^{2+}_o was raised to 3 mM but only showed a simple biphasic response with 3 mM Ca^{2+} alone [213]. These oscillations were perturbed by using EGTA to chelate Ca^{2+}_o or by addition of calcium channel blocker to block voltage-dependent calcium channels (**Figure 3.2)** [213]. Both 8-bromo-cAMP and glucagon induced cAMP pathway activation through Gs. Non-inactivating dihydropyridine (DHP)-sensitive, high threshold Ca^{2+} channels couple the intra and extra- cellular Ca^{2+} in 6-23 cells [211]. Extracellular Ca^{2+} sensitivity saturates at 3-4 mM Ca^{2+} and declines with higher extracellular Ca^{2+} [6]. A study by Thomsen in 2012 examined the biased CaSR mediated signaling in 6-23 cells [214]. Six CaSR mediated signaling were studied including Gq/11, Gi/o, Gs, extracellular signal-regulated kinases (ERK1/2), Ca^{2+}_i mobilization and calcitonin secretion [214]. They showed that

strontium as compared to calcium biases the signaling to ERK1/2 and another pathway independent of Gq/11 and Ca^{2+} mobilization [214]. There was also increased potency of strontium to mediate CT secretion and possibly using a different signaling mechanism than calcium [214]. These studies were primarily based on response to calcitonin, IP_1 and cAMP secretion.

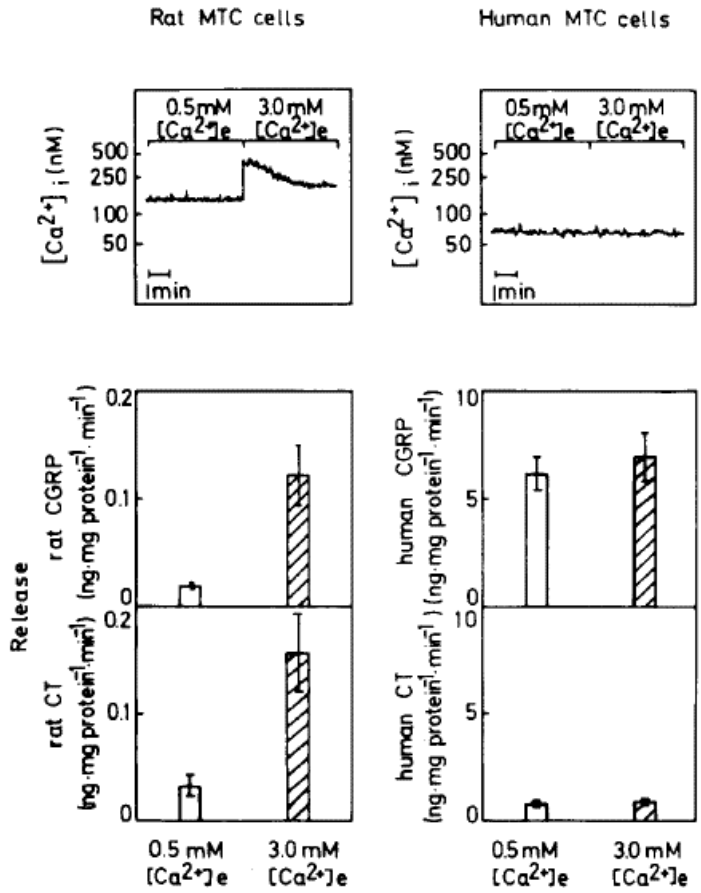

Figure 3.1 Effect of extracellular Ca^{2+} on intracellular Ca^{2+}, CT and CGRP in rat MTC 6-23 cell and human MTC TT cells. [13]

TT cells are Ca^{2+} insensitive where neither $Ca^{2+}{}_i$ nor CT is affected by extracellular Ca^{2+}. In TT, the rise of Ca^{2+} from 0.5 to 3 mM does not affect the $Ca^{2+}{}_i$, CT and calcitonin gene-related peptide (CGRP). On the contrary, CT and CGRP release was shown to be dose dependent on $Ca^{2+}{}_i$ in TT only when electropermeabilized or when ionomycin was used. Ionomycin is able to mobilize Ca^{2+} from intracellular stores. This indicates a defect in the Ca^{2+} signal transduction in the TT cell line, lack of extracellular Ca^{2+} sensitivity resulting in defective $Ca^{2+}{}_i$ release, but not the intracellular Ca^{2+} sensitivity. Rat MTC 6-23 cells respond to rise in Ca^{2+} from 0.5 to 3 mM with a transient intracellular Ca^{2+} peak and increase in CT and calcitonin gene-related peptide (CGRP).

MTC cells have varying Ca^{2+} sensing characteristics. In 1991, Fajtova et al used rMTC 44-2 cells to show that at basal state of Ca^{2+} at 0.5 mM resulted in cytosolic Ca^{2+} at 53 nM with 27% cells having spikes or oscillations **(Figure 3.5**) [12]. With changes of $Ca^{2+}{}_o$ from 0.5 mM to 4 mM, 84% cells showed rise in $Ca^{2+}{}_i$ by 2- to 10- folds as monitored by Fura-2 [12]. These responses were hampered by Ca^{2+} channel blockers cadmium and nifedipine **(Figure 3.4**) [12]. Also 20 mM K^+ elevation resulted in similar waveform [12]. Both results suggest the presence of voltage-gated Ca^{2+} channel in rMTC 44-2 cells. These cells displayed complicated $Ca^{2+}{}_i$ oscillations ranging from < 1/min to 1/min. They suggest that the discrepancy between the rMTCs, 44-2 and 6-23, cell lines could have resulted due to culture conditions or differential Ca^{2+} sensing mechanism. Moreover, rMTC 44-2 cells are known to show no IP_1, IP_2 or IP_3 generation when Ca^{2+} is increased above 1 mM [6]. This result further pointed to the possibility that oscillation is mediated by voltage-gated channel rather than IP3, or cAMP. Also, 44-2 cells showed a 9-kilobase mRNA of

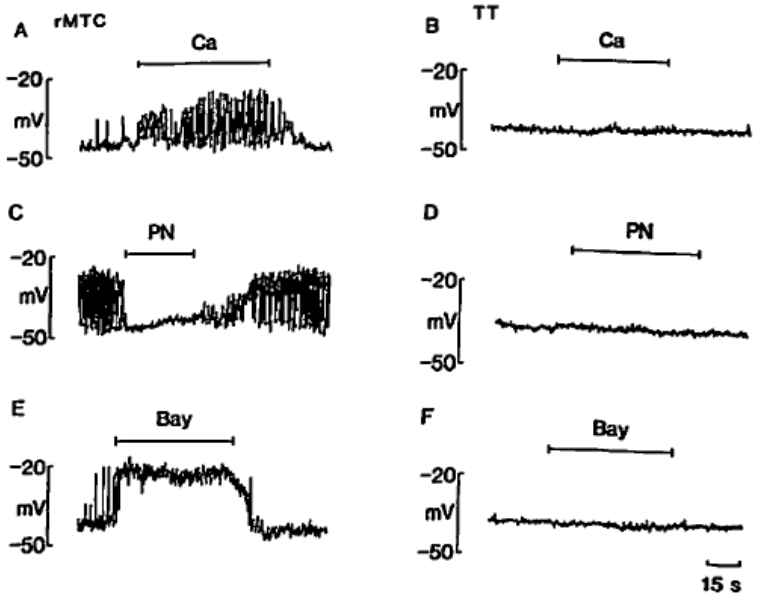

Figure 3.2 Ca^{2+} channel in 6-23 and TT cells [6].

Changes in extracellular Ca^{2+} within physiological range do not affect membrane potential of TT cells. 6-23 cells respond to 1.2-1.8 mM Ca^{2+} that elicits action potentials and or depolarizes cells by ~ 10 mV. Ca^{2+} channel blocker isradipine (PN) and agonist Bay K 8644 (Bay) were used to explore the channel activity. The results state that TT lack extracellular Ca2+ sensitive channel as compared to 6-23 cells.

full CaSR [6]. Additionally, primary parafollicular sheep cells also has shown that CaSR activation results in increased intracellular Ca^{2+} and L-type calcium channels are responsible for this increase

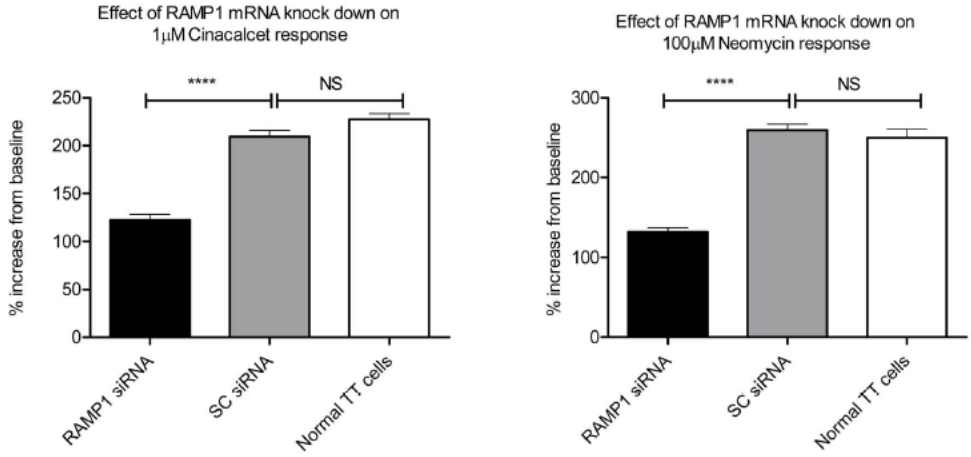

Figure 3.3 TT cells show intracellular Ca^{2+} modulation to 1.5 mM Ca^{2+} with CaSR agonists 1 μM cinacalcet and 100 μM neomycin as monitored by Fluor-4 and RAMP knockdown attenuates the signal [16]

[45].

Intracellular calcium mobilization caused by extracellular calcium is the key event in CT secretion in 6-23 cells as demonstrated by inhibition of 82% vs 48% calcitonin when stimulated by Ca^{2+} and Sr^{2+}, respectively in the presence of BAPTA-AM (calcium chelator) and absence of

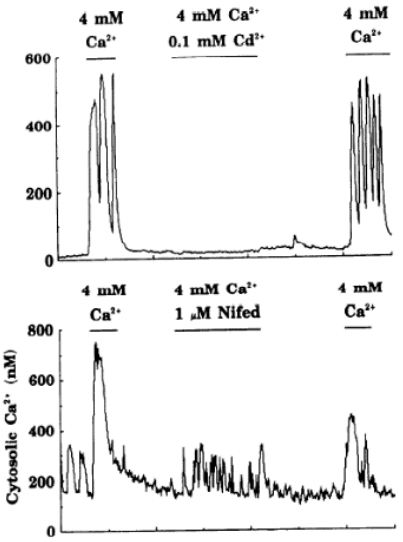

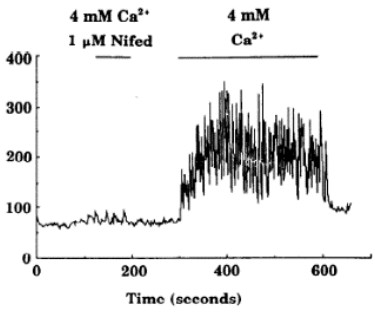

Figure 3.4 Involvement of Ca^{2+} channels in rMTC 44-2 cells as shown through attenuation by channel blockers Cd^{2+} and Nifed [12]

extracellular Ca^{2+} [214]. Similarly, in TT cells CT is shown to be dose-dependent on La^{3+} and Gd^{3+} whereas CT increased at 3 mM Ca^{2+} with increasing time course. Interestingly, rMTC 44-2 cells are known to have no sensitivity to Mg^{2+} [215]. Additionally, sheep parafollicular primary C-cells were used to study the Ca^{2+} sensing varying potency of CaSR activation by various divalent cations was shown such that $Gd^{3+}>Ba^{2+}>Ca^{2+}>>Mg^{2+}$ [45]. This paper also indicates the role of L-type voltage-gated channel and Gq/11 in the response to extracellular calcium by using channel blocker nimodipine and phosphatidylcholine PLC inhibitor, D609, respectively [45]. This study monitored serotonin (5-HT) and phospho-kinase C for CaSR mediated signaling response. The reduced Mg^{2+} sensitivity in the light of 92% sequence similarity between rat and bovine CaSR and intact Ca^{2+} binding sites could be resultant of tissue specific post-translational modifications or differential CaSR regulatory protein. This work also suggests that MTC cells as compared to the parafollicular

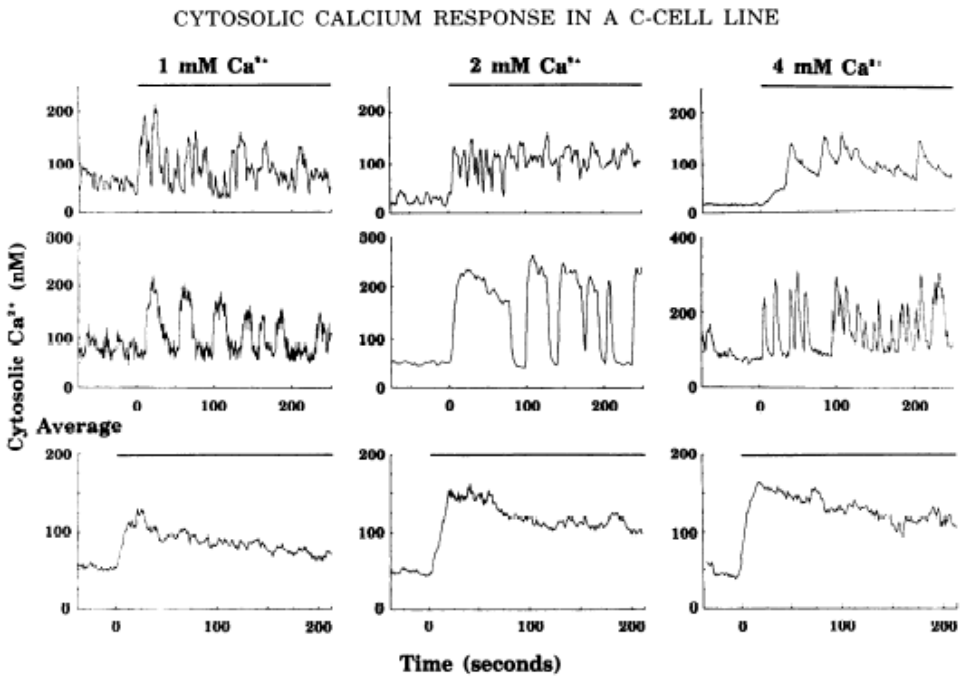

Figure 3.5 Intracellular Ca^{2+} response to extracellular Ca^{2+} in rMTC 44-2 cells show heterogenous response [12]

primary cells are more excitable like neuron cells.

Two of the major intracellular signals in C cells are intracellular Ca^{2+} and cAMP which are closely coordinated with cellular function [6]. The efficiency of signal transduction can be modified through modulation in receptor number, receptor function, desensitization or antagonistic or synergistic interactions between different signaling systems [216]. It has been found that increase in IP_1, IP_2 or IP_3 is absent with extracellular Ca^{2+} treatment above 1 mM in 44-2 cells [217]. It is to note that Ca^{2+} flux can be regulated by phosphorylation of Ca2+ channels or component linked to protein kinase such as voltage-dependent channel, cAMP-dependent phosphorylation or phosphorylation of G-protein [6]. Mechanism underlying complex oscillation in intracellular Ca2+ is still obscure.

Many of these studies have been conducted using various calcium sensors such as Fura-2 and fluor-4 or by using various inhibitors and methodologies. This could result in a discrepancy between the studies. In our work, we investigate the study of endogenous CaSR mediated $Ca^{2+}{}_i$ response mechanism further in the thyroid cancer C-cells using Fura-2 due to various $Ca^{2+}{}_o$ concentrations from 0 to 20 mM and effect of CaSR associated agonist and antagonist. We use single-cell imaging and have aimed at understanding the role of CaM in CaSR mediated Ca^{2+} signaling in C cells.

3.2.4 CaSR and CaM

CaM (CaM) is an intracellular protein that is dependent on changes in cytosolic Ca^{2+} levels and in turn, regulates numerous Ca^{2+}-signaling activities. It has two globular domains which contain two cooperatively paired EF-Hand motifs, allowing it to bind up to four Ca^{2+} ions [218]. The EF-hand site contains 29-residue helix-loop-helix structure which is highly conserved. The Ca^{2+} binding site consists of twelve residues out of which those in relative positions 1, 3, 5, 7, 9 and 12 coordinates Ca^{2+}. The equilibrium between conformational states and the interaction with

the target proteins is made possible by the apparent flexibility of trans-domain linker region (residues 76-84). The Ca^{2+}-CaM complex regulates biological processes associated with signal transduction, cell division, nerve growth, cell death, inflammation, memory, immune response and muscle contraction. The CaM reversibly or irreversibly binds its targets which possess regions of net positive charge, moderate hydrophilicity and moderate to high helical hydrophobic moments. Targets for holo-CaM contain amphipathic α helices with two suitably spaced and oriented hydrophobic anchors which can insert into the methionine rich pockets [219] and utilizes both N- and C-domains. CaM plays an important role in the calcium-signaling network, the extent of which remains to be fully mapped and understood.

3.2.5 CaM mediated GPCR signaling

An ionotropic glutamate receptor family (iGluR) called N-methyl-D-aspartate (NMDA) is a fundamental receptor involved in synaptic plasticity, LTP, learning and memory. CaM is activated by the influx of Ca^{2+} through NMDAR subsequently, binding CaMKII. Additionally, the negative feedback loop produced by the Ca^{2+}/CaM complexation inactivates the NMDAR receptor by displacing α-actinin from the C0 domain of the NR1 subunit of the receptor [220]. A G protein-coupled receptor known as the metabotropic glutamate receptors (mGluR's) bind the neurotransmitter L-glutamate for its activity. mGluR7 plays an important role in synaptic plasticity and neurotransmission in the CNS. PICK1 which regulates mGluR by recruiting PKCα for phosphorylation of mGluR7 at Ser-862 [221], competes with the Ca^{2+}/CaM for the same binding site on mGluR7, where binding of the Ca^{2+}/CaM complex releases G protein C-tail G_β and G_γ units. Additionally, CaM regulates the activity of calcium-sensing receptor (CaSR), which belongs to the family C of GPCRs along with mGluR. Huang et al. in 2010 showed that CaM interacted with CaSR to maintain the normal $Ca^{2+}{}_i$ oscillations induced by activation of CaSR through $Ca^{2+}{}_o$

[3]. CaM inhibitor, as well as CaMBD mutations, perturbed the oscillation pattern in a wild type (**Figure 3.6)**. A potential CaSR- CaM binding domain (CaMBD) between 881-894 was predicted using the CaM binding domain database. This peptide at the C-terminus of CaSR was used to prove the interaction with CaM in 1-8-14 binding mode [3]. This binding was shown to affect the secondary and tertiary structure of this region. Most importantly, CaM had a significant effect on CaSR trafficking at the plasma membrane [3].

CaM not only influenced the $Ca^{2+}{}_o$ mediated signaling via CaSR, but also the L-Phe induced signaling. Zhang et al. in her (dissertation) work showed that with the incubation with

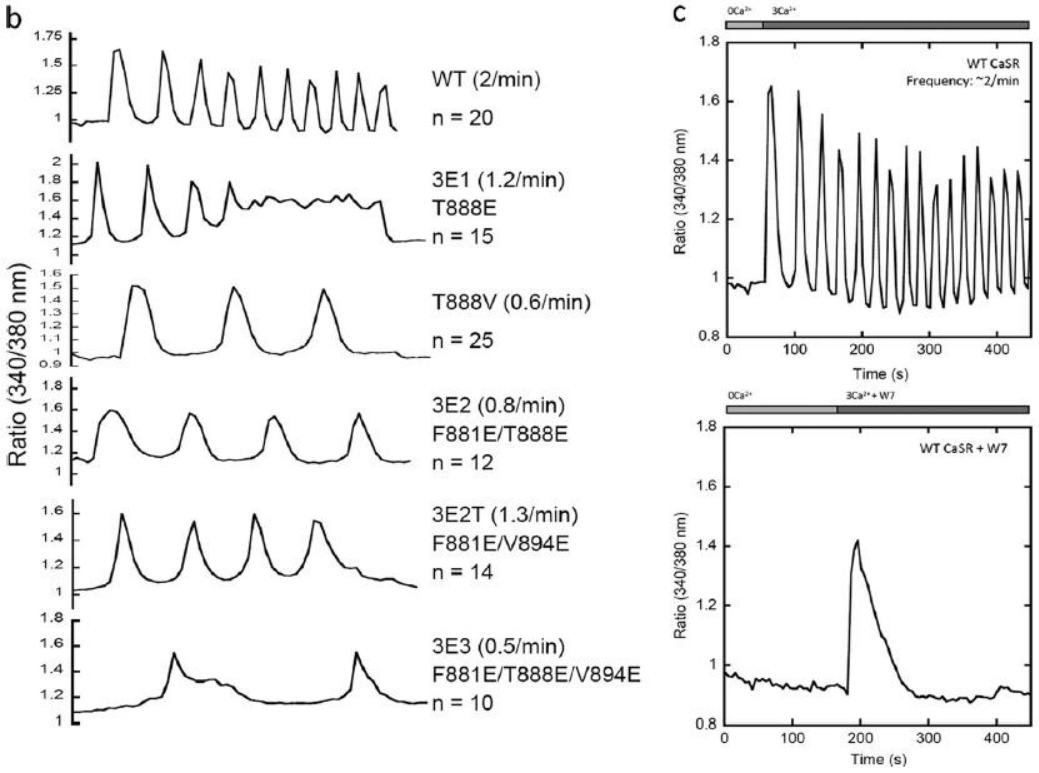

Figure 3.6 Ca^{2+} oscillation of CaSR for CaMBD mutants and with the use of CaM inhibitor W7 in HEK293 cells transfected with the corresponding pcDNA3.1 . [3] CaMBD mutants decreased the oscillation frequency and W7 resulted in transient peak

W7, the L-Phe induced sinusoidal oscillation transitioned to transient peaks as monitored with single cells imaging using FURA-2 AMAM. Furthermore, confocal imaging of the ADIS induced

by Ca^{2+} was in the presence of L-Phe was perturbed by W7. W7 also reduced the ERK1/2 activity induced by L-Phe. The Ca^{2+} induced internalization was not affected by the pre-treatment of W7 with or without L-Phe. Various C-terminus CaSR mutants were generated: F881E/V894E, F881E/T888E, F881E/T888E/V894. Most HEK293 cells transfected with these mutants showed transient peaks as their responses to the increase of $[Ca^{2+}]_o$. The addition of L-Phe could not start the oscillation at lower Ca^{2+} or increase the oscillation frequency as in case of the WT. The work also showed a direct negative relation of the mutants with the filamin binding.

3.2.6 CaSR-associated drugs

3.2.6.1 Cinacalcet

Cinacalcet (CCT) **(Figure 3.7)** binds to the transmembrane domain on CaSR and increases its potency and/or affinity of Ca^{2+} [222, 223]. It is the first calcimimetic approved by the Food and Drug Administration to treat patients suffering from secondary hyperparathyroidism in end-stage kidney disease [224]. Its side effect consists of hypocalcemic effect [225]. Studies show that CCT affected the distribution and trafficking of CaSR between the cell membrane and the endoplasmic reticulum rather than the biosynthesis of the receptor. CCT is an allosteric modulator of CaSR that increases the receptor's sensitivity to Ca^{2+} by shifting the response curve to the left and has been reported to induce its effect at a lower concentration of Ca^{2+} at 1.2 mM [226]. The experiment indicated that long-term treatment of the cells with CCT caused the redistribution of CaSR from the cell membrane to the endoplasmic reticulum–nuclear area. CCT affected the distribution and trafficking of CaSR between the cell membrane and the endoplasmic reticulum rather than the biosynthesis of the receptor [226]. At full concentration Ca^{2+} of 1.2 mM, the receptor would already be occupied by its primary agonist, and therefore, the effect of CCT might be masked [226]. CCT treatment might cause apoptosis of the esophageal cells as it was described in other

cell types [227]. CCT mediated by CaSR was also shown to trigger intrinsic mitochondrial related apoptotic pathway, and this pathway is modulated by Bcl-xL anti-apoptotic pathway in prostate cancer cells [227].

3.2.6.2 NPS-2143

NPS-2143 is a selective antagonist of CaSR with anticancer [92], and anti-inflammatory activities **(Figure 3.7)** [228]. It acts allosterically to dampen the sensitivity of CaSR to Ca^{2+} and therefore, shifts the EC_{50} to the right. It does not affect the PTH secretion at very low or high levels of $Ca^{2+}{}_{o,}$ but they do stimulate secretion of PTH under normocalcemic conditions. It is a potential drug for osteoporosis. It has been studied that NPS 2143 is effective in promoting trafficking of CaSR mutants to the cell membrane, but it negatively modulates CaSR signaling [229]. There is a contradictory study where the drug did not cause any change [230] or reduced [231] the expression of CaSR gain of function mutants. This finding suggests that the effect of NPS 2143 is mutant-specific. Additionally, NPS 2143 corrects the signaling defects in HEK293 transfected with $G\alpha_{11}$ mutated protein causing ADH2 and uveal melanoma.

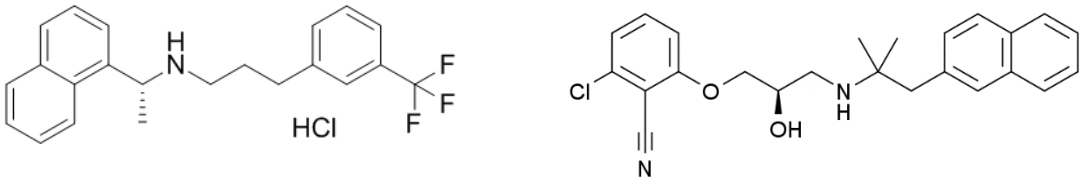

Figure 3.7 Cinacalcet and NPS 2143

3.3 Challenges

CaSR is a large membrane protein with 1068 amino acids. The presence of low endogenous expression of CaSR in cancer cells as well as heterogeneity is limiting when you are trying to characterize it and escalates the challenges for the bio-molecular techniques used in this chapter. CaSR experiences dynamic action involving folding, glycosylation, dimerization, trafficking, and

endocytosis. These dynamics causes variation in its molecular qualities. Lastly, CaSR has a multitude of binding partners involved in downstream signaling, therefore deciphering one that is causative of the differential signaling is almost impossible. There is a limitation of methods as well. The sensitivity of RT-PCR and PCR can be affected by many parameters such as primer specificity, heterogeneity of transcripts, annealing temperature, quality of RNA extracted, handling of RNA. Mass spectrometry_data is affected by glycosylation, antibody specificity, sample handling

3.4 Major Questions addressed in this chapter

a) What is the characteristic wild type CaSR mediated Ca^{2+} signaling in HEK293?

b) How do divalent cations and CaSR associated drugs impact the signaling?

c) Do human and rat thyroid cancer cells respond the same way in terms of CaSR mediated signaling?

d) Is the differential response due to expression level or presence of variants?

e) Do the CaSR- and CaBP related drugs carry similar potency in all cell types?

f) Can we use biostatistics to quantitate the difference?

3.5 Materials and Method

3.5.1 Cell culture and transfection

HEK293, 6-23, TT cells were seeded on 22 × 40 mm coverslips in 60 mm culture dishes and cultured in 5% CO_2 at 37 ºC in respective media. HEK293 cells were cultured in high glucose Dulbecco's modified Eagle's medium (DMEM) (Invitrogen) containing 10% fetal bovine serum (FBS) with 100 μg/ml penicillin-streptomycin. 6-23 cells were cultured in high glucose DMEM

containing 15% heat-inactivated horse serum, 2.5% FBS, and 100 µg/ml penicillin-streptomycin. TT cells were cultured in F12K medium from ATCC with 10% fetal bovine serum (FBS) with 100 µg/ml penicillin-streptomycin. For immunostaining assays, the cells were grown on 20 × 20 mm coverslips that were placed in 6-well plates one day before the transfection. CaSR-pcDNA and its mutants were transfected using Lipofectamine 3000TM (Invitrogen) according to the manufacturer's instructions. Cells were incubated for 48 h in respective media without or after transfection.

3.5.2 $[Ca^{2+}]_i$ responses in single cells measurements

The method is adapted from Huang et al.[232]. The wild type CaSR or its mutants were transiently transfected into HEK293 cells grown on coverslips and cultured for 48 h. On the other hand, C cells with endogenous CaSR were seeded on coverslips. Subsequently, the cells were incubated for 15-20 min using 4 µM FURA-2 AM. 2 mL of 10 mM HEPES, 140 mM NaCl, 5 mM KCl, 1.0 mM $MgCl_2$, 1 mM $CaCl_2$ and pH 7.4) was used a physiological saline buffer for loading the dye. The coverslips were mounted in a chamber with 0 mM Ca^{2+} buffer on the stage of a Leica DM6000 fluorescence microscope. The cells were illuminated with 340 or 380nm light alternately, and the fluorescence at 510 nm an emission wavelength was recorded in real time. This recording was taken for each of the increased concentration of $Ca^{2+}{}_o$ added for the experiment in the presence or absence of drugs. The ratio of the emitted fluorescence intensities resulting from excitation at both wavelengths (340/380) was utilized as the proportional change in $[Ca^{2+}]_i$ and was further plotted as a function of $[Ca^{2+}]_o$ in kgraph. All experiments were performed at 37°C. Three successive fluctuations in $[Ca^{2+}]_i$ after the initial peak was considered the oscillation.

3.5.3 $[Ca^{2+}]_i$ changes triggered by $[Mg^{2+}]_o$ in single CaSR-transfected cells

The method is adapted from Huang et al.[232]. The wild type CaSR or its mutants were transiently transfected into HEK293 cells grown on coverslips and cultured for 48 h. On the other hand, C cells with endogenous CaSR were seeded on coverslips. Subsequently, the cells were incubated for 15-20 min using 4 μM FURA-2 AM. 2 mL of 10 mM HEPES, 140 mM NaCl, 5 mM KCl, 1.0 mM $MgCl_2$, 1 mM $CaCl_2$ and pH 7.4) was used a physiological saline buffer for loading the dye. The coverslips were mounted in a chamber with 0 mM Ca^{2+} buffer on the stage of a Leica DM6000 fluorescence microscope. The cells were illuminated with 340 or 380nm light alternately, and the fluorescence at 510 nm an emission wavelength was recorded in real time. This recording was taken for each of the increased concentration of $Ca^{2+}{}_o$ added for the experiment in the presence or absence of drugs. The ratio of the emitted fluorescence intensities resulting from excitation at both wavelengths (340/380) was utilized as the proportional change in $[Ca^{2+}]_i$ and was further plotted as a function of $[Ca^{2+}]_o$ in kgraph. All experiments were performed at 37°C. Three successive fluctuations in $[Ca^{2+}]_i$ after the initial peak was considered the oscillation. $[Mg^{2+}]_o$ was increased in a stepwise manner in the presence or absence of 0.25 mM CaSRL in buffer (10 mM HEPES, 155 mM NaCl, 5 mM KCl, 2 mM NaH_2PO_4, 0 mM $MgCl_2$ and pH 7.4). The ratio of the emitted fluorescence intensities resulting [233]. The ratio of the emitted fluorescence intensities resulting from excitation at both wavelengths (340/380) was utilized as the proportional change in $[Mg^{2+}]_i$ and was further plotted as a function of $[Ca^{2+}]_o$ in kgraph. All experiments were performed at 37°C. Three successive fluctuations in $[Ca^{2+}]_i$ after the initial peak was considered the oscillation.

3.5.4 Determination of the effect of CaRL (TNCA) on Mg^{2+}-evoked $[Ca^{2+}]_i$ signaling by stimulation of CaSR in cell populations

Changes in the $[Ca^{2+}]_i$ produced by extracellular Mg^{2+} ($[Mg^{2+}]_o$) in a population of cells were measured by fluorimetry as described previously [234, 235]. A cell line stably expressing CaSR (5001) was seeded on 13.5 x 20-mm coverslips and cultured in dishes filled with DMEM. After reaching 95% confluence, cells were washed three times using loading buffer (20 mM HEPES (pH 7.4), 125 mM NaCl, 5 mM KCl, 1.25 mM $CaCl_2$, 1 mM $MgCl_2$, 1 mM NaH_2PO_4, 1% glucose, and 1% BSA) and subsequently incubated with 4 μM FURA-2 AM/4 μM pluronic F127 for 20 minutes at 37 °C to enable sufficient dye loading in the same buffer. After removing the excess FURA-2 AM, coverslips with cells were diagonally positioned in a quartz cuvette filled with 3 ml experimental buffer (125 mM NaCl, 5 mM KCl, 0.5 mM $CaCl_2$, 0.5 mM $MgCl_2$, 1% glucose, and 1% BSA). Measurements of FURA-2 AM fluorescence at 510 nm when excited at 340 or 380 nm were performed on a QM1 fluorescence spectrophotometer (PTI). The emission ratio of 340/380 was calculated and used to reflect the changes in $[Ca^{2+}]_i$ when different concentrations of $[Mg^{2+}]_o$ were applied to the cells.

To examine the co-activation of CaSR by CaSRL and $[Mg^{2+}]_o$ or $[Ca^{2+}]_o$, different concentrations of CaSRL were placed in the experimental buffer with a fixed concentration of $Ca^{2+}{}_o$ and varying concentrations of $Mg^{2+}{}_o$, or vice versa, as described in the results section. The effects of other ligands were analyzed by comparing the changes in $[Ca^{2+}]_i$ produced by $[Mg^{2+}]_o$ alone or by co-application of Mg^{2+} with other ligands.

3.5.5 Determination of $ERK_{1/2}$ phosphorylation

The 5001 cell line with stably expressed hCaSR, HEK293 cells transiently transfected wild type CaSR or 6-23 cells with endogenous CaSR was starved in serum-free DMEM medium

supplemented with 0.2% (w/v) BSA overnight, followed by washing 3-times with HBSS and a subsequent 10 minute HBSS incubation on the morning of the second day. To induce $ERK_{1/2}$ phosphorylation, varying concentrations of Ca^{2+} or $Mg^{2+}{}_o$ (0-50 mM) or $Ca^{2+}{}_o$ (0-30 mM) with or without 0.5 mM CaSRL were added to cells and incubated for 10 minutes at 37 °C. The cells were then lysed with Pierce RIPA buffer (Thermo Scientific). Total protein concentration was measured using the Bio-rad assay. Lysates containing 100 µg of total protein were loaded onto 4-20 % gradient SDS-PAGE gels for separation. After electrophoresis, proteins on the gel were transferred to nitrocellulose membranes and further analyzed by western blotting. Anti-phospho-p44/42 ERK (1:1000 dilution) and anti-p44/42 (1: 2000) polyclonal antibodies were utilized as probes to detect the phosphorylated $ERK_{1/2}$ and total $ERK_{1/2}$ respectively. A chemiluminescent detection method (AP Conjugate Substrate Kit, Bio-Rad) was applied to detect phospho-$ERK_{1/2}$ and total–$ERK_{1/2}$. The respective bands on western blots were evaluated by densitometry. The EC_{50} of $[Mg^{2+}]_o$ or $[Ca^{2+}]_o$-dependent responses were obtained by fitting the $[Mg^{2+}]_o$ or $[Ca^{2+}]_o$ concentration-response curves with the Hill equation.

3.5.6 Immunoassays

3.5.6.1 Western blot

The transfected cells grown on 60-mm plates were washed with PBS and lysed with 10 mM sodium β-glycerophosphate, 50 mM Tris-Cl (pH 7.4), 150 mM NaCl, 1 mM EDTA (pH 8.0), 1% Triton X-100, 2 mM Na_3VO_4, 50 mM NaF, 10 mM sodium pyrophosphate supplied with proteinase inhibitor cocktail (Roche, Basel, Switzerland) and 1X protease inhibitor cocktail on ice for 30 min. Cell debris was removed by centrifugation at 13,000 rpm for 10 min at 4 °C. The supernatants were denatured in SDS sample buffer (60 mM Tris-HCl, 2% SDS, 10% glycerol, 5% β-mercaptoethanol, 0.1% bromphenol blue) at 100°C for 10 min under reducing conditions and

subjected to 8.5% SDS-PAGE. The proteins resolved by SDS-PAGE were subsequently electro-transferred to a nitrocellulose membrane (Thermo Scientific). The membrane was blocked using 3% non-fat milk (Bio-Rad) in TBS. The CaSR on the blot was detected by incubation with a 1:700 dilution of monoclonal anti-CaR antibody (C0493, Abcam) followed by horseradish peroxidase-conjugated, goat anti-mouse secondary antibody. CaSR was visualized with an enhanced chemiluminescence detection reagent according to the manufacturer's instructions (Pierce Biotechnology).

3.5.7 Immunostaining

HEK293 cells and cancer cells were grown on 20 × 20 mm coverslips placed in 6-well plates. Cells subjected to transfection (if experimental design required it) and after 48 h treated for immunostaining. Cells were washed with ice-cold PBS and fixed with 3.7 % formaldehyde for 15 min at room temperature, followed by a wash with PBS three times. Cells were permeabilized using 0.2 % Triton X in PBS for 10 min at room temperature. Mouse anti-FLAG monoclonal antibody was diluted 1000 times, anti-CaSR ADD at 1:3000, anti-CaM at 1:2000 were used and incubated with cells overnight at 4°C to stain the CaSR. The cells were subsequently washed with PBS and stained with goat anti-mouse Alexa 488–conjugated or goat anti-rabbit Alexa 594 secondary antibody for 1 hour at room temperature. Nuclei were stained with 4′,6-diamidino-2-phenylindole. Fluorescence was visualized using a Zeiss LSM780 confocal microscope.

3.5.7.1 ERK1/2

`Thirty-six hours post-transfection of monolayers of HEK293 cells with CaSR or its mutants, cells were incubated in serum-free high glucose DMEM medium supplemented with 0.2% w/v BSA at 37^{o} C overnight. On the following day, cells were first incubated with HBSS for 30 min, followed by stimulation with varying levels of $CaCl_2$ (0-20 mM) with or without L-Phe (5

mM) for 10 min. At the end of the Ca^{2+}_o stimulation, cells were lysed with RIPA lysis buffer (Millipore, CA, USA). In total, 150 µg aliquots of lysate protein were loaded into either a 12.5%

$$\Delta S = \frac{[M]^n}{K_d{}^n + [M]^n} \qquad \textit{Equation 3. 1}$$

SDS-gel or a 4%-12.5% gradient gel for PAGE and analyzed by western blotting with an antiphospho- p44/42 ERK polyclonal antibody (Cell signaling Technology, Beverly, MA, USA) diluted (1:2000). A chemiluminescent method (AP Conjugate Substrate Kit) was employed to detect the phospo-p44/42 proteins. Quantitative analysis of the results was performed using ImageJ software (National Institutes of Health). The responses were normalized to the maximal effect observed with Ca^{2+}_o alone. The EC_{50} of Ca^{2+}_o-dependent responses was calculated by fitting the Ca^{2+}_o concentration-response curves with the Hill equation

where ΔS is the total signal change in the equation, Kd is the apparent binding affinity, n is the Hill coefficient, and [M] is the free metal concentration.

3.5.8 Biostatistics

In collaboration with Yan Hai from Department of biostatistics, calcium oscillations data was analyzed using 380 only with R (version 3.5.1). Based on oscillation patterns, the spikes were filtered by satisfying the conditions that the amplitude of spikes must be at least 0.1 of the maximum amplitude and single spike duration is at least 35 seconds for each treatment type. The oscillations start was considered if there are at least three spikes within a certain calcium concentration. Then the distribution (percentage of cells) of calcium oscillation, oscillation start point, oscillation endpoint and frequency (peaks/min) for each treatment type were calculated.

3.6 Results

3.6.1 CaSR and CaSR mediated intracellular Ca^{2+} response in HEK293 cells

3.6.1.1 Ca^{2+} signaling due to divalent cations

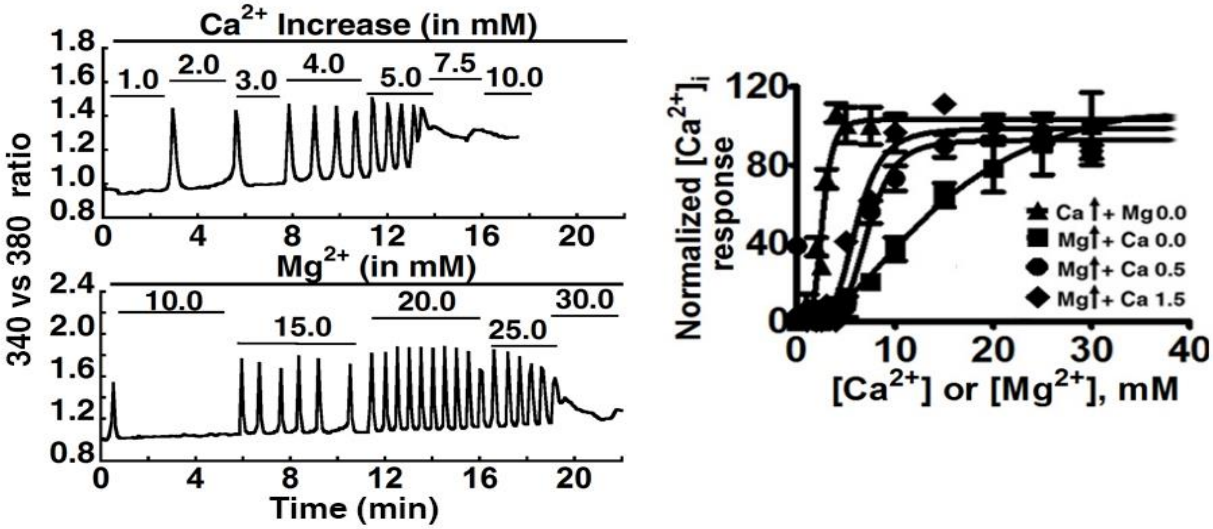

Figure 3.8 Ca^{2+} and Mg^{2+} potentiate CaSR mediated intracellular Ca^{2+} oscillation

A. CaSR mediated oscillation induced by extracellular Ca^{2+} (upper panel) and Mg^{2+} (lower panel) measured by imaging single cell calcium oscillation with FURA-2 AM using HEK293 cells transfected with CaSR. Normalized response curve at various conditions.

Divalent cations are known agonists of CaSR. Ca^{2+} is the primary activator which is able to activate CaSR with EC_{50} ~4 mM and hill number of 3. In 2016, our lab crystallized Mg^{2+} and a tryptophan derivative, TNCA, bound ECD domain of CaSR. Our CaSR mediated signaling study

Table 3.1 EC_{50} and Hill number for Mg^{2+} evoked intracellular oscillation under various Ca^{2+} concentrations

Co-activator (mM)	Single Cell Imaging	
	EC_{50}	Hill number
0.0 Ca^{2+}	12.9 ± 0.3	2.9 ± 0.2
0.5 Ca^{2+}	7.5 ± 0.3	4.7 ± 0.8
1.5 Ca^{2+}	5.9 ± 0.4	4.1 ± 0.8

by Mg^{2+} re-validated the idea that CaSR is indeed modulated by Mg^{2+}, however, with a lower potency than Ca^{2+} with EC_{50} of 13 mM and lower hill number of 2.9 **(Figure 3.8**). With site-directed mutations, E228I, E229I, at the Mg^{2+} binding sites, we were able to validate the binding sites for Mg^{2+}. Additionally, presence of 0.5 mM and 1.5 mM Ca^{2+} was able to potentiate potency of Mg^{2+} by decreasing EC_{50} for Mg^{2+} to ~7.5 and 5.9 mM respectively, which further proved the cooperative nature between Ca^{2+} and Mg^{2+} (**Figure 3.8**). Not only did we show the CaSR mediated signaling increase in case of $Ca^{2+}{}_i$ oscillation, but also through $Erk_{1/2}$ phosphorylation.

Ligand specific intracellular signaling cascades occurs in response to extracellular stimuli-followed by ligand activation GPCRs, thereby catalyzing the exchange of GDP for GTP on the Gα subunit, leading to a decreased affinity of Gα for Gβϒ. The GTP-bound Gα and Gβϒ to interact with several downstream effectors, including adenylyl cyclases, phosphodiesterases, phospholipases, tyrosine kinases, and ion channels [236, 237]. This diverse effectors of GPCR makes it a potential druggable target for numerous pharmaceutical compounds [238, 239].

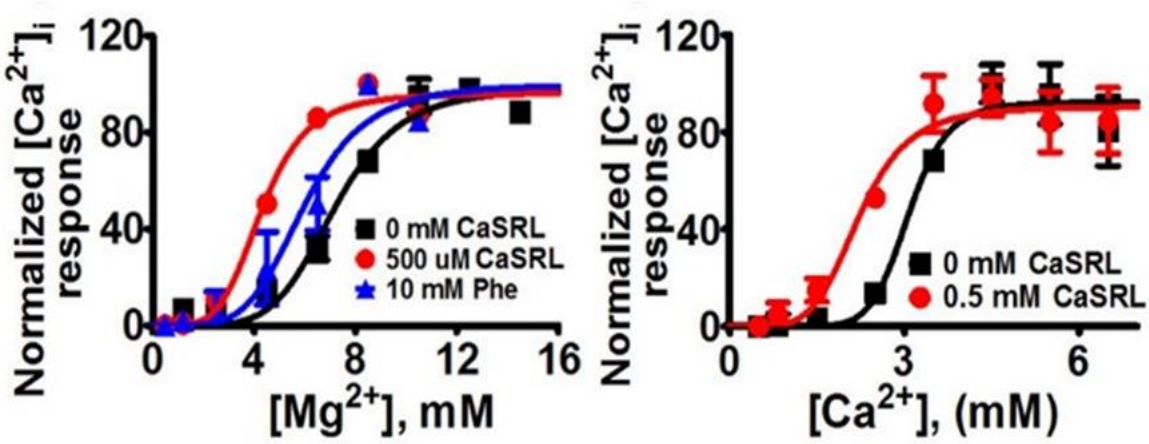

Figure 3.9 TNCA potentiates $[Mg^{2+}]_o$- or $[Ca^{2+}]_o$-evoked $[Ca^{2+}]_i$ responses
TNCA potentiates $[Mg^{2+}]_o$- or $[Ca^{2+}]_o$-evoked $[Ca^{2+}]_i$ responses in a population assay in 5001 cells measured by FURA-2 AM acetoxymethyl (AM) in the absence (black square) or presence of Phe (blue triangular) or TNCA (red closed circle).

3.6.1.2 Ca^{2+} signaling due to novel tryptophan derivative, TNCA/CaRL

Furthermore, we showed cooperative activation between the metals and tryptophan-based compound known as TNCA. The TNCA was shown to increase the sensitivity of Ca^{2+} and Mg^{2+}, thus acted as a co-agonist (**Figure 3.9, Figure 3.10**). In the presence of 0.25 mM TNCA, the EC_{50}

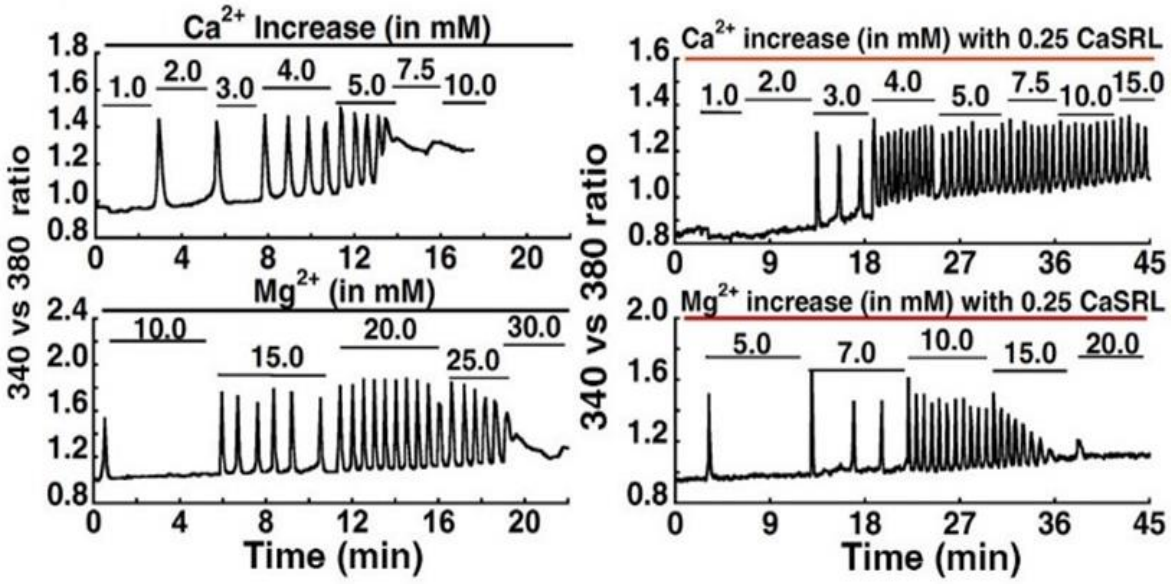

Figure 3.10 A representative oscillation pattern from a single HEK293 cell stimulated with various concentrations of extracellular Ca^{2+} or Mg^{2+} in the absence and presence of 0.25 mM TNCA.

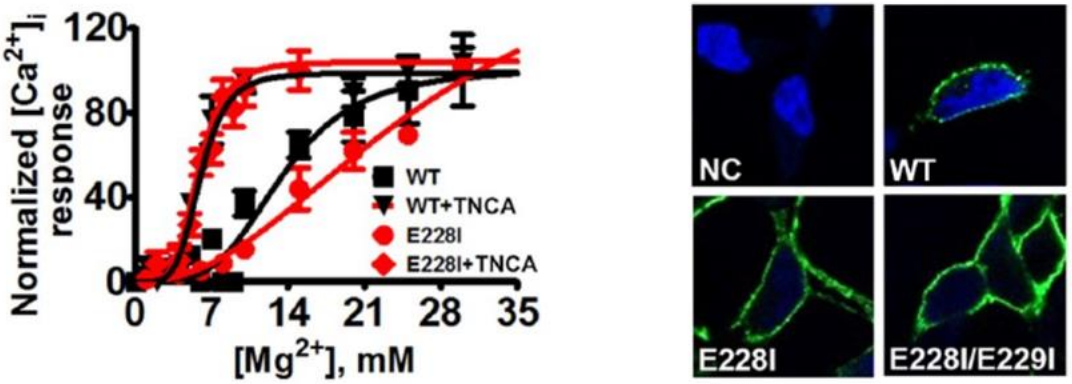

Figure 3.11 Potentiation of TNCA on $[Mg^{2+}]_o$-evoked $[Ca^{2+}]_i$ responses in WT and mutants using single cell imaging

A. TNCA potentiates $[Ca^{2+}]_i$ responses of both WT CaSR or mutant E228I to $[Mg^{2+}]_o$ stimulation in the single cell imaging assay in the absence of basal $[Ca^{2+}]_o$. B. Membrane expression of CaSR, mutant E228I and double mutant E228I/E229I. Blue: DAPI staining cell nuclei. Green: hCaSR immunoreactivity

were decreased to 2.3 mM and 4.55 mM for Ca^{2+} and Mg^{2+}, respectively. Interestingly, TNCA was able to rescue the CaSR activity in the impaired mutants **(Figure 3.11, Figure 3.12).**

3.6.1.3 Ca^{2+} signaling in the presence of cinacalcet

Cinacalcet is a known agonist of CaSR and the only FDA approved drug targeting secondary hyperparathyroidism. It has been used for patients with chronic kidney disease. It potentiates sensitivity of CaSR by decreasing the EC_{50} and shifting the concentration-response curve for extracellular Ca^{2+} to the left (**Figure 3.13**). The oscillation distributes between 0.5 to 3 mM Ca^{2+}, with the majority starting at 1mM and ending at 1 mM. Additionally, 80 % of the cells undergo oscillation frequency of 1.5-2.0 peaks/min (**Figure 3.13)**. Therefore, cinacalcet caused the enhanced activity of the cells along with the early termination of oscillation as compared to the wild type.

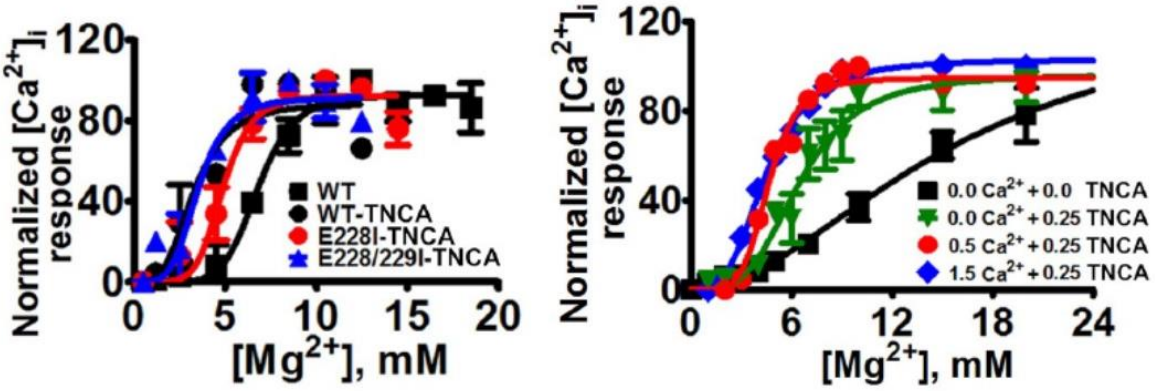

Figure 3.12 Potentiation of TNCA on $[Mg^{2+}]_o$-evoked $[Ca^{2+}]_i$ responses in WT and mutants using population studies

***A)** TNCA potentiates $[Mg^{2+}]_o$-evoked $[Ca^{2+}]_i$ responses in CaSR mutant E228I and the double mutant E228I/E229I analyzed using fluorimetry in cell population assay in 0.5 mM basal $[Ca^{2+}]_o$. **(B)** Calcium and (or) TNCA potentiate the $[Mg^{2+}]_o$ -stimulated intracellular calcium responses in the single cell imaging assay.*

3.6.1.4 Ca^{2+} signaling in the presence of NPS-2143

NPS-2143 is a known antagonist of CaSR with an IC50 of 43 nM. It is known to stimulate the parathyroid hormone secretion from bovine parathyroid cells with EC50 of 41 nM. 10 µM of NPS-2143 was used in the Ca^{2+} mixture. It was able to completely abolish CaSR mediated intracellular oscillation in HEK293 cells **(Figure 3.13)**.

3.6.1.5 Ca^{2+} signaling in the presence of W7, a CaM inhibitor

CaM is known CaSR binding partner in Ca^{2+} condition and is predicted to bind at intracellular C-tail of CaSR at 868-TIEEVRCSTAAHAFKVAARATLRRSNVSRKRSSS-901 [240]. Huang et al in 2010 have shown CaM/Ca^{2+} to be an important modulator for membrane expression of CaSR [3]. Its binding region overlaps with the phosphorylation site T888 and previous paper has shown it to be important for stabilizing CaSR. Our work by using W7, a CaM inhibitor shows a decrease in the overall number of oscillatory cells. The oscillation distributes between 1 to 5 mM Ca^{2+}, with the majority starting at 2 mM and ending at 4 mM (**Figure 3.13**). Additionally, 40 % of the cells undergo oscillation frequency of 0.5-1 peaks/min (**Figure 3.13**). Therefore, W7 caused the delay in oscillation frequency as well as the overall activity of the cells as compared to the wild type. We also carried out functional study with Co-IP where we showed the binding of CaM in Ca^{2+} dependent manner which supports the earlier study.

3.6.1.6 Additive change in Ca^{2+} signaling in the presence of cinacalcet and W7

We show that W7 is able to retard the efficacy of cinacalcet by preincubating the cells for 30 min with 50 µM W7 (**Figure 3.13**). The overall oscillation distribution, starting point, end point and oscillation frequency were found to be in between the response of W7 and cinacalcet. This also suggests that cinacalcet is able to partially rescue the inhibition of CaM.

3.6.2 CaSR and CaSR mediated intracellular Ca^{2+} response in thyroid cancer cells

CaSR has been shown to play a role in tumor growth, invasion and metastasis of several cancers including prostate cancer, breast cancer, thyroid cancer, etc. In this study, we investigate and carry out the comparative analysis of the CaSR mediated Ca^{2+} signaling in cancer cells as compared to the wild type CaSR in HEK293 cells. We observe a dramatic difference in the

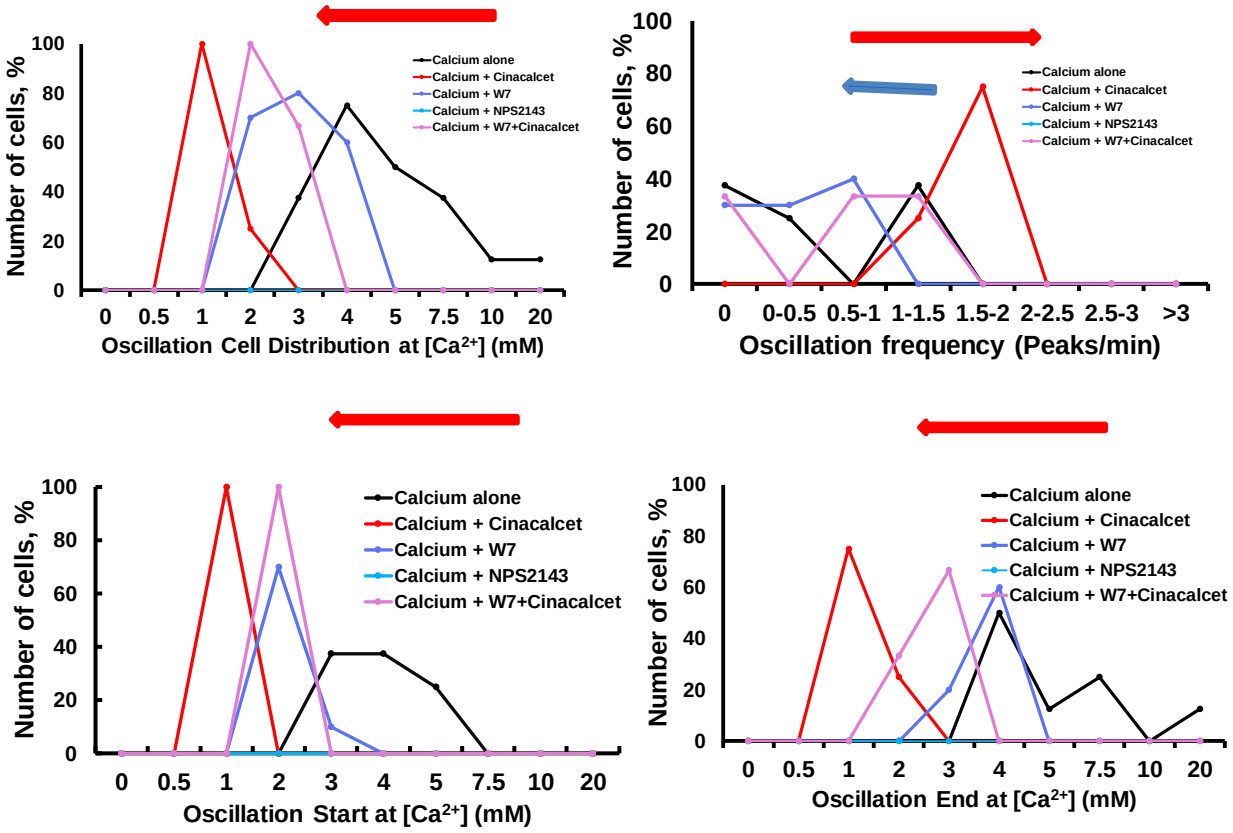

Figure 3.13 CaSR mediated oscillation pattern for wild type CaSR transfected in HEK293 cells due to extracellular Ca^{2+} and or CaSR associated drugs

Oscillation Cell distribution shows that wild type CaSR oscillates between 2-10 mM extracellular $Ca^{2+}$and frequency between 1-1.5 peaks/minute. With addition of cinacalcet the distribution is narrow between 0.5-3 mM and the frequency is increased by 2 folds. With addition of W7 the distribution is narrow between 1-5 mM and the frequency is decreased by 1fold. With addition of NPS2143 the distribution is completely obliterated. With addition of cinacalcet and pre-incubation of W7, the distribution lies between the response of cinacalcet and W7. The start and end points shift to left with all the drugs.

expression, signaling from heterogeneity in oscillation pattern, frequency, start and end of oscillation.

Medullary tumors are the third most common of all thyroid cancers and makeup about 3% of all thyroid cancer cases (*https://www.endocrineweb.com/conditions/thyroid-cancer/thyroid-cancer-medullary-cancer*). Unlike papillary thyroid cancer and follicular thyroid cancer that arise from thyroid hormone-producing cells, medullary thyroid cancer originates from the parafollicular or C cells of the thyroid. It has a low cure rate. 10-year survival rates are 90% when all the disease is confined to the thyroid gland, 70% with spread to cervical lymph nodes and 20% when spread to distant sites. CaSR not only inhibits PTH secretion but also enhances the secretion of calcitonin from thyroid parafollicular C-cells. Calcitonin is a calcium-decreasing hormone.

In a study by Haller-Brem et al. in 1987 shows that 6-23 cells respond to a rise in Ca^{2+} from 0.5 to 3 mM with a transient [13]. In TT, the rise of Ca^{2+} from 0.5 to 3 mM did not affect the Ca^{2+}_i. The calcitonin and calcitonin gene-related peptide (CGRP) release was shown to be dose dependent on Ca^{2+}_i when electropermeabilized or when ionomycin was used [13]. Ionomycin is able to mobilize Ca^{2+} from the intracellular store. This result indicates a defect in the Ca^{2+} signal transduction in the TT cell line. Another study by Eckert et al. in 1989 showed that pre-incubation of 6-23 cells with 1 µM glucagon or 1 mM 8-Bromo-cAMP caused intracellular calcium oscillation when Ca^{2+}_o was raised to 3 mM [213]. These oscillations were perturbed by using EGTA to chelate Ca^{2+}_o or by addition of calcium channel blocker to block voltage-dependent calcium channels [213]. Both 8-bromo-cAMP and glucagon induce cAMP pathway activation. rMTC 6-23 cells are calcitonin secreting line derived from transplantable WAG/Rij rat strain medullary thyroid carcinoma. Only in 1996, Freichel showed the involvement of CaSR in Ca^{2+} sensing in both of these cells. TT cells were shown to lack voltage-dependent L-type calcium channels [6, 210].

Thomsen et al. in 2012 showed that strontium biases CaSR signaling toward ERK1/2 signaling and possibly another pathway independent of Gq/11 signaling and $[Ca^{2+}]i$ mobilization [214]. Furthermore, truncated CaSR variant, CaSRb has been identified in TT cells [212]. In our study, we study the Ca^{2+} sensing mechanism further through CaSR in the C-cells.

3.6.2.1 CaSR mediated Ca^{2+} signaling in human thyroid cancer TT cell

We observed an interesting transient CaSR mediated peak with the increment of $[Ca^{2+}]_o$ (**Figure 3.14**). The application of CaSR associated drugs and W7 were able to evidently perturb the number of responding cells as well as the Ca^{2+} concentration at which the response occurred. Ca^{2+} alone was able to evoke transients at 5 mM and 7.5 mM with low percent of cells, 22% and 9 %, respectively. Cinacalcet was not only able to increase the number of responding cells to 88%, but also potentiate these transients to 2 mM. The efficacy was upregulated as the $Ca^{2+}{}_i$ rise was almost 40% greater than in other treatment conditions. NPS-2143 was able to limit the activation to mostly 5 mM and completely eradicate the response at the 7.5 mM. It also lowered the number of responding cells to 7%. W7 seemed to potentiate the response to 1, 2 and 3 mM but limited the responding number of cells to less than 17%. On the other hand, pre-incubating the cells with W7 for 30 min dramatically impeded the cinacalcet effect, validating the role of CaSR mediated signaling in Ca^{2+} sensing responses. Our results indicate the important function of CaM in CaSR functioning in human thyroid cancer cells. Like rMTC 44-2 cells, TT cells were insensitive to Mg^{2+} implying biased signaling.

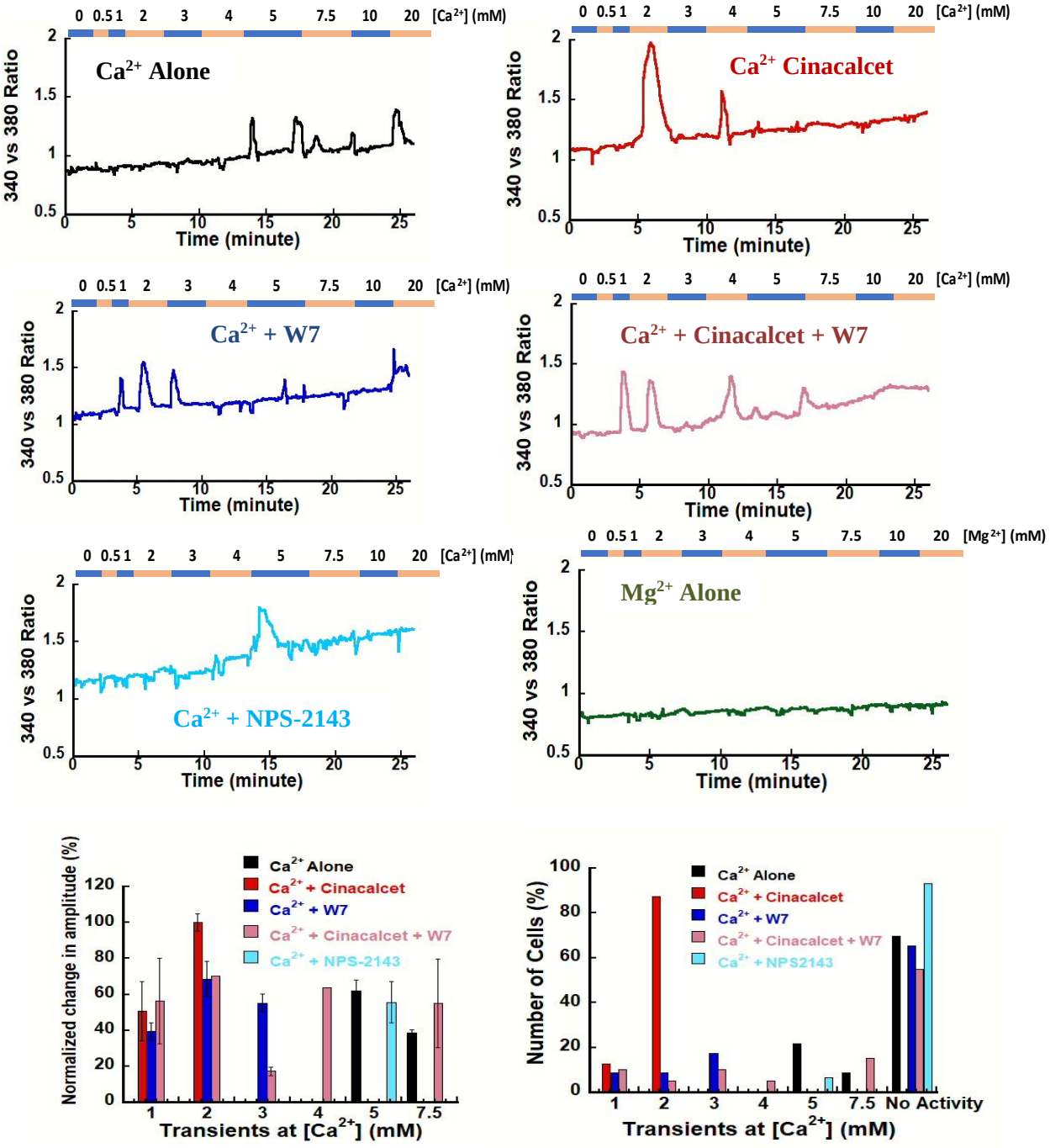

Figure 3.14 CaSR mediated signaling pattern in TT cells at various Ca^{2+} concentrations and various drugs

3.6.2.2 CaSR and CaSR mediated intracellular Ca^{2+} signaling in rat thyroid cancer cells

CaSR mediated intracellular signaling in rat 6-23 cells were highly heterogeneous with regards to not only the cell stock obtained from ATCC and passage of the cells but also amongst the cells from the same batch (**Figure 3.16**). To examine the CaSR mediated oscillation, 6-23 cells were seeded, incubated with FURA-2 AM and titrated with varying Ca^{2+} concentrations. Early passaged cells from stock obtained in 2017 displayed three distinct groups of signaling where 64% of the cells had over-activated CaSR with EC_{50} of 0.73 mM and Hill number of 1.5 for Ca^{2+}. This is almost four-fold lower in the EC_{50} as compared to the wild type and also is two-fold lower in cooperativity. Unlike the earlier reports of the requirement of the inducer of cAMP for oscillation, the cells were capable of oscillating in the presence of $[Ca^{2+}]_o$ alone.

The heterogeneity was also clearly observed when the oscillation frequency was compared between the three groups of cells with three distinct patterns (**Figure 3.16**). The majority of the cells (group A), were overactivated cells and the oscillation frequency were distributed from 0.-2.5 peak/min with 55% of those overactivated cells responding with 1.6-2.0 peak/min. The wild type CaSR has a frequency at 1.1-1.5 peaks/minute. The receptor seemed to desensitize at 15-30 mM Ca^{2+} as the oscillation frequency is almost 0-0.5 peaks/min. We observed that in group B and C which represented 18% each, had limited frequency to 0-0.5 peaks/minute at 1.5-2.5 mM Ca^{2+}. The frequency increased to 1 peaks/minute in the presence of 15-30 mM high Ca^{2+} concentration for both B and C. These results show that CaSR with varying sensitivity is present in 6-23. Not only was the CaSR mediated intracellular calcium oscillation hyper-active, but also CaSR mediated ERK1/2 indicated hyperactivity even at 0 mM Ca^{2+} with a steady increase in the ERK phosphorylation with the gradual increase in $[Ca^{2+}]_o$.

Interestingly, 6-23 cells did not show any agonistic behavior of Mg^{2+} in the absence of Ca^{2+} (**Figure 3.18**). However, 0.5mM Mg^{2+} was able to induce transition peaks in the presence of 1mM Ca^{2+}. This could indicate that the divalent cation binding domain of CaSR in 6-23 cells to be different from the wild type. They could be specific for Ca^{2+} and with the increase in Mg^{2+}, Ca^{2+} is displaced from the binding pocket and therefore, CaSR is de-activated. This could also imply that the Mg^{2+} have biased signaling. This is interesting and is supported as McGhee et al. in 1997 also illustrated the potency of CaSR activation of various divalent cations as $Gd^{3+}>Ba^{2+}>Ca^{2+}>>Mg^{2+}$ [45]. rMTC cells also are known to have no sensitivity to Mg^{2+} [215].

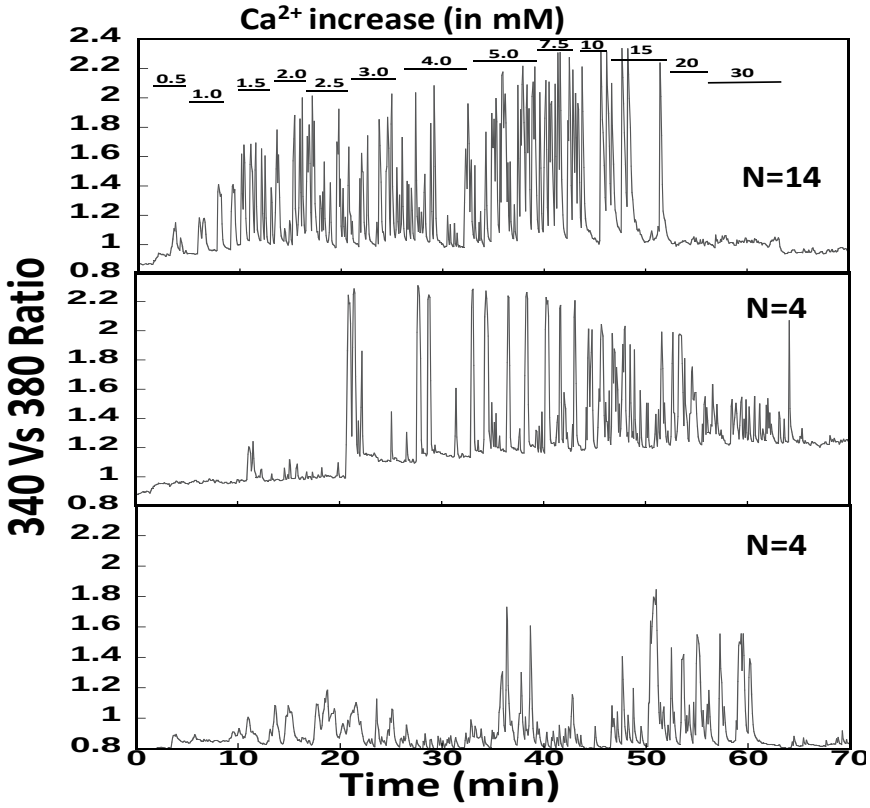

Figure 3.15 CaSR mediated intracellular Ca^{2+} response in 6-23 cells.

CaSR mediated oscillation, 6-23 cells were seeded, incubated with FURA-2 AM and titrated with varying Ca^{2+} concentrations. Most of the cells (group A), were overactivated cells and the oscillation frequency were distributed from 0.-2.5 peak/min with 55% of those overactivated cells responding with 1.6-2.0 peak/min.

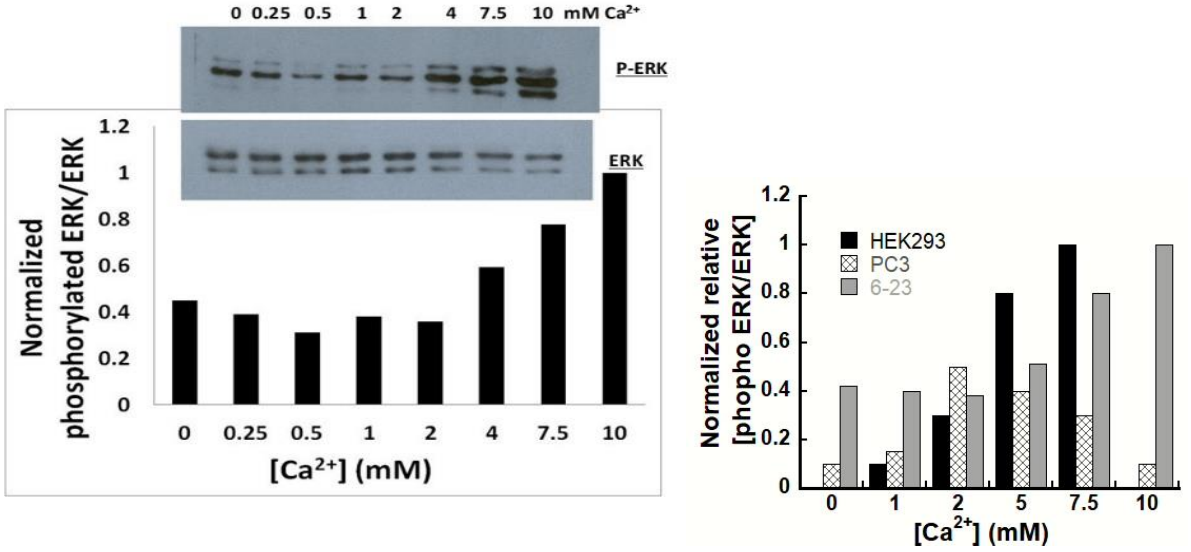

Figure 3.17 ERK1/2 phosphorylation in 6-23 and comparison with HEK293 cells

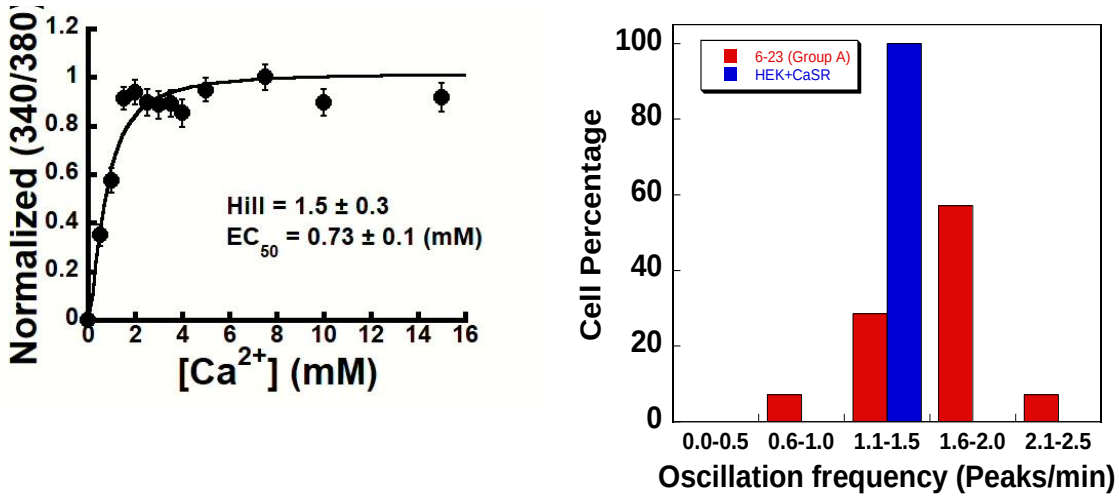

Figure 3.16, Hill curve of the response fitted and oscillation frequency of the response

The EC50 of CaSR for Ca^{2+} was 0.73 mM as compared to wild type at 3 mM. The wild type CaSR has a frequency at 1.1-1.5 peaks/minute. The receptor seemed to desensitize at 15-30 mM Ca^{2+} as the oscillation frequency is almost 0-0.5 peaks/min. We observed that in group B and C which represented 18% each, had limited frequency to 0-0.5 peaks/minute at 1.5-2.5 mM Ca^{2+}. The frequency increased to 1 peaks/minute in the presence of 15-30 mM high Ca^{2+} concentration for both B and C.

The reduced Mg^{2+} sensitivity in the light of 92% sequence similarity between rat and bovine CaSR and intact Ca^{2+} binding sites could be resultant of tissue specific post-translational modifications

or differential CaSR regulatory protein. This paper also indicates the role of L-type voltage gated channel and Gq/11 in the response to extracellular calcium by using channel blocker nimodipine and phosphatidylcholine PLC inhibitor, D609, respectively. This study used 5-HT and phosphor-kinase C for CaSR mediated signaling response.

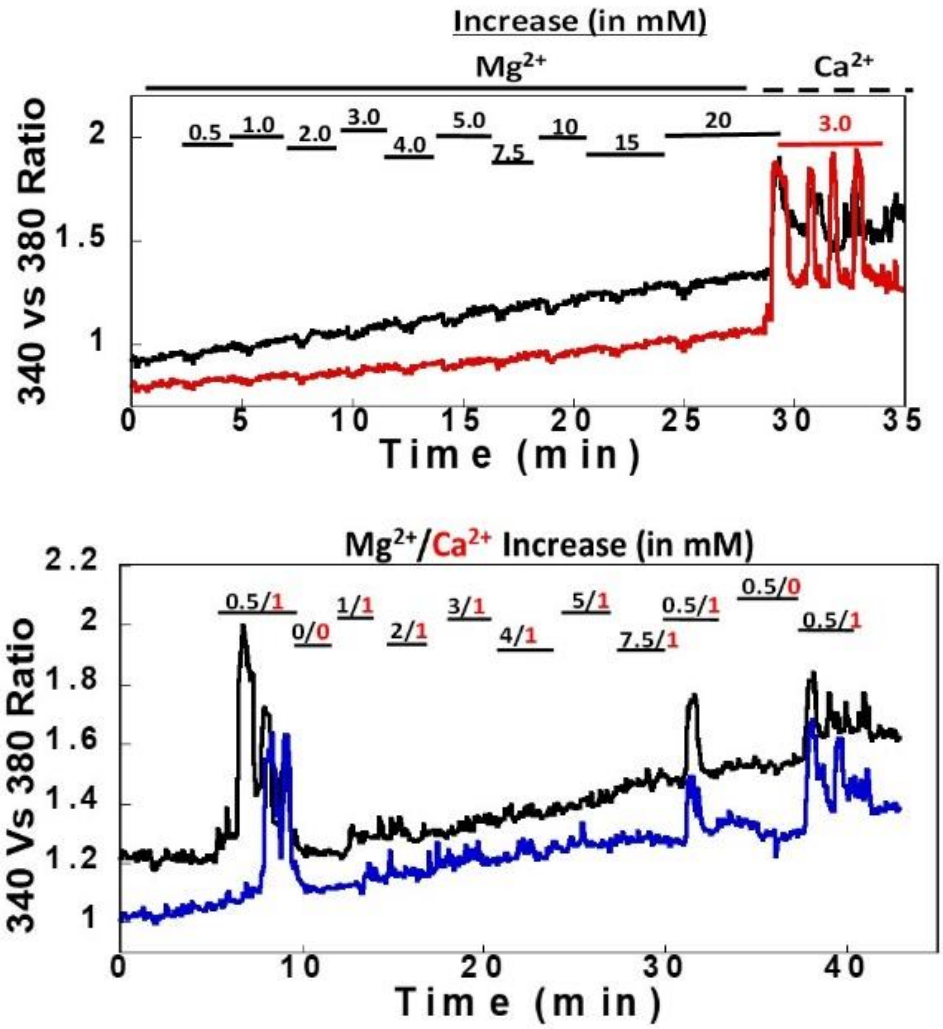

Figure 3.18 ERK and effect of Mg^{2+} in intracellular Ca^{2+} signaling in 6-23

6-23 cells did not show any agonistic behavior of Mg^{2+} in the absence of Ca^{2+}. However, 0.5mM Mg^{2+} was able to induce transition peaks in the presence of 1mM Ca^{2+}.

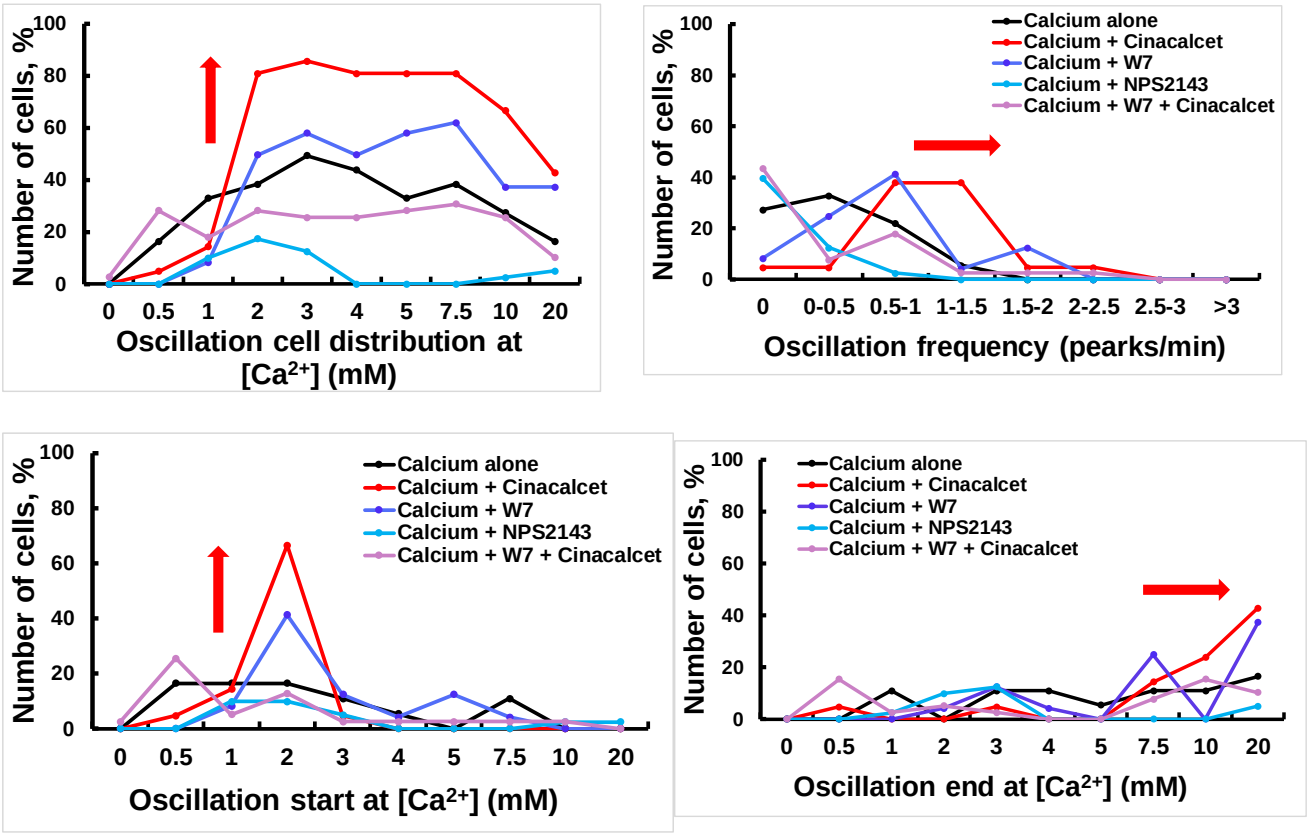

Figure 3.19 Oscillation pattern of endogenous CaSR in 6-23 cells due to extracellular Ca2+ and or CaSR associated drugs

Oscillation Cell distribution shows that endogenous CaSR oscillates between broad 1-20 mM extracellular Ca^{2+} and frequency between 1-1.5 peaks/minute. With addition of cinacalcet the percentage of the cells increase, and the frequency is increased by 1.5 folds. With addition of W7 the percentage of the cells decrease, and the frequency and percentage of cells is decreased. With addition of NPS-2143, oscillation is not completely obliterated. With addition of cinacalcet and pre-incubation of W7, the distribution lies between the response of cinacalcet and W7. Oscillation start is broad but brings to maximum at 2 mM for cinacalcet and W7. The end point is broad for all the treatments.

We collaborated with Yan Hai to use R-programming to quantitate the complicated peaks in the second batch of 6-23 from ATCC. Our results show a clear effect of cinacalcet in the number of responsive cells increasing by ~ 25% and increasing the oscillation frequency between 1-2 peaks/minute **(Figure 3.19).** Similarly, we observe the partial down-regulatory effect of NPS-2143 where the number of cells responding is drastically decreased to < 15% and oscillation frequency

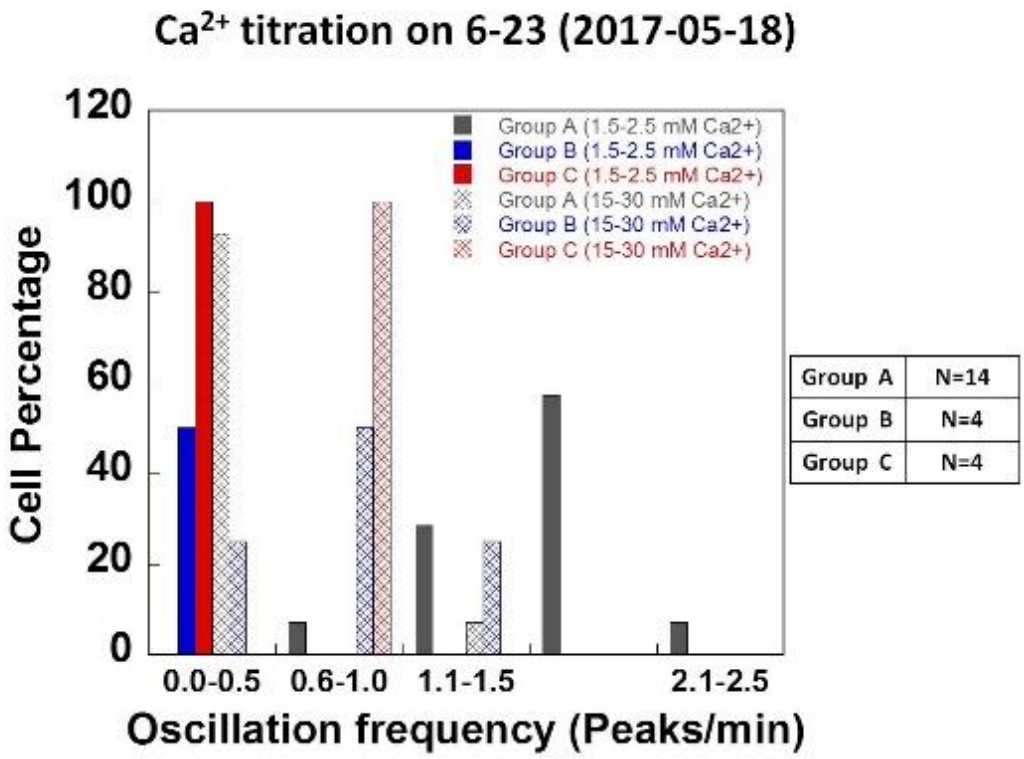

Figure 3.20 Oscillation frequency calculated between 1.5-2.5 mM and 15-30 mM Ca^{2+} in 6-23.

Group A had higher oscillation frequency distribution at 1.1-2.5 peaks/min at 1.5-2.5 mM Ca^{2+}. At higher Ca^{2+} of 15-30 mM induced much lower oscillation. Other groups B and C had lower oscillation frequency.

decreased to 0-0.5 peaks/minute. W7 on its own is able to change the oscillation pattern but doesn't have a specific trend. However, the W7 had an evident effect on cinacalcet agonism by decreasing the number of responding cells to 25% and decreasing the oscillation frequency to 0.5-1 peaks/minute. This indicates a significant role of CaM in inducing CaSR mediated oscillation in 6-23 cells. As compared to the wild type transiently transfected in HEK293 cells, the oscillation pattern is more convoluted. This might suggest an additional Ca^{2+} sensing mechanism in 6-23 cells. Like rMTC 44-2 cells, the second batch of 6-23 cells displayed complex $Ca^{2+}{}_i$ response.

3.6.3 Comparison of the differential oscillation pattern between C cells and HEK293 cells

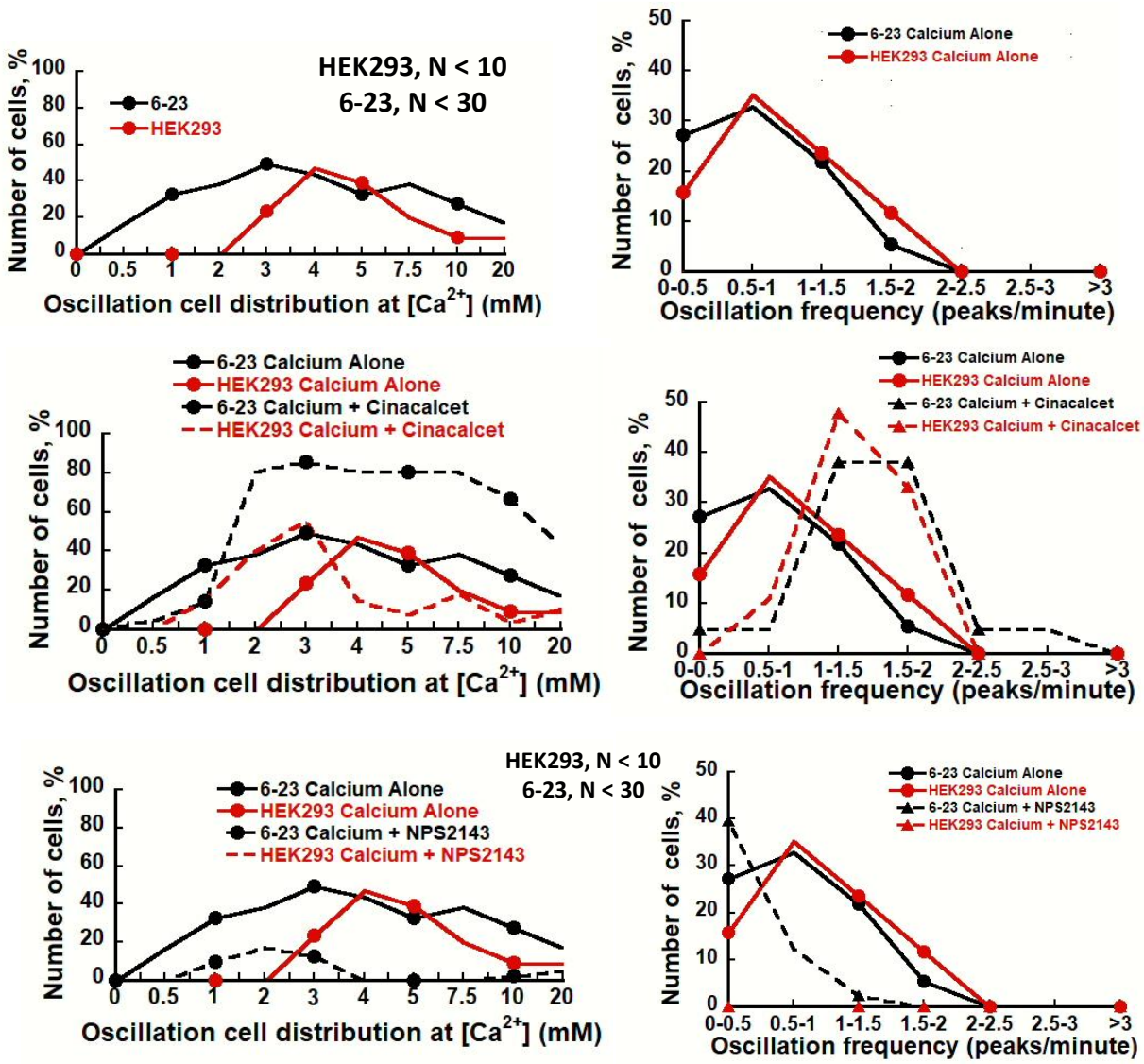

Figure 3.21 Comparison of differential oscillation pattern between 6-23 and HEK293 cells

Differential oscillation pattern was observed between the two cell lines for Ca^{2+} signaling where they had similar frequency distribution with Ca^{2+}. However, cinacalcet affects responding cell number for 6-23 and shifts distribution to the left for HEK293. Additionally, the cinacalcet affects similarly to frequency changes. Complete reduction of CaSR mediated signaling was observed due to NPS2143 in HEK293, but only partial obstruction of the CaSR mediated

signaling in distribution as well as frequency. Similarly, as in 6-23, cinacalcet increases the number of cells responding by 60% in TT cells and NPS2143 only partially obstructs response.

3.6.4 Dissecting the basis of differential CaSR mediated signaling in C cells

3.6.4.1 Expression of wild type in HEK293 and 5001

HEK293 transfected with CaSR-FLAG

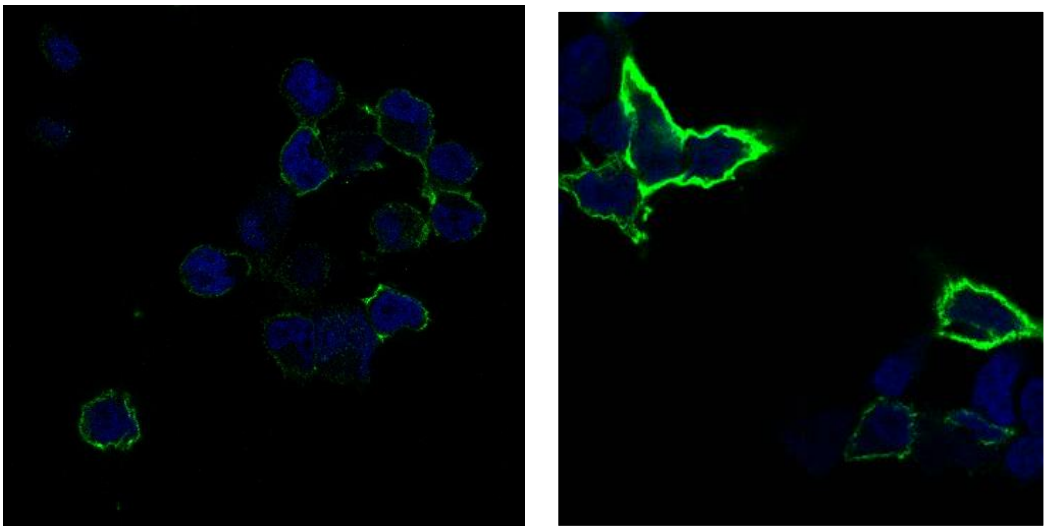

ICC: Anti-CaSR ADD

ICC: Anti-flag antibody

Figure 3.22 Immunostaining of CaSR in HEK293 cells

Efficiency of anti-ADD antibody for immunostaining is not as strong as using anti-FLAG antibody

5001 in HEK293 cells stably transfected with wild type CaSR. HEK293 cells are transiently transfected with FLAG-hCaSR pcDNA3.1. Western blot results show comparative total CaSR in both the cells types. Using two different antibodies show that anti-FLAG is much more specific for our assays. We observe plasma membrane CaSR stained in **Figure 3.22.**

3.6.4.2 Comparison of Expression of CaSR in thyroid cancer cell types

Expression of CaSR in thyroid cancer cells was compared with the wild type in HEK293 cells as shown in **Figure 3.23.** Expression of endogenous CaSR was lower by four folds in thyroid cancer cells. Interestingly, the monomer CaSR from the total had a slightly lower molecular weight in TT, similar to PC3. No monomers were detected for 6-23. The less molecular weight CaSR suggests that the CaSR detected in total are more likely immature less glycosylated CaSR. This is further supported by the immunostaining results of endogenous CaSR in thyroid cancer cells. TT and 6-23 cells were stained with anti-CaSR ADD antibody (1:3000 dilution) in permeabilized and non-permeabilized conditions. CaSR-FLAG pc DNA3.1 was transfected to examine the insertion

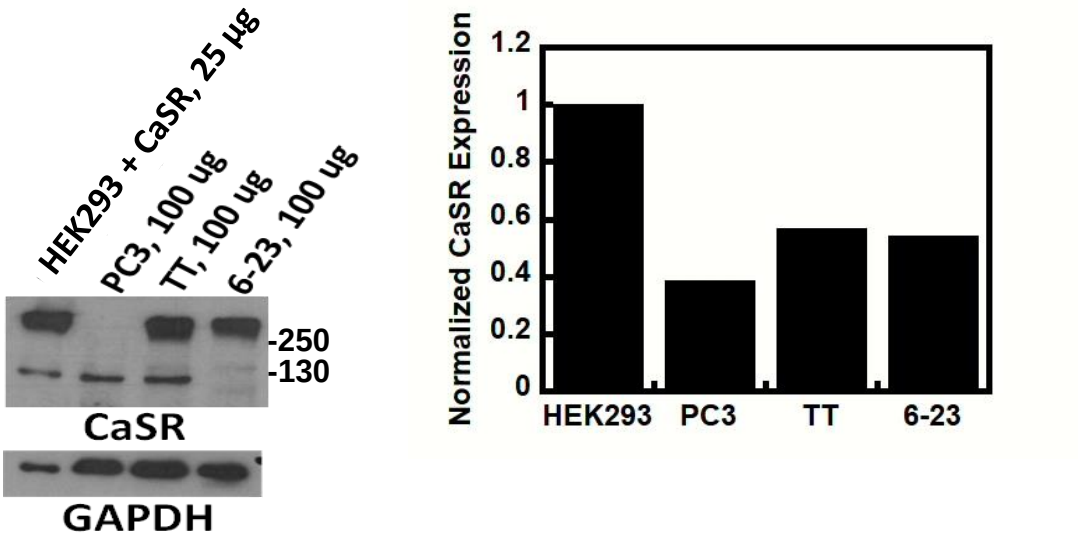

Figure 3.23 Western blot of total cell lysates in various cell lines

25-100 µg of total lysates from about 100% confluent cells were loaded to 7.5% SDS Page gel in reducing condition (5% β-mercaptonal). Oligomers at > 250 kDa in all except PC3 and monomers 110-130 kDa were observed in all except 6-23 cells.

of CaSR in the plasma membrane. Most CaSR were detected within the cell in permeabilized

condition and the significantly lower amount was observed in the plasma membrane in both 6-23 and TT cells in non-permeabilized conditions (**Figure 3.24, Figure 3.25).**

TT cells un-transfected and non-permeabilized

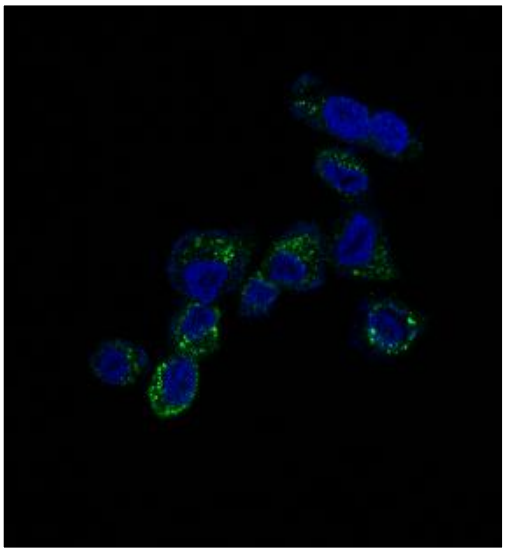

TT cells transfected with CaSR-FLAG and non-permeabilized

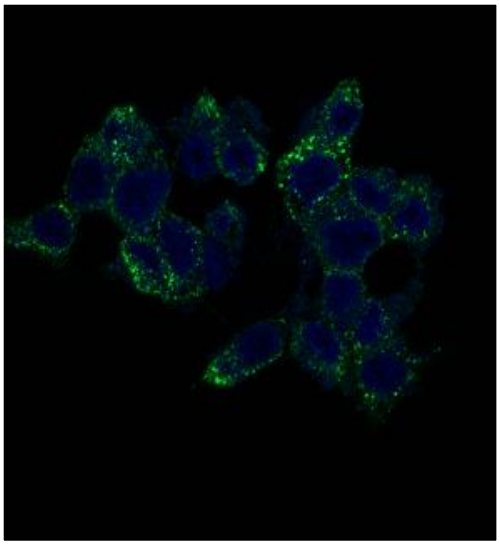

TT cells un-transfected and permeabilized

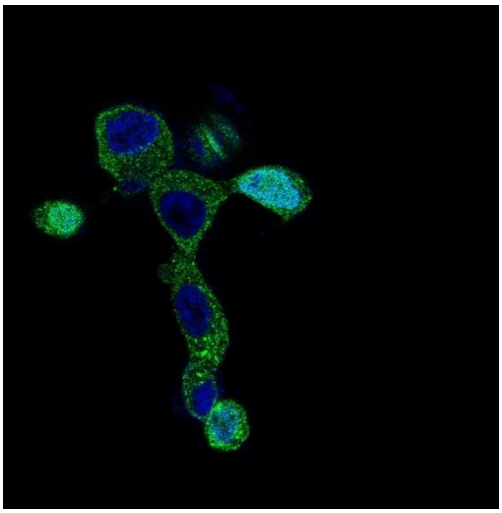

ICC: Anti-CaSR ADD antibody

Ex: 488 (CaSR)

Ex: 405 (DAPI; nucleus)

Figure 3.24 Evaluating Expression level and effect of overexpression of CaSR in TT cells Cells were seeded to 20X20 coverslips and stained with anti-mouse Alexa fluor 488 against anti-CaSR ADD and DAPI in non-permeabilized condition

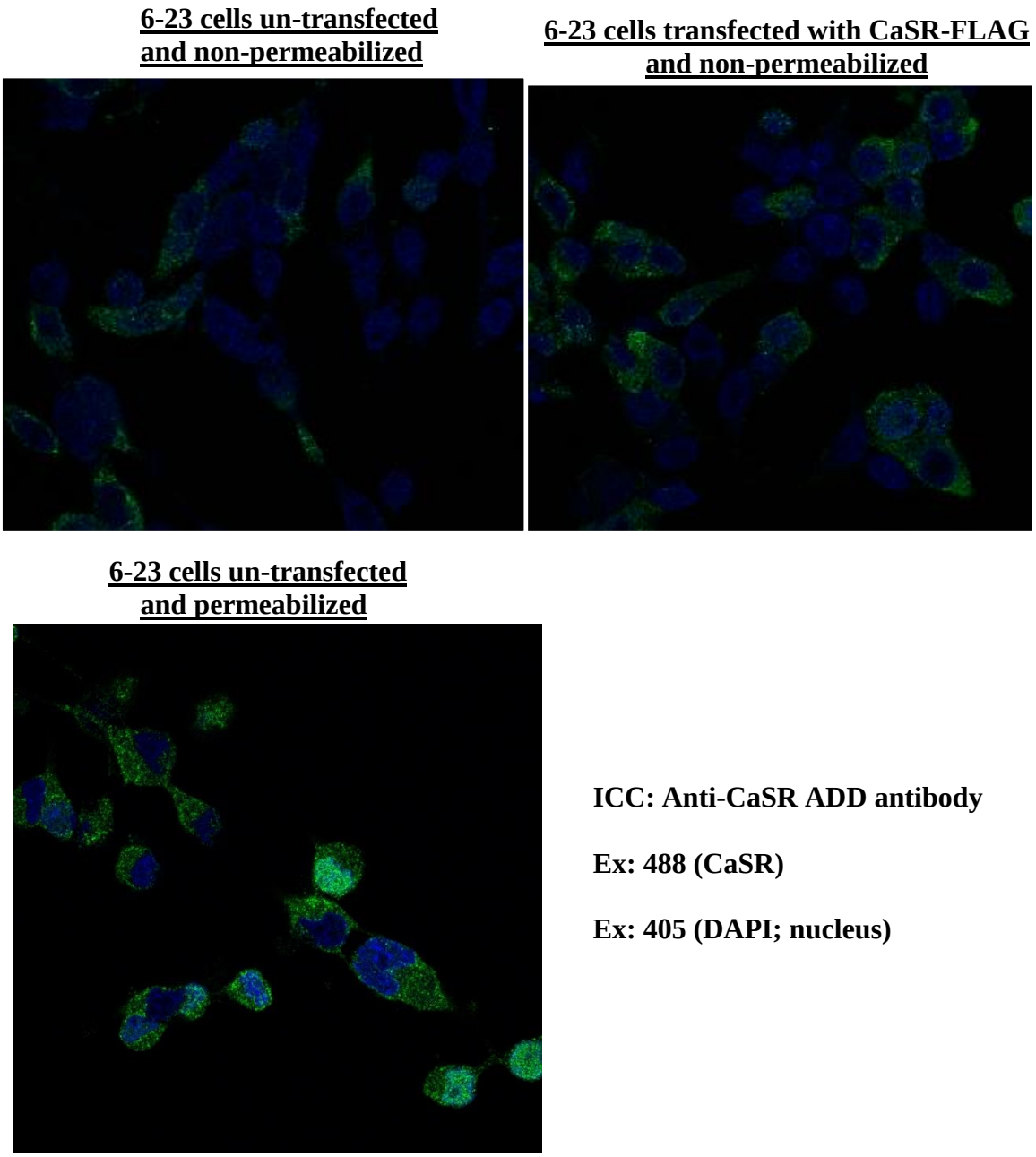

Figure 3.25 Evaluating Expression level and Effect of overexpression of CaSR in 6-23

3.6.4.3 Characterization of role of CaM as CaSR modulator in the differential CaSR mediated signaling between C cells and HEK293 cells.

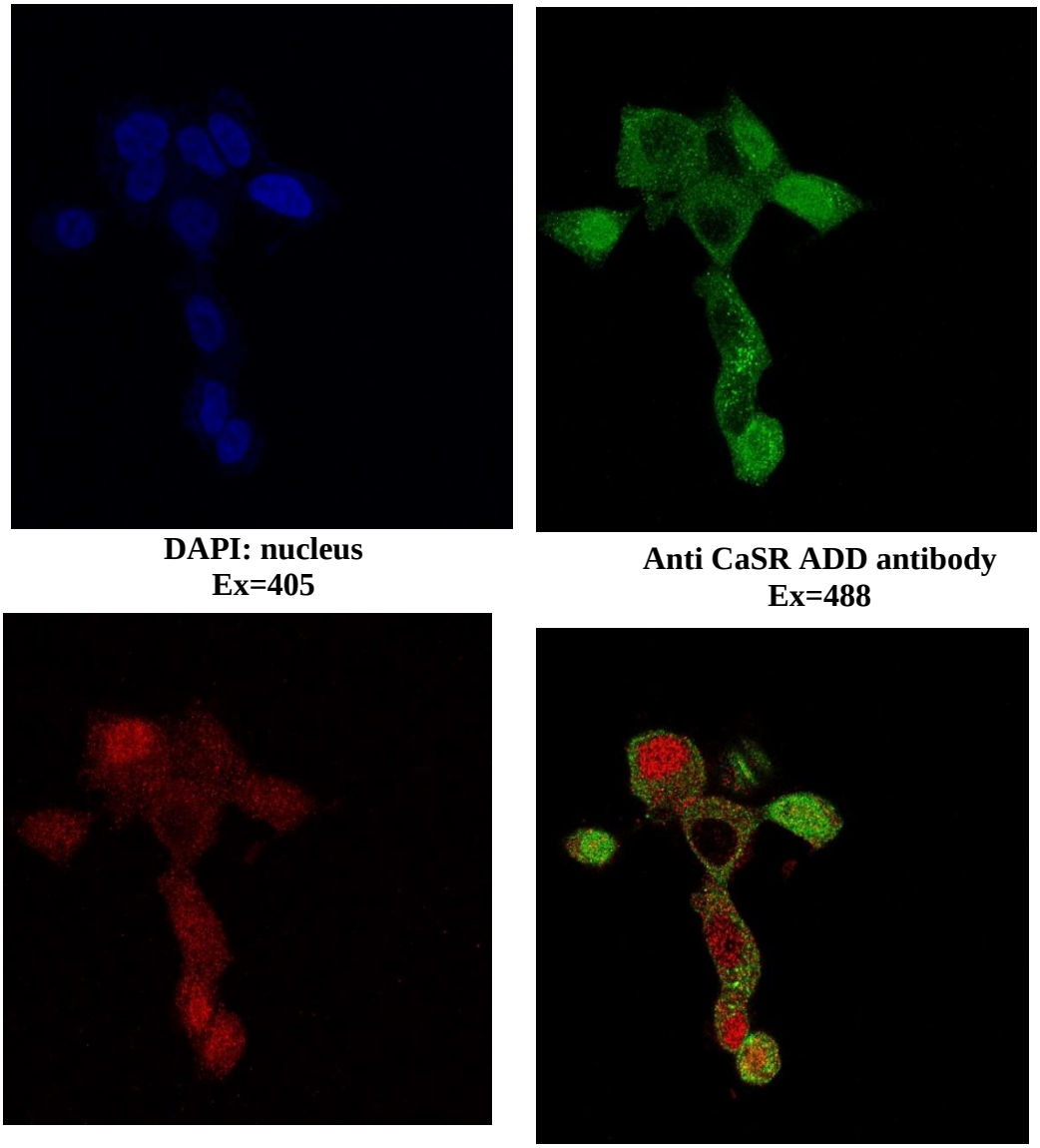

Figure 3.26 Immunostaining of CaM and CaSR in TT cells

3.6.4.3.1 CaM expression in thyroid cancer cells

Huang et al. in 2010 have demonstrated that CaM interacts with CaSR in a Ca^{2+} dependent manner and CaM binding affects the CaSR surface expression, as well as CaM binding site

mutations, hinders CaSR mediated intracellular oscillation by decreasing the oscillation frequency [3]. Since we observed CaM dependent Ca^{2+}_i response in the human and rat thyroid medullary cancer cells, we further investigated the CaM binding with co-immunoprecipitation and immunostaining.

3.6.4.3.2 CaM expression in TT cells

CaM was visualized using immunostaining with anti-CaM antibody (**Figure 3.26)**. We observed CaM throughout the cell and the merged image shows some co-localization of the CaSR and CaM. The images were taken in LSM800 with plan-apochromat 40X/1.4 oil DIC. Since the protein staining was everywhere, it is challenging to locate the definite co-localization.

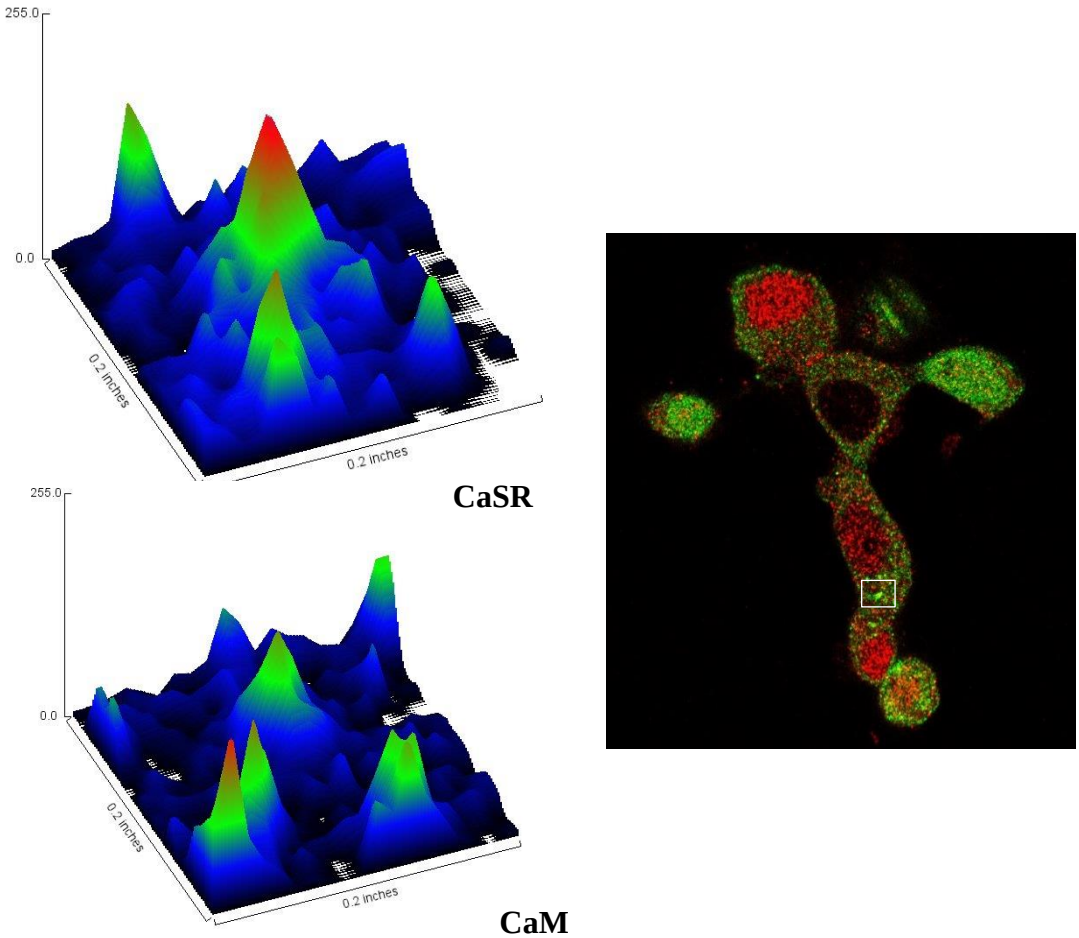

Figure 3.27 Colocalization with Pearson's coefficient of 0.78 for the whole ROI

3.6.4.3.3 CaM expression in 6-23 cells

CaM was visualized using immunostaining with anti-CaM antibody (**Figure 3.28**). We observed CaM throughout the cell and the merged image shows some co-localization of the CaSR and CaM. The images were taken in LSM800 with plan-apochromat 40X/1.4 oil DIC. Since the protein staining was everywhere, it is challenging to locate the definite co-localization.

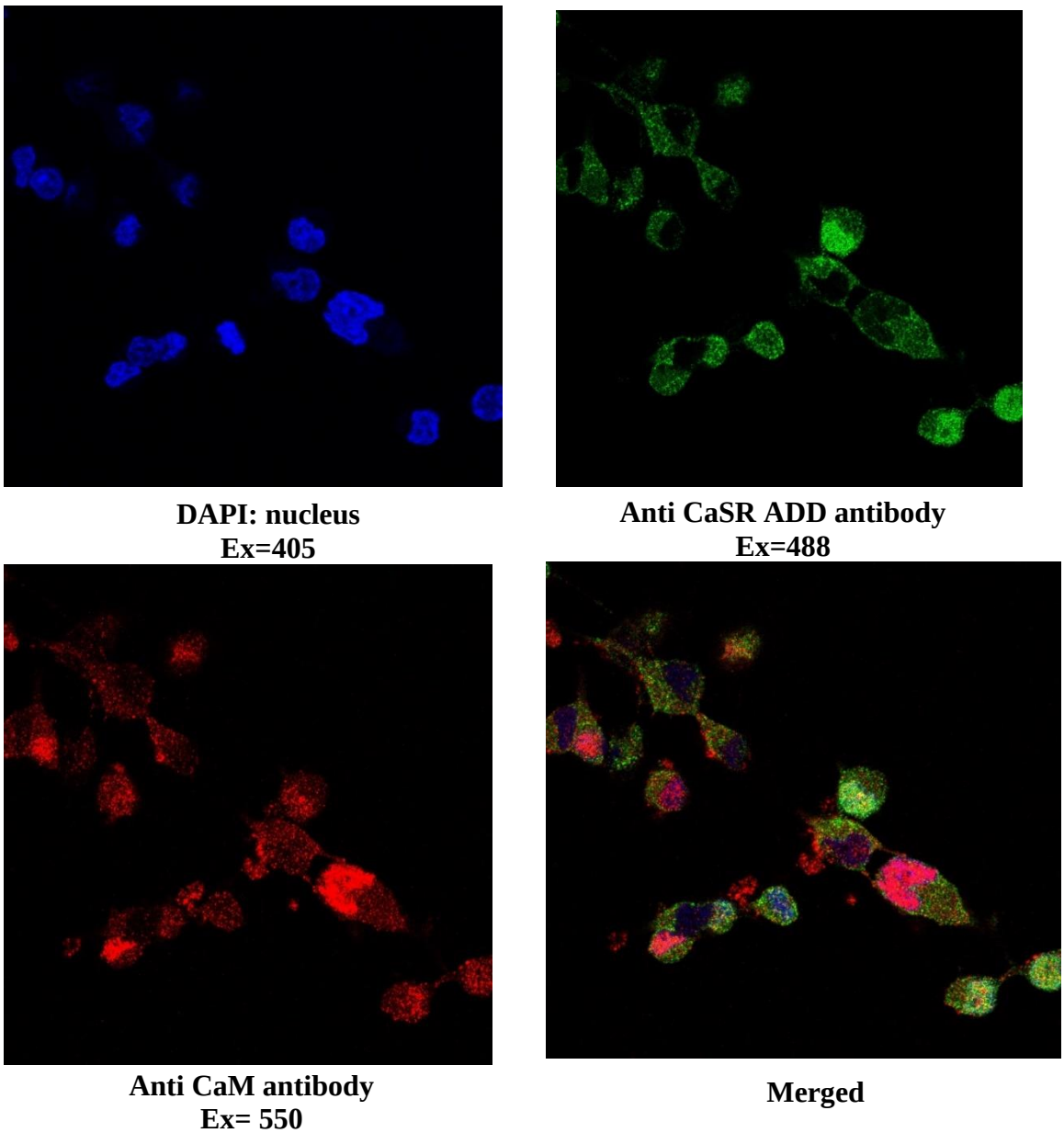

Figure 3.28 Immunostaining of CaSR and CaM in 6-23

3.6.4.3.4 Comparison of differential effects of CaM inhibitor in C cells and HEK293 cells

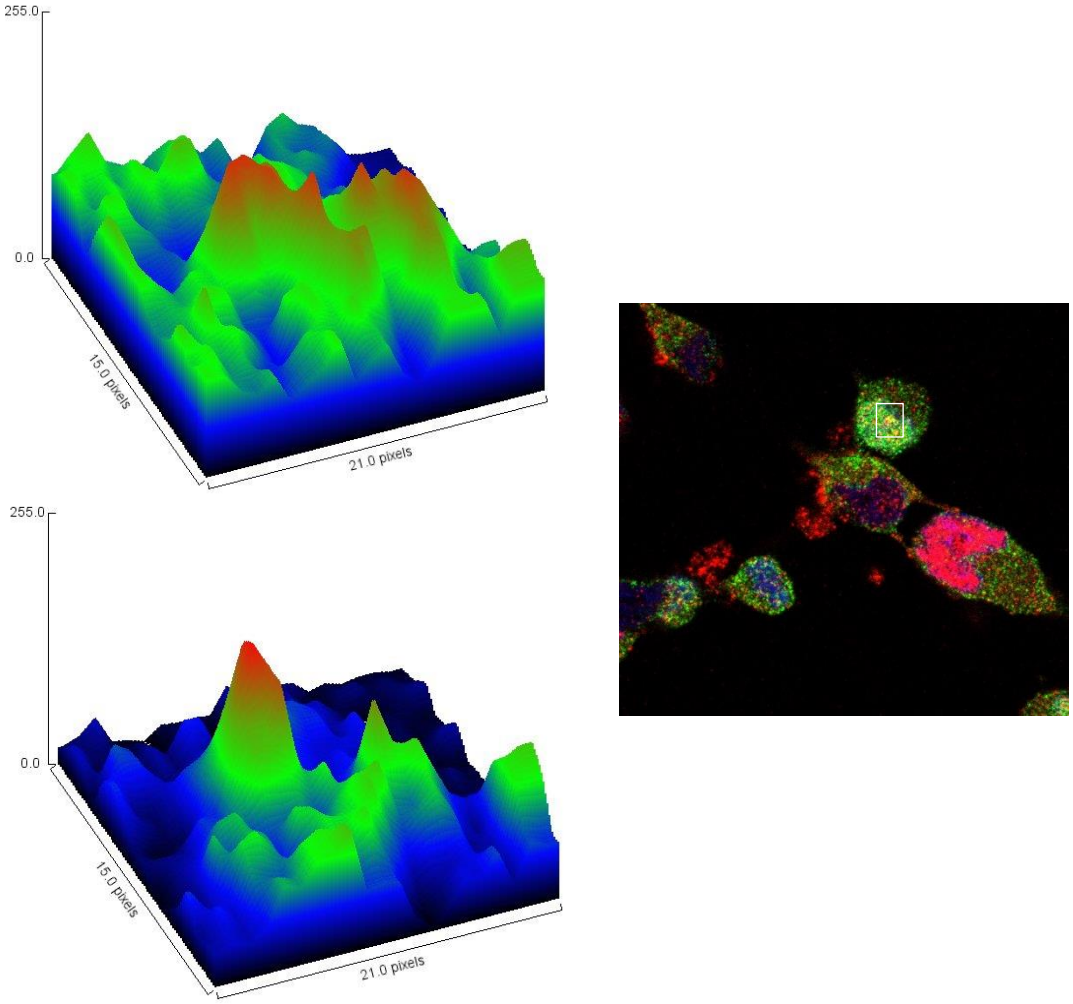

Figure 3.29 Surface plot and colocalization of whole ROI with Pearson's coefficient of 0.63 in 6-23 cells

W7 is unable to perturb C cells response to Ca^{2+}_{o}, possibly because of initial low activation. However, W7 demonstrates strong perturbation of CaSR mediated cinacalcet effect in C cells therefore, canceling its effect. This supports that CaM modulates CaSR in C cells.

3.6.4.3.5 Optimization of co-immunoprecipitation of CaSR in order to study the interaction of CaM with CaSR

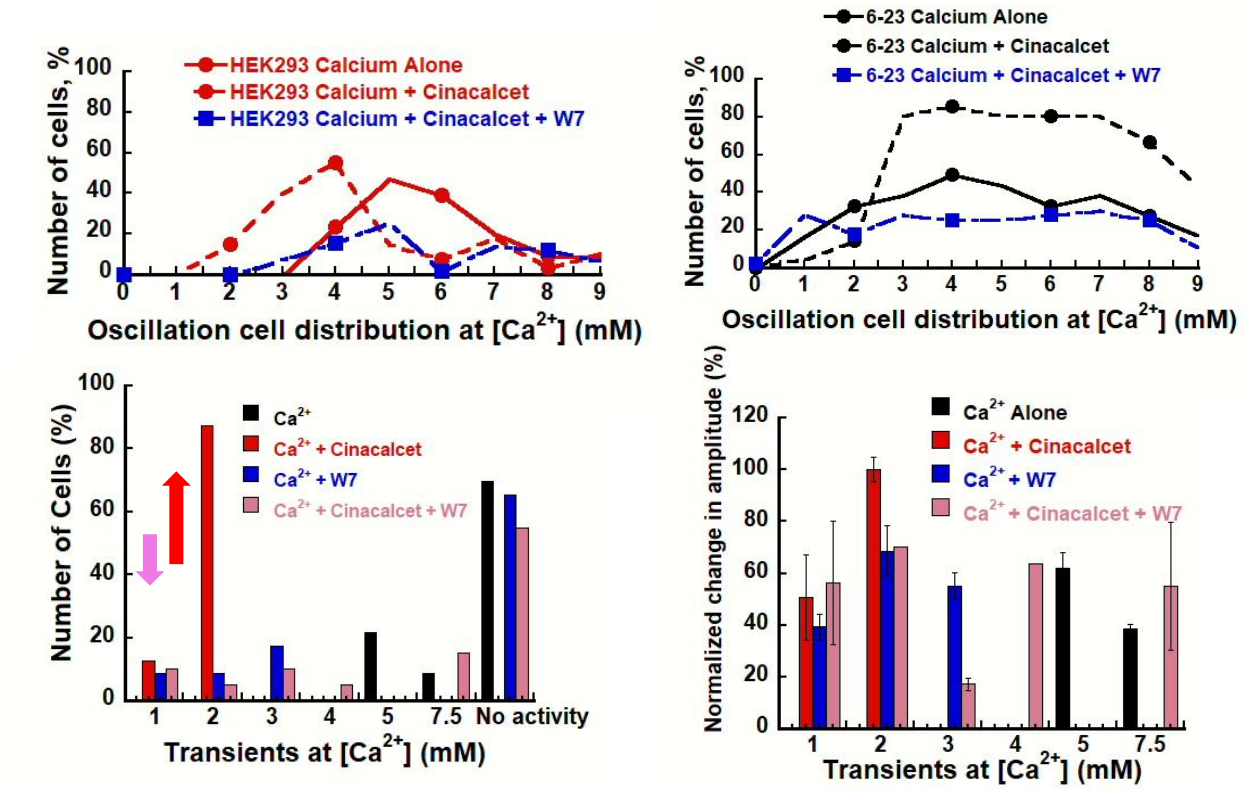

Figure 3.30 Comparison of differential effects of CaM inhibitor in C cells and HEK293 cells.

Three different anti-CaSR antibodies (C0493, 183355 and ADD) were examined and compared for the efficiency of immunoprecipitating FLAG-CaSR **()**. The cells were transfected with FLAG-CaSR pcDNA3.1, lysed and subjected to overnight binding with agarose A/G bead with the respective antibodies. We demonstrated that 183355 has the most optimal immunoprecipitation followed by C0493. However, with the endogenous CaSR such as in PC3, the input is low as well as has almost no immunoprecipitation.

For the next experiment efficiency of anti-FLAG antibody was compared with the 183355 as well

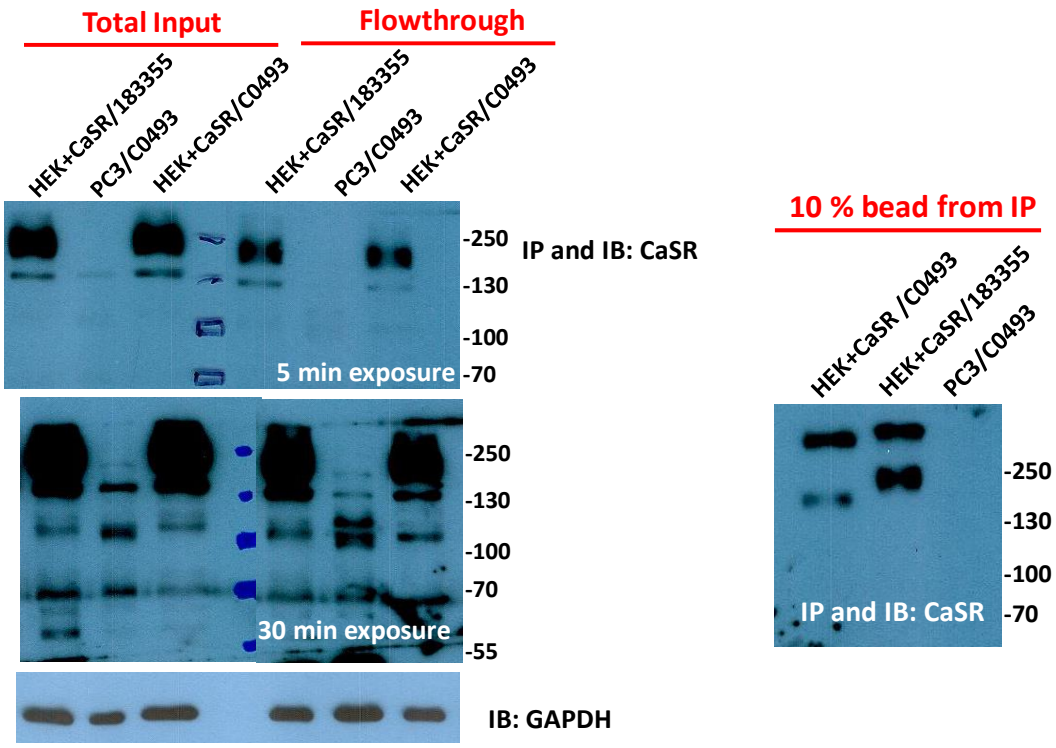

Figure 3.31 Optimization of co-IP of CasR with various antibodies. Anti-FLAG 1:100 and anti CaSR- 183355: 1:200

as we examined the co-immunoprecipitation of CaM with CaSR. The experiment was performed in duplicate. First, anti-FLAG antibody is identified to be almost 10 times higher in immunoprecipitation efficiency with HEK293 cells transfected with FLAG-CaSR using lipofectamine 2000. Un-transfected HEK293 was used as control. It was also observed that the flow-through (supernatant collected after the over-night binding process) contained a greater amount of unbound CaSR in samples with anti-CaSR 183355 antibody indicating that anti-FLAG antibody had greater efficiency of binding the CaSR.

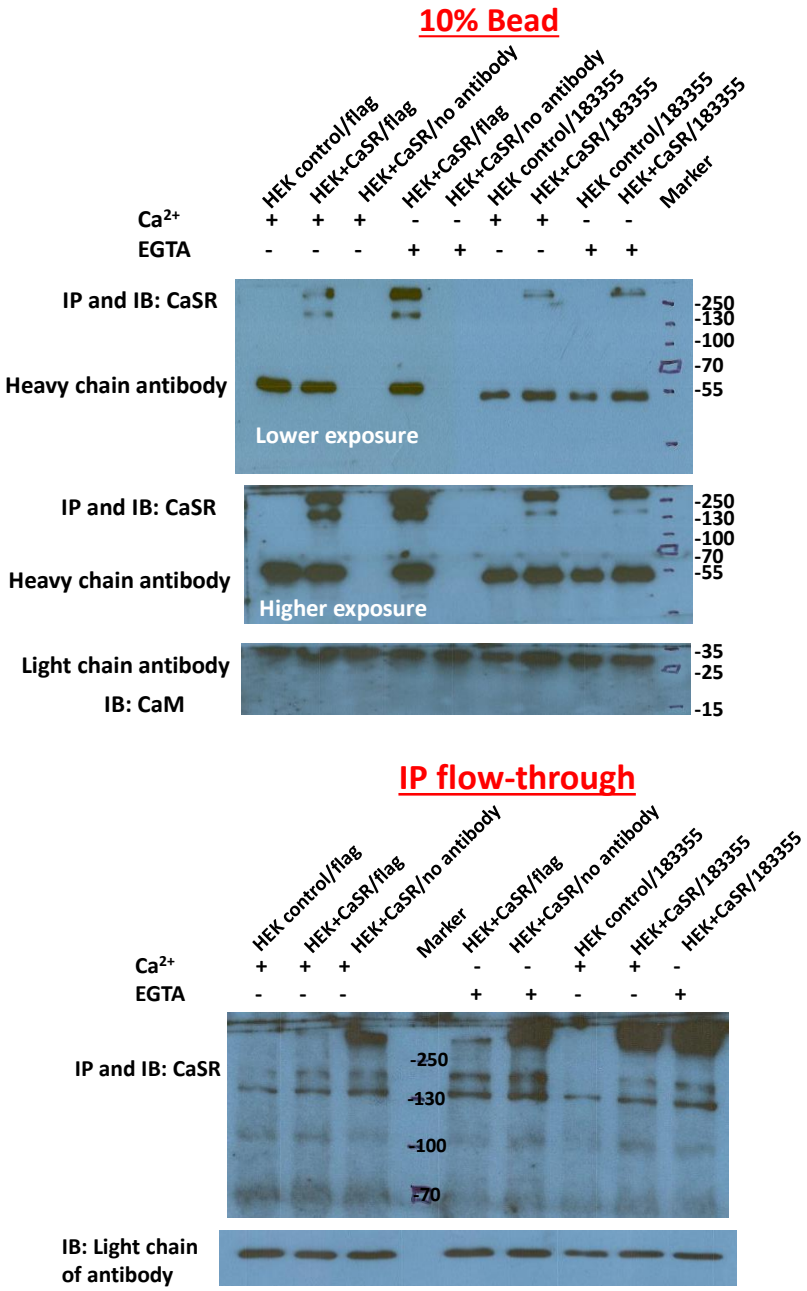

Figure 3.32 Optimization of co-IP, selecting antibodies

3.6.4.3.6 Interaction of CaM with CaSR in TT cells

In order to study the interaction in vitro, TT cells at 100% confluency in 10 cm dish were lysed and subjected to co-immunoprecipitation using the anti-CaSR 183355 antibody using dyna

bead in the presence or absence of Ca^{2+}. The experiment was conducted in duplicate. The result is not conclusive. Firstly, the immunoprecipitation of CaSR was not optimal since the anti-CaSR antibody is known to be weaker than the recombinant anti-FLAG antibodies. We observed CaM in the total and flow-through. In the duplicate experiments performed, we found a discrepancy of the CaM co-immunoprecipitated with CaSR irrespective of the presence of Ca^{2+} and CaM **(Figure 3.33).**

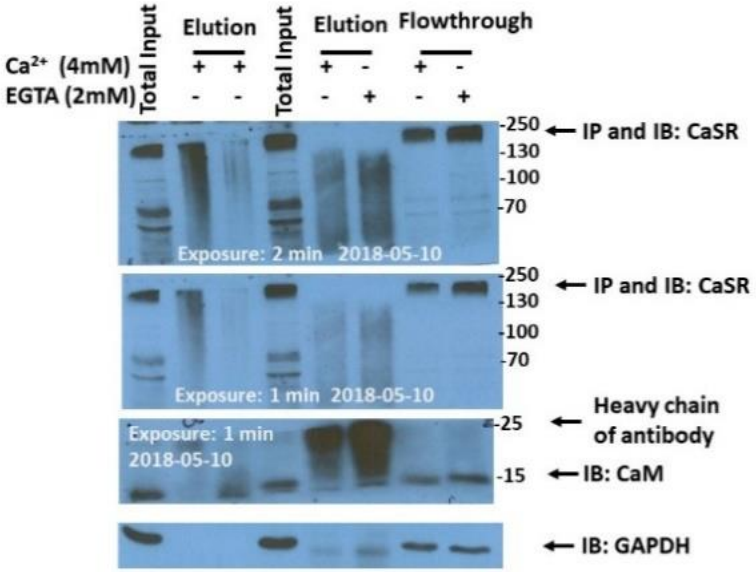

Figure 3.33 Co-IP of both CaSR not successful in WB. Co-IP of CaM in EGTA condition anti CaSR 183355

3.6.4.3.7 Ca^{2+} dependent interaction of CaM with CaSR in 6-23

In order to study the interaction in vitro, 6-23 cells at 100% confluency in 10 cm dish were lysed and subjected to co-immunoprecipitation using the anti-CaSR 183355 antibody using dyna bead in the presence or absence of Ca^{2+}(**Figure 3.34)**. The experiment was conducted in triplicate. Firstly, we show that the immunoprecipitation of CaSR was not optimal since the amount of CaSR observed to be bound to the bead was less than 20 times instead of being enriched. However, with the minimal co-IP, we observed CaM immunoprecipitated in the presence of Ca^{2+}.

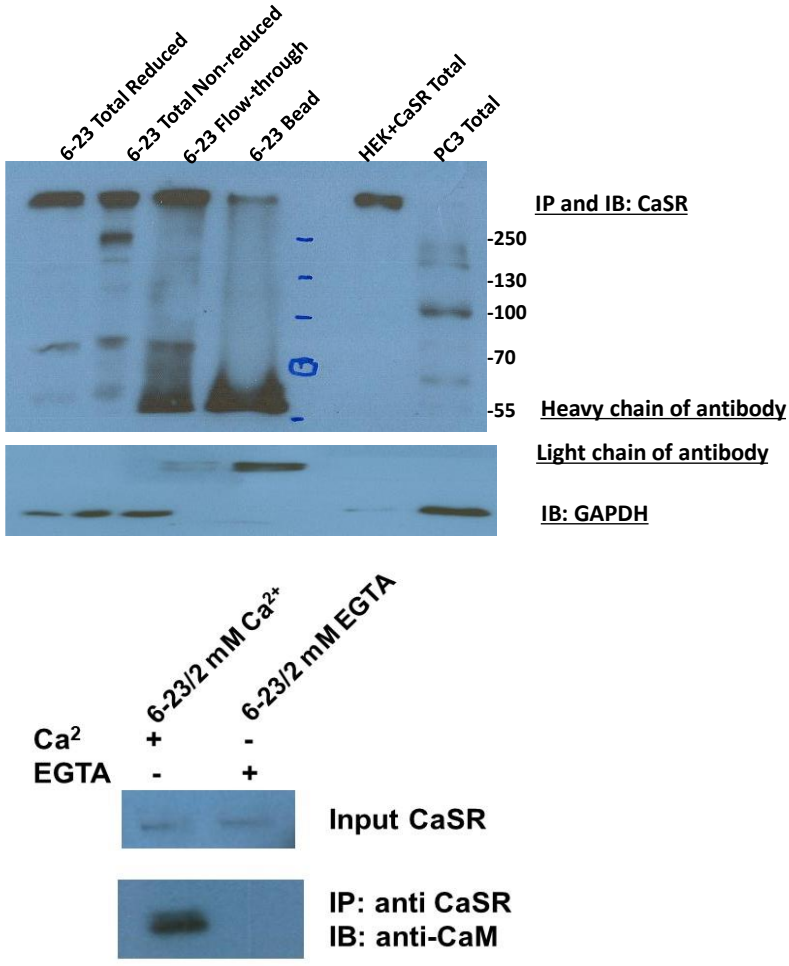

Figure 3.34 Ca^{2+} dependent CaM interaction with CaSR

3.6.5 Exploring the possibility of splice variant using RT-PCR in 6-23

More than 230 germline mutations are encoded by CASR gene that is associated with a variety of human disorders associated with abnormal Ca^{2+} homeostasis, making CaSR an important potential therapeutic target for a plethora of conditions [241]. Apart from being expressed in organs such as parathyroid, kidney, bones, heart, intestine, breast, neurons, liver, lung, etc, CaSR is highly expressed in cancer cells upon the initiation of bone metastasis[242]. CaSR may be involved in phenomena that allow for the development of many types of benign or malignant tumors, from parathyroid adenomas to breast, prostate, and colon cancers[243]. Studies have shown significant higher CaSR expression in metastatic prostate and breast cancer tissues found in the bone than that in the primary cancer tissues[90]. Therefore, CaSR in prostate and breast act as an oncogene, whereas, in parathyroid and colon act as a tumor suppressor. We explored the possibility of mutations or splice variants of CaSR in the thyroid cancer cells to inquire if this was a reason for the Ca^{2+} signaling and downstream pathways such as IP production and ERK pathways to be significantly different between the CaSR in cancer cells and native CaSR transiently transfected in HEK293.

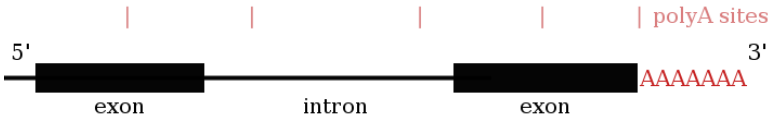

Figure 3.35 Mammalian RNA contain poly A

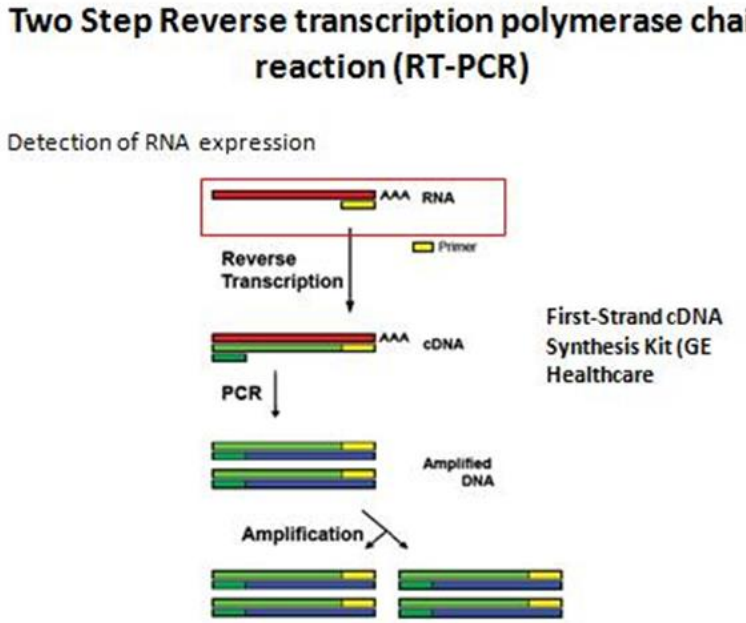

Figure 3.37 Flowchart for RT-PCR

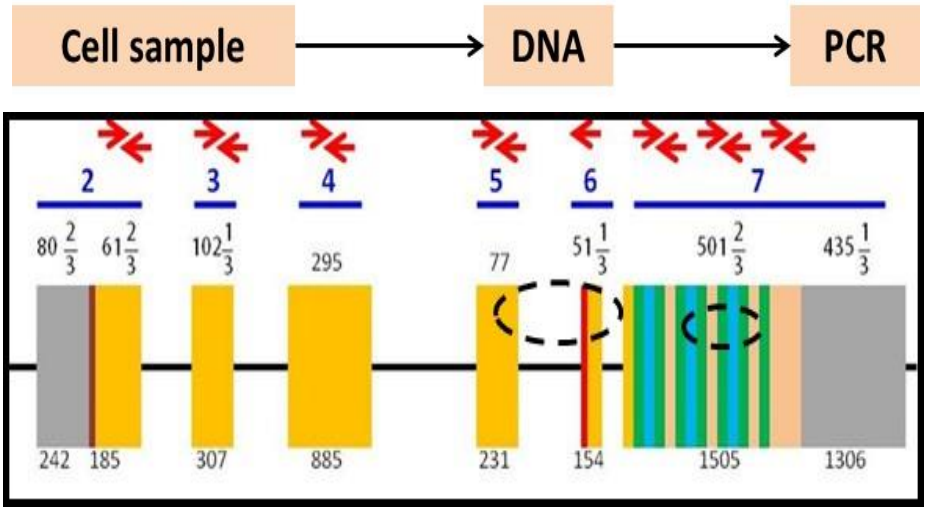

Figure 3.36 ***Primers were designed targeting each exon of CaSR from 2-7***

Primers were designed to encompass each of the seven exons of CaSR, as shown in the (**Figure 3.36**). We used polyA enrichment of the RNA while isolation and conducted reverse transcription to obtain the cDNA. A two-time PCR with nesting method was used to amplify the signal. Due to the low transcript, the first PCR usually does not generate the good signal for

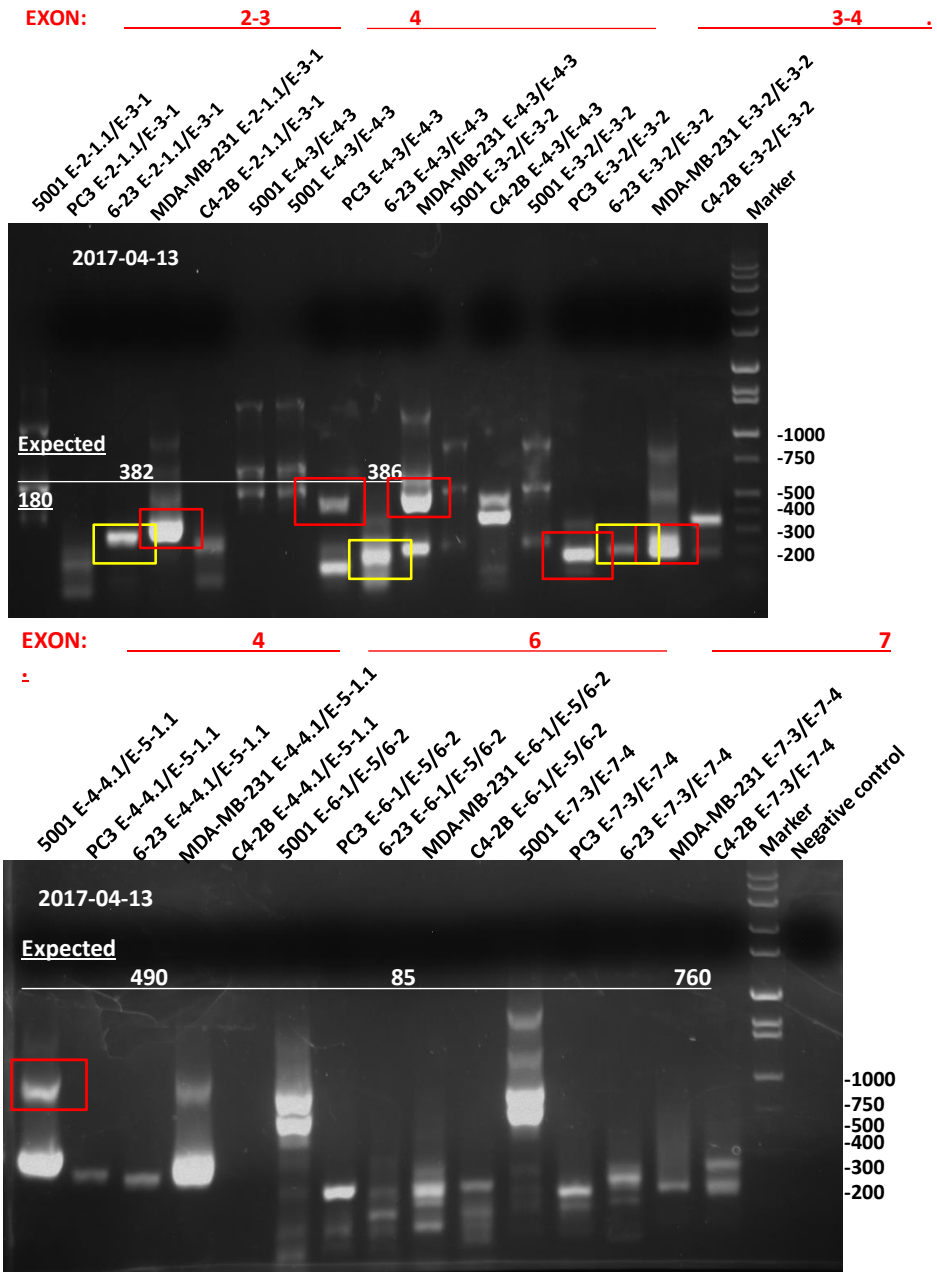

Figure 3.38 Nested PCR for 6-23. Bands corresponding to yellow bars were sequenced

endogenous CaSR transcript amplification as compared to 5001 (stably transfected HEK293 with wild type CaSR). Only exons 2, 3, 4 and 6 were able to obtain the expected PCR product for CaSR. Many bands were obtained, suggesting unspecific amplification. The bands from 2, 3, 4, and 6 exons were sequenced using sanger sequencing. We verified that the transcript of CaSR in 6-23 is isoform I precursor an additional 10 amino acid insertion. In addition to the wild type isoform II

CASR, low abundant isoform I exist which contains an additional 10 amino acid inserted after amino acid 536 in the CaSR (GenBank #U20760) (https://www.ncbi.nlm.nih.gov/protein/NP_001171536.1). This insertion is known to be rare and as to my knowledge, does not affect the function of CaSR [31]. The partial sequencing obtained from other bands does not imply any significant change in CaSR in 6-23 cells. The grey

```
AWQVLKHLRHLNFTNNMGEQVTFDECGDLVGNYS
IINWHLSPEDGSIVFKEVGYYNVYAKKGERLFINEEKILWSG                                  Exon 5

FSREPLTFVLSVLQVPFSNCSRDCLAGT.....................................560
RKGIIEGEPTCCFECVECPDG                                                      Exon 6
```

Figure 3.39 Sequencing covered for 6-23 after RT-PCR
highlighted regions are sequenced from the bands.

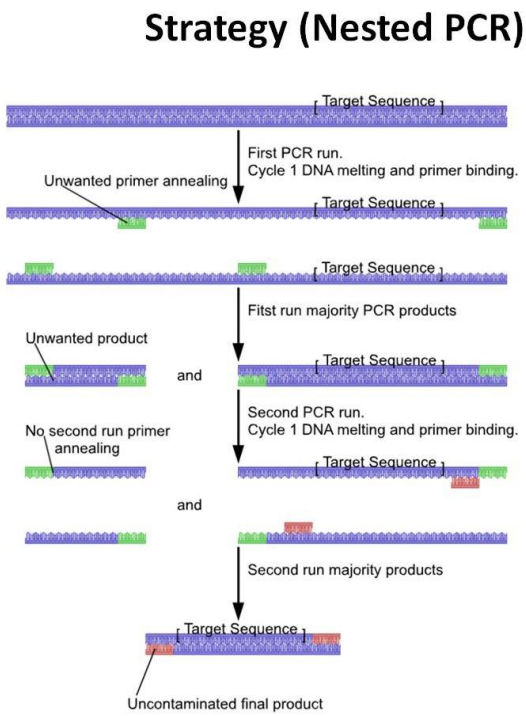

Figure 3.40 Workflow for Nested PCR strategy

Exon2: 131-557 (427)
UTR
AAGGCATCAC
AGGAGGCCTCTGCATGATGTGGCTTCCAAAGACTCAAGGACCACCCACATTACAAGTCTGGATTGAGGAA E-2-1Fwd (1)
GGCAGAAATGGAGATTCAAACACCACGTCTTCTATTATTTTATTAATCAATCTGTAGACATGTGTCCCCA
CTGCAGGGAGTGAACTGCTCCAAGGGAGAAACTTCTGGGAGCCTCCAAACTCCTAGCTGTCTCATCCCTT
GCCCTGGAGAGACGGCAGAACC

Translating
ATGGCATTTTATAGCTGCTGCTGGGTCCTCTTGGCACTCACCTGGCAC E-2-1.1Fwd (1-8)
ACCTCTGCCTACGGGCCAGACCAGCGAGCCCAAAAGAAGGGGGACATTATCCTTGGGGGGCTCTTTCCTA
TTCATTTTGGAGTAGCAGCTAAAGATCAAGATCTCAAATCAAGGCCGGAGTCTGTGGAATGTATCAG

Exon3: 558-864 (307)
GTA E-3-1Fwd (3)
TAATTTCCGTGGGTTTCGCTGGTTACAGGCTATGATATTTGCCATAGAGGAGATAAACAGCAGCCCAGCC E-3-2Fwd (3-9)
CTTCTTCCCAACTTGACGCTGGGATACAGGATATTTGACACTTGCAACACCGTTTCTAAGGCCTTGGAAG
CCACCCTGAGTTTTGTTGCTCAAAACAAAATTGATTCTTTGAACCTTGATGAGTTCTGCAACTGCTCAGA E-3-1Rev (1-8)
GCACATTCCCTCTACGATTGCTGTGGTGGGAGCAACTGGCTCAGGCGTCTCCACGGCAGTGGCAAATCTG E-3-2 Rev (1) (3-9)
CTGGGGCTCTTCTACATTCCCCAG

Exon4: 865-1749(885)
GTCAGTTATGCCTCCTCCAGCAGACTCCTCAGCAACAAGAATCAAT E-4-2Fwd (2)
TCAAGTCTTTCCTCCGAACCATCCCCAATGATGAGCACCAGGCCACTGCCATGGCAGACATCATCGAGTA
TTTCCGCTGGAACTGGGTGGGCACAATTGCAGCTGATGACGACTATGGGCGGCCGGGGATTGAGAAATTC
CGAGAGGAAGCTGAGGAAAGGGATATCTGCATCGACTTCAGTGAACTCATCTCCCAGTACTCTGATGAGG E-4-2Rev (3) E-4-3Fwd (2-10)
AAGAGATCCAGCATGTGGTAGAGGTGATTCAAAATTCCACGGCCAAAGTCATCGTGGTTTTCTCCAGTGG
CCCAGATCTTGAGCCCCTCATCAAGGAGATTGTCCGGCGCAATATCACGGGCAAGATCTGGCTGGCCAGC
GAGGCCTGGGCCAGCTCCTCCCTGATCGCCATGCCTCAGTACTTCCACGTGGTTGGCGGCACCATTGGAT
TCGCTCTGAAGGCTGGGCAGATCCCAGGCTTCCGGGAATTCCTGAAGAAGGTCCATCCCAGGAAGTCTGT E-4-4Fwd (4)
CCACAATGGTTTTGCCAAGGAGTTTTGGGAAGAAACATTTAACTGCCACCTCCAAGAAGGTGCAAAAGGA E-4-4.1Fwd (4-11)
CCTTTACCTGTGGACACCTTTCTGAGAGGTCACGAAGAAAGTGGCGACAGGTTTAGCAACAGCTCGACAG
CCTTCCGACCCCTCTGTACAGGGGATGAGAACATCAGCAGTGTCGAGACCCCTTACATAGATTACACGCA
TTTACGGATATCCTACAATGTGTACTTAGCAGTCTACTCCATTGCCCACGCCTTGCAAGATATATATACC E-4-3Rev (2) (2-10)
TGCTTACCTGGGAGAGGGCTCTTCACCAATGGCTCCTGTGCAGACATCAAGAAAGTTGAGGCGTGGCAG

Exon5: 1750-1980 (231)
G
TCCTGAAGCACCTACGGCATCTAAACTTTACAAACAATATGGGGGAGCAGGTGACCTTTGATGAGTGTGG
TGACCTGGTGGGGAACTATTCCATCATCAACTGGCACCTCTCCCCAGAGGATGGCTCCATCGTGTTTAAG E-5-2Fwd (5)
GAAGTCGGGTATTACAACGTCTATGCCAAGAAGGGAGAAAGACTCTTCATCAACGAGGAGAAAATCCTGT E-5-1.1Rev (4-11)
GGAGTGGGTTCTCCAGGGAG E-5-1Rev (4)

Exon6: 1981-2104 (124)

CCACTCACCTTTGTGCTGTCTGTCCTCCAG **(10 amino acid)**
GTGCCCTTCTCCAACTGCAGCCGAGACTGCCTGGCAGGGACCAGGAAAGG E-6-1Fwd (6) (6-12)
GATCATTGAGGGGGAGCCCACCTGCTGCTTTGAGTCTGTGGAGTGTCCTGATGGGGAGTATAGTGATGAG E-5/6-2Rev (5) (6-12)
ACAG

Exon7: 2105-4915 (2811)
ATGCCAGTGCCTGTAACAAGTGCCCAGATGACTTCTGGTCCAATGAGAACCACACCTCCTGCATTG
CCAAGGAGATCGAGTTTCTGTCGTGGACGGAGCCCTTTGGGATCGCACTCACCCTCTTTGCCGTGCTGGG
CATTTTCCTGACAGCCTTTGTGCTGGGTGTGTTTATCAAGTTCCGCAACACACCCATTGTCAAGGCCACC
AACCGAGAGCTCTCCTACCTCCTCCTCTTCTCCCTGCTCTGCTGCTTCTCCAGCTCCCTGTTCTTCATCG
GGGAGCCCCAGGACTGGACGTGCCGCCTGCGCCAGCCGGCCTTTGGCATCAGCTTCGTGCTCTGCATCTC
ATGCATCCTGGTGAAAACCAACCGTGTCCTCCTGGTGTTTGAGGCCAAGATCCCCACCAGCTTCCACCGC
AAGTGGTGGGGGCTCAACCTGCAGTTCCTGCTGGTTTTCCTCTGCACCTTCATGCAGATTGTCATCTGTG
TGATCTGGCTCTACACCGCGCCCCCCTCAAGCTACCGCAACCAGGAGCTGGAGGATGAGATCATCTTCAT E-7-4Fwd (7)
CACGTGCCACGAGGGCTCCCTCATGGCCCTGGGCTTCCTGATCGGCTACACCTGCCTGCTGGCTGCCATC
TGCTTCTTCTTTGCCTTCAAGTCCCGGAAGCTGCCGGAGAACTTCAATGAAGCCAAGTTCATCACCTTCA E-7.2-2Fwd (6)
GCATGCTCATCTTCTTCATCGTCTGGATCTCCTTCATTCCAGCCTATGCCAGCACCTATGGCAAGTTTGT E-7-3Fwd (6-13)
CTCTGCCGTAGAGGTGATTGCCATCCTGGCAGCCAGCTTTGGCTTGCTGGCGTGCATCTTCTTCAACAAG
ATCTACATCATTCTCTTCAAGCCATCCCGCAACACCATCGAGGAGGTGCGTTGCAGCACCGCAGCTCACG
CTTTCAAGGTGGCTGCCCGGGCCACGCTGCGCCGCAGCAACGTCTCCCGCAAGCGGTCCAGCAGCCTTGG
AGGCTCCACGGGATCCACCCCCTCCTCCTCCATCAGCAGCAAGAGCAACAGCGAAGACCCATTCCCACAG
CCCGAGAGGCAGAAGCAGCAGCAGCCGCTGGCCCTAACCCAGCAAGAGCAGCAGCAGCAGCCCCTGACCC
TCCCACAGCAGCAACGATCTCAGCAGCAGCCCAGATGCAAGCAGAAGGTCATCTTTGGCAGCGGCACGGT
CACCTTCTCACTGAGCTTTGATGAGCCTCAGAAGAACGCCATGGCCCACAGGAATTCTACGCACCAGAAC
TCCCTGGAGGCCCAGAAAAGCAGCGATACGCTGACCCGACACCAGCCATTACTCCCGCTGCAGTGCGGGG
AAACGGACTTAGATCTGACCGTCCAGGAAACAGGTCTGCAAGGACCTGTGGGTGGAGACCAGCGGCCAGA
GGTGGAGGACCCTGAAGAGTTGTCCCCAGCACTTGTAGTGTCCAGTTCACAGAGCTTTGTCATCAGTGGT
GGAGGCAGCACTGTTACAGAAAACGTAGTGAATT E-7-4Rev (7) (6-13)

Figure 3.41 Primers designed through exon 1-7. Color represent sets of forward and reverse primers.

Table 3.3 Primers designed to study Exon 1 & 2, to replicate previous research on exons 5 & 7, and to study Antibody specificity (exon2, 3 & 4)

Name	Primers	Expected bp (Fwd-Rev)	Exon
CaSR ADD Fwd 2016-05-27	CAATTGCAGCTGATGACGACT	75	4
CaSR ADD Rev 2016-05-27	CCTCATCAGAGTACTGGGAG		4
CaSR Ab SP5484P Fwd 2016-05-27	TATTCATTTTGGAGTAGCA	76	2
CaSR Ab SP5484P Rev 2016-05-27	GCAAATATCATAGCCTGTAACC		3
CaSR Ab ab79829 Fwd 2016-05-27	GTGGGCACAATTGCAGCTGA	58	4
CaSR Ab ab79829 Rev 2016-05-27	AGATGAGTTCACTGAAGTCGAT		4
CaSR Oda-98-1 Fwd 2016-05-27	AGGAAGTCTGTCCACAATGG	608	4
CaSR Oda-98-1 Rev 2016-05-27	CAATGATCCCTTTCCTGGTC		6
CaSR Bradbury-98-1 Fwd 2016-05-27	CTGGCGTGCATCTTCTTCAA	638	7
CaSR Bradbury-98-1 Rev 2016-05-27	GTTTTCTGTAACAGTGCTGC		7
CaSR Liao-06 Fwd-1 2016-05-27	CAACCTGCAGTTCCTGCTGG	206	7
CaSR Liao-06 Rev-1 2016-05-27	TGGCATAGGCTGGAATGAAGG		7
CaSR Liao-06 Fwd-2 2016-05-27	TTGAAAATCCGGGGGAGAG	For 28S	x
CaSR Liao-06 Rev-2 2016-05-27	ACATTGTTCCAACATGCCAG	For 28S	x
CaSR Exon1-2 Fwd-1 2016-05-27	GCCAGGAAGGACCGCACG	281	1-2
CaSR Exon1-2 Rev-1 2016-05-27	CAGCTAGGAGTTTGGAGGCT		1-2
CaSR Exon1-2 Fwd-2 2016-05-27	AGGAGGCCTCTGCATGATGTGGC	360	2-2
CaSR Exon1-2 Rev-2 2016-05-27	ACAGACTCCGGCCTTGATTTGA		2-2

Table 3.2 Primers designed for smaller sections of exon 7

Name	Primers	Expected base pair	Stop	Length	Tm	GC%	Start
CaSR E7-3.1-1 Fwd 2016-10-17	CTCATCTTCTTCATCGTCTG		26	20	58	45	6
CaSR E7-3.1-1 Rev 2016-10-17	GGATGGCAATCACCTCTA	53	97	18	58	50	79
CaSR E7-3.1-2 Rev 2016-10-17	CACCTTGAAAGCGTGAG	179	222	17	58	52.9	205
CaSR E7-3.1-3 Rev 2016-10-17	CTTCGCTGTTGCTCTTG	294	337	17	58	52.9	320
CaSR E7-3.1-4 Rev 2016-10-17	GCTCATCAAAGCTCAGTG	473	517	18	58	50	499
CaSR E7-3.1-5 Rev 2016-10-17	GAGTTCTGGTGCGTAGAA	519	563	18	59	50	545
CaSR E7-3.1-6 Rev 2016-10-17	GTCAGATCTAAGTCCGTTTC	604	650	20	57	45	630
CaSR E7-3.1-7 Rev 2016-10-17	CTCTGTGAACTGGACACTA	710	755	19	58	47.4	736
CaSR E7-3.1-8 Rev 2016-10-17	CCAGTCTTCTCCTTCCAT	785	829	18	58	50	811
CaSR E6-1 Fwd 2016-10-17	GTGCCCTTCTCCAACTG		38	17	59	58.8	21

Table 3.4 New Primers designed to study Exon 2 through 7

Name	Primer Sequence	Expected bp	Start	Stop	Length	Tm	GC%
CaSR E-2-1 Fwd 09-07-16	CTCAAGGACCACCCACATTAC	247	43	64	21	62	52.4
CaSR E-2-1 Rev 09-07-16	GACCCAGCAGCAGCTATAAA		250	270	20	62	50
CaSR E-2-2 Fwd 09-07-16	CCAAACTCCTAGCTGTCTCATC	201	195	217	22	62	50
CaSR E-2-2 Rev 09-07-16	CAGACTCCGGCCTTGATTT		396	415	19	62	52.6
CaSR E-3-1 Fwd 09-07-16	GTATAATTTCCGTGGGTTTCGC	179	1	23	22	62	45.5
CaSR E-3-1 Rev 09-07-16	GCAGAACTCATCAAGGTTCAAAG		180	203	23	62	43.5
CaSR E-3-2 Fwd 09-07-16	TGCCATAGAGGAGATAAACAGC	181	43	65	22	62	45.5
CaSR E-3-2 Rev 09-07-16	CCACCACAGCAATCGTAGA		224	243	19	62	52.6
CaSR E-4-1 Fwd 09-07-16	CAGACTCCTCAGCAACAAGAA	587	21	42	21	62	47.6
CaSR E-4-1 Rev 09-07-16	AGAAAGGTGTCCACAGGTAAAG		608	630	22	62	45.5
CaSR E-4-2 Fwd 09-07-16	TTCAAGTCTTTCCTCCGAACC	204	46	67	21	62	47.6
CaSR E-4-2 Rev 09-07-16	CATGCTGGATCTCTTCCTCATC		250	272	22	62	50
CaSR E-4-3 Fwd 09-07-16	CCCAGTACTCTGATGAGGAAGA	532	239	261	22	62	50
CaSR E-4-3 Rev 09-07-16	GGCAATGGAGTAGACTGCTAAG		771	793	22	62	50
CaSR E-5-1 Fwd 09-07-16	AGCACCTACGGCATCTAAAC	195	8	28	20	62	50
CaSR E-5-1 Rev 09-07-16	GAACCCACTCCACAGGATTT		203	223	20	62	50
CaSR E-5/6-1 Fwd 09-07-16	AGCACCTACGGCATCTAAAC	302	8	28	20	62	50
CaSR E-5/6-1 Rev 09-07-16	GGACACTCCACACACTCAAA		310	330	20	62	50
CaSR E-5/6-2 Fwd 09-07-16	TGGCTCCATCGTGTTTAAGG	194	123	143	20	62	50
CaSR E-5/6-2 Rev 09-07-16	CCATCAGGACACTCCACAC		317	336	19	62	57.9
CaSR E-7-1 Fwd 09-07-16	CCTACCTGCTGCTGCTATTATG	632	2015	2037	22	62	50
CaSR E-7-1 Rev 09-07-16	GCTGTGGCTTAGAGAGGTTAAG		2647	2669	22	62	50
CaSR E-7-2 Fwd 09-07-16	CTTTGTGCTGGGTGTGTTTATC	577	152	174	22	62	45.5
CaSR E-7-2 Rev 09-07-16	CTGGCATAGGCTGGAATGAA		729	749	20	62	50
CaSR E-7-3 Fwd 09-07-16	CTTCATCGTCTGGATCTCCTTC	795	710	732	22	62	50
CaSR E-7-3 Rev 09-07-16	CCCAGTCTTCTCCTTCCATTT		1505	1526	21	62	47.6

3.7 Discussion and major conclusion

Understanding the mechanistic functioning of CaSR is vital for drug discovery not only for CaSR related disorders but also for overall GPCR family-related pathologies. Cell lines derived from tumors represent a critical tool to understand the oncogenic mechanism as well as a preclinical tool to study the efficacy of new therapies in vitro and in vivo. In this chapter, we examined the CaSR mediated intracellular signaling mechanism in HEK293 cells and thyroid cancer cells. The intracellular calcium oscillation facilitated by CaSR activation via $[Ca^{2+}]_o$, Mg^{2+} and tryptophan derivative (TNCA) is characterized in wild type CaSR in HEK293 cells. EC_{50} of CaSR for Ca^{2+} was 4 mM with a Hill number of 3, and for Mg^{2+} EC_{50} was 13 mM and Hill number

of 2.9. Presence of 0.5 mM and 1.5 mM Ca^{2+} was able to potentiate the efficacy of Mg^{2+} by decreasing EC_{50} for Mg^{2+} to 7.5 and 5.9 mM respectively, which proved the cooperative nature between Ca^{2+} and Mg^{2+}. Mg^{2+} is a known allosteric modulator of many GPCRs. Mg^{2+} is known to increase the binding affinity of receptors to their agonists including in opioid receptors [244], beta-2 andrenergic receptor [245]and dopamine D_2 receptor [246] and generally not effective on antagonist binding. Mg^{2+} is also known to bind G-proteins directly to modulate GPCRs. Here in our work, we validate the Mg^{2+} binding pockets described in the first crystal of hCaSR ECD domain [247]. Two Mg^{2+} binding sites are shown. Site 1 is at the dimerization interface of subdomain 2 where Mg^{2+} coordinates with S^{240} and four water molecules with an ideal Mg^{2+} coordination geometry. Site 2 found on the periphery of subdomain 1 and Mg^{2+} coordinates with S^{84}, backbones of I^{81}, L^{87} and L^{88} and two water molecules. Furthermore, site 3 is described as conserved (E^{228}, E^{231} and E^{241}) acidic patch where Gd^{3+} was observed to bind. This patch is close to the subdomain 2 dimerization interface adjacent to site 1. Oscillation study with site-directed mutations (E228I or E229I/E229I double mutant) at site 3, which is also related to ADH resulted in impediment of the Ca^{2+}/Mg^{2+} CaSR sensing as well as CaSR mediated Mg^{2+} evoked $Ca^{2+}{}_i$ mobilization and calcium oscillation. Moreover, TNCA was able to act as a co-agonist and reduce the EC_{50} for both Ca^{2+} and Mg^{2+}, but more significantly for Mg^{2+} by 2.5-fold. TNCA is observed to be bound to S^{147}, A^{168}, S^{170} and Y^{218} in hCaSR ECD [247]. Previous studies have shown that aromatic amino acids including, L-Phe, L-Trp and L-Tyr, are able to allosterically regulate the extracellular Ca^{2+} sensing in CaSR [248] by binding at the Venus-fly trap domain near the orthosteric site to potentiate the activity of extracellular Ca^{2+} on various downstream pathways [74, 248-250]. GPCRs such as GABAB is modulated by aromatic (L-Phe) and aliphatic (L-Leu

and L-Ile) amino acids [251]. Here, TNCA shows about 1000-fold more potency than Phe in reducing the Mg^{2+} or Ca^{2+} activation of CaSR.

In the second part of the chapter, we examined the CaSR mediated Ca^{2+} sensing in transfected HEK293 cells, human (TT) and rat thyroid medullary cancer cells (6-23) by monitoring intracellular Ca^{2+} response to extracellular Ca^{2+} as well as CaSR associated drugs. It is known that CaSR is expressed and functions in tissue- and pathology- specific manner. Using R-programming, $Ca^{2+}{}_i$ peaks for the 6-23 cells and manual counting for TT cells with prominent peaks were quantitated. The oscillation distribution by hCaSR in HEK293 cells (n= > 5) was shifted to the lower Ca^{2+} concentrations of 0.5 to 3 mM by cinacalcet instead of 2 to 10 mM in lone Ca^{2+} treatment implying the potency of cinacalcet to enhance stimulation of CaSR mediated signaling. Cinacalcet also increased the oscillation frequency from 0.5-2 peaks/minute to 1-2.5 peaks/minute. Previous studies have noted that calcimimetic agents increase the intracellular calcium concentration in a dose dependent manner [252]. Antagonist (NPS-2143) was able to completely obstruct the Ca^{2+} sensing. W7, an inhibitor of CaM, a CaSR regulating protein was able to decrease the oscillation frequency to 0-1 peaks/minute as shown by Huang et al [3]. We report for the first time that W7 is able to obstruct the cinacalcet overactivation partially, or that cinacalcet can rescue the W7 inhibition.

Effectiveness of divalent cations such as Ca^{2+} and Mg^{2+} metal ions as well as CaSR associated drugs and the role of CaM in inducing CaSR activation as observed as $Ca^{2+}{}_i$ is ambiguous in C cells. Changes in $Ca^{2+}{}_i$ is directly associated with hormone production in C cells. Therefore, understanding the efficacy and potency of CaSR in alteration in $Ca^{2+}{}_i$ is imperative for drug discovery associated with CaSR dysfunction in MTC cells. Previous works have suggested a dominant L-type voltage gated channel as Ca^{2+} sensing mechanism in 6-23 and its absence in TT

cells. Another study showed Ca^{2+}_i transients and/or oscillation to 3 mM Ca^{2+}_o and CaSR agonists including, Gd^{3+}, La^{3+} and neomycin as monitored by Fura-2 [212]. Additionally, calcitonin increase was observed with 3 mM Ca^{2+}_o with an added time course and with La^{3+} and Gd^{3+} in dose-dependent manner. Moreover, recent work by Desai et al in 2014 showed that normal TT cells displayed higher intracellular Ca^{2+} to 1.5 mM Ca^{2+} in the presence of cinacalcet and neomycin (CaSR agonist) than the TT cells with siRNA knockdown of RAMP (receptor activity modifying protein), a CaSR regulator [16] as monitored using Fluo-4AM. Ca^{2+} sensing at higher Ca^{2+}_o concentration is missing in these studies.

TT cells demonstrated CaSR mediated transient peaks at 5 and/or 7.5 mM extracellular Ca^{2+} by < 30 % of the cells (n=23). Whereas, the addition of 10 µM cinacalcet evoked the transients at 2 mM Ca^{2+} in 88% of the cells and resulting in 40% increase in the amplitude as compared to other treatments (n=24). NPS2143 was able to inhibit the Ca^{2+} response at 7.5 mM and preincubation with 50 µM W7 was able to impede the agonistic behavior of cinacalcet, implying that cinacalcet and W7 have an additive effect the CaSR mediated signaling. On the other hand, a highly non-synchronous CaSR mediated oscillatory behavior was revealed in 6-23 cells in the first batch obtained in 2017. These cells contained a mixture of CaSR with variable activity, some with low EC_{50} for Ca^{2+} at 0.5 mM and a lower Hill number of 1.5 and some that were un-responsive to Ca^{2+}. The intracellular Ca^{2+} responses were erratic with sharp peaks similar to rMTC 44-2. On the other hand, rMTC 44-2 cells are known to show no IP_1, IP_2 or IP_3 generation when Ca^{2+} is increased above 1 mM [6], but a study by Thomsen in 2012 examined 6-23 and monitored IP_1 generation in 6-23. This study also reported that strontium as compared to calcium biases the signaling to ERK1/2 and another pathway independent of Gq/11 and Ca^{2+} mobilization [214]. There was also increased potency of strontium to mediate CT secretion and possibly using a

different signaling mechanism than calcium [214]. These studies were primarily based on response to calcitonin, IP_1 and cAMP secretion. In our study, we report a pattern of Ca^{2+}_i, the knowledge of which can allow us to decipher CT and IP_1 responses as well. Extracellular Ca^{2+} sensitivity saturates at 3-4 mM Ca^{2+} and declines with higher extracellular Ca^{2+} [6] which was not observed in our study.

Again, using R-programming, Ca^{2+}_i peaks for cells with prominent peaks were quantitated in 6-23 (n= > 16). We report that cinacalcet can up-regulate the Ca^{2+}_i response of cells and the percentage of cells responding is increased by 25% and increases oscillation frequency from 0-0.5 peaks/minute to 1-2 peaks/minute. Pre-incubation with W7 can down-regulate the effects of cinacalcet by 50% and also down-regulate the oscillation frequency from 1-2 peak/minute to 0.5-1 peaks/minute. NPS-2143 was able to inhibit Ca^{2+}_i response by 65%. The remaining response suggests an alternative Ca^{2+} sensing mechanism which has been previously reported in 6-23 as well as other rMTC 44-2 cells [6] as the L-type voltage-gated channel. Interestingly, CaSR in both the C cells were selective to Ca^{2+} and not to Mg^{2+} implying biased signaling. This has also been previously shown in sheep parafollicular primary C-cells where the Ca^{2+} sensing varying potency of CaSR activation by various divalent cations was shown such that $Gd^{3+}>Ba^{2+}>Ca^{2+}>>Mg^{2+}$ [45].

Next, efforts were made to dissect the molecular reason behind the above-mentioned difference in Ca^{2+} sensing between HEK293 cells and C cells. We firstly report four-fold lower expression of endogenous CaSR in both 6-23 and TT cells as compared to stably wild type CaSR transfected HEK293 cells (5001) or transiently transfected HEK293 cells. 6-23 is missing the CaSR monomers even in reducing condition, implying a varying molecular composition of CaSR. CaSR immunostaining results show that surface expression of CaSR in both C cells is low relative to the cytosolic CaSR or membrane expression in 5001 and transiently transfected wild type CaSR

in HEK293 cells. Our results (1) validates the oscillation and transient peaks were partially but to a greater extent CaSR mediated in C- cells, and (2) re-validates that CaSR functions tissue- and species- specifically. Our findings provide an important insight into potential differential modes of modulation of intracellular Ca^{2+} signaling and thereby, control of calcitonin, through regulation of endogenous CaSR activation in pathologies related to dysregulation of Ca^{2+} homeostasis. Interestingly, the second batch of 6-23 from ATCC in 2018 showed a differential $Ca^{2+}{}_i$ response than the first batch. One way of explaining this difference is that 18-36% of the cell lines are usually misidentified or cross-contaminated with other cell lines, thus this could have compromised our results. This has been shown in previous studies [253-255].

Next, we examined the role of CaM in CaSR mediated signaling in C cells. Co-localization of CaSR and CaM in TT and 6-23 cells show a significant Pearson's coefficient of 0.78 and 0.63, respectively. Surface plot of the intensity of minuscule co-localized spots also supports that the two proteins exist at close contact. We also provide evidence of co-immunoprecipitation of CaM with endogenous CaSR in 6-23 in the presence of 2 mM Ca^{2+}. This is the first direct evidence of role of CaM in CaSR mediated Ca^{2+} sensing in 6-23 cells. However, the co-immunoprecipitation of CaM with CaSR in TT cells were not successful. This could be resulted due to lower expression level and non-optimized condition for CaSR immunoprecipitation in TT cells. Additionally, it has been a challenge to use anti-CaSR antibody for CaSR immunoprecipitation which is > 10-fold less efficient than using anti-FLAG antibody in recombinant CaSR in HEK293 cells. Further, we used RT-PCR method to characterize the CaSR in 6-23 but due to a low transcript, the sequencing was partial. However, we showed for the first time that 6-23 contained CaSR with isoform I with 10 amino acid insertion in its 6^{th} exon. For this I collaborated with Dr. Yu Li from Emory and Xiaojuan Tan to optimize RT-PCR for low transcript gene. First, primers with were re-designed

with 18-24 bases, 45-60% GC content, starting and ending with G/C pair and with melting temperature at ~60°C. The high RNA concentration and poly-A primer was used to enrich cDNA from pathological cells.

All in all, we show that oscillation distribution pattern is highly differential implying tissue- and species-specific function of CaSR. NPS-2143 was unable to completely inhibit $Ca^{2+}{}_i$ response suggesting an alternative Ca^{2+} sensing mechanism in C cells. C cells respond with an increase in the number of responding cells to cinacalcet and additionally, an increase in frequency in 6-23 cells. Mg^{2+} is unable to activate the Ca^{2+} mobilization in C cells implying biased signaling. We also established for the first time that CaM binds with CaSR and modulates CaSR mediated signaling in C cells and demonstrated lower expression level and differential mode of oligomerization of CaSR in cancer cells.

4 CHAPTER IV: CALCIUM-SENSING RECEPTOR IN PROSTATE CANCER: ITS CHARACTERIZATION, PROTEOMICS AND ROLE IN BONE METASTASIS

4.1 Abstract

The calcium-sensing receptor (CaSR) mediated $[Ca^{2+}]_o$ signaling is known to play a role in tumor growth, invasion and metastasis of several cancers including prostate cancer (PCa). PCa is one of the leading causes of death in men. Higher CaSR has been observed in prostate cancer tissues metastasizing to bones as compared to normal prostate or primary prostate cancer tissues without bony metastasis. In this study, we aimed at understanding the intracellular Ca^{2+} signaling mediated by CaSR and molecular characterization in PCa, which is largely missing. PC3 cell line

derived from prostate tumors metastasizing to bones can represent a critical tool to understand the oncogenic mechanism and Ca^{2+} sensing. We report that the CaSR mediated $G\alpha_{q/11}$ associated $Ca^{2+}{}_i$ response, such as the intracellular calcium transients/oscillation and IP_1 are absent in PC3. Additionally, the CaSR mediated ERK1/2 signaling in PC3 is impeded as compared to the wild type in HEK293 cells. In order to explore if these variabilities were derived from differential expression, we used immune-assays and RT-PCR for molecular characterization. We report that CaSR in PC3 is a monomer in non-reducing condition with a lower molecular weight of 110 kDa suggesting that endogenous CaSR may exist as a potential variant with splicing or lower glycosylation which results in its incapability to form an oligomer. Immunostaining results show that most CaSR is expressed within the cell as compared to functional plasma membrane CaSR. Using RT-PCR we validated that a full CaSR with all seven exons is present. These results lean towards the possibility that the lack of Ca^{2+} sensing is due to CaSR in PC3 predominantly existing intracellularly in an immature stage.

We further show that PC3 is able to generate an oligomer CaSR when transiently transfected. However, this overexpression of wild type CaSR in PC3 cells or application of CaSR agonists such as TNCA and cinacalcet cannot rescue the intracellular Ca^{2+} response which further indicates that CaSR in PC3 may lack other necessary regulators required for the Ca^{2+} signaling. Next, we used mass spectrometry we characterize the overall proteome of PC3. A total of 3327 proteins were detected. Gαq is not detected however, CaM and other G-proteins such as Gαi-2, Gαs and Gβ are detected with strong MS/MS count. But, CaSR was not detected with PSM of 0 which supports the retarded Ca^{2+} sensing and low transcript generated in RT-PCR. Only 22 (e.g., programmed cell death protein 6 (PDCD6), BH3 interacting domain death agonist (BID), mitogen-activated protein kinase1 (MAPK1), mitochondrial import inner membrane transmembrane

(TIMM13), E3 ubiquitinating-protein ligase UBR5, exosome complex component MTR3 (EXOSC6), coiled-coil domain containing protein 86 (CCDC86), and histidine-tRNA ligase (HARS)) were at least two-fold up-regulated in expression in the presence of Ca^{2+} and 17 (e.g., deubiquitinating protein (VCPIP1), BAG family chaperone regulator (BAG3)) were downregulated in the presence of Ca^{2+}. Because we were interested in prognosis markers, we compared the known markers in prostate cancer from the human protein atlas. We found two proteins, Epoxide hydrolase 1 (EPHX1) and Catebhol O-methyltransferase (COMT) with good abundance with the stringency of ≥ 4 average PSM and with average LFQ intensity in the range of 10^9. These markers were decreased with the Ca^{2+} treatment in PC3 by < 0.9-fold as compared to one treated with EGTA. However, these were ≥ 3-fold increased as compared to HEK293 cells. Isoforms of other good prognostic markers including the ubiquitin (RNF114), Ubiquitin-conjugating enzyme (UBE2D2/3) and SLCs were detected with good stringencies.

Next, we used gene ontology on the MS results to understand the role of extracellular Ca^{2+} in alteration of proteomics in PC3 cells as compared to HEK293 cells. We noted that global proteome is generally upregulated in PC3 as compared to HEK293 cells. In the presence of Ca^{2+}, ≥ 4-fold upregulated proteins are associated with pathways including, trans-Golgi network vesicle budding and citric acid cycle. Further, in vivo studies were conducted to understand and re-enforce involvement of CaSR in PC3 colonization in bones by preventing cell apoptosis of cancer cells, inhibiting invasion, and promoting mesenchymal-epithelial transition. My work showed a significant decrease in tumor growth when injected in mouse tibia with PC3 with CaSR knockdown as compared to the control knockdown. Our work indicates that even in the presence of normal CaSR, PC3 displays unique Ca^{2+} signaling that is independent of Gαq, possibly undergoing signaling bias.

4.2 Introduction

4.2.1 Prostate Cancer

Prostate cancer is the second leading cause of cancer-associated deaths in American men, with metastatic prostate cancer having poor survival rate; the median survival rate of around 3 years and 30% for 5-year survival rate [89, 256]. Prostate cancer microscopic lesions are localized to prostate. However, the prostate cancer cells metastasize exclusively to bones primarily to spine, femur, pelvis, rib cage, skull and humerous [257]. This causes problems such as bone fractures, pain, spinal cord compression and bone marrow suppression [88, 258]. Causing disabling pain and complications. Unfortunately, there is no cure for skeletal metastasis of prostate cancer and the application of radiation, hormonal manipulations and/or chemotherapy are only palliative [259].

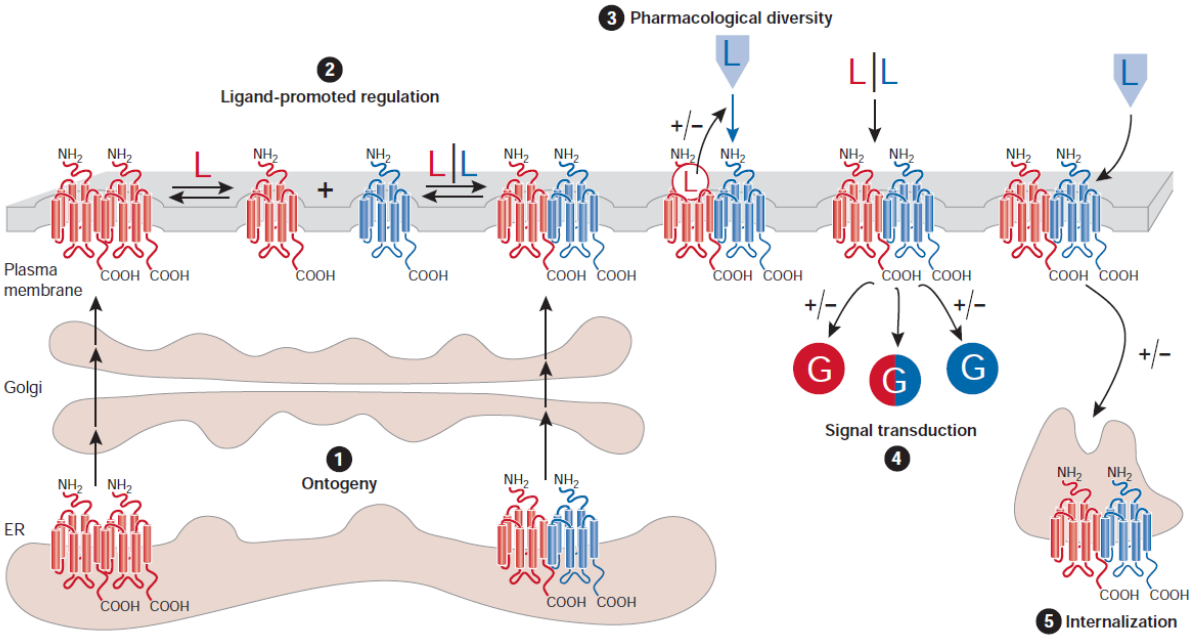

Figure 4.1 GPCR dimerization essential for many functions such as trafficking, signaling, ligand binding, cooperativity and internalization. Adapted from [7]

4.2.2 Prostate Cancer, CaSR and Ca^{2+}_o

Ca^{2+} signaling is associated with tumor progression through processes including proliferation through induction of early response genes FOS, JUN and MYC in G1 cycle [260]. It is also involved in invasiveness and migration as Ca^{2+} controls phosphorylation of contractile proteins and induces matrix metalloproteinases [261]. Ca^{2+} signaling also plays an important role in cell death in case of greater cytosolic Ca^{2+} accumulation such as in-case of the defect in SERCA pump [262]. PTEN loss is associated with IP_3R degradation [263]. The processes thus involved with Ca^{2+} signaling allow for the development of resistance to cancer therapies.

Several studies implicate the role of Ca^{2+}_o and CaSR in prostate cancer bone metastasis. Stephen Paget's theory on "seed and soil" postulates the importance of the microenvironment (soil), in the secondary site in organ-specific metastasis [89]. The blood plasma Ca^{2+} concentration is ~2.2-2.6 mM whereas, the bone plasma is around 10 mM and 20 mM in extracellular space of bone tissue [22]. Osteoclasts are known to generate extracellular Ca^{2+} from the matrix during bone resorption resulting in up to 40 mM local Ca^{2+} concentration [264]. High Ca^{2+} could act as a favorable microenvironment for the metastasized cells. Calcium homeostasis is an indispensable process that is regulated through the Calcium-Sensing Receptor (CaSR) which is a class C, G-protein coupled receptors (GPCR). This critical homeostasis regulates three of the important cellular processes that determine the cellular fate such as cell proliferation, differentiation and apoptosis [30, 66].

46 years ago, the accompaniment of secondary hyperparathyroidism (SHPT) in late-stage prostate cancer patients (6) has been described and recent clinical reports show the increased level of serum PTH in advanced prostate cancers [265]. The probable mechanism for this association is

the activation of CaSR due to hypocalcemia caused by osteoblastic lesion in skeletal sites of metastatic prostate cancer and which in turn results in increased PTH production and secretion [227, 265]. Additionally, PTH is known to increase the cell proliferation of human prostate cancer in vitro (7) and promote bone metastasis in xenograft mouse model of prostate cancer (80). Therefore, down-regulation of PTH secretion through modulation of CaSR activity could work to obstruct SHPT in prostate cancer patients [227]. Same study also shows that cinacalcet trigger mitochondria-related apoptotic pathway mediated by CaSR and modulated by Bcl-xL anti-apototic pathway [227]. PTHrP is known to be the chief mediator of hypercalcemia related malignancy and osteolysis [259]. In bones, Ca^{2+} plays a critical role in osteoblasts [10, 233, 266] and is known to be associated indirectly through PTH or other endocrine factors [267]. Extracellular Ca^{2+} and CaSR were shown to play an essential role in potentially protecting osteoblasts against apoptosis by monitoring their effects on proliferation and bone formation [268]. However, the role of CaSR in bone is unclear.

In 2001, a 5.2 kb transcript of CaSR similar to that in parathyroid CaSR was verified in PC3 and LNCaP prostate cancer cell using northern analysis [259]. The same study verified a 480 bp transcript of CaSR using RT-PCR and subsequently, CaSR protein was validated by western blot results [259]. This study was directed in understanding the CaSR mediated parathyroid hormone related protein (PTHrP) release induced by CaSR agonists Ca^{2+}, neomycin, and spermine. They showed a dose-dependent PTHrP secretion with maximal stimulation at 7.5-10mM Ca^{2+} [259]. The requirement of higher Ca^{2+} level around resorbing osteoclast could be the result of the natural high Ca^{2+} present around that area. This high Ca^{2+} requirement has also been seen in normal keratinocytes [269], normal cervical epithelial cells [270], oral squamous cancer cells [271], JEG-3 cells [272], and H-500 rat Leydig cells [273], which is used as a model for hypercalcemia of

malignancy. CaSR was shown to be associated with prostate cancer. However, this study failed to look at the detailed expression of CaSR as compared to the wild type. Feng et al. in 2014, also showed CaSR expression to be higher in the bone metastasis than in the primary prostate tissues metastasis with microarray data [274]. [90]. Furthermore, Liao et al. in 2006, had shown a higher proliferation of skeletal metastatic cells, PC3, in increased Ca^{2+} condition as compared to LNCaP cells that metastasize to lymph nodes, and this mechanism is mediated by CaSR as shown by the decrease in proliferation when CaSR is knocked-down [91]. Along with PTH, another Ca^{2+} homeostasis related hormone, calcitonin, and calcitonin receptor (CTR) abundance known to be upregulated in malignant prostates, and positively correlate with Gleason grade of prostate cancer [275]. Calcitonin is also associated with various cancer regulated processes such as the tumor growth, invasion, angiogenesis, chemoresistance and metastasis [276-278]. It was shown that PC3 cells lacked CTR[275]. In addition to prostate cancer, CaSR has been shown to be highly expressed in patients with primary renal cell tumors with bone metastasis in comparison to lung metastases or no metastases. Further, the proliferation and migration induced by Ca^{2+} treatment in RCC cells obtained from patients with bone metastasis was inhibited by CaSR inhibitor NPS2143 [92].

4.2.3 PC3 and LNCaP cells lines

Prostatic cancers are usually adenocarcinomas that form gland and express markers for androgen receptor (AR) and prostate-specific antigen (PSA) [279]. On the other hand, another form of prostate cancer is prostatic small cell neuroendocrine carcinoma (SCNC) which do not form glands and are negative for AR and PSA [279]. This SCNC is extremely aggressive and present in locally advanced disease or distant metastasis and patients usually die within months of diagnosis [280, 281]. These do not respond to hormonal therapy [282, 283] and occurs as a minor population in prostatic epithelial malignancies. These are small, with fine chromatin pattern, scant

cytoplasm and nuclear molding [279]. These account for less than 1% of prostate cancer but is recurrent in patients with conventional prostatic adenocarcinoma and who take hormonal therapy. PC3 [284] is a epithelial cell used as a model for PCa with spectrum of aggressive form and with AR dependence. On the other hand, LNCaP [285, 286], also an epithelial cell, is used as a model for indolent form of PCa with castration-resistance. Study by Tai et al in 2011 showed that PC3 have features of SCNCs and LNCaP with conventional adenocarcinoma [279].

4.2.4 Ca^{2+} signaling in bone environment

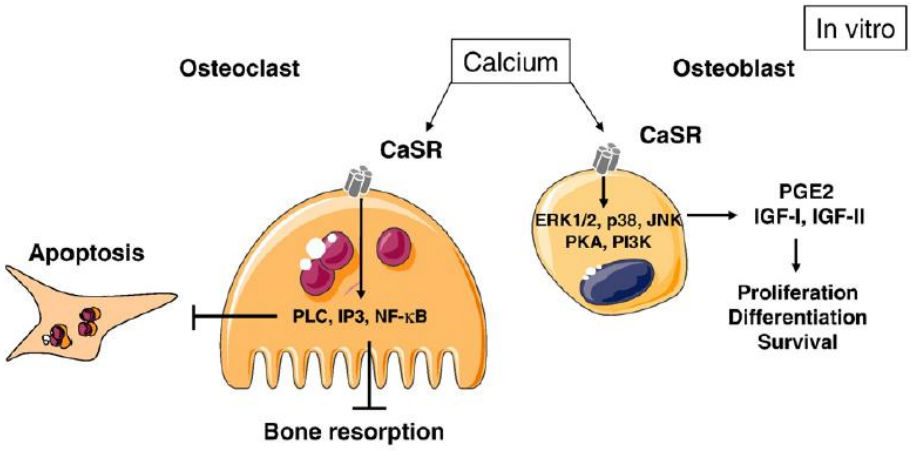

Figure 4.2 Extracellular Ca^{2+} induced CaSR mediated signaling in bone cells [10]

4.2.5 Prognosis of prostate cancer

The most common screening used for early detection of PCa is prostate-specific antigen (PSA). But higher PSA levels are also present in non-malignant conditions such as benign prostatic hyperplasia (BPH) [274, 287]. Other prognostic markers for PCa include performance status (PS) score, hemoglobin level, age factor, albumin, lactate dehydrogenase (LDH), Gleason score, pain intensity and metastasis characteristics [288]. For biomarker profiling, cDNA microarray between 50 normal and neoplastic protease specimen and three typical prostate cancer cells, including PC3,

LNCaP, and DU-145 were conducted. Common genes such as the tumor suppressor PTEN and CDH1 (E-cadherin) were downregulated, and proto-oncogene MYC and fatty acid synthase were up-regulated [274]. Further hepsin, a transmembrane serine protease and pim-1, a serine/threonine kinase were also correlated with PCa [274]. Other related gene mutations in MYC, RB1, MET, BRCA1/2 and ATM are known [289, 290].

4.2.6 The human protein atlas on prostate cancer proteome

According to the proteome analysis using TCGA transcriptomics data and antibody-based protein data, they suggest a prognostic based on transcriptomics data from 494 patients, 134 genes associated with unfavorable prognosis and only 25 genes associated with favorable prognosis (https://www.proteinatlas.org/humanproteome/pathology/prostate+cancer).

4.2.7 CaSR alternative splicing

CaSR gene (CASR) encodes for calcium-sensing receptor and is a ~100-kb spanning single copy gene that maps to human 3q13.3-21. Out of the eight exons, exons 2 to 7 encode the CaSR protein of 1068 amino acids. Exons 1A and 1B are able to encode for two alternative 5′-untranslated region (UTR) that may splice to a common segment encoded by exon 2 [31]. Exon 2 contains 242 nucleotides of the 5′-UTR upstream of the ATG translation initiation codon [31]. CASR is expressed in multiple tissues and organs at various levels. The variation of expression of CASR gene as multiple alternative transcripts in multiple tissues/organs hint at the ability to diversify its functions and regulations. A splice variant with an exon 3-deleted CASR transcript in thyroid TT cells, placental cytotrophoblast, and in parathyroid, thyroid, and kidney [31, 291] causes poorly expressed and trafficking of CaSR to the cell surface. Another alternative transcript of CaSR exists in human keratinocytes where exon 5 is deleted (with a 77-amino acid in-frame deletion in the exodomain) [292]. The relative amounts of full-length is lowered during

keratinocyte differentiation and the alternatively spliced variant is shown to cause the full-length protein to be less responsive to Ca^{2+}. This variant of CaSR is also known to be upregulated in skin and kidney in the knockout mice and is shown to compensate for the absence of the full-length CaSR in bone and cartilage [31].

Table 4.1 20 genes with highest significance associated with favorable prognosis in prostate cancer .
https://www.proteinatlas.org/humanproteome/pathology/prostate+cancer

Gene	Description	Predicted localization	mRNA (cancer)	p-value
CRACR2A	calcium release activated channel regulator 2A	Intracellular	1.6	2.85e-6
TMEM158	transmembrane protein 158 (gene/pseudogene)	Membrane	6.7	6.43e-5
EPHX1	epoxide hydrolase 1	Intracellular	73.3	1.32e-4
TSKU	tsukushi, small leucine rich proteoglycan	Secreted	16.9	1.66e-4
AOC1	amine oxidase, copper containing 1	Secreted	5.7	1.71e-4
TXN2	thioredoxin 2	Intracellular	47.1	2.04e-4
SESN1	sestrin 1	Intracellular	11.9	2.07e-4
AK5	adenylate kinase 5	Intracellular	2.3	3.88e-4
GPAT4	glycerol-3-phosphate acyltransferase 4	Membrane	11.0	4.15e-4
RFPL2	ret finger protein like 2	Intracellular	5.6	4.16e-4
ATP6V1E1	ATPase H+ transporting V1 subunit E1	Intracellular	35.5	4.18e-4
RNF122	ring finger protein 122	Membrane	3.5	5.37e-4
COMT	catechol-O-methyltransferase	Intracellular,Membrane	27.8	5.67e-4
UBE2D4	ubiquitin conjugating enzyme E2 D4 (putative)	Intracellular	5.7	5.77e-4
HBEGF	heparin binding EGF like growth factor	Membrane	7.0	6.00e-4
NTNG2	netrin G2	Secreted	1.3	6.06e-4
SLC35B2	solute carrier family 35 member B2	Membrane	37.9	6.07e-4
FOXQ1	forkhead box Q1	Intracellular	2.3	6.68e-4
ARL2	ADP ribosylation factor like GTPase 2	Intracellular	21.3	7.70e-4
FOS	Fos proto-oncogene, AP-1 transcription factor subunit	Intracellular	225.2	7.81e-4

4.2.8 Alternative splicing

Alternative splicing (AS) of pre-mRNAs is extensively prevalent throughout most eukaryotes, occurring in 40-60% of all genes [293] and in as many as ~95% of human multi-exon

genes [294]. This has allowed for the high levels of tissue specificity and functional diversity in higher organisms [295]. AS plays a vital role in many cellular functions including the regulation of neuronal development [296], metabolism [297], immunity [298], and signaling pathways through changes in protein-protein interactions [296, 299].

4.2.9 Proteomics

Mammalian cell lines are an indirect means to understand the much larger and fundamental biological processes. These processes are dictated by proteomics and cellular response that are common or differential. By using mass spectrometry, we can identify and quantify proteins in a global manner which can further indicate the molecular processes that are altered between such systems. Many previous works have used global proteomics but have been either limited with their number of detected proteins, such as Bukart et al. [300] compared seven cell lines and detected ~2000-4000 proteins per cell line and were limited to more abundant proteins. The human genome consists of about 20,000 genes with much more complex proteomes. It has been estimated that a single cell can express about 10,000 proteins [301]. Geiger el al in 2012 characterized over 10,000 proteins in each cell lines. The same group also characterized potential biomarkers for breast cancer [302]. In our work, we employ the latest proteomics technique to achieve further understanding of the proteostasis affected by the Ca^{2+}_{o} in PC3 as well as compare the proteome between PC3 and HEK293 cells. This may allow us to uncover the biomarkers pertaining to prostate cancer.

4.3 Challenges

As mentioned in chapter III, the challenges of studying CaSR in the endogenous form in pathological cells is the four-fold lower expression level, heterogeneity of CaSR transcripts and variants, dynamic CaSR lifecycle, and multitude binding partners involved in signaling. There is

a limitation of methods as well. The sensitivity of RT-PCR and PCR can be affected by many parameters such as primer specificity, heterogeneity of transcripts, annealing temperature, quality of RNA extracted, handling of RNA. Mass spectrometry_data is affected by glycosylation, antibody specificity, sample handling

4.4 Major Questions addressed

1. How do the characteristic feature of CaSR in prostate cancer cell different from the wild type CaSR?
2. Do CaSR mediated signaling follows the conventional scheme in prostate cancer cells?
3. How do divalent cations and drugs impact CaSR mediate signaling?
4. Is the differential response due to expression level or presence of variants?
5. How does Ca^{2+}_o affect the proteostasis of PC3 cells?
6. How does the proteomics of PC3 cells differ from HEK293 cells?

4.5 Materials and Methods

4.5.1 Antibodies

Anti-FLAG antibody, mouse (Sigma-Aldrich, Canada) was used to precipitate the CaSR/interactor complex. Anti-CaSR C0493, mouse (Abcam, Cambridge, MA, USA) and Anti-GAPDH mouse (Abcam, Cambridge, MA, USA) were used for western blot.

4.5.2 Total protein extracts

Transfected HEK293 cells from 90-100 % confluent 100 mm dishes were harvested after the treatment with 4 mM Ca^{2+} or 2 mM EGTA. They were washed with ice-cold Phosphate-buffered saline (PBS) with 0 mM Ca^{2+} 3 times. 600 µL of 10 mM Sodium β-glycerophosphate, 50

mM Tris-Cl (pH 7.4), 150 mM NaCl, 1 mM EDTA (pH 8.0), 1% Triton X-100, 2 mM Na_3VO_4, 50 mM NaF, 10 mM sodium pyrophosphate supplied with proteinase inhibitor cocktail (Roche, Basel, Switzerland) was used to lyse cells for 30 min in ice with frequent vortex and subsequently centrifuged to pellet cell debris. Cleared cell lysates were subjected to anti-FLAG immunoprecipitation before immunoblotting

4.5.3 Cell culture and transfection

HEK293 cells were seeded on 22 × 40 mm coverslips in 60 mm culture dishes and cultured in 5% CO2 at 37 ºC in respective media. HEK293 cells were cultured in high glucose Dulbecco's modified Eagle's medium (DMEM) (Invitrogen) containing 10% fetal bovine serum (FBS). CaSR-pcDNA with flag tag was transfected using Lipofectamine 3000TM (Invitrogen) according to the manufacturer's instructions. Cells were incubated for 36-48 h in respective media after transfection.

4.5.4 Cell lysis

10 mM Sodiumβ-glycerophosphate, 50 mM Tris-Cl (pH 7.4), 150 mM NaCl, 1 mM EDTA (pH 8.0), 1% Triton X-100, 2 mM Na_3VO_4, 50 mM NaF, 10 mM Sodium pyrophosphate supplied with Sigma proteinase inhibitor cocktail was used to lyse cells for 30 min in ice with frequent vortex. For each condition, ~1-2 mg total protein was used. antibody (flag 10ug) and dyna bead was incubated for 30 min incubation of at room temperature in 200ul PBS and 0.01% Tween20 and washed once with lysis buffer. Antigen was incubated overnight at 4 degrees. Or, the Dyna bead, lysate and antibody were incubated at 4 degrees overnight. Next day, the beads were washed two times with lysis buffer and 1 time with PBS with Ca^{2+} or EGTA. Or for the $[Ca^{2+}]_o$ perturbation experiment, cells were incubated with 0.1% BSA Ca^{2+} depleted DMEM (low glucose) for 30 min and Ca^{2+} and EGTA were added to the medium and incubated for 2 h at 37 degrees. After overnight

incubation, the beads were washed four times, two with lysis buffer and two with PBS without additional Ca^{2+} or EGTA.

10% beads were suspended in 30 ul of 2X sample buffer with 5% beta mercaptonol and heated for 10 min at 70 or 100 degrees.

4.5.5 RNA preparation

Illustra RNAspin Midi RNA Isolation kit (GE Healthcare) was used to separate the RNA from the PC3 cells as described by the manufacturer's protocol. 6 X 10^6 cells were lysed using buffer RA1 and β-mercaptoethanol. After vortexing vigorously, the chaotropic salts in the lysis buffer break open the cells and inhibit RNases. β-mercaptoethanol helps to inhibit RNases and break up RNA-protein complexes. The lysate was filtered by centrifugation through an RNAspin filter unit. 70% ethanol was added to the cleared lysate and applied to a silica column. The chaotropic salt in the lysis buffer plus the ethanol promotes binding of RNA > 200 nucleotides long to the silica membrane. Denatured proteins are collected in the flowthrough following centrifugation. After the addition of ethanol, a stringy precipitate may become visible. All the precipitate were loaded onto the column. The membrane was desalted using desalting buffer to wash away salts. RNase-free DNase I was added to digest membrane-bound DNA and incubated briefly at room temperature. Finally, the column was washed to inactivate DNase, then washed with a low-salt buffer containing ethanol to remove residual salts and other contaminants. After drying the membrane, the purified total RNA was eluted using RNase-free water and immediately placed on ice or frozen.

4.5.6 RT-PCR

Purified RNA is a mixture of mRNA and rRNA. In mammalian system, poly-A enrichment is used to enrich the mRNA and separate the rRNA out. Next, Superscript III (Thermo Scientific)

was used to isolate RNA and KOD hot start was used to carry out PCR. The protocol was as described by the manufacturer. A 20-µl reaction volume as used for 500 ng of mRNA. 1 µl of oligo(dT)20 (50 µM), 500 ng mRNA, 1 µl 10 mM dNTP mix (10 mM each dATP, dGTP, dCTP and dTTP at neutral pH) sterile, 13 ul distilled water was added to a nuclease-free microcentrifuge tube. The mixture was heated to 65°C for 5 minutes and incubate on ice for at least 1 minute. The contents of the tube were collected by brief centrifugation and 4 µl 5X First-Strand Buffer, 1 µl 0.1 M DTT, 1 µl RNaseOUT™, Recombinant RNase Inhibitor (Cat. no. 10677-019, 40 units/µl) were added. The solution was mixed by pipetting gently up and down. The tube was incubated at 50°C for 30–60 minutes. Finally, the reaction was inactivated by heating at 70°C for 15 minutes.

The cDNA (0.794 ug/ul) was used as a template for amplification in PCR. To remove RNA complementary to the cDNA, E. coli RNase H was added at 1 µl (2 units) and incubated at 37°C for 20 minutes. PCR reaction tube was prepared by adding 10X PCR Buffer [200 mM Tris-HCl (pH 8.4), 500 mM KCl], 3 µl 25 mM MgCl2, 5 µl 2 mM dNTP,1.5 ul Sense primer (10 µM) 1.5 µl, Antisense primer (10 µM), 1 µl KOD hot-start polymerase (5 U/µl) (Novagen), 2 µl cDNA, 31 µl autoclaved-distilled water to make a 50 µl solution. The reaction was heated to 95°C for 2 minutes to activate polymerase and again 95°C for 20 sec to denature. The annealing was carried out at 56 °C for 30 sec. 30 cycles of PCR was used for an extension at 70 for 60 sec each cycle.

4.5.7 Immunoblotting

A total input protein of 50 ug and 30 ul of the 10 % bead samples were loaded in 8.5 % acrylamide gels and subjected to sodium dodecyl sulfate-polyacrylamide gel electrophoresis (SDs-PAGE) to separate proteins, then transferred to nitrocellulose membranes. The membranes were blocked with 3 % nonfat milk (w/v) in TBS for 2 hours at room-temperature with constant shaking. The antibodies of interest were diluted in 3 % non-fat milk (w/v) and 0.2% Tween-20 in TBS

(TBST). Anti-CaSR C0493, mouse (Abcam, Cambridge, MA, USA) was used at 1:700 dilution and HRP-conjugated mouse secondary antibody were used (Sigma-Aldrich, United States) at 1:3000 dilution to probe CaSR. For, GAPDH, anti-GAPDH mouse (Abcam, Cambridge, MA, USA) was used at 1:3000 dilution and HRP-conjugated mouse secondary antibody was used (Sigma-Aldrich, United States) at 1:10,000 dilution. Membranes were incubated with the primary and secondary antibodies for 1 hour at room temperature with constant shaking and finally washed with TBST. The secondary antibody was visualized using ECL detection reagents (GE Healthcare, Little Chalfont, UK) developed on X-OMAT^{TM} imaging film (Kodak, Rochester, NY).

4.5.8 Immunostaining

HEK293 cells were grown on 20 × 20 mm coverslips placed in 6-well plates one day before the transfection. Cells subjected to transfection and after 48 h treated for immunostaining. Cells were washed with ice-cold PBS and fixed with 3.7 % formaldehyde for 15 min at room temperature, followed by a wash with PBS three times. Cells were permeabilized using 0.2 % Triton X in PBS for 10 min at room temperature. Mouse anti-FLAG monoclonal antibody was diluted 1000 times and incubated with cells overnight at 4°C to stain the CaSR. The cells were subsequently washed with PBS and stained with goat anti-mouse Alexa 488–conjugated secondary antibody for 1 hour at room temperature. Nuclei were stained with 4′,6-diamidino-2-phenylindole. Fluorescence was visualized using a Zeiss LSM780 confocal microscope.

The stains were analyzed using Image J. After splitting the channels, the red and green channels were given rainbow RGB and were analyzed for the surface plot for the area of interest for co-localization. The corresponding peaks corroborate the co-localization of the two stains and therefore, of two proteins. Similarly, after splitting the channels, plugin coloc2 was used to analyze

the Pearson's coefficient between two channels. Channels other than red or green were given Pseudo RGB using zenlite for Image J to read.

4.5.9 IP_1 assay

HEK293 cells and PC3 cells were seeded in 24-well plates at 3 x 10_5 cells per well in 500 µl of culture medium. After transfection with WT CaSR or its various mutants, cells were further cultured for 24 hours at 37°C. Cell monolayers were first washed with Ringer's buffer without calcium (121 mM NaCl, 2.4 mM K_2HPO_4, 0.4 mM KH_2PO_4, 10 mM HEPES, 5.5 mM glucose, 1.2 mM $MgCl_2$) and then incubated for 1 hour at 37□C in stimulation buffer (140 mM NaCl, 5 mM KCl, 10 mM $LiCl_2$, 0.55 mM $MgCl_2$, 10 mM HEPES) containing varying concentrations of $CaCl_2$. After treatment, cells were lysed for 30 min at 37°C with 50 µl of 2.5% IP_1 ELISA Kit Lysis Reagent (CIS Bio International, Gif-sur-Yvette, France). The accumulation of IP_1 was measured using an immunoassay based on competition between free IP_1 and horseradish peroxidase (HRP) conjugated IP_1 for binding to the monoclonal anti-IP_1 antibody. The results for IP_1 were expressed as percentage inhibition of IP_1-HRP binding = [1-IP_1-HRP binding in stimulated cells/IP_1-HRP binding in unstimulated cells] x 100.

4.5.10 Mass spectrometry

LC-MS/MS Q-Extractive Orbitrap was used. LFQ intensity of each protein for each treatment condition was averaged from two total lysate samples from each from HEK293 and PC3 cells in treated with Ca^{2+} or EGTA. The missing values were imputed as previously described using Perseus [130]. Enrichment of proteins was considered significant if the intensities had at least two-fold difference, i.e., $\log_2(Ca^{2+}/EGTA)$ -PC3 or $\log_2$ (PC3/HEK293)-$Ca^{2+} \geq 1.00$. For robust stringency, we employed a requirement of minimum PSM of 2 for no less than two replicates and identification with at least one unique peptide.

4.5.11 Gene ontology

Protein-protein interaction was performed using the Search Tool for the Retrieval of Interacting Genes/Proteins (STRING) version 10.0. Interaction network view was used to identify and visualize the degrees of interaction amongst the upregulated proteome (*homo sapiens*). STRING uses evidence from experimental and knowledge-based databases to provide confidence in functional associations or interaction through the Edge Confidence. Size of colored nodes represent evidence of known or predicted 3-dimensional protein structure.

The Database for Annotation, Visualization, and Integrated Discovery (DAVID), version 6.8, was used for the functional annotation and analysis of enriched proteins. The set of total proteins identified and quantified (n = 3327) was used as the background. The numbers of enriched proteins of interest and background lists are compared in each functional cluster. A two-tailed modified fisher's exact test (EASE score of 1) with classification stringency at "medium" was employed to generate statistically significant enrichment annotations and to categorize them under annotation terms: cellular compartments, biological processes, molecular function and KEGG pathways. Correction for multiple hypothesis testing was carried out using standard false discovery rate control methods. A Bonferroni-corrected $P \geq 0.05$ and an enrichment ≥ 1.3 were used as a cut-off [131].

4.5.12 CaSR knock down

Using shRNA technology, CaSR was knocked down in PC3 luc cells. pLKO.1-CaSR was co-transfected into HEK293T cells with psPAX2 and pMD2 plasmids. The target gene was as described by Liao et al CTGGGTGTGTTTATCAAG in the seventh exon.

4.6 Results

4.6.1 CaSR mediated intracellular signaling in PCa cells is arrested

4.6.1.1 Intracellular Oscillation is inhibited in PCa cells

The PC3 cells with endogenous CaSR show little to no response to the increasing Ca^{2+} in terms of the CaSR mediated intracellular oscillations (**Figure 4.3)**. PC3 cells (prostate cancer cells

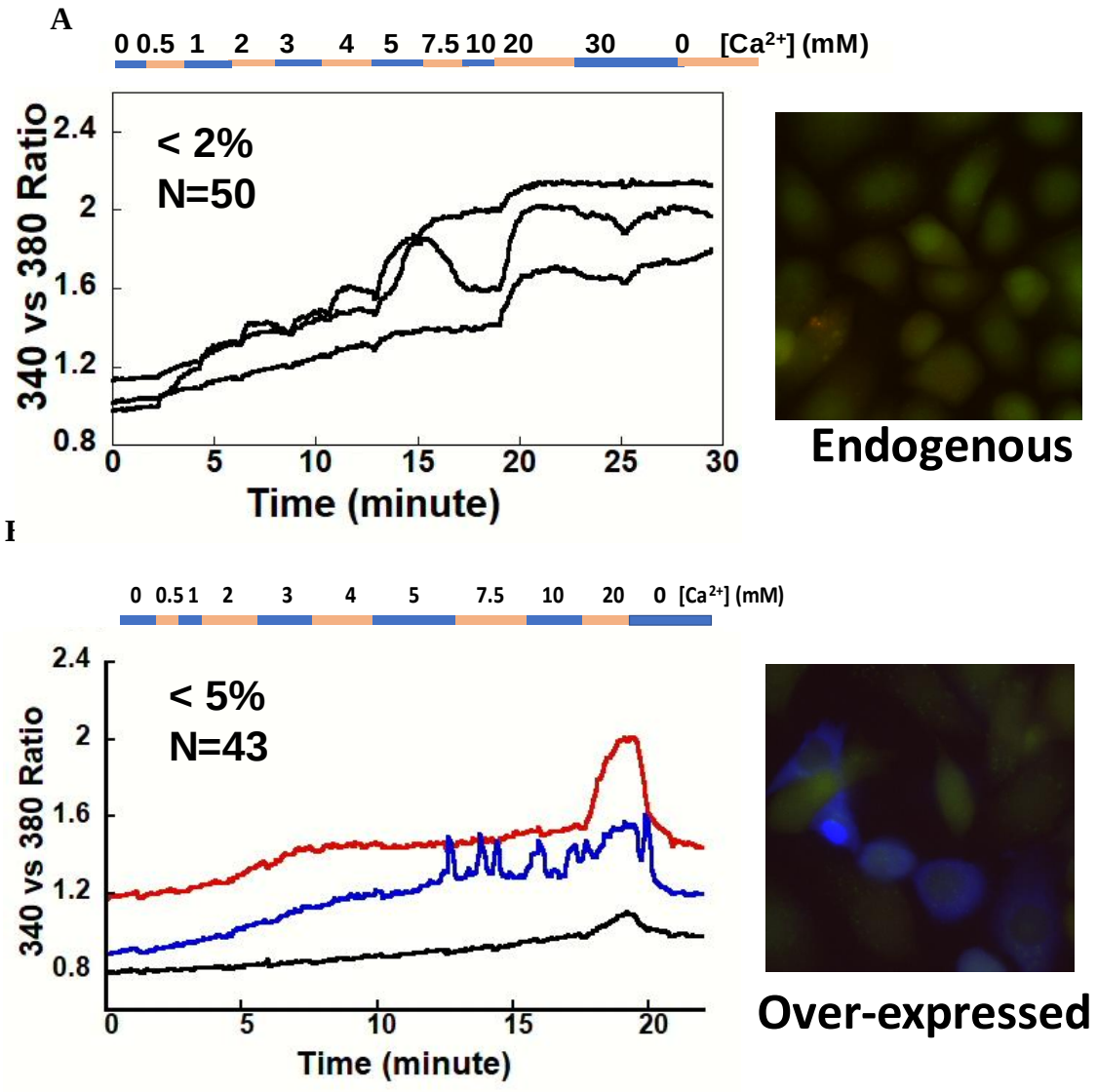

Figure 4.3 Intracellular Ca^{2+} response to extracellular Ca^{2+} by PC3 with endogenous CaSR (A) or that triansiently transfected with GFP-CaSR (B)

that metastasize to bones) display heterogeneity where 98% of the cells do not oscillate, 2% of them carry out the sinusoidal oscillation with low frequency at ~5 or 10 mM $[Ca^{2+}]_o$ and 3% carry out transient peak at ~ 10-20 mM Ca^{2+} (n=50). Interestingly, we observe 50% of LNCaP cells (Prostate cancer cells that metastasize to lymph nodes) responding with a transient at a high Ca^{2+}

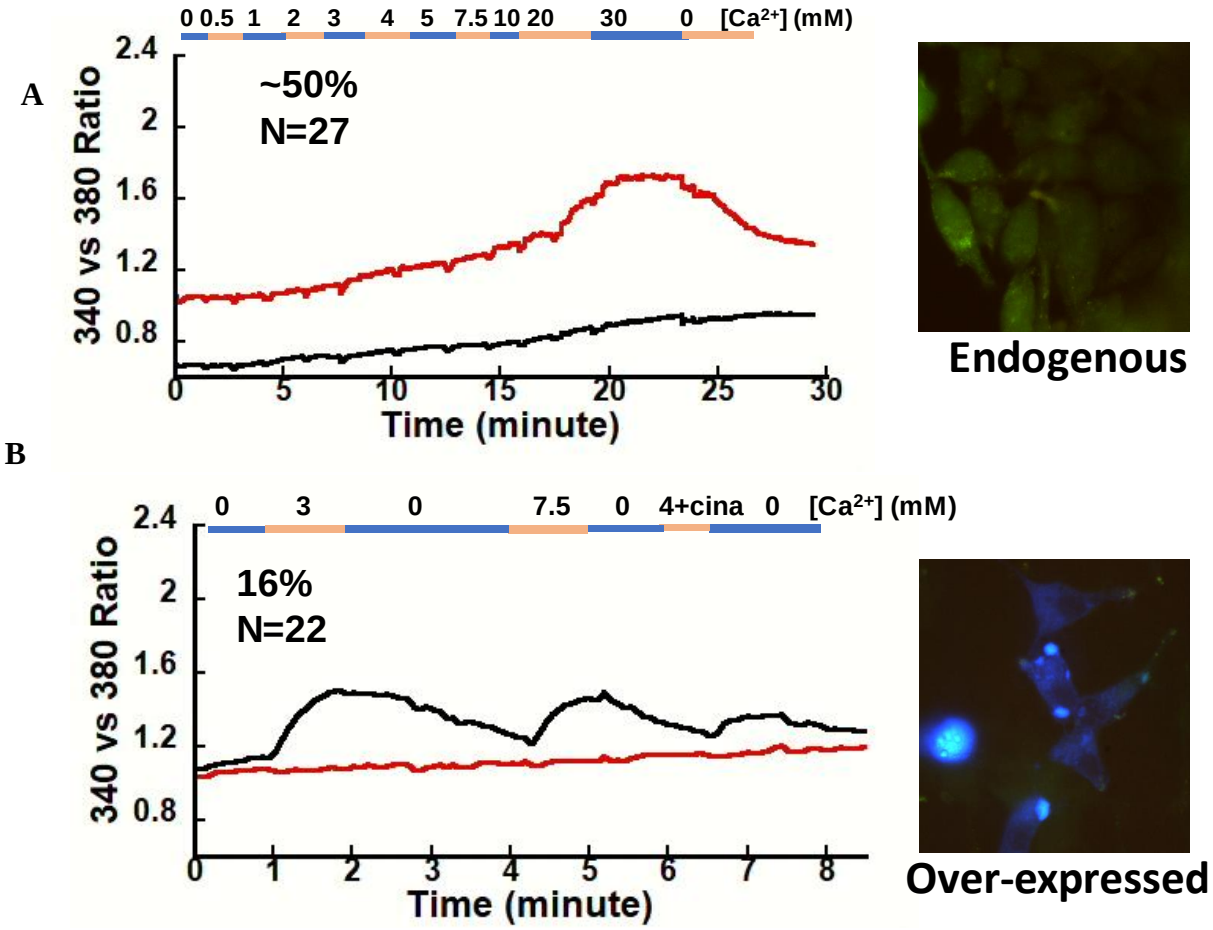

Figure 4.5 Intracellular response by LNCaP cells

50% LNCaP cells with endogenous CaSR showed intracellular Ca^{2+} response at 30 mM. 4.5 2 % LNCaP cells transfected with wild type GFP-CaSR showed minimal response with transient Ca^{2+} peaks at 3 and 7.5 mM Ca^{2+}

concentration of 30 mM (n=27) with 0.5 units (340/380 ratio) height (). We further exempted the idea that a CaSR variant caused this discrepancy by transiently transfecting PC3 and LNCaP cells with wild type CaSR with 1.5-2 ug of DNA (**Figure 4.3, Figure 4.5).** The GFP-CaSR transfected PC3 cells do not display any oscillations, only rise in intracellular Ca^{2+} in 2% of the PC3 cells at

20 mM which could be washed away with 0mM Ca^{2+}. These raises were variable in amplitude with 0.1-0.4 units (340/380 ratio) rise from the baseline. A clear oscillation at 5 mM was observed in only 1 cell out of the 43 transfected cells examined. But the pattern did not represent the WT and with 0.20 units (340/380 ratio) (**Figure 4.3**). LNCaP cells interestingly responded by 16% with increased intracellular Ca^{2+} transients by lower Ca^{2+} concentrations of 3 or 7.5 mM with ~0.5 units (340/380 ratio) height in LNCaP cells (**Figure 4.5**). This suggests a significant difference in intracellular signaling or a dysfunctional Ca^{2+} sensing machinery in prostate cancer cells irrelevant to the region of metastasis with different Ca^{2+} environments. Also, the mechanism of Ca^{2+} sensing is differential between the PC3 and LNCaP cells. Similarly, Mg^{2+} and TNCA had no effect on CaSR mediated intracellular oscillation in these cells.

4.6.1.2 CaSR mediated inositol monophosphate (IP_1) accumulation in PC3

Additionally. to examine the function of CaSR, IP_1 accumulation was studied in PC3 and compared with 5001 (HEK293 stably transfected with wild type CaSR). IP_1 is a stable downstream

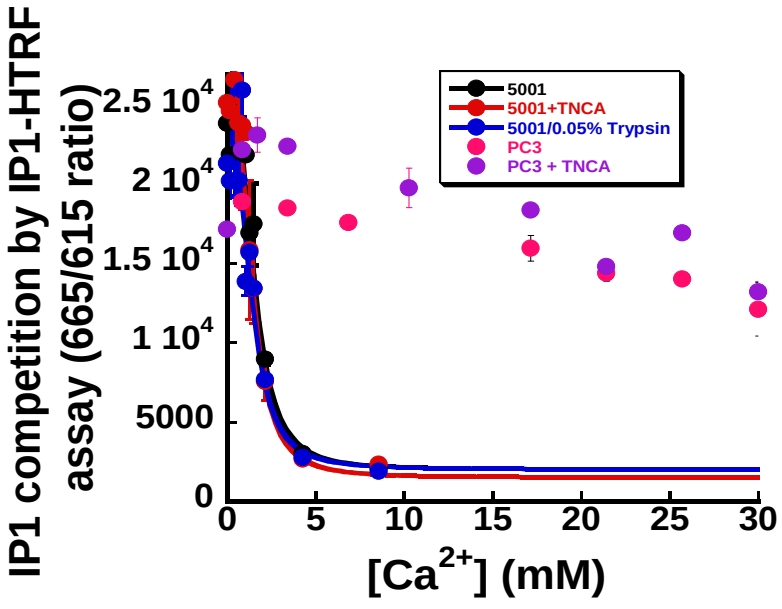

Figure 4.6 IP1 accumulation in PC3 is absent even in the present of CaSR agonist TNCA

metabolite of IP_3 induced by activation of a phospholipase C (PLC) cascade through CaSR **(Figure 4.6)**. IP_1 accumulation is absent in PC3, which supports the oscillation data and indicates that CaSR in PC3 is unable to induce $G\alpha_{q/11}$ mediated signaling.

It has been studied in the past that $G\alpha_{q/11}$ was only present in RWPE-1 and LNCaP prostate cancer cells, but not in PC3 cells [303]. We checked the $G\alpha_{q/11}$ expression level in PC3 using immunoblot and MS. We show contradictory result where immunoblot (**Figure 4.7)** shows the presence whereas, MS does not.

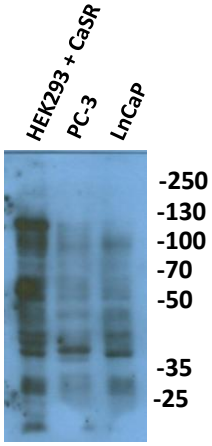

Figure 4.7 Expression of Gαq in PCa cells

4.6.1.3 CaSR mediated ERK1/2 in PC3

CaSR mediates ERK phosphorylation through Gαi. It is a well-characterized signal and is known to affect another downstream signaling. We observe that the ERK1/2 is stunted in PC3 as compared to the wild type (**Figure 4.8**). This further support that PC3 lack Ca^{2+} sensing through Gαq and Gαi.

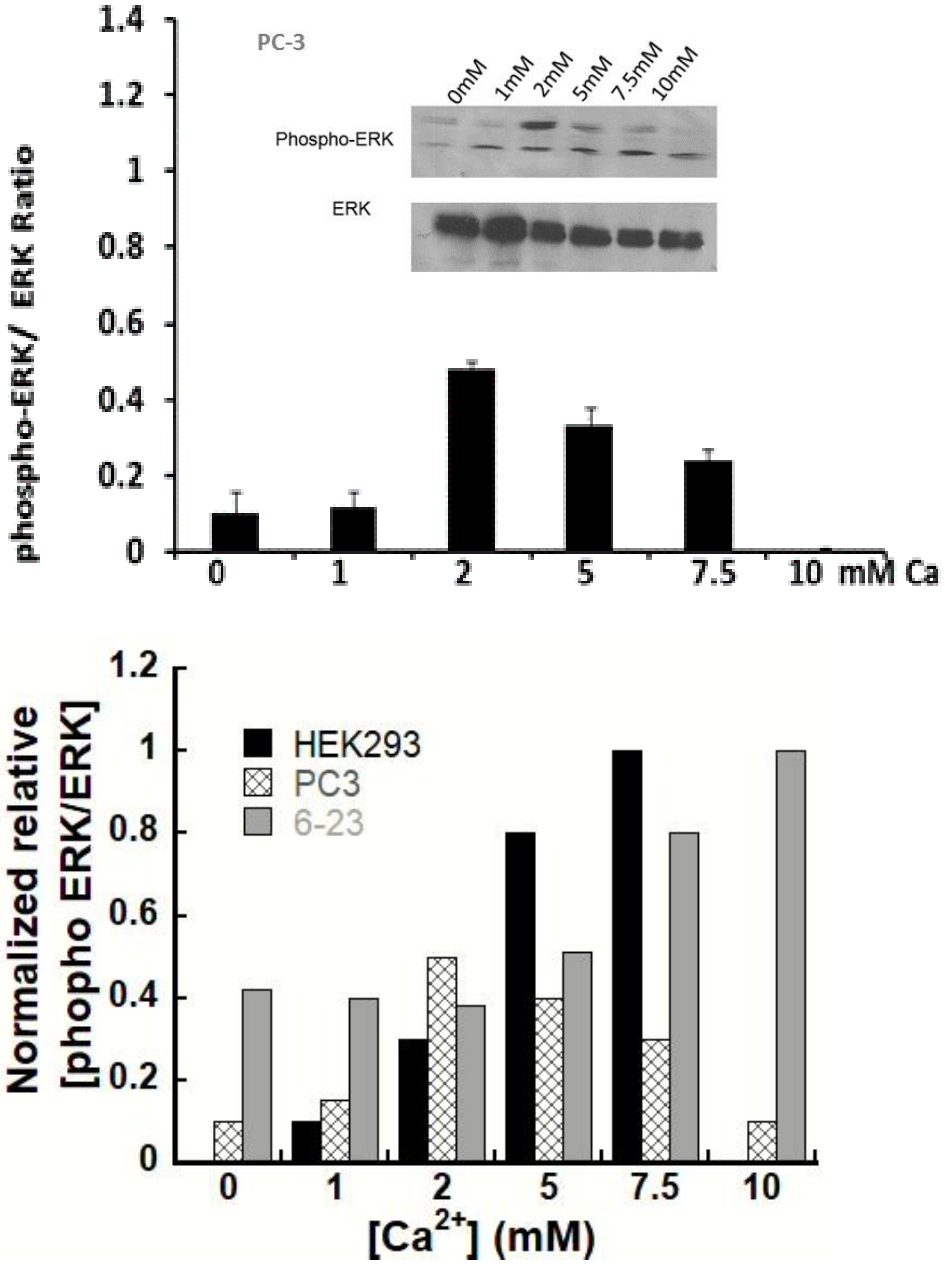

Figure 4.8 ERK in PC3 and comparison to HEK293 cells and 6-23 cells

4.6.2 Dissecting the basis of differential CaSR mediated signaling in prostate cancer cells and HEK293 cells.

4.6.2.1 Expression of CaSR in PC3

4.6.2.1.1 Western blot

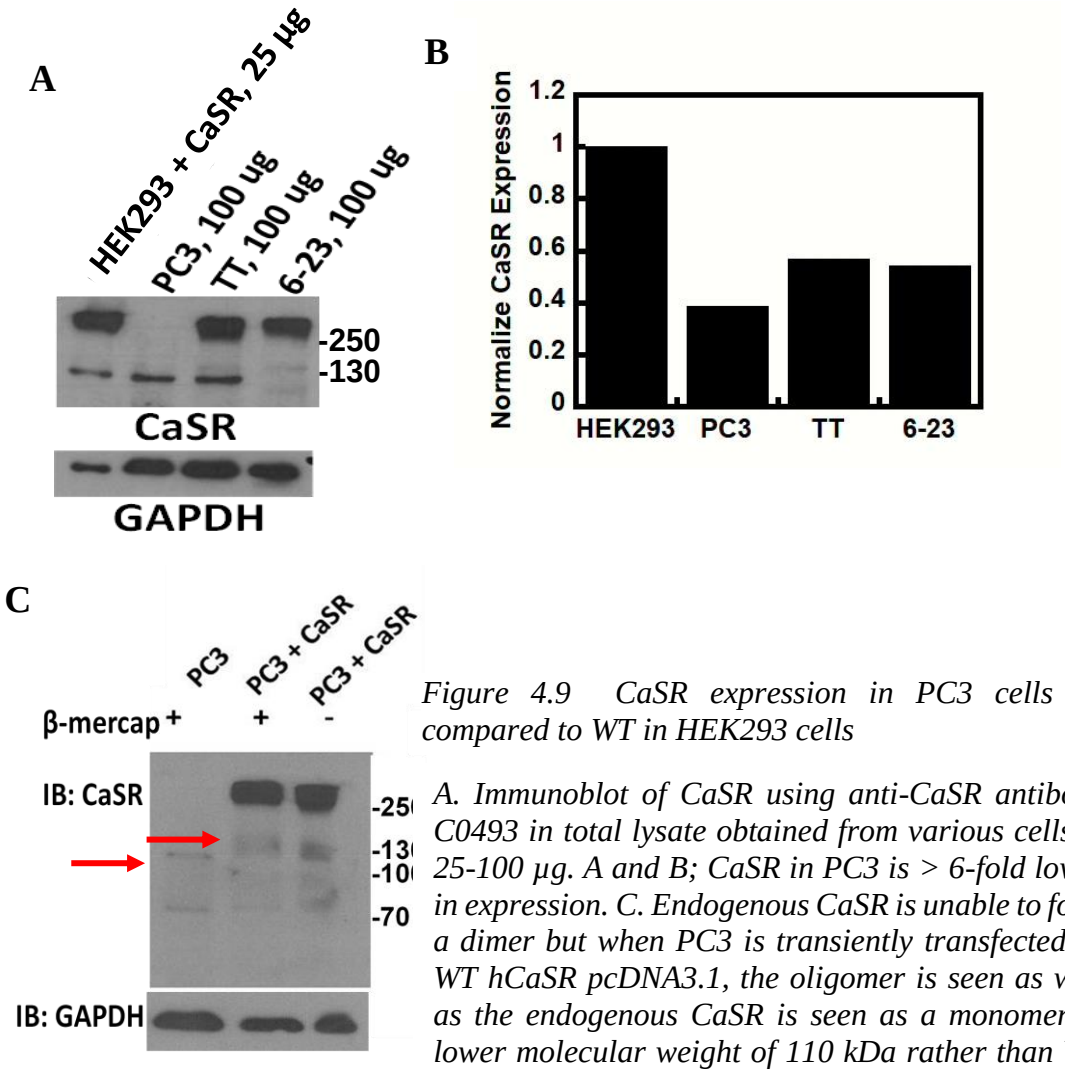

Figure 4.9 CaSR expression in PC3 cells as compared to WT in HEK293 cells

A. Immunoblot of CaSR using anti-CaSR antibody C0493 in total lysate obtained from various cells at 25-100 µg. A and B; CaSR in PC3 is > 6-fold lower in expression. C. Endogenous CaSR is unable to form a dimer but when PC3 is transiently transfected by WT hCaSR pcDNA3.1, the oligomer is seen as well as the endogenous CaSR is seen as a monomer at lower molecular weight of 110 kDa rather than WT 130-150 kDa.

Expression of endogenous CaSR was examined using the western blot of the total CaSR obtained from PC3 cells after the lysis. Anti CaSR – C0493 antibody was used for blotting

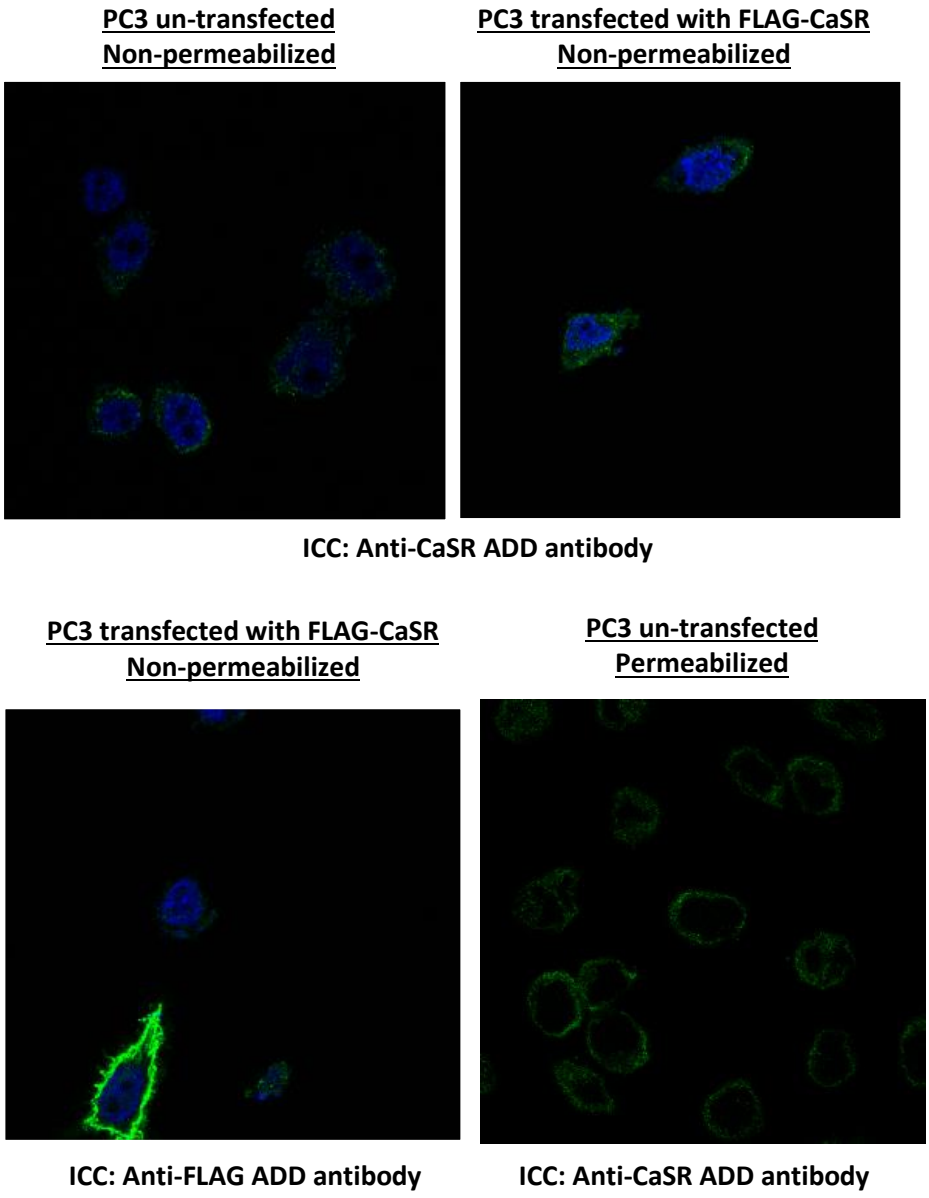

Figure 4.10 Detection of endogenous and transiently transfected CaSR on the membrane of PC3

endogenous CaSR. Two plates for PC3, TT and 6-23 samples were lysed and one plate for 5001. 100 µg was loaded for each cancer sample and 25 µg for 5001 sample (**Figure 4.9**). The expression level of endogenous CaSR was about 6-fold lower than HEK293 cells transiently transfected with

wild type CaSR or the PC3 transiently transfected with wild type CaSR. We also observe the molecular difference in the monomers; CaSR in PC3 has lower molecular weight at 110 kDa as compared to the wild type CaSR at 130-150 kDa in HEK293 or PC3 transiently transfected.

Interestingly, overexpression of recombinant wild type CaSR in PC3 was able to form an oligomer unlike the endogenous CaSR in PC3. These results may indicate the presence of splicing or lower glycosylation in endogenous CaSR to result in the lower molecular weight. Our result also suggests that PC3 has glycosylation enzymes needed to glycosylate the WT CaSR so that the defect may lie on the endogenous ones. Previous studies by Liao et al. has shown the expression of PC3, but they do not specifically indicate the molecular weight they detected. However, they validate that PC3 with bony metastasis has higher CaSR as compared to C4-2B, an androgen-independent variant of LNCaP that metastasizes to bone [91, 304, 305].

4.6.2.1.2 Immunostaining

We observe endogenous CaSR on the membrane but in lower amount as compared to the wild type transiently transfected in HEK293 or PC3 cells (**Figure 4.10**). Overexpressing wild type CaSR in PC3 increases the amount of staining. Using anti-FLAG antibody, we can see a membrane expression of CaSR on PC3 cells, but the transfection efficiency is low where the number of transfected CaSR is low. Anti-FLAG antibody is more efficient at staining the FLAG-CaSR as

compared to the anti-ADD as determined in Chapter III. The reason for not being able to observe a significant difference between anti-ADD stained transfected and endogenous CaSR in PC3 must be due to in-efficiency of transfection.

Figure 4.11 Primers were designed to investigate presence of DNA at each exon All corresponding bands matched in 5001 and cancer cell lines expect for exons 5/6 and 7-

4.6.2.2 Investigation of splice variant of CaSR in PC3

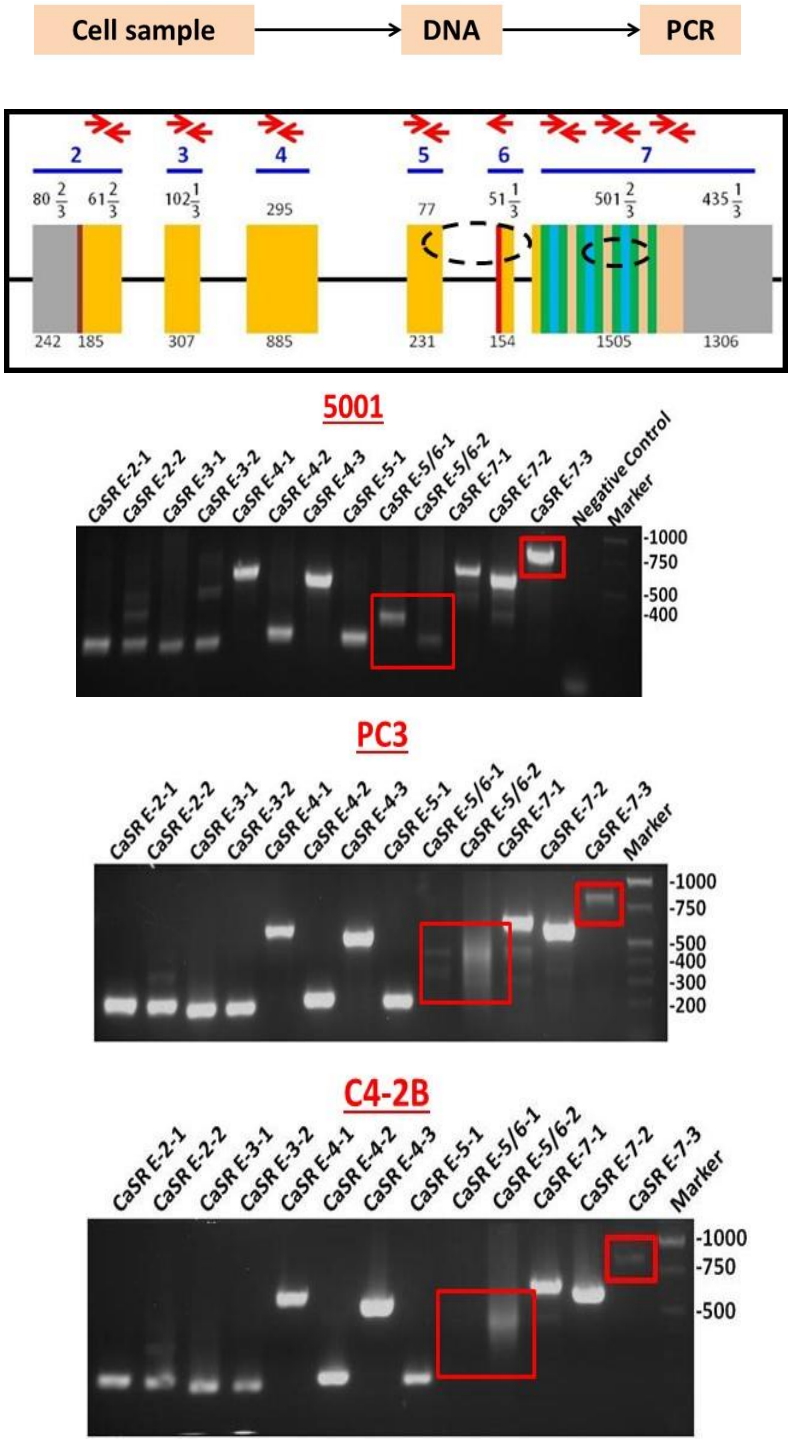

Figure 4.12 Primers were designed to investigate presence of DNA at each exons. All corresponding bands matched in 5001 and cancer cell lines expect for exons 5/6 and 7-3

4.6.2.2.1 Probing DNA of coding region of CaSR in PC3 cells.

In order to find the cause for the lower molecular weight as well as the signaling difference, we investigated the CaSR in PC3 at the gene level. We isolated the RNA using Illustra RNAspin Midi RNA Isolation kit from GE healthcare and carried out a poly-A enrichment where Superscript III (Thermo Scientific) was used to isolate RNA and KOD hot start was used to carry out PCR. We found the CaSR transcript to below. This could have resulted due to RNA being unstable. Therefore, we used amplification of genomic DNA first, which is more robust.

We were able to match all corresponding bands in PC3 as compared to the positive control 5001 except for exons 5/6 and 7-3 when we amplified CaSR fragments with CaSR specific primers using genomic DNA **(Figure 4.12**). We further went to design primers within 5/6 and 7-3 regions accounting for shorter probes.

4.6.2.2.2 Probing DNA at Exon 6 and 7-3 Region of PC3 cells

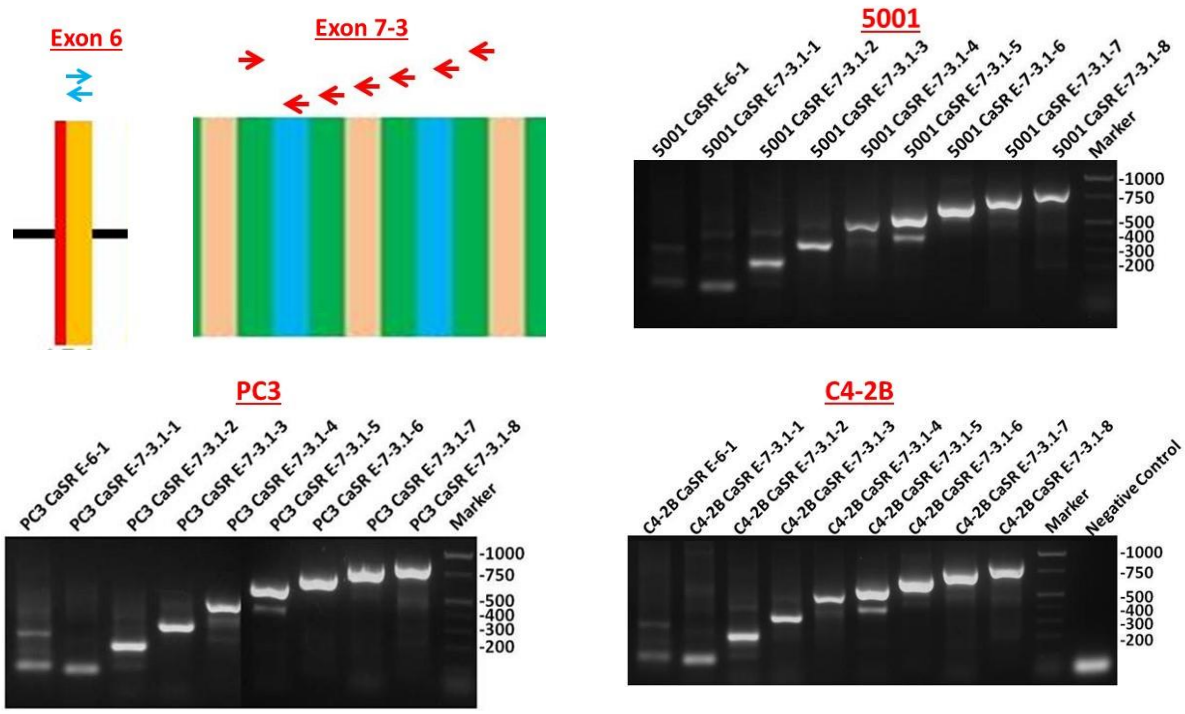

Figure 4.13 Exon 6 and 7-3 do not show any difference between the cell lines at DNA level

For genomic PCR, all exons showed prominent expected bands (**Figure 4.13**). This indicated that PC3-CaSR at the genomic level, was identical to that of positive control or wild type CaSR.

4.6.2.2.3 Probing RNA spanning in all exons in prostate cancer cells

4.6.2.2.4 Amplification between Exon ¾ and 5,6, and 7

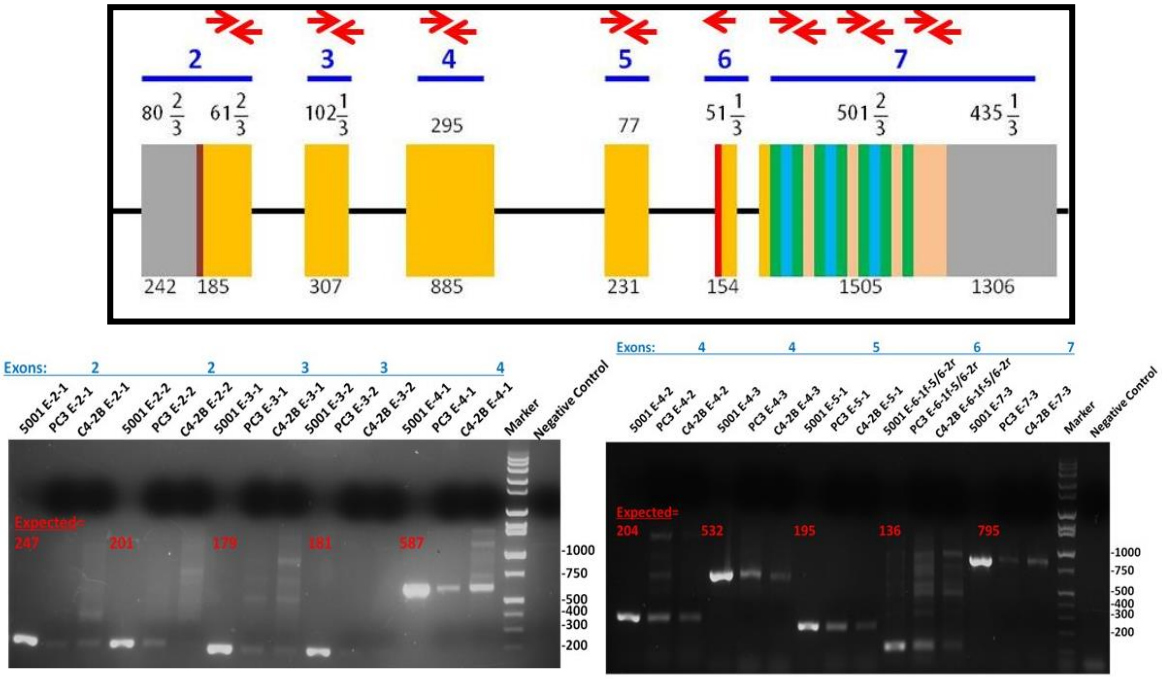

Figure 4.14 Expected bands for each exons suggest presence of CaSR without splicing. 5 ul for 5001 and 25 ul loaded for others. 1,5% gel. cDNA was obtained using 6-7 times more RNA amplicon for PC3 and C4-2B with 1R primer

After many optimization and trials, we were able to obtain each corresponding band at each exon **(Figure 4.14)**. This indicates that a wild type with all the fragments in all coding exons is present in PC3. However, since our gel was not clear, we cannot rule out the possibility of other CaSR variants.

4.6.2.2.5 Sequencing RT-PCR product

We were able to carry out sanger sequencing. The sequence covered are presented below in grey highlights. The sequence covered

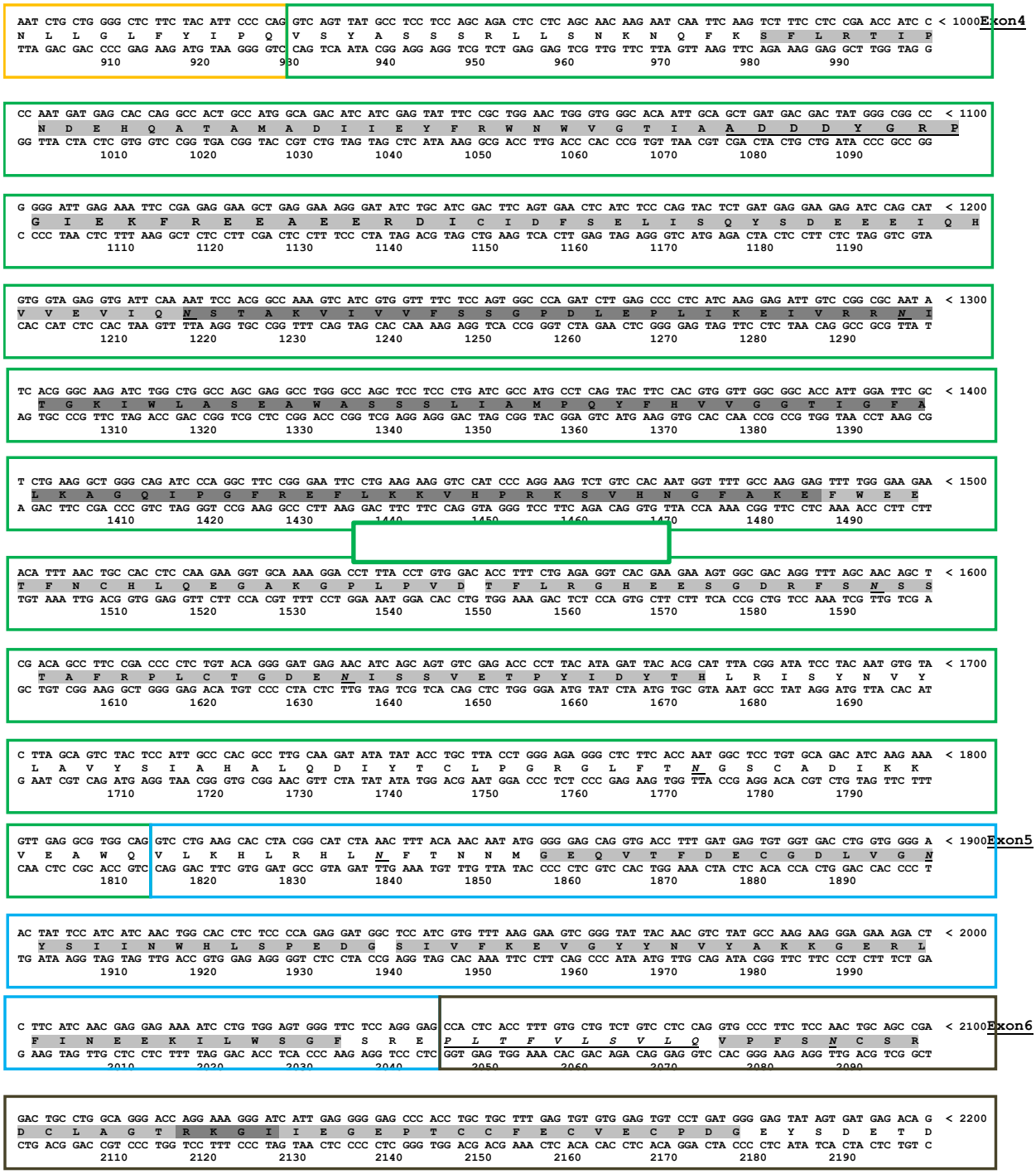

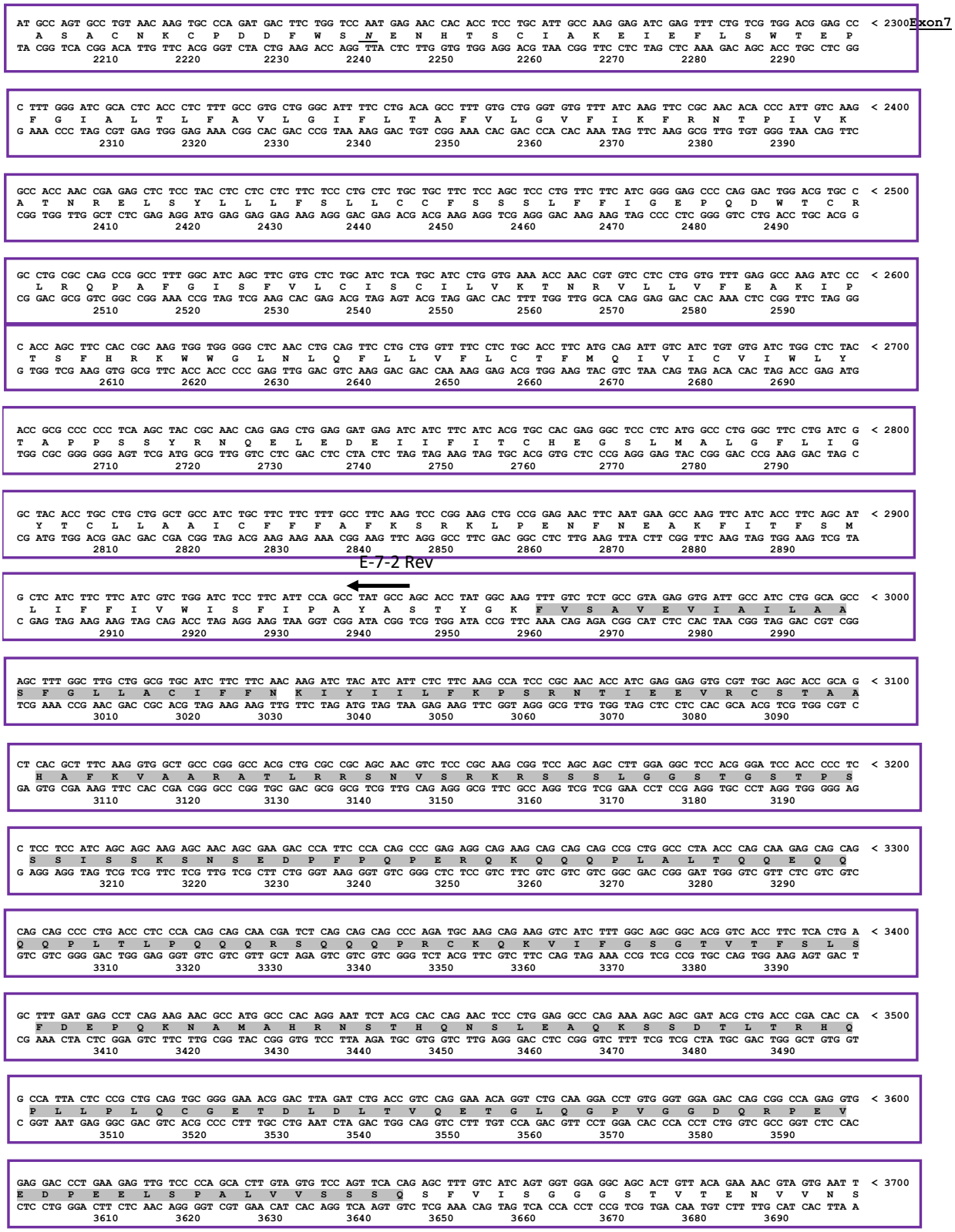

Figure 4.15 PC3: part of exon 4, 5, 6 and 7 were sequence at Biology Core. An insertion was seen at exon 4

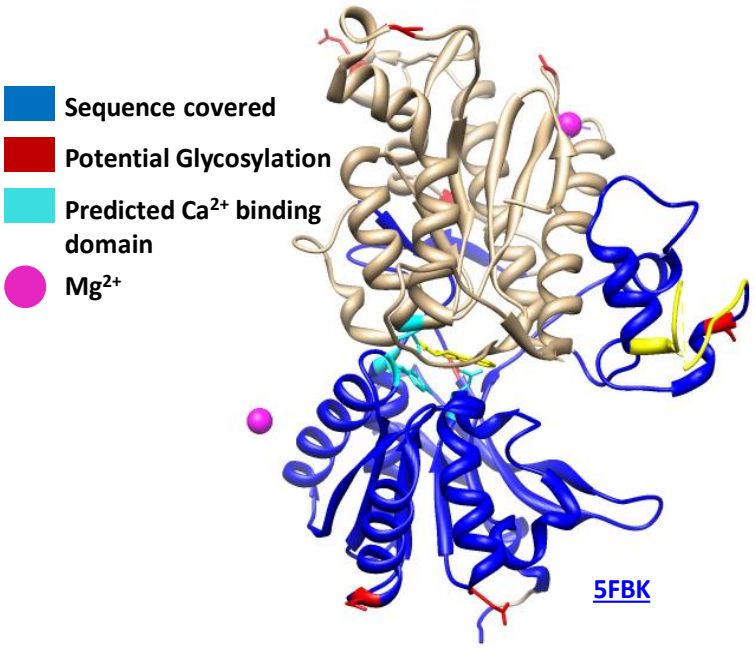

Figure 4.16 PC3 overall sequence covered from PCR products

4.6.2.2.6 RNAseq study

A study done in 2015 with an RNA sample from PC3 cells (OtA8101-2) in collaboration with Otogenetics company could not achieve high confidence mapping for CaSR. 46 million read were obtained for two transcripts. The read pairs mapped CaSR transcript covering exon 3 (121976084 – 121976234). One of the reads extended ends of exon 3 to 2 nucleotides in intron and with last 2 bases mutated from AG to CA. The second one mapped had low confidence.

Table 4.2 RNAseq study on CaSR gene in PC3 in 2015

Variant	Reference Gene ID	Transcript ID	Coverage
#2 (WT)	CASR|NM_000388	NM_000388	0.0268
#1 (Insertion)	CASR|NM_001178065	NM_001178065	0.0266

The second set of study design was carried out in collaboration with Dr. Yi Li from CDC and work was carried out at Otogenetics in 2017 using various cell lines. RNA was extracted using Illustra RNA spin mini from GE healthcare. cDNA was generated using superscript III from thermos scientific and eight times more template from cancer cells. The result shows that even if 5001 had about 5 times lower read the output provided was higher. The combination of cDNA of other pathological cell types had poor output. Overall, the Q30 which describes the library material quality or the sequencing adapter was poor

Table 4.3 RNAseq study on CaSR gene in various cells with endogenous CaSR

cDNA libraries	Initial round of sequencing (03/02/2017)	03/06/2017	Notes
5001 (control)	1.7M reads	1 Gb of sequencing; pr quality	Q30 (poor library material or sequencing adapter)
PC3+ C4-2B	375 K reads	1 Gb of sequencing: 0.34Gb or 3M reads	
HEKn, MDA MB-213, HUVEC, VSMC	7 M reads	1 Gb of sequencing: 2Gb with 17 M reads	

4.6.2.3 Proteomics study in PC3

PC3 cells in 80% confluency were first starved and then treated with 4mM Ca^{2+} or 2 mM EGTA. We employed mass spectrometry to detect total proteins in the cell. Not only could this assay give us the presence of a protein but also provide the relative quantitative amount of abundance.

4.6.2.3.1 Ca^{2+} signaling related proteomics in PC3

A total of 3327 proteins were detected in HEK293 and PC3 combined. In order to understand the implication of proteome in signaling, we examine the relative expression of Ca^{2+} signaling related proteins in PC3 and used HEK293 proteome as a positive control as we see the WT Ca^{2+} signaling in HEK293 cells. With the stringency of ≥ 2 average PSM, we note that Gαq is absent both in PC3 and HEK293 cells (**Table 4.5**Error! Reference source not found.**)** and therefore, implying its detection to be unreliable. CaM and other G-proteins such as Gαi-2, Gαs and Gβ are detected with strong MS/MS count. Additionally, CaSR was not detected in PC3 with PSM of 0, which supports the retarded Ca^{2+} sensing and low transcript generated in RT-PCR and RNAseq. On the contrary, 10^9 LFQ intensity was observed for HEK293 cells transfected with FLAG-CaSR with an average PSM of 22 (**Table 4.5)**. Further, SERCA (ATP2A2) is present with strong average PSM of 20 and LFQ intensity of 10^9. However, IP_3R and related phosphodiesterase and phosphatases were detected at low PSM of < 1 in both PC3 and HEK293 cells (**Table 4.5**).

4.6.2.3.2 Proteomics related to prognostic markers

Because we were interested in prognosis markers, we compared the known markers in prostate cancer from the human protein atlas. This database integrates human proteomic results from various omics technologies (mass-spectrometry, antibody-based imaging, and transcriptomics). According to this database, there are 25 favorable prognostic markers for PCa. We found two proteins Epoxide hydrolase 1 (EPHX1) and Catebhol O-methyltransferase (COMT) with good abundance with the stringency of ≥ 4 average PSM and with average LFQ intensity in the range of 10^9 (**Table 4.4**). These markers were decreased with the Ca^{2+} treatment in PC3 by < 0.9-fold as compared to one treated with EGTA. However, these were ≥ 3-fold increased as compared to HEK293 cells. Apart from the two, we also detected isoforms of other good

prognostic markers, including the ubiquitin (RNF114), Ubiquitin-conjugating enzyme (UBE2D2/3) and SLCs with good stringencies. PC3 as compared to Ca^{2+} and EGTA and with HEK293 cells, these markers did not have a specific dependence on Ca^{2+}.

4.6.2.3.3 Role of Ca^{2+} in proteomics related to metastasis

Bone is a well-established site of metastasis for prostate with a high Ca^{2+} environment of 10-40 mM. Previous work has shown that higher extracellular Ca^{2+} of 2.5 mM plays a role in facilitating prostate cancer metastasis and localization in bone [91]. Our work in the lab by Dr. Jie Feng has also shown that CaSR may act to protect and facilitate localization of these tumors in high Ca^{2+} environment through reducing apoptosis and invasion of the cancer cells and allowing mesenchymal to epithelial transition (MET) pathway. We explored metastasis-related biomarkers in PC3 proteomics. Ironically, cell-adhesion proteins such as E-cadherin and integrin as well as biomarkers associated with MET, including, e-cadherin, catenin, actin, and vimentin were not upregulated in the Ca^{2+} treated PC3 cells. γ-catenin was not detected at all (**Table 4.5**). The

Table 4.4 Heat map of expression of metastasis related biomarkers

			Average Intensity HEK293		Average MS/MS count HEK293		Average Intensity PC3		Average MS/MS count PC3		Log_2(intensity)		
Majority protein IDs	Protein names	Gene names	Ca^{2+}	EGTA	Ca^{2+}	EGTA	Ca^{2+}	EGTA	Ca^{2+}	EGTA	PC3-(Ca^{2+}/EGTA)	(PC3/HEK293) Ca^{2+}	(PC3/HEK293) - EGTA
P35221	Catenin alpha-1	CTNNA1	7.23E+08	7.31E+08	5	7	0.00E+00	4.41E+06	0	0	2.3276	-5.0297	-7.3729
P23229-7	Integrin alpha-6;Integrin alpha-6 heavy chain; light chain;Processed integrin alpha-6	ITGA6	0.00E+00	0.00E+00	0	0	0.00E+00	1.76E+07	1	0.5	1.2066	2.0601	1.1365
O96019	Actin-like protein 6A	ACTL6A	1.28E+09	1.11E+09	6	5.5	1.10E+09	1.00E+09	7	3.5	0.1345	-0.2226	-0.1476
P16144-4	Integrin beta-4	ITGB4	0.00E+00	1.08E+07	0	0	3.43E+09	3.33E+09	20.5	15	0.0467	8.2499	8.2726
B4DGU4	Catenin beta-1	CTNNB1	3.32E+08	2.37E+08	1.5	1.5	9.79E+08	9.51E+08	7	8	0.0414	1.5614	2.0024
P05556	Integrin beta-1	ITGB1	1.14E+08	2.80E+08	1	0.5	3.10E+09	3.13E+09	14.5	12	-0.0127	4.7663	3.4845
P26006	Integrin alpha-3; alpha-3 heavy chain; alpha-3 light chain	ITGA3	0.00E+00	0.00E+00	0	0	2.27E+08	2.30E+08	1.5	1.5	-0.0243	5.1328	5.1992
P17301	Integrin alpha-2	ITGA2	0.00E+00	5.24E+07	0	0	2.26E+09	2.43E+09	15	12.5	-0.1047	7.1362	5.535
P68133	Actin, alpha skeletal muscle	ACTA1;ACTC1;ACTG2;ACTA2	1.36E+10	1.39E+10	6	6	1.78E+10	1.94E+10	7.5	7	-0.1175	0.3973	0.4787
A0A087WXI5	Cadherin-1;E-Cad/CTF1;E-Cad/CTF2;E-Cad/CTF3	CDH1	4.67E+07	0.00E+00	0	0	3.41E+08	3.77E+08	1	2	-0.1436	2.869	6.1747
P63261	Actin, cytoplasmic 2;Actin, cytoplasmic 2, N-terminally processed	ACTG1	1.23E+11	1.25E+11	111.5	119.5	1.73E+11	1.94E+11	132	118	-0.1655	0.4927	0.6256
A0A087WUB9	Beta-catenin-like protein 1	CTNNBL1	4.07E+08	4.27E+08	1.5	3	5.96E+08	6.85E+08	4.5	5	-0.2011	0.551	0.6802
P08670	Vimentin	VIM	2.26E+10	2.29E+10	47.5	49.5	1.28E+09	1.57E+09	6.5	9.5	-0.2875	-4.1421	-3.8733
C9JZR2	Catenin delta-1	CTNND1	3.28E+08	2.74E+08	1.5	1.5	1.49E+09	1.88E+09	10.5	13	-0.3332	2.1847	2.774
P60709	Actin, cytoplasmic 1;Actin, cytoplasmic 1, N-terminally processed	ACTB	2.99E+09	2.87E+09	4	4	0.00E+00	1.23E+09	4.5	4	-7.1915	-8.4736	-1.2268

proteins with higher LFQ intensity such as cantenin α-1 and integrin α-6 had unreliable PSM (**Table 4.4, Table 4.5**Error! Reference source not found.).

Next, we analyzed the proteins present in PC3 and compared between treatment groups with Ca^{2+} and EGTA. Secondly, we compared the global proteomics in PC3 and compared it to HEK293 cells in order to understand the differences that might cause the signaling differences.

Table 4.5 Heat map for selected protein detected in PC3 and HEK293 cells through MS.

			Average MS/MS count HEK293		Average Intensity HEK293		Average MS/MS count PC3		Average Intensity PC3		Log_2(intensity)		
Majority protein IDs	Protein names	Gene names	Ca^{2+}	EGTA	Ca^{2+}	EGTA	Ca^{2+}	EGTA	Ca^{2+}	EGTA	PC3-(Ca^{2+}/EGTA)	(PC3/HEK293) Ca^{2+}	(PC3/HEK293) EGTA
P21333-2	Filamin-A	FLNA	79.5	85.5	1.71E+10	1.65E+10	100	103	2.65E+10	2.93E+10	-0.147	0.6285	0.8277
O75369-2	Filamin-B	FLNB	17	13	2.77E+09	2.59E+09	91.5	101.5	2.10E+10	2.26E+10	-0.1108	2.9198	3.1273
P16615	Sarcoplasmic/endoplasmic reticulum calcium ATPase 2	ATP2A2	14	13	2.55E+09	2.44E+09	23	21	5.25E+09	5.18E+09	0.0191	1.0391	1.0863
P63244	Guanine nucleotide-binding protein subunit beta-2-like 1; beta-2-like 1, N-terminally processed	GNB2L1	29.5	26.5	1.22E+10	1.05E+10	20.5	21	1.24E+10	1.32E+10	-0.0873	0.0293	0.3258
H0Y7A7	Calmodulin	CALM2;CALM1	12	14	7.62E+09	7.88E+09	10.5	12.5	6.33E+09	6.70E+09	-0.0813	-0.267	-0.2348
P62873	Guanine nucleotide-binding protein G(I)/G(S)/G(T) subunit beta-1	GNB1	5	5	2.03E+09	1.92E+09	10	9.5	2.41E+09	2.55E+09	-0.0822	0.2501	0.4138
P04899	Guanine nucleotide-binding protein G(i) subunit alpha-2	GNAI2	9.5	7.5	9.01E+08	8.13E+08	10	12	1.68E+09	2.02E+09	-0.2697	0.8973	1.3154
P21964-2	Catechol O-methyltransferase	COMT	1	1	3.63E+08	2.84E+08	6	6.5	1073500000	1183500000	-0.1407	1.5648	2.0596
P07099	Epoxide hydrolase 1	EPHX1	1.5	0.5	2.19E+08	1.72E+08	6	5.5	1034700000	1046740000	-0.0167	2.2419	2.6041
P62879	Guanine nucleotide-binding protein G(I)/G(S)/G(T) subunit beta-2; subunit beta-4	GNB2;GNB4	3	2.5	6.59E+08	6.44E+08	3.5	3.5	6.17E+08	6.77E+08	-0.1323	-0.0937	0.0721
P63092-3	Guanine nucleotide-binding protein G(s) subunit alpha isoforms short;XLas	GNAS	1	0	1.44E+08	6.70E+07	3	2.5	2.47E+08	2.74E+08	-0.1517	0.7809	2.0328
Q14315-2	Filamin-C	FLNC	0	0	0.00E+00	0.00E+00	1.5	2.5	9.62E+07	1.01E+08	-0.0645	2.0331	3.9922
P63218	Guanine nucleotide-binding protein G(I)/G(S)/G(O) subunit gamma-5	GNG5	1	1.5	2.92E+08	3.76E+08	1	1	0.00E+00	1.37E+08	-2.9641	-4.0619	-1.4631
Q9BY32	Inosine triphosphate pyrophosphatase	ITPA	2	2	1.77E+08	1.69E+08	1	1.5	0.00E+00	1.11E+08	-3.8429	-4.5235	-0.6091
Q14573	Inositol 1,4,5-trisphosphate receptor type 3	ITPR3	0.5	1.5	0.00E+00	0.00E+00	0.5	0.5	0.00E+00	5.33E+06	1.2904	-0.317	-0.9872
Q01970-2	1-phosphatidylinositol 4,5-bisphosphate phosphodiesterase beta-3	PLCB3	0	0	0.00E+00	0.00E+00	0.5	1	0.00E+00	3.15E+07	0.1916	2.5717	2.0951
P08754	Guanine nucleotide-binding protein G(k) subunit alpha	GNAI3	0	0	1.93E+08	1.92E+08	0.5	1	1.25E+08	1.33E+08	-0.0891	-0.6271	-0.5249
P29992	Guanine nucleotide-binding protein subunit alpha-11	GNA11	0.5	1	2.56E+08	2.27E+08	0	0	2.90E+07	0.00E+00	3.1503	-3.1448	-6.1233
P63096	Guanine nucleotide-binding protein G(i) subunit alpha-1	GNAI1	0	0.5	6.47E+07	6.75E+07	0	0	0.00E+00	2.17E+07	0.5147	-1.0628	-1.639
Q14571	Inositol 1,4,5-trisphosphate receptor type 2	ITPR2	0.5	0.5	0.00E+00	3.07E+07	0	0	0.00E+00	3.22E+07	-0.1045	1.1117	0.0688
Q9UBI6	Guanine nucleotide-binding protein G(I)/G(S)/G(O) subunit gamma-12	GNG12	0	0.5	9.56E+07	8.65E+07	0	0	0.00E+00	9.18E+07	-2.3866	-2.4461	0.0863
E7ENE0	Extracellular calcium-sensing receptor	CASR	0	0	2.60E+06	5.04E+06	0	0	1.34E+08	0	3.6869	5.69	1.0497
E7ENE0	Extracellular calcium-sensing receptor	CASR*	19	24	5.395E+09	9431450000							
* HEK+CaSR													

4.6.2.3.4 Global Proteomics of PC3 and effect of $[Ca^{2+}]_o$

We observed changes in few proteins due to the effect of presence of Ca^{2+}. For this, we employed successive stringencies to ensure robust upregulation, reproducibility, and detection**:** (i). at least 2 folds change of the average between the compared groups, (ii). PSM of equal or greater

to 2 in both the duplicates of the up-regulated group, (iii) at least 1 unique peptides of the up-regulated group. We determined that 39 proteins in PC3 had a differential expression that was dependent on Ca^{2+} (**Figure 4.17**). 22 were at least two-fold up-regulated in expression in the presence of Ca^{2+} and 17 were downregulated in the presence of Ca^{2+}. Gene ontology study was tried on these set of proteins, but we could not generate any group attributed to a particular biological function. Some cell death associated proteins such as programmed cell death protein 6 (PDCD6), BH3 interacting domain death agonist (BID), mitogen-activated protein kinase1 (MAPK1), mitochondrial import inner membrane transmembrane (TIMM13), E3 ubiquitinating-protein ligase UBR5 were upregulated. Notably, exosome complex component MTR3 (EXOSC6), coiled-coil domain-containing protein 86 (CCDC86), and histidine-tRNA ligase (HARS) were upregulated by > 8 folds. Alongside, deubiquitinating protein (VCPIP1), BAG family chaperone regulator (BAG3), were down-regulated. Notably, microsomal glutathione S-transferase 1 (MGST1) was down-regulated by log2 intensity ratio of 6.65.

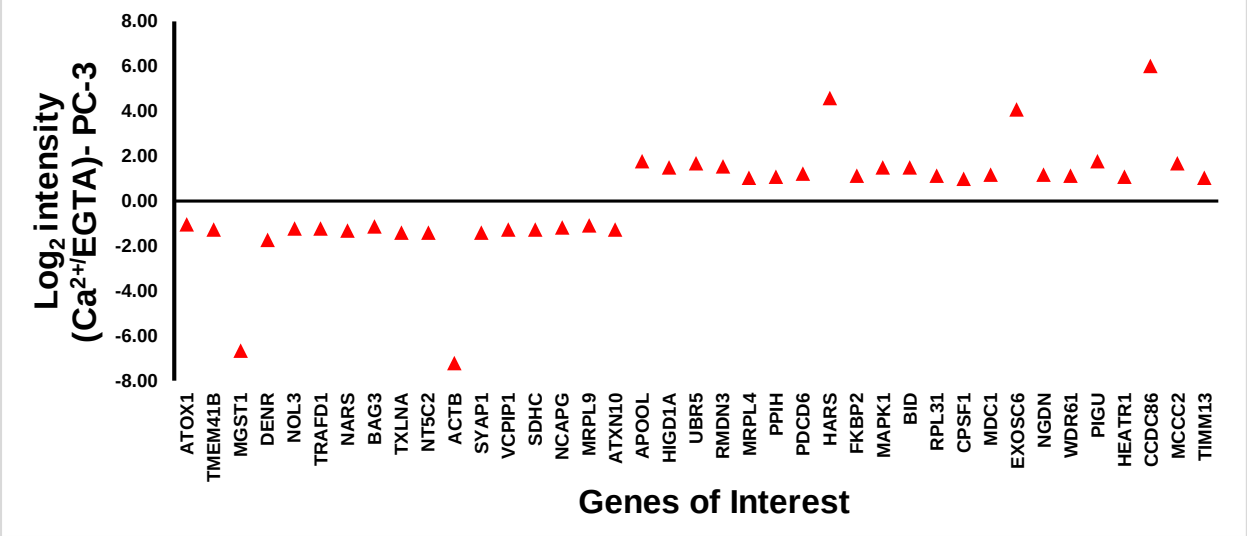

Figure 4.17 Differential proteome in PC3 compared between Ca^{2+} and EGTA treatments PC3 were treated with Ca^{2+}, and after tandem MS on cell lysates, Ca^{2+} and EGTA groups were compared

4.6.2.3.5 Upregulation of proteomes in PC3 as compared to HEK293 in Ca^{2+}

464 proteins were observed as up-regulated by at least two-fold in PC3 as compared to HEK293 cells in Ca^{2+} treated conditions (**Figure 4.18**). 396 were commonly up-regulated in PC3 between Ca and EGTA conditions. These processes must be Ca^{2+} independent and significant in PC3 for its distinctive cellular processes. 25 most highly expressed proteins contain the core histones, enolase, GAPDH, tubulin and heat shock proteins as well as proteins of the ribosome (2012 Geiger). 25 proteins with the lowest MS signals included several novel and uncharacterized proteins as well as isoforms of well-known proteins. This abundance estimation is a rough estimation of the actual expression levels. Also, the proteome could be incomplete, as we can assume that proteins with low expression levels, could not be identified.

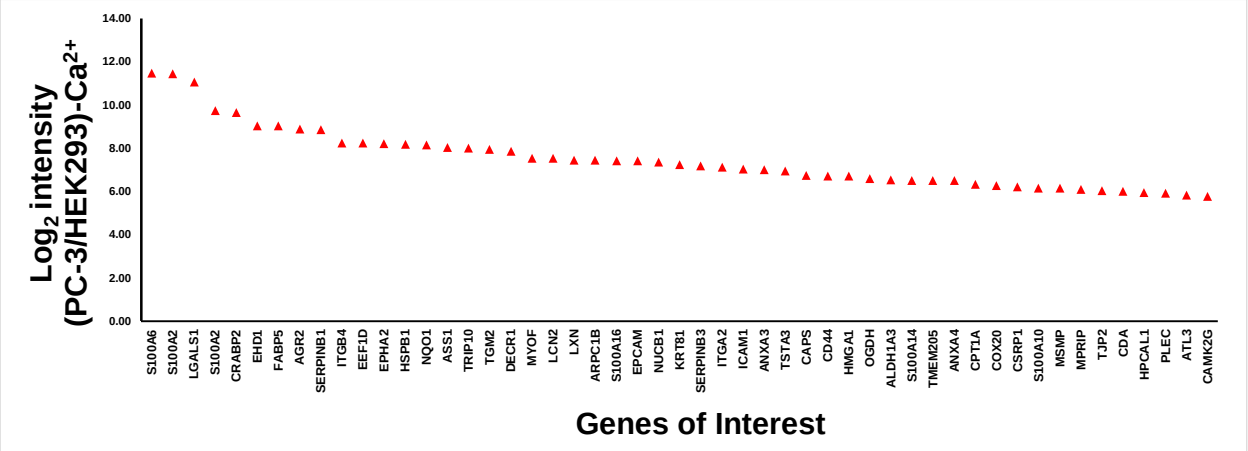

Figure 4.18 Top 50 up-regulated proteome in PC3 as compared to HEK293 cells in Ca^{2+}

PC3 and HEK293 cells transiently transfected with CaSR were treated with Ca^{2+}, and after tandem MS on cell lysates, the top 50 proteins upregulated by various degrees in Ca^{2+} are plotted.

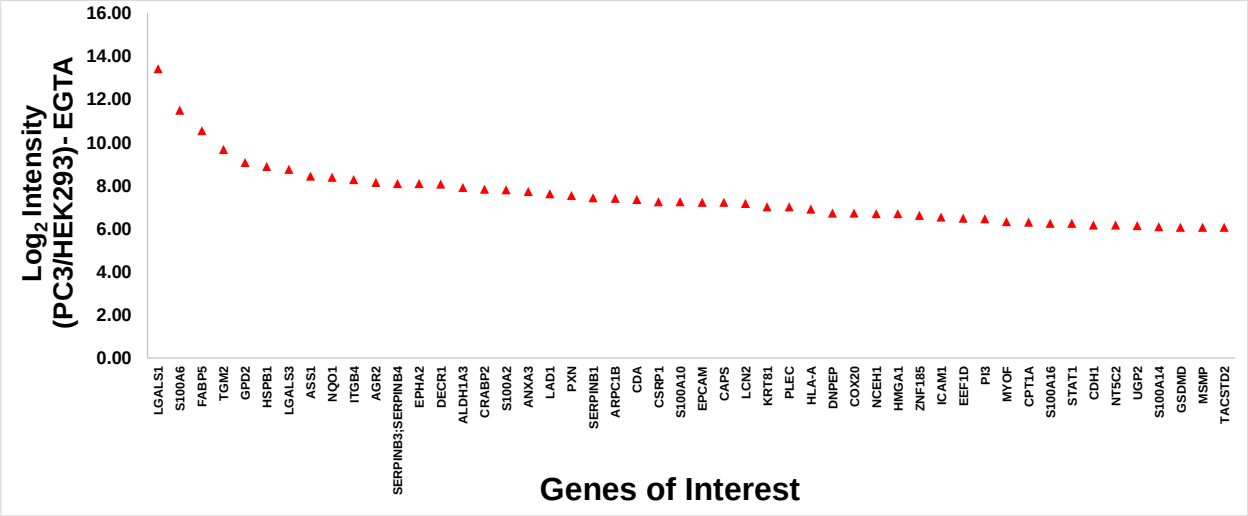

Figure 4.19 Top 50 up-regulated proteome in PC3 as compared to HEK293 cells in EGTA

4.6.2.4 Functional analysis using Cytoscape and ClueGo

Metabolic pathways such as fatty acid metabolism, amino acid metabolism and glutathione metabolism were highly variable (2012 Geiger), indicating differential energy production and biosynthetic pathways. Additionally, large difference existed in the actin cytoskeleton, which indicates their difference in morphology. Amongst the more constant processes involved basal transcription machinery and protein translation. These are fundamental and nonredundant pathways.

The up-regulated proteins were input into Cytoscape and plugin ClueGo was used to derive the functional annotations associated with them. We show pathways associated with TCA cycle, trans-Golgi network vesicle budding, and triglyceride synthesis were upregulated in Ca^{2+} in PC3 as compared to HEK293 cells. Instead of these pathways, the up-regulated pathways in EGTA in PC3 as compared to HEK293 cells were arginine/proline metabolism and amino sugar/nucleotide sugar metabolism (**Figure 4.20).**

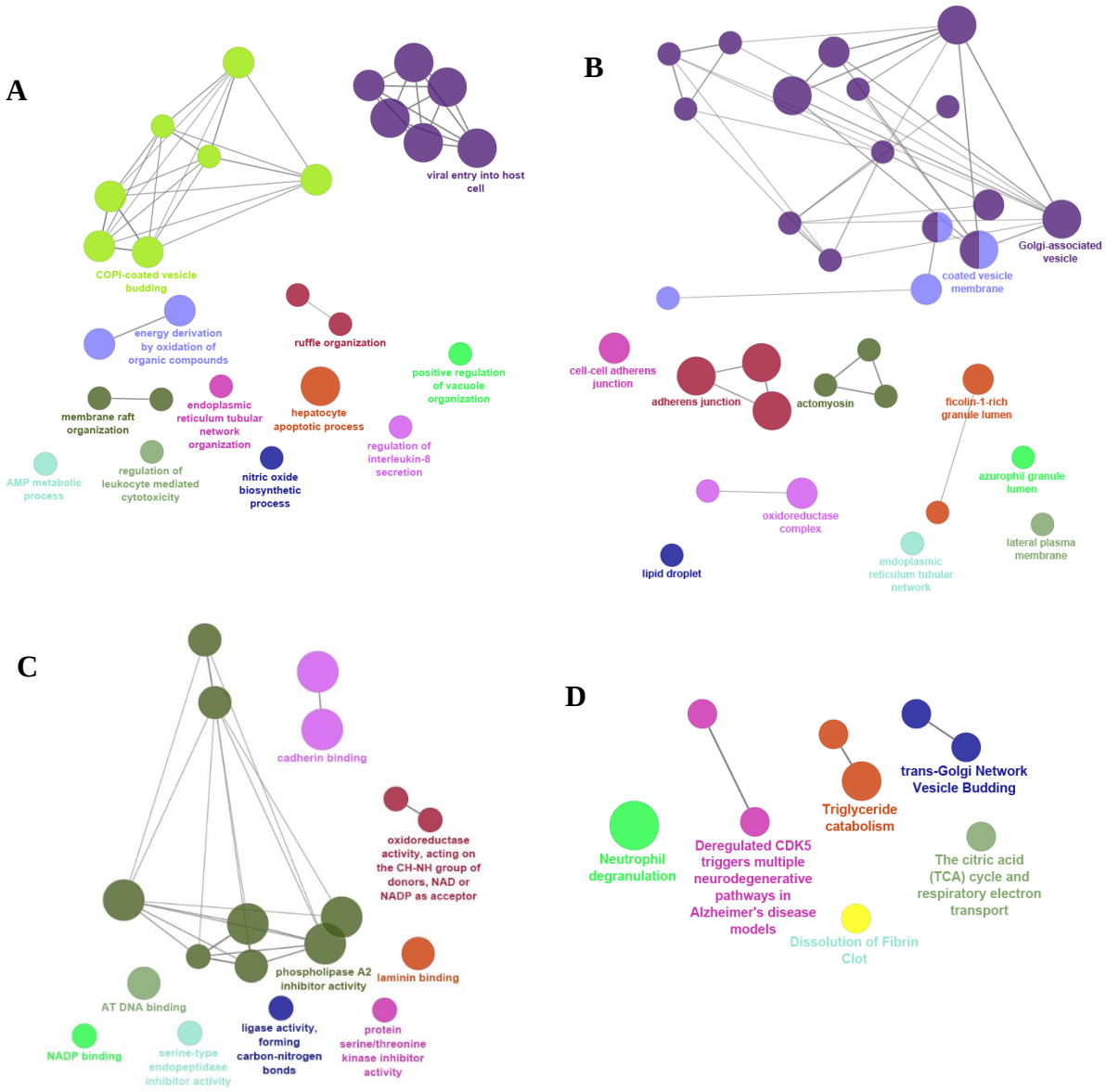

Figure 4.20 4-fold up-regulated proteome in PC3 as compared to HEK293 cells in 4mM Ca^{2+}.

The upregulated annotations are shown above as A. Biological Process, B. Cellular Compartment, C. Molecular Function and D. Pathway

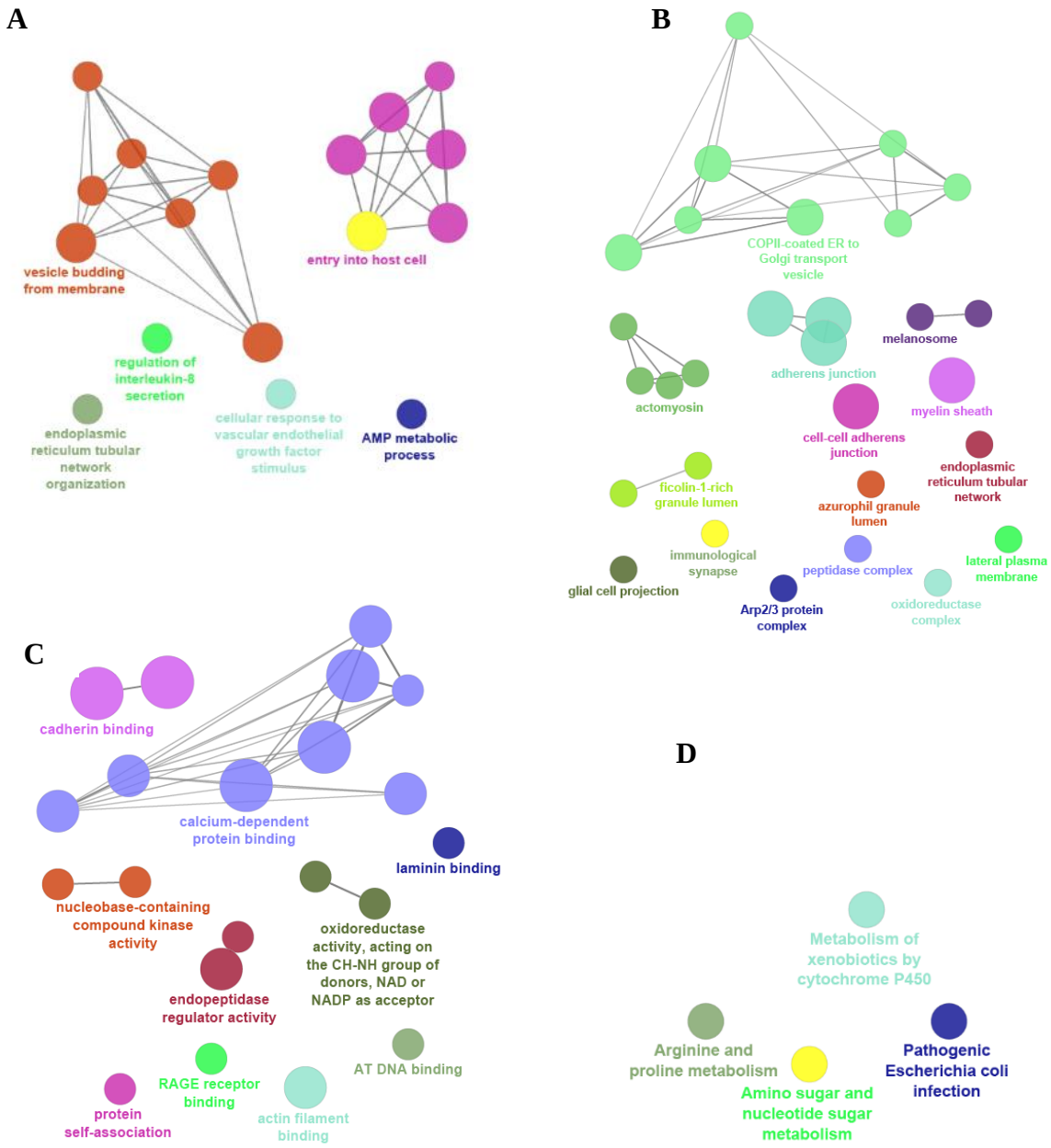

Figure 4.21 4-fold up-regulated proteome in PC3 as compared to HEK293 cells in EGTA. The upregulated annotations are shown above as A. Biological Process, B. Cellular Compartment, C. Molecular Function and D. Pathway

.

4.6.2.5 In-Vivo study of the role of CaSR and extracellular Ca^{2+} in bony metastasis

It has been previously shown metastasis localization is promoted by higher extracellular Ca^{2+} through CaSR mediated signaling [91, 92]. CaSR may play a role in PCa in bony metastasis. This was shown by Dr. Jie Feng that CaSR knockdown in PC-3 cells resulted in a decrease in tumor cell viability at higher Ca^{2+} environment and an increase in apoptosis and invasion by greater than 50-folds. Additionally, significant increased levels of cell-adhesion proteins, e-cadherin and integrin, and decreased levels of matrix metalloproteinases (MMP-2 and MMP-9) in PC-3 with CaSR. Furthermore, CaSR knockdown caused phenotypic changes associated with epithelial-mesenchymal transition, i.e., decreasing E-cadherin and γ-catenin and increasing smooth muscle actin and vimentin.

4.6.2.5.1 Generation of a PC3 luc CaSR knockdown cells

Using lentiviral infection and shRNA technology, CaSR was knocked down in PC3 luc cells. pLKO.1-CaSR was co-transfected into HEK293T cells with psPAX2 and pMD2 plasmids.

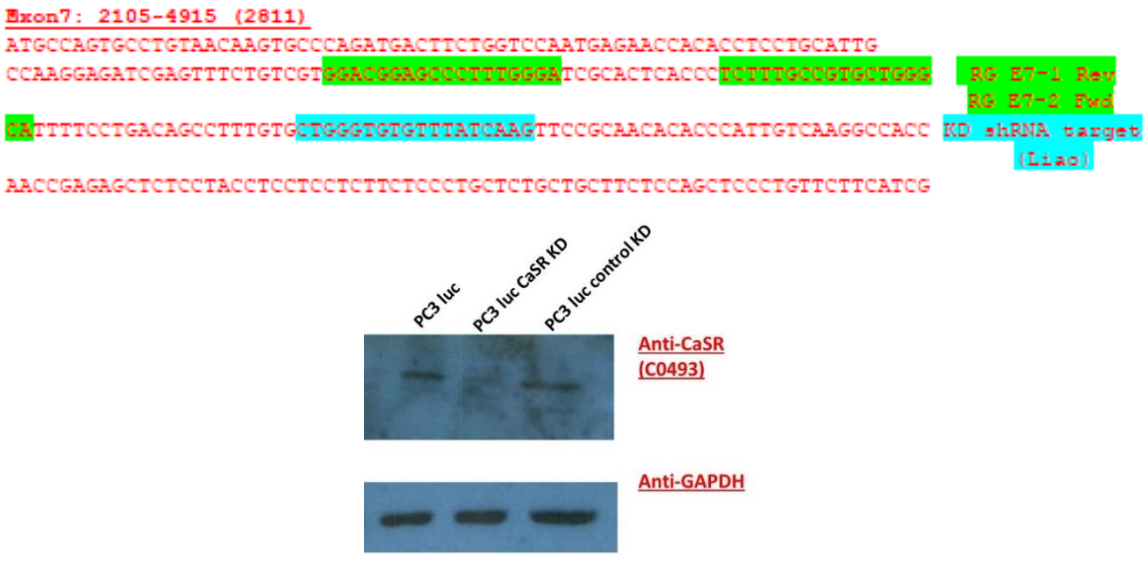

Figure 4.22 Generation and validation of CaSR KD in PC3 luc cells

The target gene was as described by Liao et al CTGGGTGTGTTTATCAAG in the seventh exon (**Figure 4.2, Figure 4.22**).

4.6.2.5.2 Effect of Ca^{2+} on the metastatic biomarkers is complex

In order to understand the role of extracellular Ca^{2+} on bone metastasis, we studied the effect on biomarkers such as E-cadherin, γ-catenin, vimentin, and N-cadherin in PC3 luc cells. 5 mM Ca^{2+}

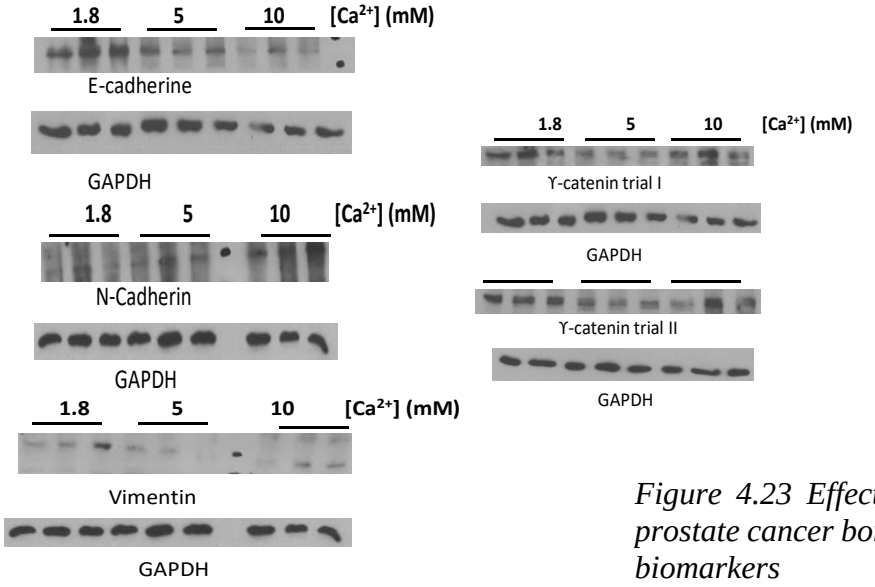

Figure 4.23 Effect of Ca^{2+} on prostate cancer bone metastasis biomarkers

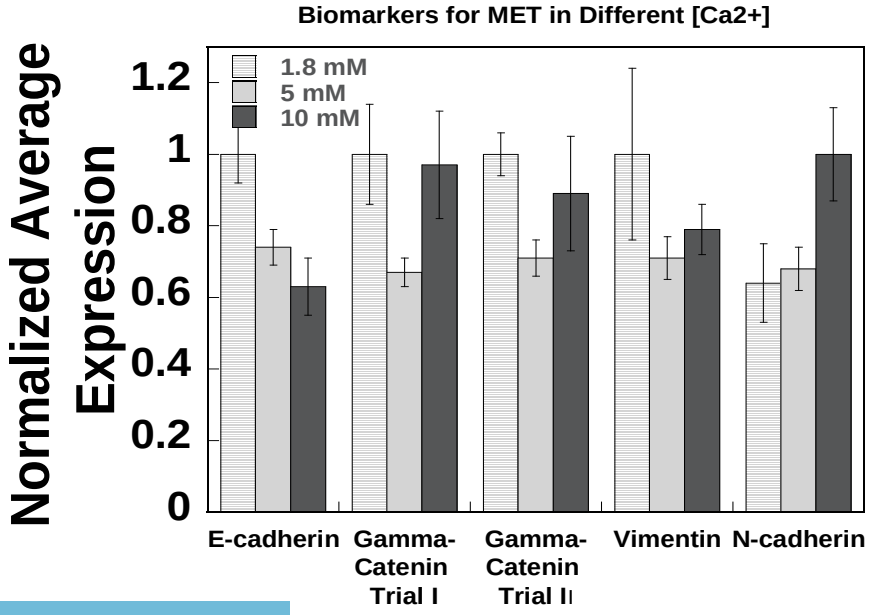

decreased the expression of E-cadherin, γ-catenin, and vimentin, however, the N-cadherin was not affected **(Figure 4.23)**. 10 mM Ca^{2+} had a different effect where it further decreases the expression in E-cadherin and vimentin whereas it increases the expression of N-cadherin and doesn't have any effect on γ-catenin. This trend doesn't support MET where E-cadherin and γ-catenin should increase, and N-cadherin and vimentin should decrease. It offers a dynamic role of Ca^{2+} on various biomarkers suggesting more complex role. This study needs to be compared with PC3 luc with CaSR KD and control KD to make more sense.

4.6.2.5.3 In-vivo study of the role of CaSR and Ca^{2+} in bony metastasis

First, the PC3 cells were measured for the luciferase signal by Dr. Kanza from Dr. Daqing Wu's Lab in Augusta University (**Table 4.6**). The firefly reading is the real number since PC3-luc uses a firefly luciferase vector. The Renilla reading is the background, which is extremely low, given the 10-second collecting time of signals. There was a ~30-fold difference between the control and KD cells, which may be due to many reasons, including the amounts of cell lysates used in the assay and different expression levels of KD vectors.

Table 4.6 Luciferase reading on PC3 luc cells

	RLU Firefly	RLU Renilla
PC3-luc control KD	325679	766
PC3-luc CaSR KD	10195	723

The in-vivo work showed a significant decrease in tumor growth when injected in mouse tibia with PC-3 with CaSR knockdown as compared to the control knockdown. Our results strongly support that CaSR is involved in promoting PC-3 colonization in bones with high calcium by preventing cell apoptosis of cancer cells, inhibiting invasion, and promoting mesenchymal-epithelial transition. It suggests that CaSR may serve as a potential therapeutic biomarker for PCa metastasis.

Table 4.7 The experimental log of weights for mouse in-vivo for injection of PC3 cells

	Mouse in experiment								
PC3 Ctrl luc (PBS)									
	2	22.6	20.3	20.26	23.2	25	25.8	24.8	24.3
	3	23.8	21	22.3	24.5	25.5	26	25.3	24.5
	4	24	22.6	21.3	25	26	26.7	26.5	26.2
PC3 Ctrl luc (Zoledronic acid 0.2mg/kg)									
	1	22.2	23.3	24.5	26.4	27.8	27.9	27.3	26.3
	2	22.6	24.2	24.9	27.2	26.2	25.2	24.5	22.2
	3	23	22.6	21.3	23.7	24.9	26.2	26.9	25.4
	4	22.5	22.7	20.9	23	24.9	26	26.7	28
	5	24.4	24.5	23.9	26.5	26.9	27.5	27.3	25.5
PC3 CaSR KD (PBS)									
	1	22	19.4	18.7	21	20.6	24.3	25.8	25.4
	2	23.2	20.7	19	21.9	21.2	23.6	25	24
	3	23	20.7	20	22.6	21.9	24.8	25	24.5
	4	22.2	20.5	20	22.5	22.6	25.4	25.4	24.2
	5	23.7	22	21.4	23.8	22.6	24.6	25.7	24.9
PC3 CaSR KD (Zoledronic acid 0.2 mg/kg)									
	1	25	23	23.2	24.2	25.4	28.4	26.9	26.5
	2	21.18	19.8	19.6	21.3	22	24.5	24.5	24.2
	3	25.8	23.8	24.8	26.5	26.2	27.6	27.2	27
	4	23.6	21.6	19.5	22.1	21.9	23.8	23.6	23.3
	5	24.5	22.6	21.8	24.4	24.5	27.7	23.6	26.2

The following experiment was conducted in collaboration with Dr. Daqing Wu in Augusta University. The postdoctoral fellow Kanza Manmouni conducted the experiment. Tibia of the nude male mouse which were 4 weeks old was injected via subcutaneous route twice a week with cells, either PC3 luc control or PC3 CaSR KD starting on October 3rd 2017 **(Table 4.7**). Subcutaneous injection of PBS as a negative control or bisphosphonate (zoledronic acid) at 0.2 mg/kg was carried out twice per week for 4 weeks. By using image J, we can say that the tumor growth is substantially

larger in both PC3 control and CaSR KD (**Figure 4.24**). This supports the idea that Ca^{2+} is essential for tumor survival and growth in bones.

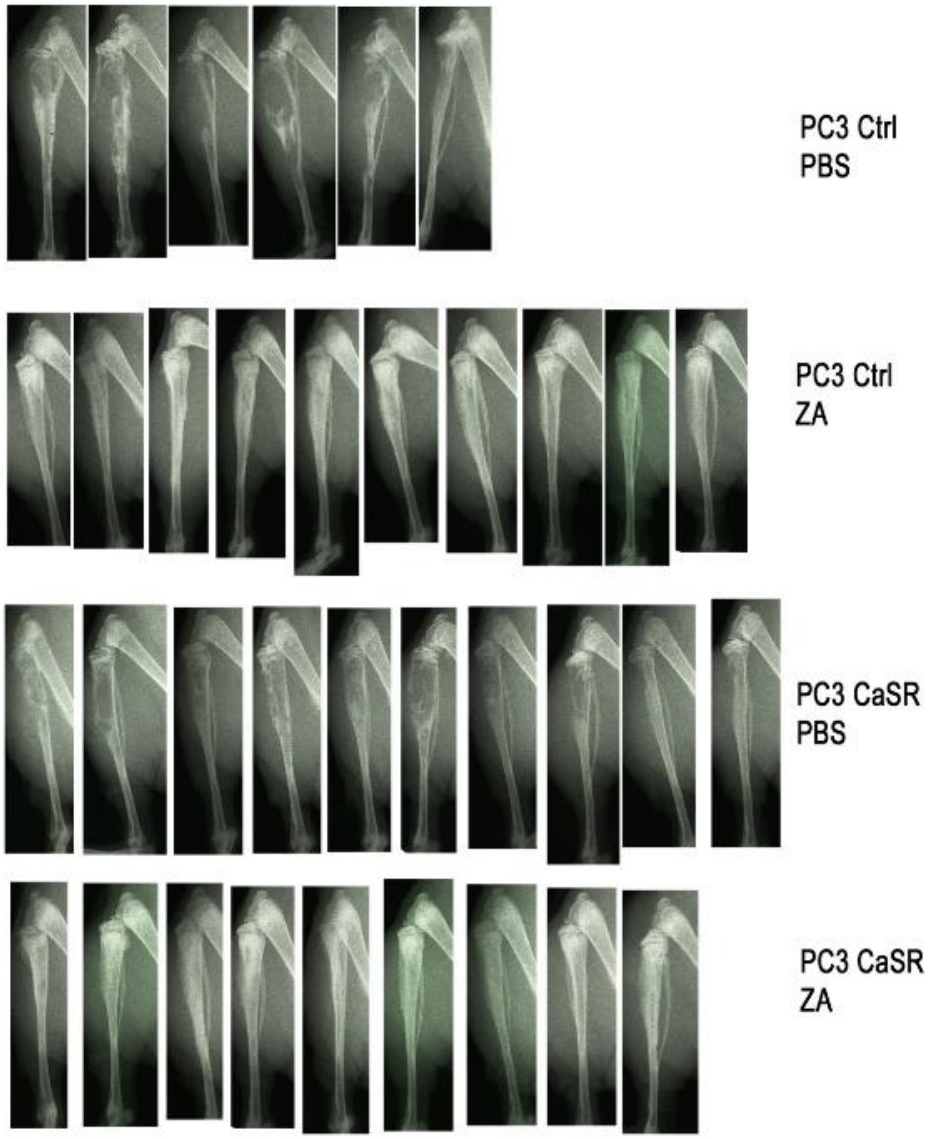

Figure 4.24 In vivo study to study the proliferation of PC3 cells when injected in tibia or a mouse

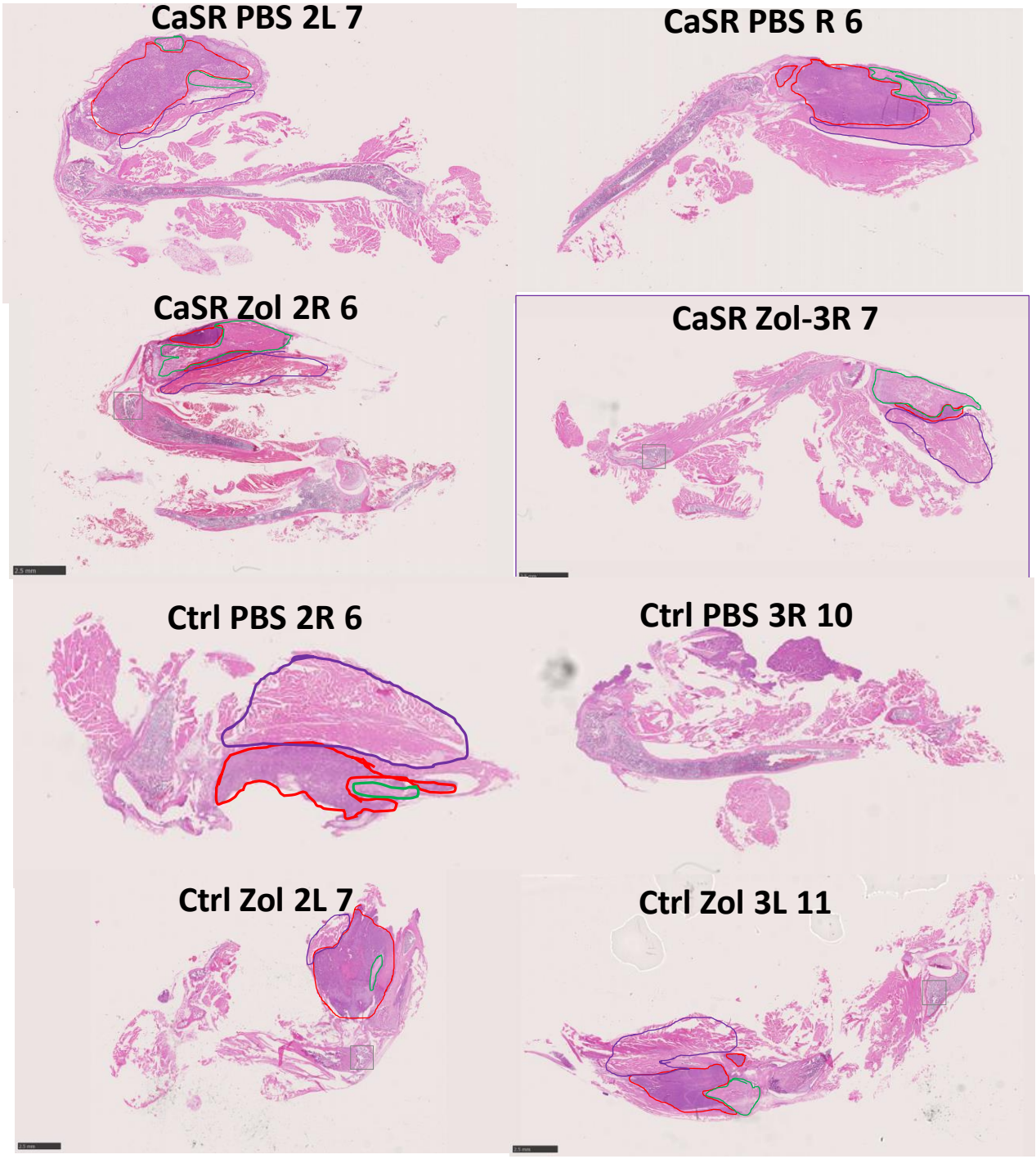

Figure 4.25 H&E staining of the bone tissue from the mouse to understand the role of CaSR in PC3 proliferation in bone

Representative two slices from each conditions are shown. Third slice did not have proper demarcated tumor, therefore, were excluded. For CaSR Zol, only 1 slice was taken. The area represented under the red curve is tumor in darker red. The green represent bone in tibia and purple represents muscle. A. PC3 luc cells with CaSR KD in PBS medium. B. PC3 luc cells with CaSR KD in zoledronic acid medium. C. PC3 luc cells with control KD in PBS medium and D. PC3 luc cells with control KD in zoledronic acid medium

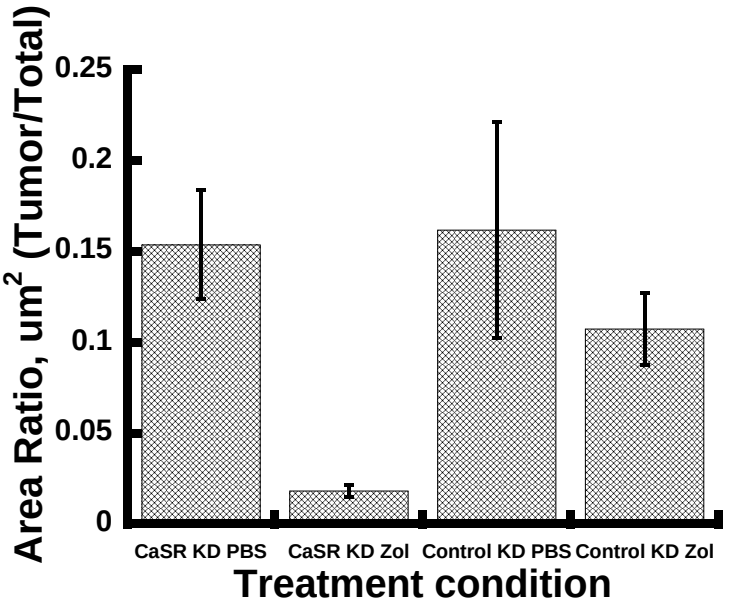

Figure 4.26 Measurement of area of tumor growth calculated from H&E staining

Next, we can see that the tumor growth is almost completely subsided with the use of bisphosphonate (**Figure 4.24, Figure 4.25)**. Bisphosphonates are nonhydrolyzable pyrophosphate analogs. They are known to cause inhibition of osteoclast generation, maturation, and osteoclastic bone resorption activity [306-308]. Zoledronic acid is a new generation bisphosphonate with imidazole ring and high potency[309]. Our theory is that the increase in extracellular Ca^{2+} promotes the bone metastasis in PC-3 cells expressing CaSR**.** It can bind to hydroxyapatite and therefore might decrease the Ca^{2+} available to the cancer tissues. Therefore, bisphosphonates have multiple mechanisms in bone and may limit the interactions between Ca^{2+} and tumor cells. This approach partially supports the hypothesis. The previous study by Corey has shown that zoledronic acid may inhibit prostate cancer cell proliferation in vitro, but they were unable to show this in-vivo [310]. H&E staining and TRAP staining on the bone tissue were conducted to have a better quantitative analysis. The bones were stored in 10% formalin at 4 degrees.

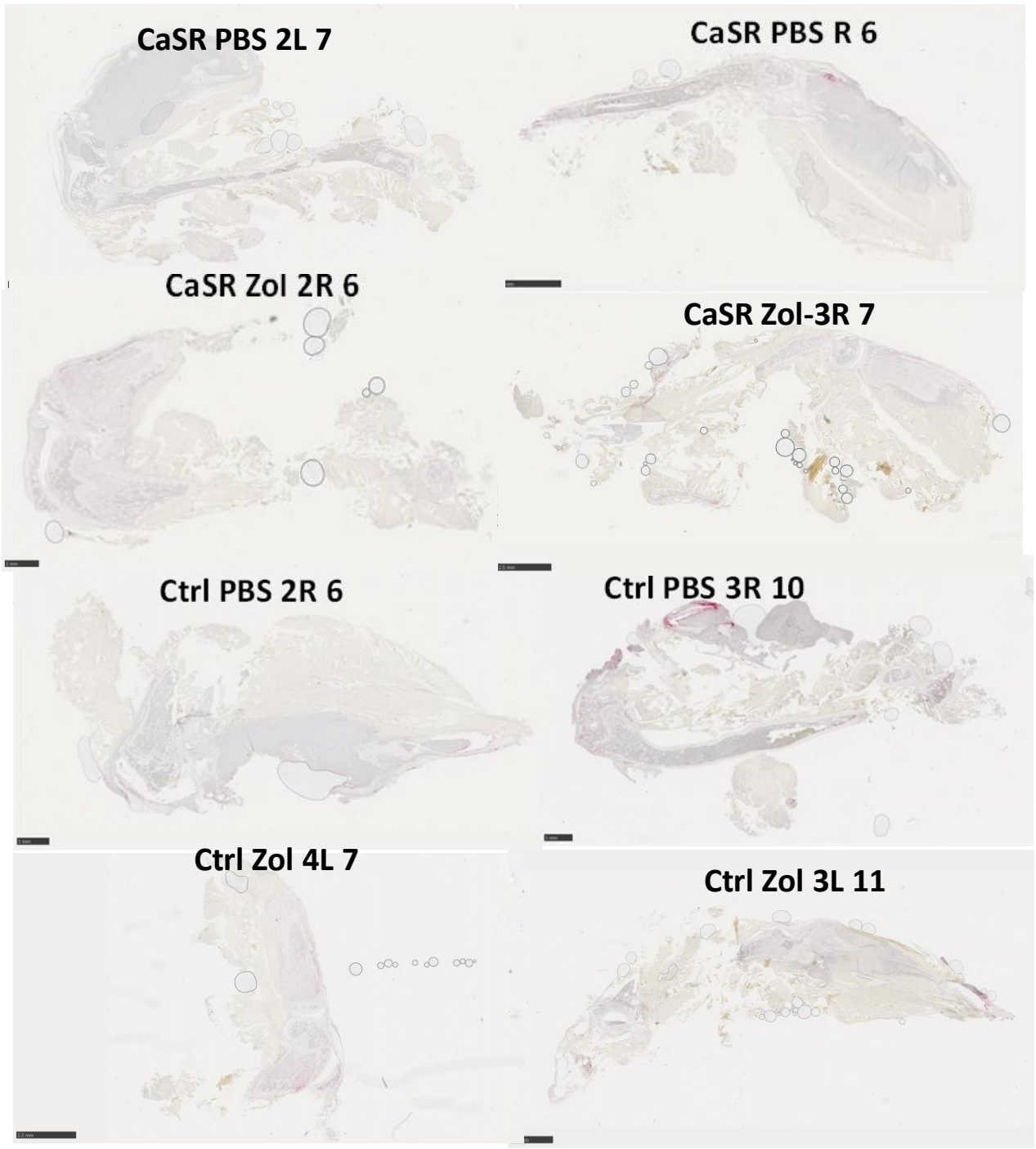

Figure 4.27 TRAP staining on bone tissue from mouse tibia injected with PC3 luc with and without CaSR

4.6.2.6 Interaction of CaM with CaSR in PC3

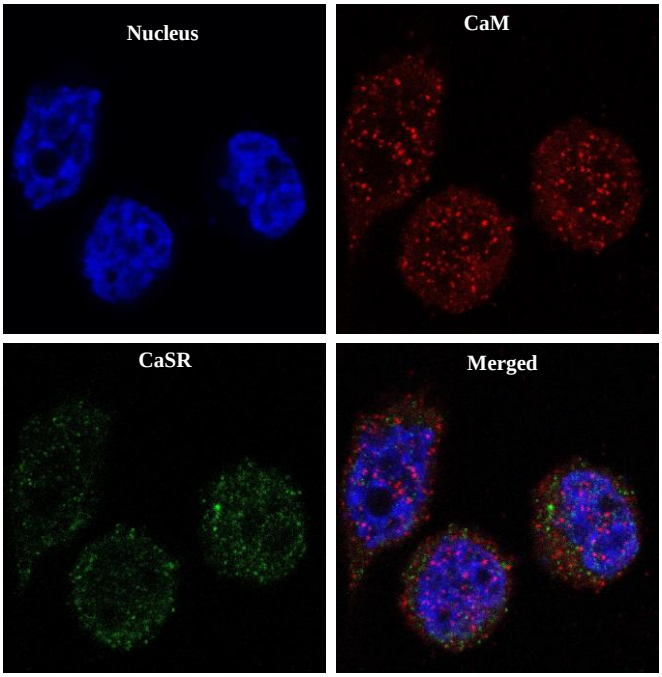

Figure 4.28 Co-localization of CaM with CaSR with a Pearson's coefficient of 0.67

CaM expression was established using immunostaining where CaM and CaSR were seen to co-localize with a Pearson's coefficient of 0.67 (**Figure 4.28)**. Ca^{2+} dependent binding of CaM with endogenous CaSR in PC3 was analyzed using Co-IP and western blot validation. The Ca^{2+} dependence is not established as both conditions show the elutions at the higher molecular weight (**Figure 4.29**). This can be explained by the higher molecular weight immunoprecipitation of CaSR at > 250 kDa where CaM is seen in the blot.

4.7 Discussion

Bone is a common site of metastasis for prostate cancer cells. The Ca^{2+} concentration in the bone is 10-40 mM and this provides a unique environment for the tumor cells. The CaSR in PC3 has been implicated in tumor proliferation and survival. In our work, we explore the intracellular

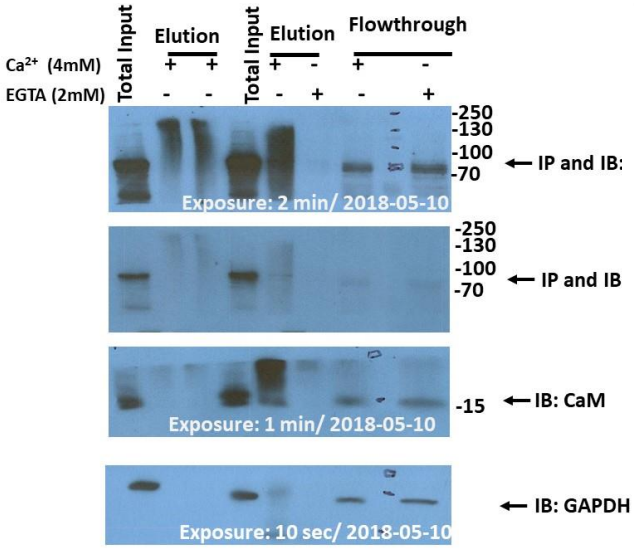

Figure 4.29 Interaction of CaSR with CaM

10% gel. Overnight transfer. Blocked 2 hrs with 3% milk; antibodies incubation with 3% BSA. Heated with 5% beta-mercaptanol for 10 min on the same and day and ran samples

Ca^{2+} response of PC3, precisely the CaSR mediated responses. We report that the CaSR mediated $G\alpha_q$ associated $Ca^{2+}{}_i$ response, such as the intracellular calcium oscillation and IP_1 are absent in PC3. Oscillation with very low frequency was observed in 2-3% of the cells. Overexpression of wild type CaSR in these cells could not rescue these signaling. Apart from the intracellular Ca^{2+} response, we observe that ERK1/2 and IP1 are also missing in PC3 cells. This suggests that the PC3 is extracellular Ca^{2+} insensitive and therefore, the G-protein mediated signaling are stunted. CaSR associated drugs such as cinacalcet and TNCA could not rescue these signaling. To understand the signaling in other PCa cells, we explored the intracellular response in LNCaP cells, which are PCa cells that metastasize to lymph nodes. They also lack the response. However, previous studies have suggested that these cells have lower CaSR [91], so that could be the reason we observe no oscillation. However, interestingly, we observe more significant number of transients in 50% of the LNCaP cells at 3 mM Ca^{2+}.

In order to understand the molecular reason for this discrepancy in signaling, we explored the protein and genomic expression of CaSR as well as the overall proteomics in PC3 cells. We noted that CaSR monomer in PC3 occurs as a monomer in non-reducing condition and has a lower

molecular weight with 110 kDa, indicating incapability to form a dimer or presence of a variant with a splice-variant or lower glycosylation. WT CaSR usually shows up at 130-150 kDa. PC3, on the contrary, is able to generate a dimer when artificially transfected. Immunostaining showed that most endogenous CaSR occurs within the cell as compared to functional plasma membrane CaSR. These results suggest that endogenous CaSR in PC3 may deflect from the WT in molecular composition and this may result in obstructed Ca^{2+} signaling. Therefore, we further went to use RT-PCR to examine the expression of CaSR at the genomic level. We show that a full CaSR with all seven exons are present in PC3. But we cannot rule out the presence of other splice variants as primers were designed based on known WT CaSR for PCR. Also, mutations or small deletions could not be detected with this process. Unfortunately, our endeavor to use RNAseq for complete CaSR sequence was not successful due to the low transcript of CaSR and therefore, resulting in almost no detection of CaSR.

Another possibility of lower molecular weight of endogenous CaSR in PC3 could be due to the presence of immature CaSR with less glycosylation. However, our result that transiently transfected CaSR occurred as proper molecular weight species and immunostaining showed at least some cells were able to express the WT CaSR at the surface, but this still could not rescue the g-protein signaling, suggest against the logic that glycosylation could be the reason behind the differential Ca^{2+} signaling. Other possible reason for differential signaling in PC3 cells could be biased signaling or defect with its regulators in the cells. In order to examine this, we carried out immunoassay which shows the presence of essential CaSR regulators $G\alpha_q$ and CaM. However, proteomics study in the past had shown that $G\alpha_{q/11}$ was only present in RWPE-1 and LNCaP prostate cancer cells, but not in PC3 cells [303]. This is contrary to what we have found. We could also argue that the $G\alpha_{q/11}$ blot obtained was slightly lower than that in LNCaP and HEK293 cells

which indicates a variant of $G\alpha_{q/11}$ in PC3 resulting in the differential signaling. Proteomics study of PC3 cells indicates the absence of $G\alpha_{q/11}$ but presence of $G\alpha_{i.}$ ERK1/2 is induced by $G\alpha_i$ and intracellular oscillation by $G\alpha_{q/11}$ usually. ER Ca^{2+} channel SERCA was present with reliable PSM and high LFQ intensity. However, IP3R detection was not reliable for PC3 cells. We cannot say that mass spectrometry result is a complete picture. MS may not be able to detect the $G\alpha_{q/11}$ and IP3R even in HEK293, a positive control.

Proteomics of total cell lysate was carried out and a total of 3327 proteins were detected. Apart from Gαq, CaM and other G-proteins such as Gαi-2, Gαs and Gβ are detected with strong MS/MS count. Additionally, CaSR was not detected with PSM of 0 which supports the retarded Ca^{2+} sensing and low transcript generated in RT-PCR and RNAseq. On the contrary, 10^9 LFQ intensity was observed for HEK293 cells transfected with FLAG-CaSR with an average PSM of 22. Only 22 proteins were at least two-fold up-regulated in expression in the presence of Ca^{2+} and 17 were downregulated in the presence of Ca^{2+}. More research is required to understand their implication in PC3 cells. Additionally, because we were interested in prognosis markers, proteins detected in PC3 were compared to known markers in prostate cancer from the human protein atlas. We found two proteins, Epoxide hydrolase 1 (EPHX1) and Catebhol O-methyltransferase (COMT) with good abundance with the stringency of ≥ 4 average PSM and with average LFQ intensity in the range of 10^9. These markers were not significantly Ca^{2+} dependent, as Ca^{2+} treatment in PC3 caused < 0.9-fold decrease as compared to one treated with EGTA. However, these were ≥ 3-fold increased as compared to HEK293 cells. Isoforms of other good prognostic markers including the ubiquitin (RNF114), Ubiquitin-conjugating enzyme (UBE2D2/3) and SLCs were detected with good stringencies.

We were also interested to see what cellular processes are upregulated in PC3 as compared to HEK293 cells. We employed gene ontology on the up-regulated proteins from MS to understand the role of extracellular Ca^{2+} in alteration of proteomics in PC3 cells as compared to HEK293 cells. We noted that global proteome is generally upregulated in PC3 as compared to HEK293 cells. In the presence of Ca^{2+}, $\geq$ 4-fold upregulated proteins are associated with pathways including, trans-Golgi network vesicle budding and citric acid cycle. This has been recently shown that TCA cycle is hyperactivated in PCa cells using GC-MS and RNA-seq analysis by another group[311]. This is shown to result due to decreased PCa epithelial cells accumulating zinc and thereby, increasing citrate oxidation [311]. This may allow more energy production in PC3 cells. Fatty acid uptake [312] and enzymes required for beta-oxidation [313] has been shown to be increased in PCa tumors. This can provide ATP and acetyl-coenzyme A to accelerate the citrate oxidation. Additional analysis and literature mining is underway to understand the upregulated proteome in PC3 and better understanding will be achieved if the proteome is compared between the malignant, normal and non-malignant cells or tissues since comparing PC3 and HEK293 are from distinctive origin, our analysis can be diluted.

Further, in vivo studies were conducted to understand and re-enforce involvement of CaSR in PC3 colonization in bones by preventing cell apoptosis of cancer cells, inhibiting invasion, and promoting mesenchymal-epithelial transition. My work showed a significant decrease in tumor growth when injected in mouse tibia with PC3 with CaSR knockdown and the control knockdown in the presence of a Ca^{2+} chelator, Zoledronic acid. This work shows the Ca2+ dependent proliferation of PC3 cells in bones. The work does not show a significant change between the PC3 with CaSR knockdown and the control knockdown as quantified by our limited two H&E staining.

Our work indicates that even in the presence of normal CaSR, PC3 displays unique Ca^{2+} signaling that is independent of Gαq, possibly undergoing signaling bias.

5 CHAPTER V: REGULATION OF CONNEXIN26 GAP JUNCTION CHANNEL THROUGH EXTRACELLULAR CALCIUM AND CALMODULIN

5.1 Abstract

Living beings are an amalgam of processes and regulations. One of such vital biological processes is cellular communication which regulates hormone signaling, neural transmission and cell-to-cell adhesion. Gap junction (GJ) proteins consist of intercellular aqueous channels between adjacent cells that permit the exchange of important hydrophilic molecules such as ATP, cAMP, IP_3, glutamate, calcium, and many more. Connexin26 (Cx26) is the second most ubiquitous GJ proteins, and hundreds of mutations in Cx26 is implicated in many hereditary deafness and dermatological disorders. Many studies have pointed out the dependence of GJ channels on calcium ions and CaM (CaM) for the intra- and inter-cellular communications, respectively. However, the mechanism is obscure. In our study, first, we aimed at optimization of the expression and purification of the full-length hemichannel and dodecamer Cx26. Next, we investigated the molecular changes and binding affinities of Cx26 to $Ca^{2+}{}_o$ in hemichannels and intracellular calcium activated CaM protein using resonance energy transfer.

The expression of hemichannel Cx26 was successfully optimized using the C43(DE3)pLysS bacterial stain, induced with 1 mM IPTG and grown at 37°C for 18 h. 3.5% empigen was determined as the most suitable detergent for solubilization of intact and stable Cx26

membrane protein. However, the yield was limited to 0.6 mg/L and the purification was challenging due to the oligomerization and precipitation of the protein during the process. Using fluorometry, we noted that the binding affinity of the hemichannel Cx26 to Tb^{3+} was 1.8 μM and indirect Ca^{2+} competition of bound Tb^{3+} exhibited a weak K_d of 37 mM. However, we found the result to be questionable due to non-linearity of the fluorescence change and the protein concentration during the competition. Additionally, we observed the dependence of fluorescence of the protein on the time of pre-incubation with Tb^{3+}. Both observations suggested protein conformation change or precipitation during these processes. Therefore, the result we obtained is not conclusive.

In order to understand the interaction between Cx26 and CaM, wt-CaM was successfully purified at 37 mg/L. Effect of Cx26 peptide (residue 1 to 21, $Cx26p_{1-21}$) on the domain-specific Ca^{2+}-binding affinity of CaM was examined by monitoring the intrinsic fluorescence intensity change of Phe and Tyr. In the presence of $Cx26p_{1-21}$, the K_d of CaM to Ca^{2+} increased from 1.35 to 4.10 μM and 2.9 to 3.87 μM for the N-domain and C-domain, respectively. This suggested greater conformational change of the N-terminal lobe by greater than 2.5 folds than that of C-lobe of CaM upon $Cx26p_{1-21}$ binding. Further, the interaction between CaM and Cx26 in the living cell was examined using bioluminescence resonance energy transfer (BRET). Interaction between CaM with the yellow fluorescence fusion protein, Venus-C1, and Cx26 with the Renilla luciferase (Rluc-C1) fusion protein was found to be insignificant. This implies that the interaction does not occur between the CaM and the C-terminus of Cx26. The surface plasmon resonance study showed no significant binding between CaM and $Cx26p_{1-21}$. This preliminary result indicates that the interaction between CaM and N-terminus of Cx26 is insignificant.

5.2 Introduction

Gap junctions (GJ) are integral membrane proteins which assist in communication and coordination between cells through processes including, exchange of metabolites and electrical signal. In humans, GJs are expressed in all tissues except differentiated skeletal muscle, erythrocytes, and mature sperm cells [100]. GJ proteins consist of intercellular aqueous channels between adjacent cells that permit the exchange of hydrophilic molecules such as ions, and metabolites (ATP, NAD^+, small peptides and nucleotides), and secondary messengers (Ca^{2+}, cAMP, IP_3) of less than 1kDa [100]. They are known to modulate a wide range of functions such as immune response, inflammation, memory, apoptosis, water channels, metabolism and muscle contraction [100].

5.2.1 Regulation of Cx26 hemichannel by Calcium

It has been known since 1991 that $[Ca^{2+}]_o$ leads to the opening of connexin hemichannels. Muller et al. studied the conformational change of Cx26 hexameric extracellular hemichannel surface using atomic force microscopy (AFM) imaging at 1.2 nm lateral resolution and discovered the occurrence of significant narrowing of the entrance of Cx26 from 1.5 nm to 0.6 nm in the

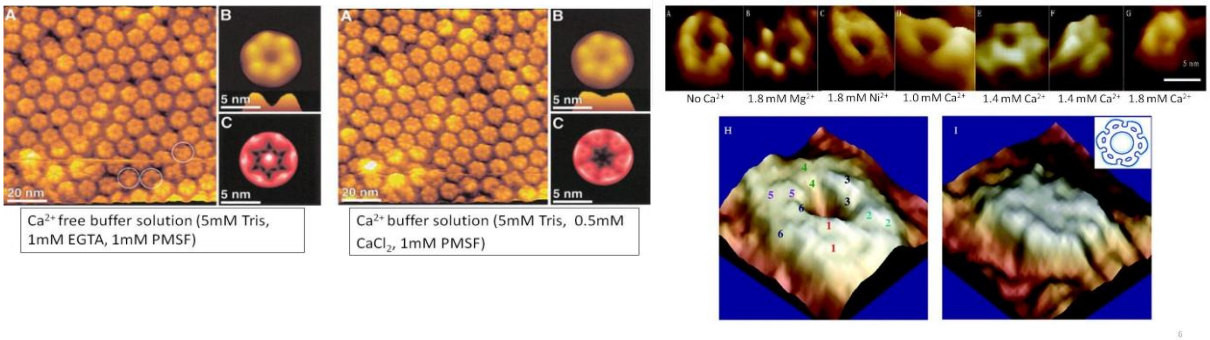

Figure 5.1 A. Ca^{2+} induced conformational change of the extracellular Cx26 connexon surface [9]. B. Conformational change in Cx43 with increasing $[Ca^{2+}]$ [18]

presence of calcium at 0.5mM **(Figure 5.1A)** [9]. Additionally, conformational change with increasing Ca^{2+} concentration was demonstrated in Cx43 at a higher Ca^{2+} concentration of 1.8 mM, by Thimm et al suggesting a differential sensitivities **(Figure 5.1B)** [18]**.** It was established that the conformational change was fully reversible and specific to Ca^{2+} ions. Divalent cations like Zn^{2+}, Cd^{2+}, Co^{2+}, Ba^{2+} and Mg^{2+} have been shown to inhibit the channel activity in general with their increasing concentration [314-316]. Calcium also induced the formation of microdomains and increase in the plaque height. Intracellular and extracellular hemichannel sensitivity to calcium concentration differs (intra: µM and extra: mM range). This suggests that there is a different gating mechanism for channel closure for the extracellular surface and cytoplasmic surface [100]. According to many types of research, the likely candidate for the plug for the GJ protein are the NT, CT or CL domains. Increase in $Ca^{2+}{}_i$ uncouples gap junction. Dr. Xue Wang has predicted the potential Ca^{2+}-binding sites in Cx26 at amino acid positions Glu42, Asp46, and Glu47 from EL1 and Glu187 from EL2 using computational algorithm MUG^{SR} **(Figure 5.2)**. This predicted binding sites are largely conserved in many Cxs and localize within the loop gating region. Several disease related mutations such as deletion of Ca^{2+}-binding residues Glu42, Glu47Lys, and Gly45Glu affect GJ channel function dramatically and are associated with keratitis ichrhyosis deafness syndrome. Peracchia et al. have suggested the effect of Ca^{2+} is via CaM protein modulation [317]. Inhibitors of CaM has shown to prevent uncoupling of GJ in a number of cell types [317]. Increasing activity of CaM also showed an increase in Ca^{2+} sensitivity of Cx32 [318].

5.2.2 CaM

CaM is one of the most extensively studied calcium-binding proteins. It is a small, 17 kDa, a bilobed protein consisting of four EF-hand motifs each binding a Ca^{2+} ion [317]. It is a ubiquitous, 148 amino acid containing protein whose sequence is well conserved in most plants

and animal [317]. It has the N-and C- terminals connected by an internal flexible linker domain. Upon binding to Ca^{2+}, the N-and C- terminals undergo structural rearrangements exposing a hydrophobic binding pocket that recognizes target proteins. The conformational change supports CaM's Ca^{2+} dependent recognition mechanism and its flexibility allows in binding > 500 diverse set of substrates. It has also been found that CaM is able to bind some target proteins in its apo-form [319], suggesting the dynamic nature of CaM modulation. Its targets include phosphodiesterase, myosin light chain kinase, CaM kinase, calcineurin, NO synthase, etc [319]. The EF hand consists of 29 residues; 9 in helix, 12 in loop and 8 in the second helix [320]. The loops are responsible in binding to four Ca^{2+} ions. Ca^{2+} ions take on pentagonal-bipyramid geometry; five oxygen atoms being on the same plane, and two oxygen atoms being above and below the plane. It coordinates to seven oxygen from side chain residues 1, 3, 5, 9 & 12, carbonyl mainchain and bridged water. Positions 1, 6, and 12 most highly conserved with Asp, Gly & Glu [320]. Various studies have reported domain-specific affinity values by monitoring changes in intrinsic fluorescence of Phe and Tyr residues [321, 322]. These studies report that the C-domain of CaM binds Ca^{2+} with higher affinity ($K_d \approx 2.0$) than the N-domain ($K_d \approx 10.0$) [321, 323]. The result is consistent with the reported order of site occupancy where the binding of Ca^{2+} to the C-domain is known as the rate-limiting step in Ca^{2+}/CaM complex formation, as the on/off-rates of Ca^{2+} can be 30- to 150-fold slower for the C-domain than for the N-domain; however, binding of CaM with the PEP-19 enzyme appears to increase the on-rate for Ca^{2+} up to 40-fold, so the Ca^{2+}/CaM complex formation isn't solely regulated by temporal and spatial changes in cytosolic Ca^{2+} and CaM concentrations [324]. Several studies using peptide models have shown Holo CaM in the collapsed binding form binding to sites located in the second half of the intracellular loop of

α-subfamily connexins ($Cx50p_{141–166}$, $Cx44p_{132–153}$ and $Cx43p_{136–158}$). This is a 1–5–10 subclass binding mode. Here, each number represents the presence of a hydrophobic residue [325].

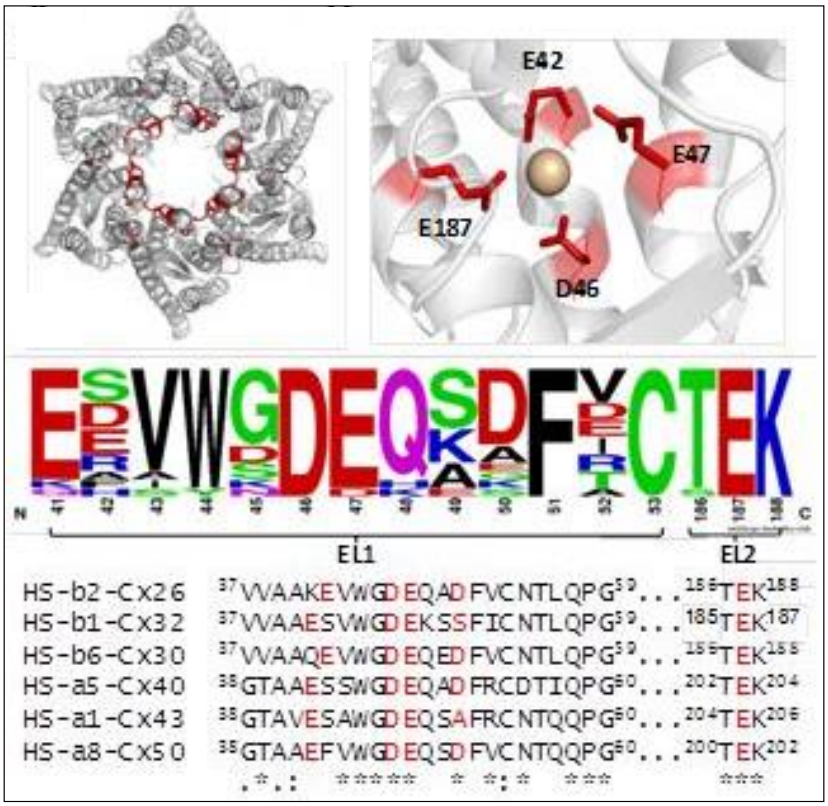

Figure 5.2 A. Crystal structure of Cx26. B. Predicted calcium binding sites in Cx26 using MUG[SR]. Glutamate and aspartate residues were predicted. C. Conservation of the predicted residues through various connexins.

5.2.3 Regulation of GJ by CaM

The N- and C-domains are known to have different binding affinities and kinetic properties. This allows for CaM to differentiate between the local and global Ca^{2+} changes to regulate their targets using various interaction modes [326]. Several connexins from all subfamilies such as Cx43, Cx44, Cx45 and Cx50 have been shown to be modulated by CaM by indirect methods such as silencing CaM expression or using CaM antagonist [317]. In 2017, Zou et al showed for the

first-time direct interaction of Ca^{2+}/CaM with Cx45 using bioluminescence resonance energy transfer (BRET) in live cells [327].

5.2.4 Expression Systems: The host cells

The host cell for protein synthesis impacts the quality and generation of the protein. Bacterial expression of proteins has many advantages with fast growth kinetics, high cell density cultures, inexpensive culture media and easy and fast transformation with exogenous DNA [328]. Furthermore, it produces a high yield of the protein lacking posttranslational modification such as glycosylation which may impair interpretation of NMR data and most importantly, it enables hetero-labeling study using NMR. However, multiple challenges are associated with expressing a membrane protein in bacteria. For our purpose, we needed to generate hemichannels which was possible with a bacterial expression system. However, with this system, usually proteins don't fold properly, the host lacks enzymes responsible for post-translational modifications such as glycosylation which may hinder expression, rare codons in mammals need to be inserted into the host, and synthesis of toxic proteins hinder the optimum production of proteins. Therefore, it is important to optimize the expression system considering the induction period, the temperature of expression, vectors being used, etc. The main advantage of mammalian cell expression as compared to bacterial expression system is that the signals for synthesis, processing and secretion of eukaryotic proteins are properly and efficiently recognized by mammalian cells and therefore, resulting in properly folded proteins [329]. On the other hand, the baculovirus expression system is lengthy and intensive, but it yields larger amount of recombinant protein than the bacterial system.

5.2.5 Fluorescence Resonance Energy Transfer (FRET)

At room temperature electrons in molecules occupy the lowest vibrational energy levels of

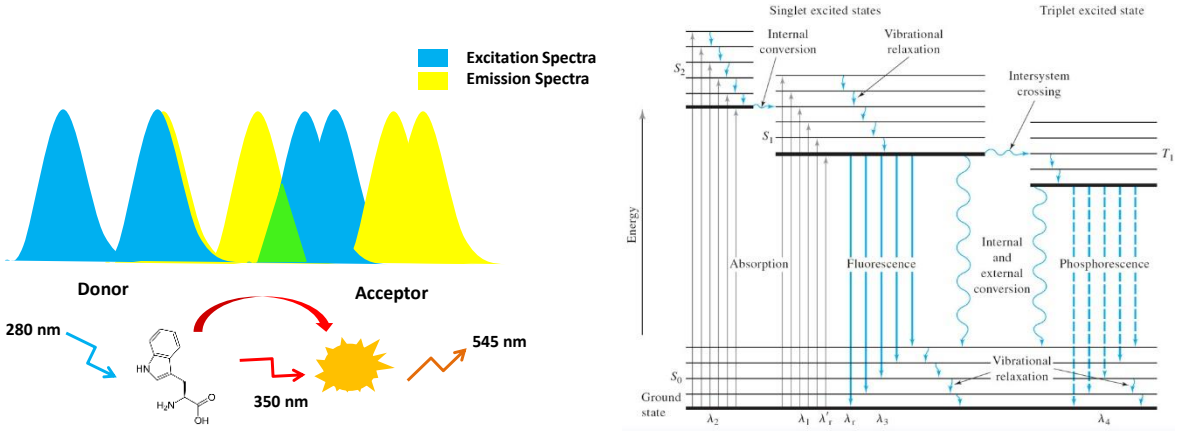

Figure 5.3 A. Principle of fluorescence resonance energy transfer (FRET). B. Partial energy-level diagram for a photoluminescent system

the ground electronic state, and when they absorb light, they are transferred to excited states. **Figure 5.3** demonstrates the absorption process by molecules to produce either the first, S_1 or second S_2, excited states. Fluorescence contains two processes; the first absorption occurs between different energy levels and then subsequent emission at longer wavelengths due to the vibrational energy loss. Since the wavelength that is being detected is different from the incident one, sensitivity is much higher due to the absence of background in excitation source. It is possible to measure fluorescence in the 10^{-7} M range, which has a better limit of detection than other absorption spectroscopy techniques [330]. There is a linear relationship between fluorescence intensity (F_λ) and concentration (C) of the fluorophore only for dilute solutions of the fluorophore (absorbance at excitation wavelength less than 0.05), represented in the equation below:

$$F_\lambda = B\,C;\; B = I_0 2{,}3\;\varepsilon_{(\lambda)}\,l\,\Phi\,Z \qquad \textit{Equation 5. 1}$$

Nanoseconds is usually the range for lifetime of a fluorophore in the excited state, however, this time is sufficiently long to interact with the environment. Fluorescence parameters can be

affected by different factors such as interactions of the fluorophore with the solvent molecules which will eventually affect the maximum λ_{em}, quantum yield, and lifetime. Generally, an increase in the polarity of the solvent (or environment) has two effects: (a) a decrease in the fluorescence intensity, and (b) a redshift in the λ_{max} of emission [330]. These effects of the environment on fluorescence parameters have been used extensively in monitoring protein-protein interactions.

5.2.5.1 Stoke Shift

The absorption energy is given by $E_a=hc/\lambda_a$ and emission energy is given by $E_{em} = hc/\lambda_{em}$. Since, $E_{em} < E_a$ we have: $\lambda_{em} > \lambda_a$, where λ_a and λ_{em} are absorption and emission spectra peaks. Thus, the emission spectrum has its maximum shifted to longer wavelengths compared to the maximum of the absorption spectrum. The distance between this maximum absorption and emission spectra is called the Stokes shift [330].

5.2.5.2 Lifetime Fluorescence Spectroscopy

After the excitation of the molecules, they tend to remain in the excited state for a short time before returning to the ground state, therefore, the lifetime of the molecules in the excited state is equal to the mean time during which molecules remain in the excited state, and the time is considered as the fluorescence lifetime. This time ranges from the nanoseconds (10^{-9} s) to picoseconds (10^{-12} s) [330]. So, the fluorescence lifetime determines the time available for the fluorophore to interact with or diffuse in its environment. For the fluorophore illustrated in **Figure 5.4,** the lifetime is $\tau = 1/ (\Gamma+k_{nr})$, where the emissive rate of the fluorophore is called (Γ) and its rate of nonradiative decay to S_0 is called (k_{nr}). The lifetime is an average value of the time spent

$$k_T(r) = \frac{1}{\tau_D}\left(\frac{R_0}{r}\right)^6 \qquad \textit{Equation 5. 2}$$

in the excited state. The natural lifetime can be calculated from the measured lifetime (τ) and quantum yield (Q): $\tau_n = \tau/Q$

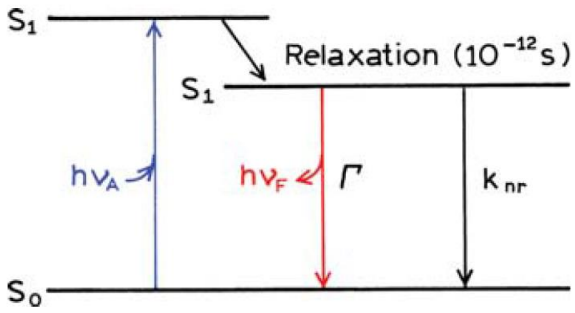

Figure 5.4 A simplified Jablonski diagram to illustrate the meaning of quantum yields and lifetimes

5.2.5.3 Fluorescence Quantum Yields

The fluorescence quantum yield is defined as the ratio of the number of photons emitted to the number absorbed. The fraction of fluorophores that decay through emission, and hence the quantum yield, is given by $Q = \Gamma/(\Gamma + k_{nr})$. The quantum yield can be close to unity if the nonradiative decay rate is much smaller than the rate of radiative decay which means is $k_{nr} < \Gamma$.

5.2.5.4 Fluorescence Resonance Energy Transfer (FRET)

Fluorescence resonance energy transfer (FRET) has various applications in the field of fluorescence such as medical diagnostics, DNA analysis, and optical imaging. FRET usually occurs between a donor (D) molecule in the excited state and an acceptor (A) molecule in the ground state. The donor molecules typically emit light at shorter wavelengths which then overlap with the absorption spectrum of the acceptor. Energy transfer occurs without the generation of any photon and it is the result of long-range dipole-dipole interactions between the donor and acceptor. **Figure 5.5** demonstrates the RET process. In this process, the acceptor can be a non-fluorescent agent. The distance between the donor and acceptor is the key determinant for the extent of energy transfer, and the extent of spectral overlap. The spectral overlap is described in **Figure 5.5** in terms

of the Förster distance (R_0). The efficiency of energy transfer for a single donor–acceptor pair at a fixed distance is $E = R^6_o/(R^6_o + r^6)$, where r is the distance between the donor (D) and acceptor (A) and τ_D is the lifetime of the donor in the absence of energy transfer. Therefore, the extent of transfer depends on the distance (r) [330]. The Förster distances are comparable in size to biological macromolecules: 30 to 60 Å. For this reason, energy transfer has been used as a "spectroscopic ruler" for measurements of the distance between sites on proteins.

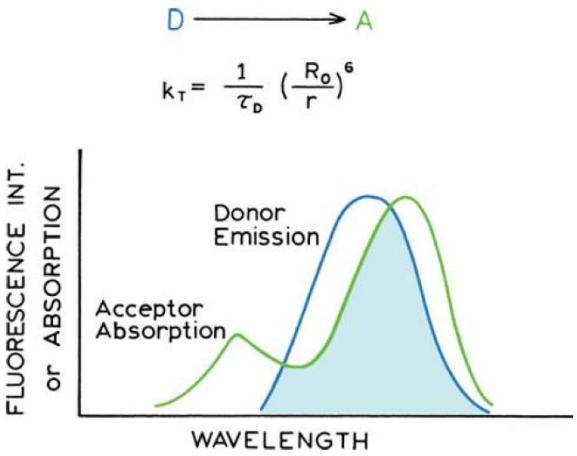

Figure 5.5 Spectral overlap for fluorescence resonance energy transfer (RET).

5.2.5.5 BRET

The BRET method is an advanced, non-destructive, cell-based assay technology based on the forster resonance energy transfer leading to a non-radiative energy transfer between an energy donor and an energy acceptor [330]. The energy donor is a luciferase, which emits light in the presence of its corresponding substrate. The energy acceptor is a fluorophore, typically a fluorescent protein, which absorbs light at a given wavelength and reemits light at a longer wavelength. To fulfill the conditions for energy transfer, the emission spectrum of the donor must overlap with the excitation spectrum of the acceptor. To investigate protein-protein interactions,

one protein is fused to the donor and the other to the acceptor. If the two fusion proteins do not interact, only light emitted from the substrate transformation by the energy donor can be monitored. If the two fusion proteins interact and the distance between the energy donor and acceptor is less than 10 nm, a resonance energy transfer occurs and an additional. light signal corresponding to the acceptor reemission can be detected. When the energy donor and acceptor are fused to the same protein, an intramolecular BRET can be monitored in this double-fusion protein. Depending on the position at which the energy donor and acceptor are fused, structural rearrangements (conformational changes) within the protein of interest can be measured as changes of the intramolecular BRET signal.

5.2.6 Surface plasmon resonance

Surface Plasmon Resonance is a phenomenon that occurs when polarized light hits a metal film at the interface of media with different refractive indices. A light is incident upon a metal film through a prism and the reflected beam is collected and analyzed. At an appropriate angle (resonance angle), the incident light excites the surface plasmons in the sensor chip (metal film) and the intensity of the reflected light drops to a minimum. The electromagnetic field created by SPR penetrates the fluidic medium and probes molecular binding processes taking place on the surface and the refractive index changes in the fluidic medium. The excitation of surface plasmons

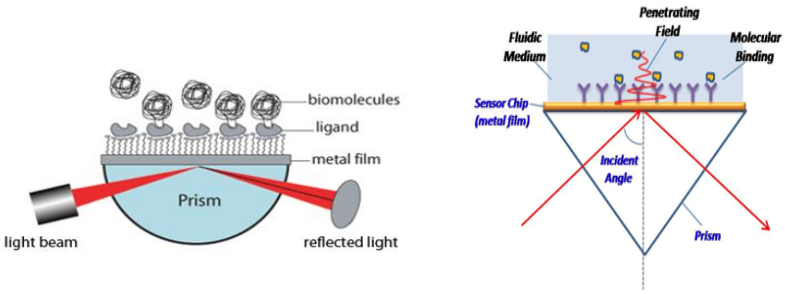

Figure 5.6 Principle of surface plasmon resonance

results in a dark line in the reflected beam, and the angular position of the dark line shifts as a molecule binding event takes place. SPR Scanning Angle Response. SPR causes an intensity dip in the reflected light at the sensor surface. A shift in the curve represents molecular binding. The angular shift vs. time provides a good study of binding kinetics. The reverse process, molecular dissociation, can be studied in a similar way. Ideally for a kinetic analysis, the maximal RU signal should be ~ 100 RU for protein:protein, protein:DNA interactions and ~ 25 RU for small molecules (< 1000 – 1200 Da).

5.3 Challenges

As mentioned in chapter I, challenges faced in studying connexins include oligomerization, lower solubility and difficulty and limitations associated with expression *E.coli.*, and insect cells due to the fact that bacteria lack proper mechanism for eukaryotic protein folding, translocating, trafficking, disulfide bond formation and post-translational modifications. Also, the phospholipid composition in bacteria and insects varies from that of eukaryotic cells. These may result in improper surface expression of membrane proteins such as connexins. These limitations in membrane proteins result in unavailability of crystal structures. Additionally, understanding the calcium modulation is a challenge due to its weak binding and that Ca^{2+} binding has high on- and off- rate. Furthermore, calcium is silent spectroscopically which makes the study challenging.

5.4 Major aims and questions in this chapter

a) Aim I: Optimize a full length hCx26 expression and purification system from bacteria

- What parameters can optimize the expression of hCx26?
- What detergents and strategies are optimal for purification of hCx26?
- What are the biophysical characteristics/stability of the purified protein?

b) Aim II: Understanding the gating of hemichannels through Ca^{2+}_o using the hCx26 expressed from bacteria

- What is the stoichiometry, metal binding affinity and metal selectivity of the hCx26?
- How does Ca^{2+} induce conformational changes, stability and assembly?

c) Aim II: Understanding the interaction of Cx26 with CaM using synthetic Cx26 peptide

- What is the major mechanism of interacts between CaM/Ca^{2+} and Cx26?

5.5 Materials and methods

5.5.1 Molecular cloning

5.5.1.1 Recombinant hCx26 gene was cloned into pRSETA vector

This was carried out between *BamHI* (5' end of gene) and *EcoRI* (3" end of gene) restriction enzyme sites. Polymerase chain reaction (PCR) was used to amplify the hCx26 gene. 100ul reaction mixture was obtained using 66 ul of autoclaved water, 10ul of 10X buffer, 10ul of 2mM dNTPs, 6ul of 25mM $MgSO_4$, 0.5ul of ~1500ng/ul plasmid, 2ul of reverse and forward primers and 2ul of polymerase KOD. The forward primer designed was CGCGGATCCATGGATTGGGGCACACTC and the reverse was CCGGAATTCGACTGGTCTTTTGGACTT (T_m=56ºC). Denaturation was carried out at 94ºC for 2 min, annealing at 56ºC for 30 sec, extension at 72ºC for 20 sec for 30 cycles, final extension at 72ºC for 20 sec. Using double digestion, the CaSR gene was cleaved from the pRSETA vector and similarly, hCx26 target gene with His tag was cleaved from the pHisTrcA vector. The digested products were run in DNA gel, extracted and ligated with rapid ligase. Various concentrations of PCR product and vectors were tried. 1:7, 3:5, and 5:3 worked. The ligation reaction was allowed

to incubate at room temperature for ~3hrs. The ligated product was transformed into XL10-gold. Next day, a colony was inoculated into a 5ml LB and grown at 37^{o}C o/n. DNA was extracted using Quick MiniPrep and sent for sequencing.

5.5.1.2 Generation of C43(DE3)pLysS competent cells

Plasmids from Rosetta 2(DE3) pLysS cells and C43(DE3) were isolated and pLysS was cleaved from the Rosetta2(DE3) pLysS. Next, C43(DE3) and the mixture with pLysS and Rosetta2(DE3) were co-transformed and selected.

5.5.1.3 Cloning BRET constructs

This was carried out using the previously described method [327]. The yellow fluorescent protein fusion protein expression vector pVenus-N/pVenus-C1 and the Renilla luciferase (RLuc) protein fusion protein expression vectors were received from Dr. Hepler (Emory University, GA). The mouse Cx26 plasmid in pcDNA3.1/Hygro(+) was from Dr. Veenstra (SUNY Upstate Medical Univesity, NY). Cx26-pVenus was synthesized by insertion of the PCR product of the mouse Cx26 into vector pVenus-N1 at Nhe I and Xma I enzyme sites upstream of eYFP. Forward and reverse primers were CTA GCT AGC ATG AGT TGG AGC TTC CTG ACT and TCCC CCC GGG AAT CCA GAC GGA GGT CTT CCC. CaM-RLuc8 was generated by insertion of rat CaM gene into vector RLuc8-N1 at Xho I and BamH I. Forward and reverse primers for generation of CaM-RLuc8 were CCG CTC GAG ATG GCT GAC CAG CTG ACC and CGC GGA TCC CTT GCG AGT CAT CAT CTG. All DNA sequences were verified by GENEWIZ.INC (www.genewiz.com).

5.5.2 Transformation and expression of hCx26

Expression conditions were varied and optimized using various the competent cells, temperature and induction times **(Figure 5.10)**. hCx26 plasmid was transformed into competent cells such as: *E. coli* C43(DE3), C43(DE3)pLysS, Rosetta gammi pLysS or Shuffle. A single colony was inoculated into 200ml or 100ml medium (LB or M9) and allowed to grow o/n (< 16hrs) at 37^{o}C or 28^{o}C at 250 rpm along with respective antibiotics. 1ml antibiotic was added into the 0.5 L autoclaved medium. ~3.5ml was transferred into 0.5 L medium in 1 L flask at respective temperatures and allowed to grow at 250 rpm. When OD reached 0.9-1.2 (1.0 is optimum), 1mL of 1 M IPTG was added to induce expression for 16-20 hrs. Once expression was complete, the bacterial cells was harvested at 7000rpm for 10 min at 4^{o}C. The pellets were stored at -80^{o}C for future purification process after adding 300ul of 1M PMSF. The expression was quantified using western blot and SDS-page gels. (Minimal medium (M9) contained Na_2HPO_4, KH_2PO_4, NaCl, NH_4Cl (0.5 g), $MgSO_4$, $CaCl_2$(1 M), $FeSO_4$ (0.01 M), Glucose (5 g), Thiamine (0.5 mg/mL), Vitamin (BLE)). (LB: Tryptone (10 g), Yeast Extract (5 g), NaCl (10 g))

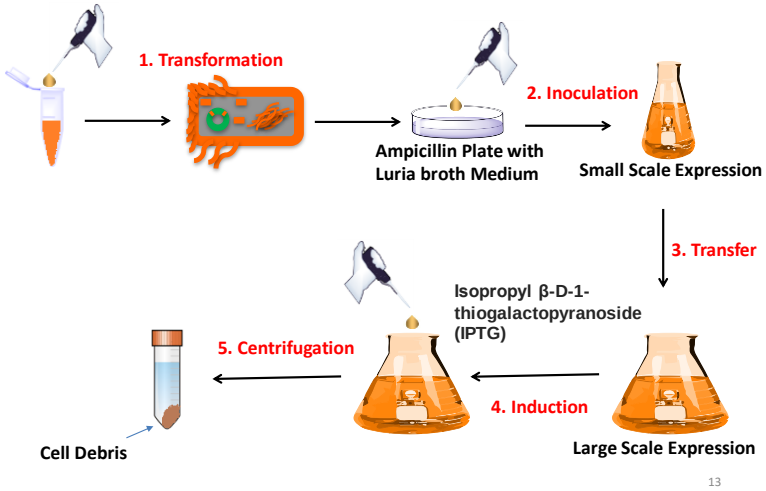

Figure 5.7 Workflow of expression of protein from bacterial strain.

5.5.3 Purification of hCx26

Various buffer systems and detergents were used in order to optimize the yield and quality of Cx26.

5.5.3.1 Purification of hCx26 using 2% DDM:

Pellets was thawed on ice. ~30mL of lysis buffer (75mM Tris HCl, 30mM NaCl, pH 7.7, 1mM PMSF and 1 ul benzononase nuclease per 50 mL) was added little at a time to homogenize the pellets. The mixture was ultra-centrifuged at 30,000 rpm, 4^{o}C for 1hr. Supernatant was collected in a clean beaker and filtered through 0.45um filter. 10mM Imidazole was added and pH was adjusted to 8. 1mM PMSF, 0.05-0.1% DDM was added. Beads were prepared and washed with deionized water and lysis buffer with 10mM imidazole. The supernatant was combined with beads properly in a beaker and stirred for 2-3 hrs or o/n in cold box. The pellet was re-suspended gently using hand homogenizer. Solubilization buffer (10mM HEPES, 0.005% NaN_3, 500mM NaCl, pH=7.5 2% working concentration of DDM (Stock=10%, stored at -20^{o}C) with 1mM PMSF) was added. The lid was Para filmed and was allowed to shake overnight at 4^{o}C in a circular shaker. Next day, solubilization buffer at pH 7.5 with 2% DDM was added to the pellet solution and brought the volume to ~32ml. Then ultracentrifuged it at 28,000 rpm for 1hr. The supernatant was filtered through 0.45um filter into a clean beaker and the pellet was stored at -20^{o}C. 10mM imidazole was added to get rid of non-specific binding proteins and adjusted the pH to 8. The same process was carried out as done day before for the supernatant, but with 2% DDM to extract remaining membrane proteins. The supernatant was incubated with bead for 2-3hrs. The supernatant-bead mix was transferred to the column. The column was rinsed with wash buffer I (10mM HEPES, 500mM NaCl, 10mM Imidazole, 0.1% DDM, pH=8) and wash buffer II (10mM HEPES, 500mM NaCl, 0.1% DDM, 40mM Imidazole, pH=8). Finally, protein was eluted out in

2ml fractions in each of the five falcon tubes using 10mM HEPES, 150mM NaCl, 300mM Imidazole, pH 7.5. Column was cleaned using 2 M imidazole was used to clean the column, followed by deionized water (5X) and stored in 20% ethanol at 4^{o}C.

5.5.3.2 Purification of hCx26: Using 3.5% empigen

Table 5.1 Buffers used for various protein purification optimization

Purification Buffers	3.5% Empigen	NLS-OG System	Urea/Unfolding-Refolding
Lysis Buffer	75mM Tris HCl, 30mM NaCl, 0.2mM EDTA, pH 7.7	75mM Tris HCl, 30mM NaCl, pH 7.7	[25mM HEPES, 0.5M NaCl, 1% sarkosyl, pH 7.2] **X 2**
Solubilization buffer	3.5% Empigen	55mM N-laurylsarcosine, 0.2M NaCl, 50mM Na2HPO4, 1.09M glycerin, 10mM Tris, pH 9.5 → diluted to 0.5% NLS	M Urea, 20mM Tris-HCl, 0.5M NaCl, 2% TritonX-100, pH 8
Wash buffer I	10mM HEPES, 0.5M NaCl, 10mM Imidazole, 3%Empigen, pH=8	0.5% NLS, 0.2M NaCl, 10mM Tris, pH 8	6M Guanidine HCL, 1mM 2-mercaptoethanol, 20mM Tris-HCl, 0.5M NaCl, 5mM Imidazole pH8
Wash buffer II	10mM HEPES, 0.5M NaCl, 3% Empigen, 40mM Imidazole, pH=8	30mM OG, 0.2M NaCL, 10mM Tris, pH 8	[20mM Tris, 0.5M NaCl, *20mM Imidazole, 6M Urea*, 1mM 2-Mercaptoethanol, pH8 4M → 2M → 0M Urea
Elution buffer	10mM HEPES, 0.15M NaCl, 0.3M Imidazole, 0.1% DDM, pH 7.5	30mM OG, 0.5M Imidazole, 10mM Tris, pH 8	500mM Imidazole

The same method as above was used. After sonication, 1ml of 35% Empigen solution was added for every 10ml of lysate and tumbled in round rotor for 30 min -1hr. After ultracentrifugation at 30,000 for 1hr at 4^{o}C, the supernatant was treated same way as above with the beads for 2-3 hrs or o/n in cold box. The mixture was allowed to settle in the column and washed with wash buffer I and II, and finally eluted using same reagents as above.

5.5.3.3 Purification of hCx26 Using NLS-OG System

55 mM N-laurylsarcosine and 30 mM Octyl beta-glucoside (OG) was used to extract the membrane protein. Details on buffers used for this process is given in the table.

5.5.4 Expression of wt CaM (CaM)

Wild type CaM plasmid was transformed into BL21(DE3)pLysS (50ul) using heat shock method. The mixture with 1ml LB was incubated for 30 min at 37^{o}C. 50 ul of the mixture was transferred dropwise on the plate and the plate was coated all over. It was incubated overnight (o/n) at 37^{o}. 200ul of ampicillin (100mg/ml) was transferred into the 200ml LB, followed by inoculation of a single colony into the 200 ml medium. It was incubated o/n (<16hrs) at 37^{o}C at 200 rpm. 1ml ampicillin was added into the 1 L autoclaved LB. 20ml from the 200 ml culture was added into it and shaken vigorously to homogenize. It was then incubated at 37^{o}C at 200 rpm. OD was checked every 1 hr until it reached 0.7 OD. 200uL of 1M Isopropyl beta-D-1-thiogalactopyranosides (IPTG) was then added for induction. It took 3 hrs to reach ~0.7 OD and the expression was allowed to run for another 5 hrs. Once expression was complete, the bacterial cells were transferred into a clean centrifuge bottle. It was centrifuged at 7000rpm for 20 min at 4^{o}C. The pellets can be stored at -20^{o}C for the future purification process.

5.5.5 Purification of WT CaM:

After the pellet was thawed, 30mL homogenization buffer was added to 1L of cell pellet. Allowed to homogenize 4^{o}C to homogenize for 30 min using homogenization buffer (2mM EGTA, 50mM Tris, pH 7.5, 1mM PMSF (Phenylmethylsulfonyl fluoride), 1mM DTT. The samples were sonicated for 20sec, followed by 5 min rest for the pellets to cool down. This process was repeated 6 times. Sonicated samples were heated for 5min at 80-85^{o}C. The mixture was transferred to small centrifuge tubes, balance and centrifuge for 17,000 rpm for 40min at 4^{o}C. Then, supernatant and

pellet was separated out and stored for further analysis. 5mM $CaCl_2$ was added to supernatant. Supernatant was transferred into a clean beaker and was filtered through a 0.45um. It was ready for running through the hydrophobic WT-CaM column.

CaM wash buffer 1: 0.5mM CaCl2, 50mM Tris, pH 7.5 (75-100ml)

CaM wash buffer 2: 0.5mM CaCl2, 50mM Tris, 50mM NaCl, pH 7.5 (75-100ml)

CaM elution buffer: 50mM Tris, 5mM EGTA, pH 7.5 (75-100ml)

Preparing column:

The HIC WT CaM column was adjusted for the flow rate of 1-2 ml/min. The column was cleaned with filtered 20% ethanol (~50-75ml) to wash off the non-specific bindings, followed by filtered dd water (50-75ml) to remove ethanol, followed by wash buffer 1. The protein was allowed to run through the column overnight to ensure all the CaM is bound to the column. The column was washed with wash buffer 1, followed by wash buffer 2 to remove any unspecific-bound proteins from the column. Lastly, elution buffer was run through to elute out fractions of desired protein into six, 15ml falcon tube (collect 12-13ml/each). The purified CaM was dialyzed with 2L 10mM Tris buffer at pH 7.5 at 4^{o}C. The buffer was replaced every 1 hr three times. The last dialysis was left for O/N.

5.5.6 Western Blot:

Once the 7.5% gel is run, the gel is sandwiched between nitrocellulose membrane (0.45um) and filter paper. The box was filled with 1X transfer buffer and transfer chamber is run at 260mA for 2hrs or o/n at 22V at 4^{o}C. Next, tris-buffered saline with 0.1% tween (TBST) buffer was used to rinse the membrane off the salt from transfer buffer. The membrane was blocked with 5% bovine serum albumin (BSA) in the TBST for 1hr at RT for any non-specific binding proteins. Anti His 1˚ antibody mixture was prepared with 1:3000 dilution for Cx26-his-tagged protein and the

$$[Ca^{2+}]_{free} = K_d \cdot \frac{F - F_{min}}{F_{max} - F}$$ *Equation 5. 3*

membrane was incubated with the antibody o/n in cold box on. The membrane was rinsed with TBST for 15 min on a shaker at room temperature 3 times. The membrane was incubated with anti-mouse 2˚ antibody for 1hr, followed by TBST washes of 3 times, 15 min each. Finally, 1ml substrate and 25 ul of enhancer (enzyme) mix were applied for 5min in dark. The membrane was dried and chemiluminescence was used to visualize the western blot.

5.5.7 Fluorescence spectroscopy

Steady-state fluorescence spectra were recorded using a QM1 fluorescence spectrophotometer (PTI) in a 1 cm path length cell with a xenon short-arc lamp at 25°C. Intrinsic tryptophan (Trp) emission spectra were recorded using 2 μM and 4uM protein sample in 10mM HEPES at pH 7.4. The Trp fluorescence spectra were recorded from 500 to 600 nm with the excitation wavelength at 285 nm. The slit widths were set at 1.5 and 3.0 nm for excitation and emission, respectively. The Tb^{3+} titration experiments were performed by gradually adding 1-5 μl aliquots of Tb^{3+} stock solutions (200 mM) into the protein samples (2 and 4 μM). For the Ca^{2+} competition studies, the solution containing Tb^{3+} and protein was set as the starting point. The stock solution of 1M $CaCl_2$ with the same volume of Tb^{3+} was gradually added in the initial mixture. The fluorescence intensity was normalized by subtracting the contribution of the baseline slope using logarithmic fitting.

Equilibrium Ca^{2+} titrations were performed at room temperature using a previously described method [327]. CaM (8 μM) with $Cx26p_{1-21}$ peptide (molar ratio of 1:1.2) in 50 mM HEPES (pH 7.4), 100 mM KCl, 5 mM nitrilotriacetic acid (NTA) and 0.05 mM EGTA was titrated with 15 mM or 50 mM Ca^{2+} solution prepared in the same buffer. The intrinsic fluorescence of tyrosine (λ_{ex} = 277 nm, λ_{em}= 320 nm) or phenylalanine (λ_{ex} = 250 nm, λ_{em}= 280 nm) was used to

monitor the Ca^{2+} binding to the CaM C- and N-domains, respectively. The fluorescent Ca^{2+} indicator dye (0.2 μM) Oregon Green 488 BAPTA-5N (Oregon Green) was used to determine the free Ca^{2+} concentration at each titration point using equation as previously described.

Where, F represents the fluorescence intensity of Oregon Green at each titration point, while F_{max} and F_{min} represent the fluorescence intensity of dye at Ca^{2+}-saturated and Ca^{2+}- free states, respectively. Ca^{2+} titrations of CaM samples were repeated at least three times and fitted to a non-linear Hill equation.

$$f = \frac{[Ca^{2+}]^{n}_{free}}{Kd + [Ca^{2+}]^{n}_{free}} \qquad \textit{Equation 5. 4}$$

Where f is the fractional change in intrinsic fluorescence intensity, $[Ca^{2+}]^{n}_{free}$ is the concentration of free ionized Ca^{2+} in solution, K_d represents Ca^{2+} dissociation constant and n is the Hill coefficient.

5.5.8 Mass spectroscopy

The MALDI mass spectrometry analysis was performed by Dr. Chen Ma and Dr. Jingyou to analyze the purity of the sample with either contamination or degradation.

5.5.9 Mammalian Cell Expression

Frozen HeLa cells were recovered and allowed to grow in low glucose DMEM medium with 10% fetal bovine serum (FBS). They were split twice before they were prepared for transfection. For splitting cells, HBSS medium was used to rinse the excess DMEM (Dulbecco's Modified Eagle Medium), 1X trypsin was used to detach the cells and finally, DMEM was used to flush and homogenize the cells. These cells were transferred into smaller dishes with slides until the right confluency appeared. Lipofectamine 2000 (3X plasmid volume) was used to transfect the

cells with hCx26-EGFP plasmid (2ug each for small dishes) in OPTI-MEM serum reduced medium. After 5-6 hours of transfection, the medium was changed to DMEM.

5.5.10 Silver staining

12.5% gel was first fixed with 50% methanol, 12% HAc, 0.005% formalin. It was followed by a wash with 35% EtOH and sensitized with 0.002% $Na_2S_2O_3$. 0.25 silver nitrate, 0.0076% formalin was used to wash it. The gel was finally developed with 6% Na2CO3, 0.05% formalin. To stop the reaction, 50% methanol and 12% HAc was used.

5.5.11 Bioluminescence Resonance Energy Transfer (BRET)

The BRET assay was carried out on a TriStar LB941 multimode microplate reader. The HEK293 cells cotransfected with Venus-CaM and Cx26-Rluc were detached and suspended in sterilized BRET buffer (140 mM NaCl, 2.7 mM KCl, 1 mM CaCl2, 1 mM MgCl2, 0.37 mM NaH2PO4, 24 mM NaHCO3, 25 mM HEPES, 0.1 % Glucose) and distributed into 96-well plates. Before measurement, coelenterazine was added to a final concentration of 5 μM and sequential measurements were performed at 460 ± 25 nm and 525 ± 25 nm. In some cases, cells were treated either with BAPTA-AM (50 μM) or CaCl2 (5 mM $CaCl_2$ and 10 μM Ionomycin) or W7 (50 μM) for 20 min, 10 min, and 30 min, respectively, before BRET measurement. The average BRET signals from three experiments were plotted as a function of the ratio of acceptor over the donor.

5.5.12 Cx26p$_{1-21}$ peptide

The peptide derived from the cytoplasmic loop of Cx26 (Cx26p1-21, Ac-1MDWGTLQTILGGVNKHSTSI21-NH2) was obtained commercially from AnaSpec Inc. The peptide was > 90% pure on the basis of high-performance liquid chromatography and was used without further purification. Acylated N-termini and aminated C-termini were designed to mimic the protein environment and remove extra charges.

5.5.13 Circular Dichroism

CD spectra were recorded on a Jasco-810 spectropolarimeter at ambient temperature using a 0.1-cm path length quartz cuvette, an integration time of 1s and a scan rate of 100 nm/s. The far UV CD spectra of Cx26 full-length protein at 8 μM was carried out and each spectrum shown is the ellipticity (mdeg) as a function of wavelength.

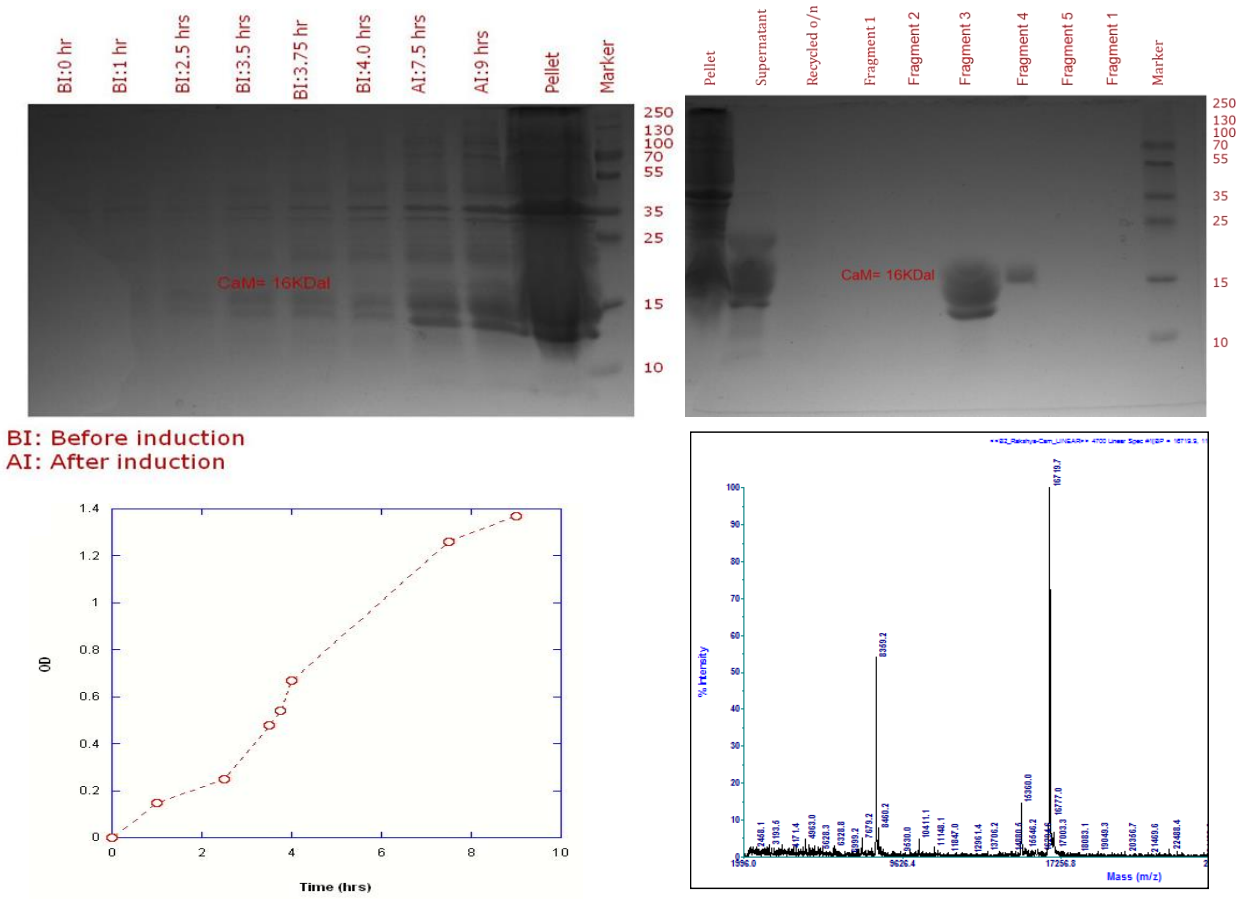

Figure 5.8 Expression and purification analysed

A. Expression Gel for WT CaM showing a distinct band for CaM at ~ 14 kDa. B. Purification Gel for WT CaM showing two distinct bands. wtCaM was successfully expressed and purified with a yield of 37.1 mg/L. C. Growth Curve for WT CaM expression is shown. D. MALDI spectrum indicated pure wtCaM.

5.6 RESULTS

5.6.1 Expression and purification of wtCaM

The purified CaM was quantified using absorbance at 277 nm contributed due to the tyrosin residue. Two fractions F3 and F2 showed the presence of CaM. 27ml of CaM protein was concentrated to ~3.2ml and gel was run for the purified CaM **(Figure 5.8)**. The concentration of purified CaM was found as 676 µM and yield was 37.1 mg/L. Two bands were observed that was close to 16kDa which were two forms of CaM bound with EGTA or Ca^{2+}. MALDI was carried out and it showed two peaks, one for 16 kDa and other for 8 kDa **(Figure 5.8D)**. The smaller indicates a degradation band.

5.6.2 Expression of hCx26 using C43(DE3)pLysS

The expression of hCx26 was optimized using varying temperatures, competent cells, IPTG concentrations and induction times. Similarly, purification was optimized using various detergents and methods. Table 1 is a summary of most of the optimization for expression. It was established that C43(DE3)pLysS in LB grown at 37°C induced at 1.4 OD with IPTG of 1 mM and

Table 5.2 Results of Various Expression Conditions

Competent cell	Medium	Temperature (°C)	OD at induction	Expression hours (h)	Expression Results
C43(DE3)pLysS	M9	27 or 30	1.1 (11 h)	17	Good
C43(DE3)pLysS	LB	37	1.4 (4.5 h)	18	Best
Rosetta gammi (DE3) pLysS	LB/M9	28/37	~1.0	16	None
Shuffle	M9	16 or 30	1.1 (9 h)	18-19	None
Shuffle	LB	16 or 30	1.1 (5.5 h)	21	OK (30 >16)°C
C43(DE3)	LB	27 or 37	1.1 (11 h)	17	Moderate
C43(DE3)	M9	27 or 37	1.4 (4.5 h)	18	Moderate

expression of 18 hr was the most optimal. DE3 lysogen contains T7 polymerase when induced by IPTG.

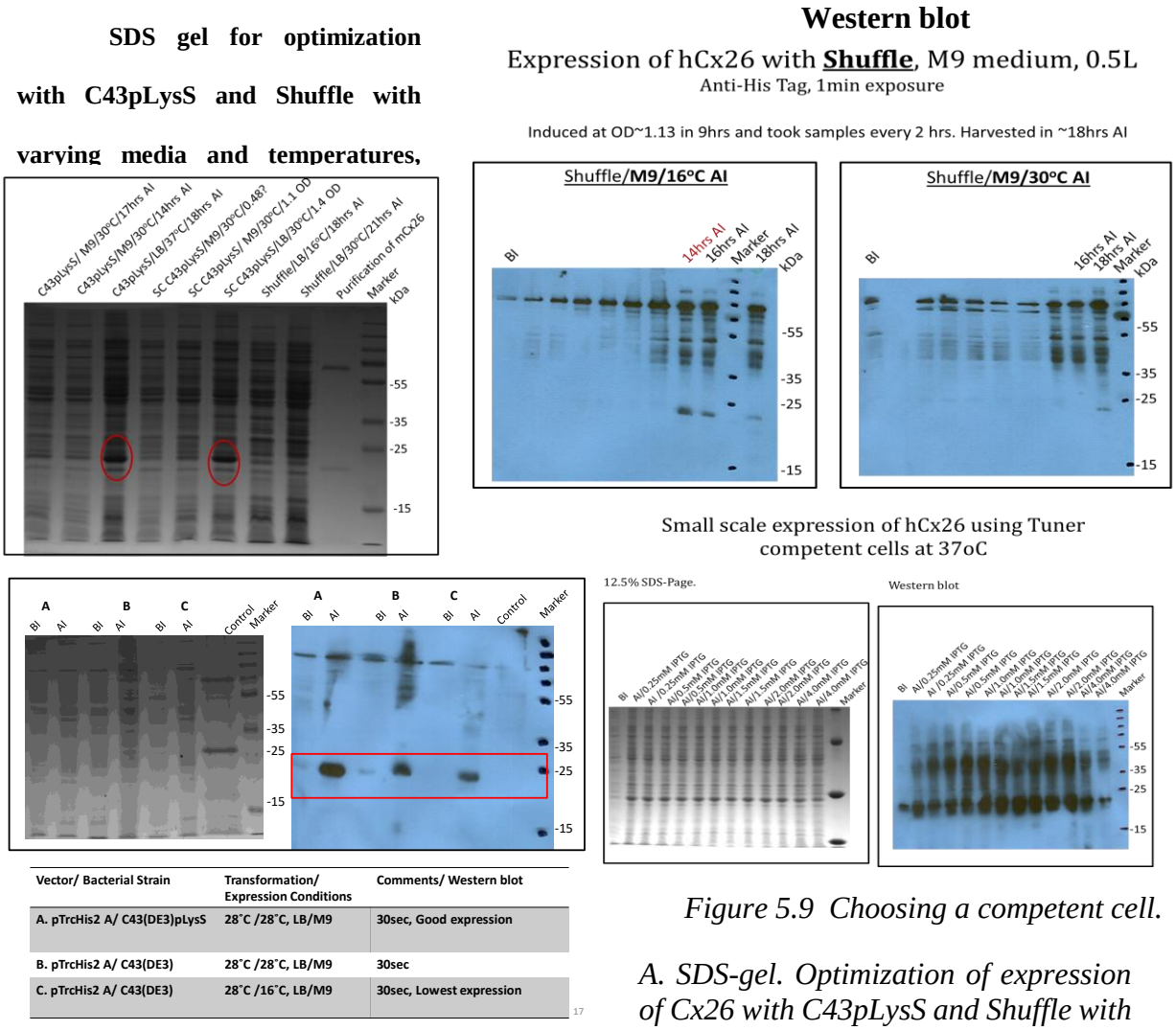

Figure 5.9 Choosing a competent cell.

A. SDS-gel. Optimization of expression of Cx26 with C43pLysS and Shuffle with varying media and temperatures, time of expression and ODs for induction. B. Western blot.

Additionally, the pLysS plasmid produced T7 lysozyme to reduce basal level expression of the gene of interest. Therefore, all in all, this strain of C43(DE3)pLysS is effective in expressing toxic and membrane proteins. We also used shuffle because it expresses chromosomal copy of disulfide

bond isomerase DsbC and promotes the correction of mis-oxidized protein into correct form, thus, correctly folds proteins with multiple disulfide bonds in the cytoplasm.

5.6.3 Purification of hCx26 using C43(DE3)pLysS

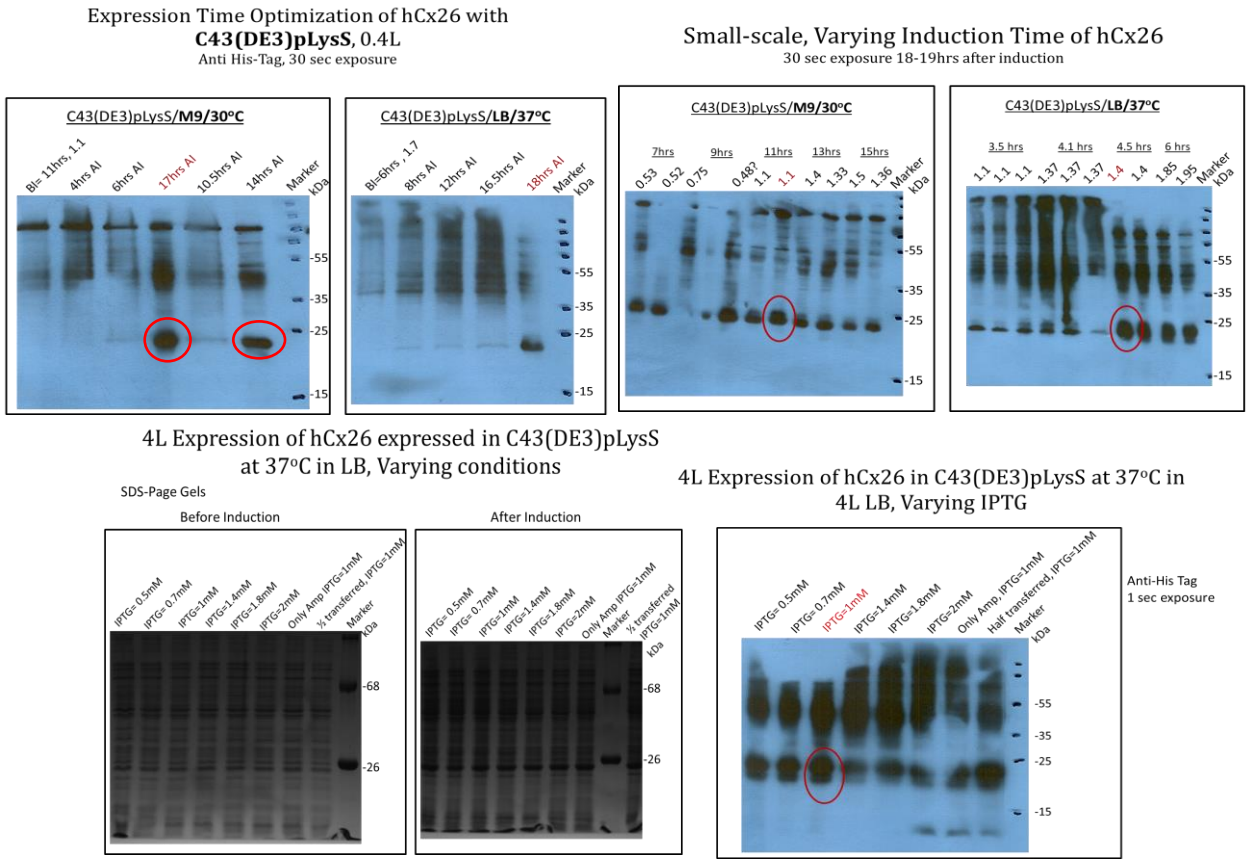

Figure 5.10 Optimization of expression of Cx26 in C43(DE3)pLyss.

It was determined that induction at 1.4 OD at 4.5 hrs of transfer of the small-scale strains, IPTG of 1mM and growth for 18 hrs after induction is the most optimal for maximum expression.

Various detergents and methods were applied to purify the hCx26.

Empigen and DDM: According to the preliminary comparison of the western blots of eluted fractions, empigen worked best to yield higher result. Due to presence of imidazole in our fractions, we couldn't quantify the fractions without the dialysis or anion exchange column, therefore, used western blot. 3.5% empigen was used to solubilize the membrane protein from the

supernatant and pellet separately after the cells were lysed and separated. Using 3.5% empigen on the cell pellets (condition I) produced prominent SDS bands for dimers (~52kDa) and anti-His tag

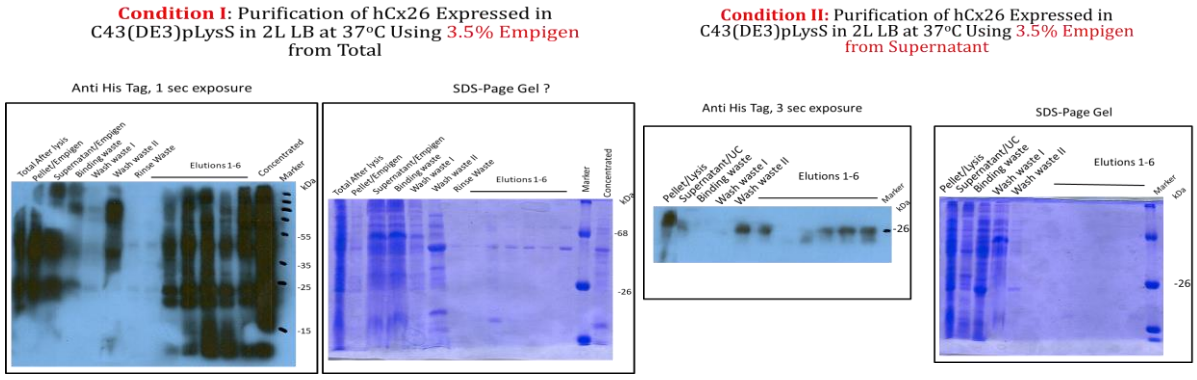

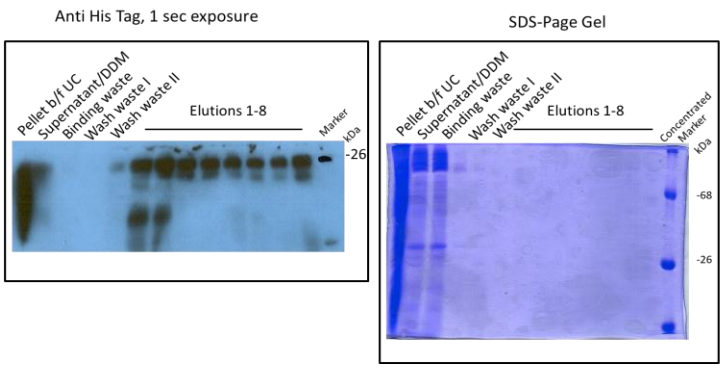

Figure 5.11 Using empigen for Cx26 purification

Condition I and II were used for purification where empigen was first used to solubilize the membrane proteins followed by either empigen or DDM to finally used to sustain the membrane protein in elution. Empigen worked better but the yield was low in uM range.

Purification Buffers	Condition I	Condition II
Lysis Buffer	75mM Tris HCl, 30mM NaCl, pH 7.7	75mM Tris HCl, 30mM NaCl, 0.2mM EDTA, pH 7.7
Solubilization buffer	10mM HEPES, 0.005% NaN_3, 500mM NaCl, pH=7.5	
Buffer I		40mM HEPES, 300mM NaCl, 3%Empigen, 1mM TCEP, pH=7.5
Wash buffer I	10mM HEPES, 500mM NaCl, 10mM Imidazole, 3%Empigen, pH=8	40mM HEPES, 300mM NaCl, 3%Empigen, 40mM Imidazole, 1mM TCEP, pH=8
Wash buffer II	10mM HEPES, 500mM NaCl, 3% Empigen, 40mM Imidazole, pH=8	0.1% DDM, 25mM sodium phosphate dibasic, 1mM TCEP, pH 7.2
Elution buffer	10mM HEPES, 150mM NaCl, 300mM Imidazole, pH 7.5	0.1% DDM, 1M imidazole, 1mM TCEP, pH 7.8
Dialysis buffer		1mM TCEP, 20mM Ammonium bicarbonate, pH 7.4

western blot confirmed the presence of both dimers and monomers. Condition II where we used with 3.5% empigen and 2% DDM on supernatant and cell pellet respectively produced less promising bands than that the first condition. The SDS bands were not visible, although the western blot still showed the monomers. After dialysis and quantitating the yield, the concentration was low µM range.

N-laurosarkosyl and octyl-glucoside: N-laurosarkosyl was used to lyse the total cell lysate and protein was eluted out in octyl-glucoside. 5L was purified again using the NLS-OG. The elution was concentrated to 0.5ml and gel filtration was carried out to separate the monomers. The elutions 8-10 and 20-23 were collected for gel analysis. Using UV_{280} the main fraction 14 was found to have 6.3 µM and yield of ~0.6mg/L.

Even after gel filtration, a lot of contamination or degraded products was observed in our fractions as can be seen in the silver stained gel and western blot above. Western blot and absorption at 280 showed that fraction 14 and 15 contained most protein. Fraction 15 was sent for MALDI analysis which show poor result for any protein close to 26 or 52 kDa. The peaks at 26kDa show small peak indicating our protein and other peaks indicated contamination/degradation.

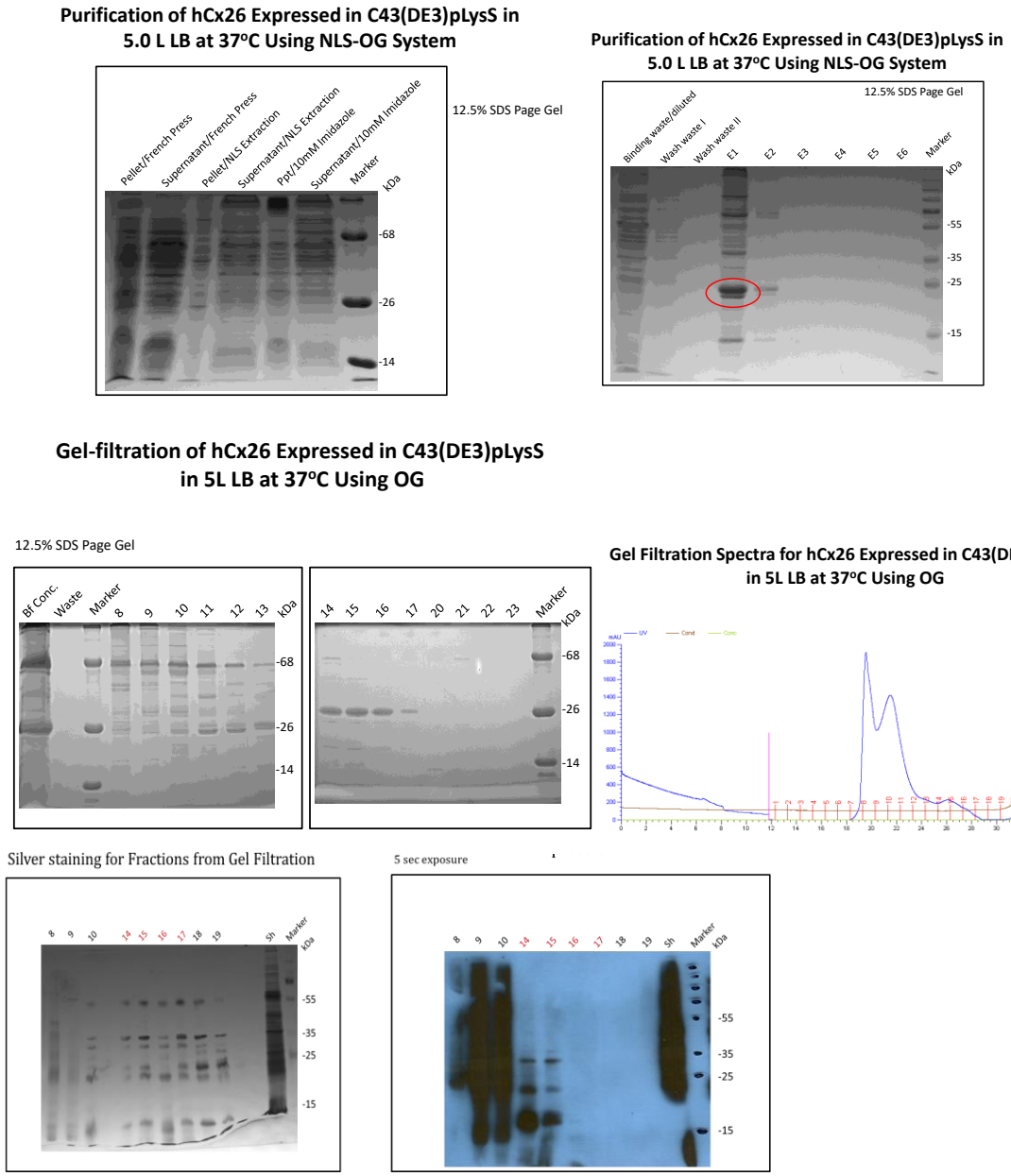

Figure 5.12 NGS/OG purification system.

N-laurosarkosyl was used to lyse the total cell lysate and protein was eluted out in octyl-glucoside. 5L was purified again using the NLS-OG. The elution was concentrated to 0.5ml and gel filtration was carried out to separate the monomers. The elutions 8-10 and 20-23 were collected for gel analysis. Using UV_{280} the main fraction 14 was found to have 6.3uM and yield of ~0.6mg/L.

5.6.4 Biophysical characterization of the hCx26 from bacteria

5.6.4.1 MALDI Mass spectrometry

MALDI showed a spectra at 37 and 35 kDa with low intensity instead of a 26 kDa monomer or an oligomer of 52, 78 or 156 kDa.

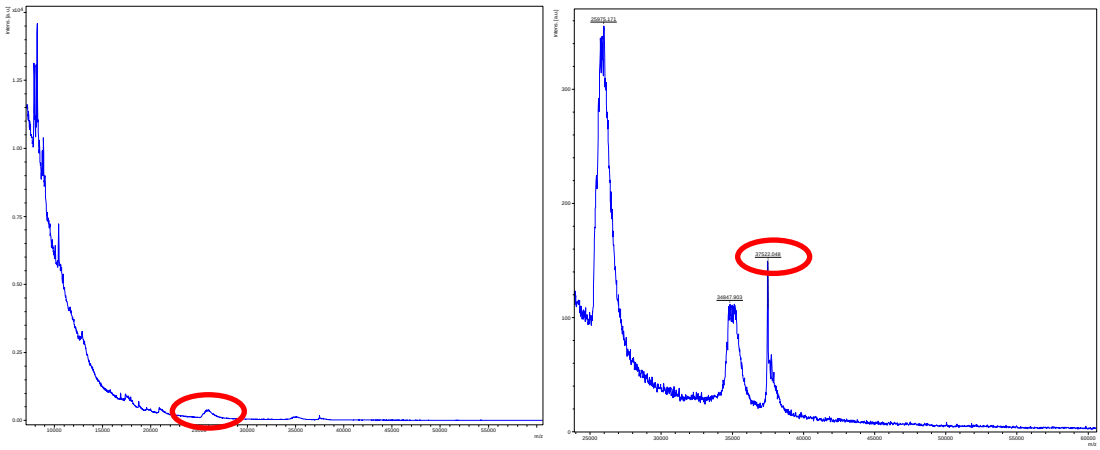

Figure 5.13 MALDI. Molecular weight of 37 kDa was observed.

5.6.4.2 Stability of secondary and tertiary structure of purified hCx26 from bacteria

Circular dichroism displayed a typical α-helical structure with an inverse peak between -208 and -222 nm for hCx26 purified. With Ca^{2+} and EGTA the structure changed but still retained the α-helical structure. In order to determine the proper folding of the protein, tryptophan emission of the purified Cx26 was compared with the free tryptophan. A blue shifted tryptophan emission spectrum was observed when the tryptophan emission at 340 was compared with free tryptophan which indicated that the tryptophan in our protein structure were in hydrophobic environment and therefore, well folded. The parameters used was:

[hCx26]= 2uM in 10mM Tris, 30mM OG, 200mM NaCl and pH=6.8; 800uL

Ex=280nm; Em=300-400nm; Slit: Ex=1.25; Em=2.50

The presence of detergent and NaCl in the buffer affected the CD spectra adding noise.

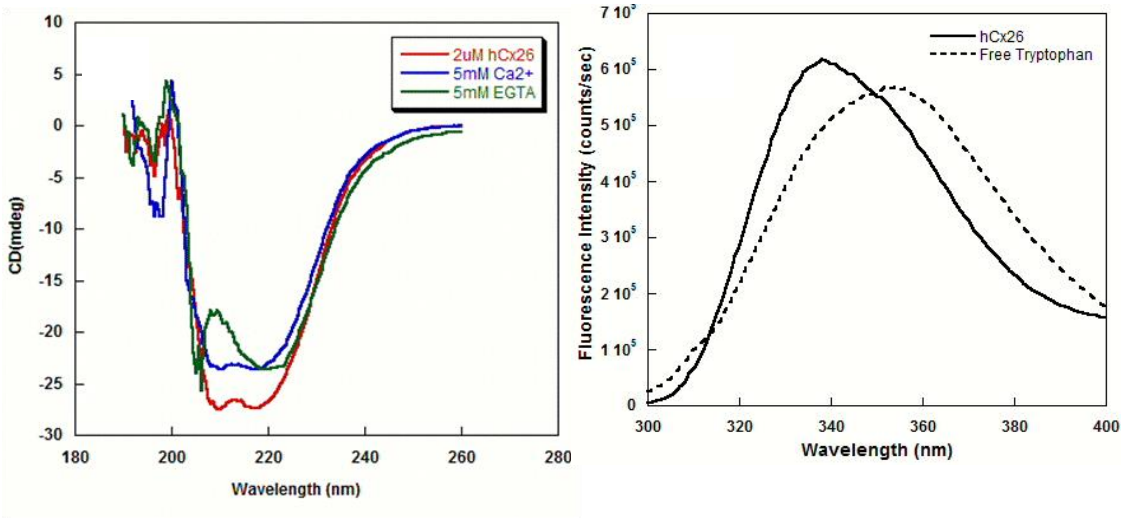

Figure 5.14 *Stability of secondary and tertiary structure of purified hCx26 from bacteria*

A. Typical α-helical structure was observed with an inverse peak between 210 and 220 nm for hCx26 purified. With Ca^{2+} and EGTA the structure changed but still retained the α-helical structure. B. The tertiary structure was observed comparing the tryptophan emission with free tryptophan.

5.6.4.3 Binding affinity using Tb^{3+}/Ca^{2+} fluorescence measurement

The purpose of this experiment is to obtain a binding affinity of Ca^{2+} to hCx26. Since, Ca^{2+} is not directly observed, Tb^{3+} is used in competition assay to get the K_d. 200mM of Tb was titrated into a 800 ul 6uM hCx26 in a 1cm pathlength cuvette. 500-600 nm spectrum was acquired with an excitation wavelength at 285nm. Energy transfer between two chromophores (namely, Trp and Tb^{3+}) is measured. Trp is excited by wavelength of 285nm and this is transferred to the nearby Tb^{3+}. The excited Tb^{3+} emits out the fluorescence between 500-600nm while returning to the

ground state. The efficiency of this transfer is dependent on the distance between the two chromophores, shorter the higher. The parameters used were [hCx26]= 2µM or 4uM in 10mM Tris, 30mM OG, 200mM NaCl and pH=6.8; 800uL, Ex=285nm; Em=500-600nm; Slit: Ex=1.25; Em=2.50

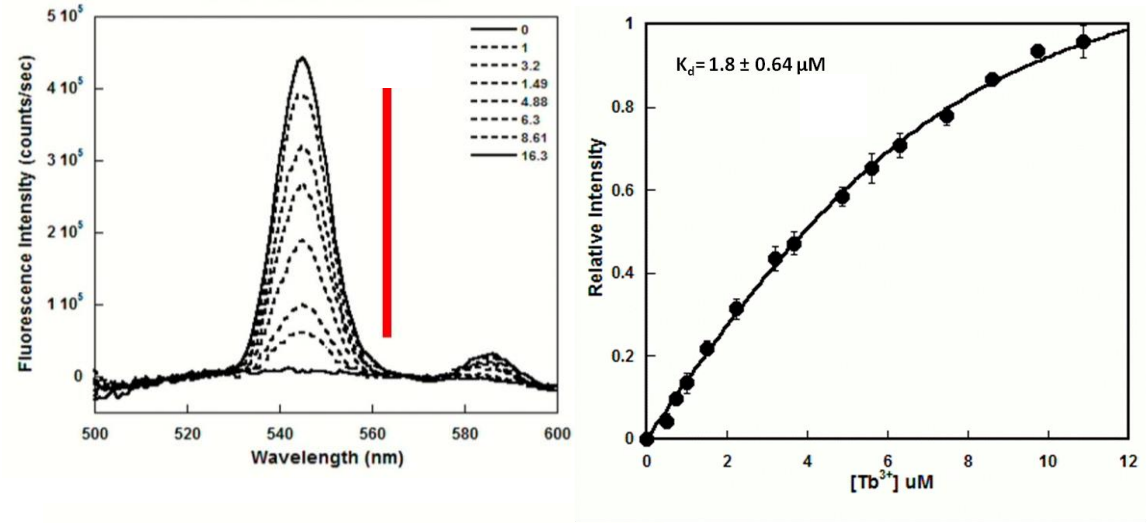

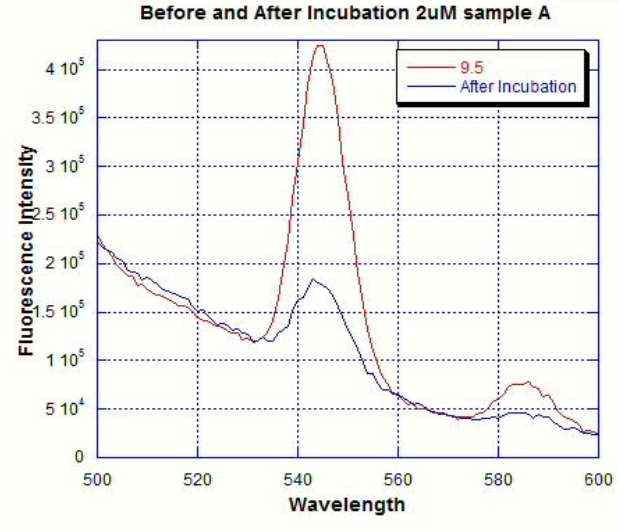

1.1.1.1 ***Figure 5.15*** *Binding affinity using Tb^{3+}/Ca^{2+} fluorescence measurement*

A. Tb^{3+} titration was carried out using 2uM hcx26 and carried out in triplicate. B. The Kd was found to be ~0.6 uM. It was comparable to the Kd observed by previous lab members on full length Cx26 from SF9. After incubation of protein with Tb^{3+} for 0.

K_d for Tb^{3+} for hCx26 from *E. coli*, was found to be in µM range similar to rCx26 from SF9 and E-1 grafted in CD2 from previous members **(Figure 5.15)**. K_d for Ca^{2+} for hCx26 from *E. coli* was found to be 37 mM **(Figure 5.16)**. Tb^{3+}/Ca^{2+} FRET assay indicated that Tb^{3+}/Ca^{2+} binds to hCx26. In order to make sure that the fluorescence change was directly proportional to the protein concentration, the Tb^{3+} titration was performed with 2uM and 4uM hCx26. But interestingly, the enhancement of the peak was not doubled at expected. Additionally, to check if the integrity of the protein were preserved, the fluorescence was observed before and after ~30min of incubation of the hCx26 with Tb^{3+}. The peak decreased drastically which must impact the calcium competition titration and K_d calculation. However, we still can observe the gradual decrease in the peak after calcium titration in hCx26 sample and not in the control buffer sample. This suggests that Tb^{3+} binding must change the protein conformation and therefore, the availability of tryptophan to Tb^{3+}, or that the protein precipitated during this incubation. However, we still can observe the gradual decrease in the peak after calcium titration in hCx26 sample and not in the control buffer sample.

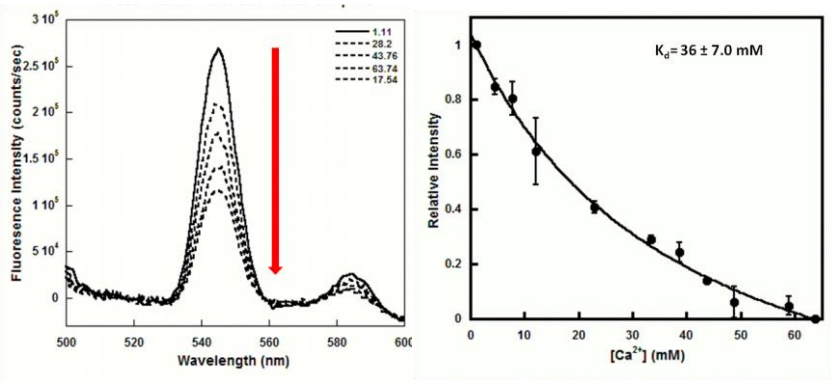

Figure 5.16 Ca^{2+} competition titration. K_d for Ca^{2+} for hCx26 from E. coli *was found to be 36 mM.*

5.6.4.4 *Effect of Cx26p$_{1-21}$ on the domain specific Ca^{2+}- binding affinity of CaM*

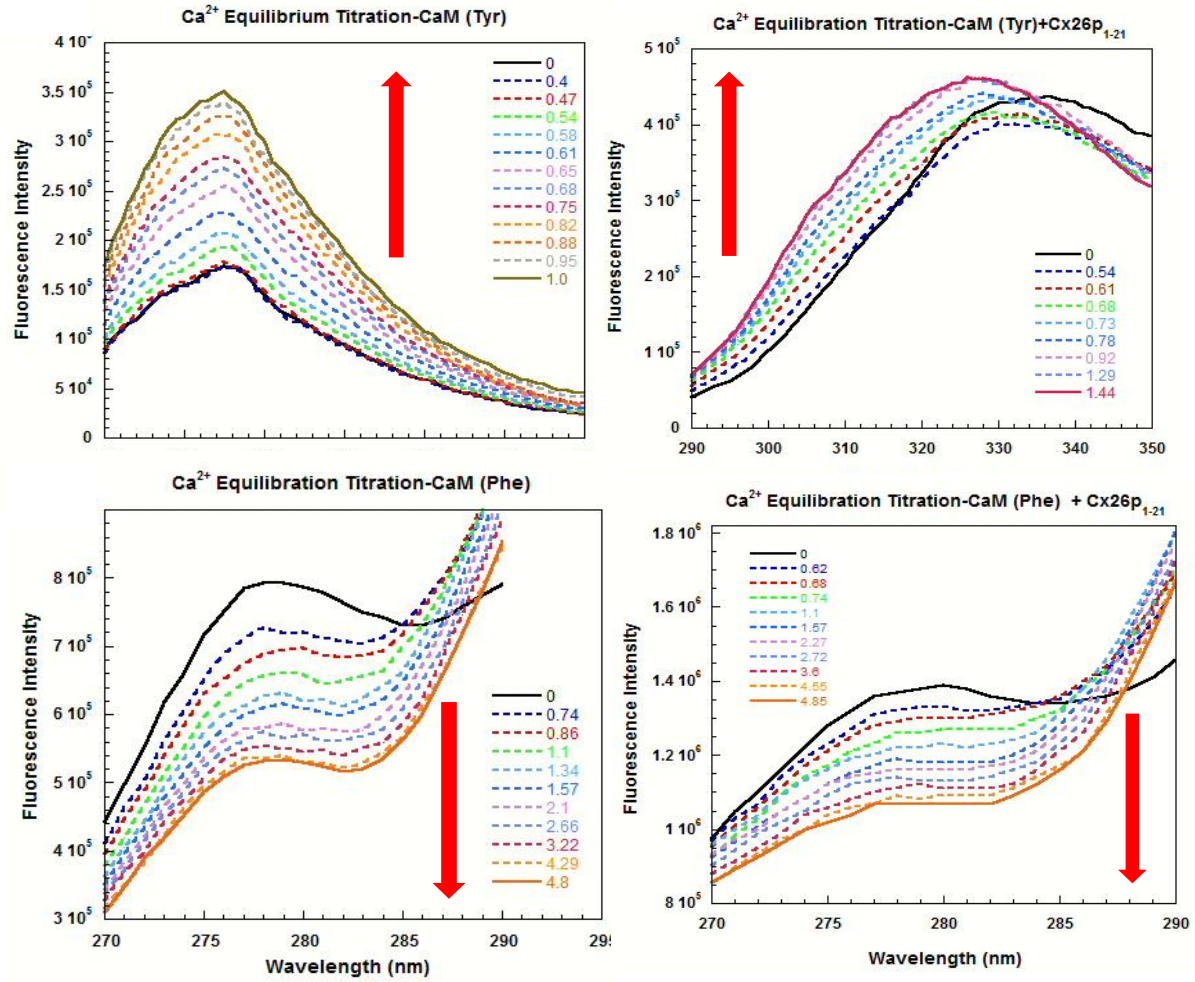

Figure 5.17 Effect of Cx26p$_{1-21}$ on the domain specific Ca^{2+}- binding affinity of CaM.

In the presence of Cx26p$_{1-21}$, the K_d of CaM to Ca^{2+} increased from 1.35 to 4.10 µM (A and B) and 2.9 to 3.87 µM (C and D) for the N-domain and C-domain, respectively. This suggested greater conformational change of the N-terminal lobe by greater than 2.5 folds than that of C-lobe of CaM upon Cx26p$_{1-21}$ binding

To examine Cx26p$_{1-21}$ contribution to the calcium binding affinity of CaM, calcium binding affinity of both N- and C-domain of CaM was determined by monitoring the intrinsic fluorescence intensity change of Phe and Tyr respectively. Binding of Ca^{2+} to the N-domain (Site I and II)

induced the decrease of Phe fluorescence intensity in the absence of Cx26p$_{1-21}$. The Phe fluorescence intensity upon addition of Ca^{2+} was plotted as a function of free calcium concentration determined by calcium indicator Oregon Green 488 BAPTA-5N and fitted by Hill equation. In the presence of Cx26p$_{1-21}$ (molar ratio of CaM: Cx26p$_{1-21}$ =1:1.2), the K_d increased from 1.35 to 4.10 µM indicating that calcium binding affinity to N-domain of CaM was significantly decreased. Similarly, binding of Ca^{2+} to the C-domain (Site I and II) induced the increase of Tyr fluorescence intensity in the absence of Cx26p$_{1-21}$. The Tyr fluorescence intensity upon addition of Ca^{2+} was plotted as a function of free calcium concentration determined by calcium indicator Oregon Green

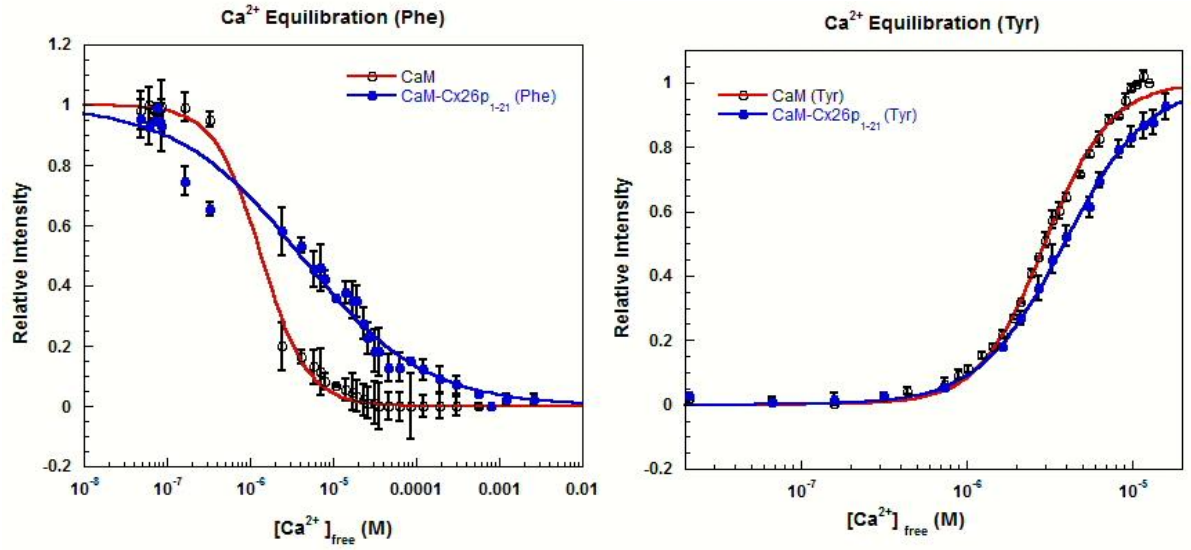

	Kd (uM)	Hill
CaM (Tyr)	2.9±4.28E-02	2.19±0.07
CaM-Cx26p1-21 (Tyr)	3.87±6.96E-02	1.7±0.05
CaM (Phe)	1.35± 9.8E-02	1.54±0.09
CaM-Cx26p1-21 (Phe)	4.10 ± 4.4E-1	0.58 ±0.03

Figure 5.18 Effect of Cx26p$_{1-21}$ on the domain specific Ca^{2+}- binding affinity of CaM fitted to Hill equation

The titration from figure 18 was fitted to Hill equation. In the presence of Cx26p$_{1-21}$, the K_d of CaM to Ca^{2+} increased from 1.35 to 4.10 µM (A) and 2.9 to 3.87 µM (B) for the N-domain and C-domain, respectively. This suggested greater conformational change of the N-terminal lobe by greater than 2.5 folds than that of C-lobe of CaM upon Cx26p$_{1-21}$ binding

488 BAPTA-5N and fitted by Hill equation. In the presence of $Cx26p_{1-21}$ (molar ratio of CaM: $Cx26p_{1-21}$ =1:1.2), the K_d increased from 2.9 to 3.87 µM indicating that calcium binding affinity to N-domain of CaM was significantly decreased.

5.6.5 Bioluminescence Resonance Energy Transfer (BRET)

Several combinations for the Cx26 and vectors Rluc and Venus were cloned. After sequencing results, it was confirmed that the Cx26-EYFPC1 and Cx26-RlucN1 were successfully cloned. To determine whether CaM associates directly with Cx26 full length in live cells, we used BRET. Here, in case of the association, the energy is transferred between the bioluminescent and fluorescent tags. Cx26 was tagged with bioluminescent Renilla reniformis luciferase (Rluc) at the C terminal and yellow fluorescent tag, Venus-C1, as cloned into CaM. The cells were co-transfected with fixed amount of Cx26 and increasing amount of Venus-CaM. Signal was determined as the ratio of light emitted at 525 nm over the light emitted at 460 nm. The BRET result with and without Ca^{2+} for Cx26 shows that there is no interaction between CaM with yellow fluorescence fusion protein, Venus-C1 and Cx26 with the Renilla luciferase (Rluc-C1) fusion protein. However, Cx45-Rlu was used as a control where Venus-CaM was capable of producing a significant BRET. Elevating $Ca^{2+}{}_i$ by pre-incubating cells with Ca^{2+}-ionomycin notably increased the BRET ratio one-fold. Taken together, these results suggest that there is. This implies that the interaction does not occur between the CaM and the C-terminus of Cx26.

5.6.6 Surface plasmon resonance

Ideally for a kinetic analysis, the maximal RU signal should be ~ 100 RU for protein: protein interaction. We observe a robust immobilization of Cx26 peptide but no response was observed for the CaM titration. This suggest that $Cx26p_{1-21}$ does not interact with CaM.

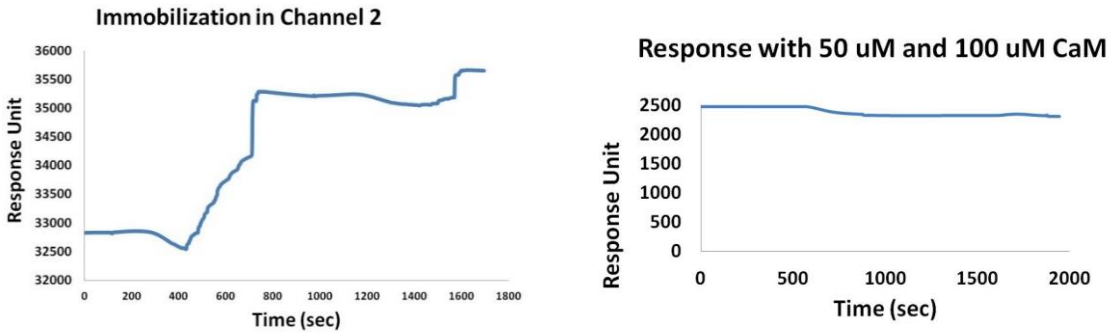

Figure 5.19 Surface plasmon resonance measuring interaction between Cx26 peptide and CaM.

A. A robust immobilization of Cx26 peptide was observed but B. no response was observed for the CaM titration. This suggest that $Cx26p_{1-21}$ does not interact with CaM.

5.7 Conclusion and Discussion

To study the modulation of hemichannel activity through $[Ca^{2+}]_o$, we first aimed at optimizing the expression and purification of hCx26 in bacteria. There were many limitations while working with the Cx26 protein. (1) Stability was limited at 4ºC for a narrow span of 12-24 hours post-purification, (2) the gravity column was required along with manual purification due to high probability of the oligomerization and therefore, clogging the FPLC column and (3) limitation with final yield of the protein even after the exhaustive steps of expression and purification. Even with the challenges, the expression of hCx26 was improved drastically with the use of C43(DE3)pLysS expressed in LB at 37ºC. The optimal OD for induction and expression period were 1.4 and 18hrs, respectively. Additionally, 1mM IPTG is optimum for maximal induction of

expression. Addition of glucose or $MgSo_4$ to the growth medium did not improve the expression level. 3.5% empigen was determined as the most suitable detergent for solubilization of intact and stable Cx26 membrane protein. However, the yield was limited to 0.6 mg/L and the purification was challenging due to the oligomerization and precipitation of the protein during the process.

The secondary and tertiary structures of the intact proteins were studies using circular dichroism and Trp fluorescence. CD displayed a typical α-helical structure with an inverse peak between -208 and -222 nm. With Ca^{2+} and EGTA the structure changed but still retained the α-helical structure. In order to determine the proper folding of the protein, tryptophan emission of the purified Cx26 was compared with the free tryptophan. A blue shifted tryptophan emission spectrum was observed when the tryptophan emission at 340 nm was compared with free tryptophan which indicated that the tryptophan in our protein structure were in hydrophobic environment and therefore, well folded.

Next, after obtaining the protein, fluorometry was used to determine the binding affinity of the hemichannel Cx26 to Tb^{3+} which was 1.8 μM and indirect Ca^{2+} competition of bound Tb^{3+} exhibited a weak K_d of 37 mM. However, we found that the fluorescence change was non-linear to the protein concentration during the competition. Additionally, we observed the dependence of fluorescence of the protein on the time of pre-incubation with Tb^{3+}. Both observations suggested protein conformation change or precipitation during these processes. Therefore, the result we obtained are not conclusive.

In order to understand the interaction between Cx26 and CaM, wt-CaM was successfully purified at 37 mg/L. Effect of $Cx26p_{1-21}$ on the domain-specific Ca^{2+}-binding affinity of CaM was examined by monitoring the intrinsic fluorescence intensity change of Phe and Tyr. In the presence of $Cx26p_{1-21}$, the K_d of CaM to Ca^{2+} increased from 1.35 to 4.10 μM and 2.9 to 3.87 μM for the N-

domain and C-domain, respectively. This suggested greater conformational change of the N-terminal lobe by greater than 2.5 folds than that of C-lobe of CaM upon $Cx26p_{1-21}$ binding. Further, the interaction between CaM and Cx26 in the living cell was examined using bioluminescence resonance energy transfer (BRET). Interaction between CaM with the yellow fluorescence fusion protein, Venus-C1 and Cx26 with the Renilla luciferase (Rluc-C1) fusion protein was found to be insignificant. This implies that the interaction does not occur between the CaM and the C-terminus of Cx26. This was further supported by surface plasmon resonance study where no significant binding was observed between CaM and $Cx26p_{1-21}$.

5.8 Major significance and future work

The expression of hCx26 has been improved with the use of C43(DE3)pLysS competent cells. Purification with 3.5% empigen has been found optimal for the intact hCx26 from bacterial. However, further optimization needs to be sought to improve the yield as well as purity and longer stability of hCx26 for additional biophysical interrogation. Using Tb^{3+} titration and Tb^{3+}/Ca^{2+} competition, it has been determined that K_d of hCx26 for Tb^{3+} as 0.6 μM and K_d for Ca^{2+} as 36 mM. It has been established that the C-terminus of Cx26 does not interact with the CaM using BRET. Other constructs need to be cloned and various combinations between Cx26- /CaM- and Rluc/ Venus needs to be studied using BRET to study the interactions in live cell.

6 CHAPTER VI: MAJOR FINDING AND FUTURE DIRECTIONS

Ca^{2+} is a universal signaling ion that regulates life. In this study, we focus on understanding the integral role of extracellular Ca^{2+} on the regulation of two major proteins, the first being the CaSR that maintain systemic calcium homeostasis and the second being the Cx26 that maintains cellular homeostasis. Chapter II touches on the importance of knowledge of the mode of regulation and regulators of the CaSR is enormous as it is widely expressed throughout the body sustaining life by maintaining Ca^{2+} homeostasis. In order to achieve this, we employed and established protocols after many optimizations for immunoprecipitation of CaSR and tandem mass spectrometry. With our finding of 98 new putative CaSR interactors and the first protein-protein interaction network, we take the field of calcium signaling and CaSR signaling to a new height. The knowledge allows us to survey potential pathways and regulators of CaSR that could potentially allow us to develop drugs to modulate CaSR activity, its biosynthesis, trafficking or degradation. This could very well be a potential target for other cGPCRs. Chapter II also probes and validates the critical role of extracellular Ca^{2+} in regulating these CaSR interactions. The direct role of CaSR as a mediator of extra- and intra- cellular Ca^{2+} signaling and the novel role of Ca^{2+}_o in modulating the CaSR mediated proteostasis of CaSR interactors/regulators is colossal. The putative CaSR interactors are significantly enriched in the ER as shown by the gene ontology analysis related to protein folding in the presence of Ca^{2+}_o. The work also indicates the direct role of CaSR mediated Ca^{2+} signaling with ER Ca^{2+} signaling and ER proteostasis. The cellular state is largely dependent on the ER Ca^{2+} homeostasis and therefore, this inter-relationship between Ca^{2+}, CaSR, and ER is large and allows us to take our research further into many avenues. Taken together, this study offers an insight into the interconnection of GPCR function, intracellular trafficking, and potential targets for Ca^{2+} homeostasis related pathogenesis of diseases.

CaSR-binding of some of the proteins such as Bip/GRP78 and CHIP has been validated through immunoassay and ICC. This chapter is a significant finding for the role of extracellular Ca^{2+} in CaSR biosynthesis and function, and it offers many potential future questions and projects: (1) Do most of the interacting proteins come from the ER compartment? If so, why? (2) Do proteins in the ER interact with functional plasma membrane CaSR through the process involved with bringing ER and plasma membrane to close proximity such as in the case of ORAI/STIM? (3) Is CaSR ubiquitination dependent on Ca^{2+}? Why? (4) Do the putative interactors directly or indirectly bind CaSR? (5) What is the mechanism for this alteration? (6) Do pathological cells such as cancer cells or tissues have similar interactors of CaSR as in HEK293 cells? (7) How does the ER Ca^{2+} signaling change during this process? (8) What are the interactors in normal cells in physiological conditions? Here, (1) and (2) can be explored using TIRF microscopy in live or fixed cells. (3) can be answered using ubiquitination assay. Ubiquitination of CaSR can be examined using co-IP in HEK293 cells and HEK293 cells with CHIP or RanBP2 shRNA knockdown. (4) and (5) need mechanistic studies with individual interactors. (6) and (8) can be achieved with the same experimental design with pathological tissues or cell or normal cells, respectively. To achieve (7), we can use ER sensors to measure and probe ER Ca^{2+} fluctuations in a live cell.

Chapter III examines the differential CaSR mediated intracellular signaling mechanism in HEK293 cells and thyroid cancer cells. Understanding the intracellular Ca^{2+} response due to CaSR activation is an important and most direct way of studying CaSR mechanism. Response to stimuli from extracellular Ca^{2+}, Mg^{2+}, drugs, and regulators provide us invaluable information on how to modulate CaSR and its effects at the molecular level. Furthermore, information on the dysfunction of CaSR in pathological cells offers us with the clue on how to mend CaSR to allow for better treatment conditions. The intracellular calcium oscillation facilitated by wild type CaSR activation

via Ca^{2+}_{o}, Mg^{2+} and tryptophan derivative (TNCA) is characterized in HEK293 cells. Ca^{2+} is more potent than Mg^{2+} to activate CaSR, and Ca^{2+} and Mg^{2+} cooperatively work together. This can be explained by the similar and shared residues both the ions coordinate to in their respective binding sites as shown in the crystal structure and the predicted binding site. Moreover, TNCA was able to act as a co-agonist and reduce the EC_{50} for both Ca^{2+} and Mg^{2+}, but more significantly for Mg^{2+} by 2.5 folds. Mutations at the Mg^{2+} binding sites, also ADH related mutations (E228I and E229I) resulted in impediment of the Ca^{2+}/Mg^{2+} CaSR sensing as well as CaSR mediated Mg^{2+} evoked Ca^{2+}_{i} mobilization and calcium oscillation. This information allows us to have a better understanding of mechanistic functioning of wild type CaSR as well as provides us with insight into ADH related dysfunctions.

Next, a thorough CaSR mediated mechanism in Ca^{2+} sensing mechanism was investigated in endogenous CaSR in thyroid carcinoma cells, human (TT) and rat thyroid medullary cancer cells (6-23), to understand the CaSR mediated Ca^{2+} sensing and were compared to the wild type hCaSR in HEK293 cells. A highly non-synchronous CaSR mediated oscillatory behavior was revealed in 6-23 cells. These cells contained a mixture of CaSR with variable activity, some with EC_{50} for Ca^{2+} at 0.5 mM and a lower Hill number of 1.5 and some that did not respond to Ca^{2+} even at 10 or 20 mM. Interestingly, the responding CaSR were selective to Ca^{2+} and not to Mg^{2+} implying biased signaling or Ca^{2+} selective binding site. On the contrary, TT cells demonstrated exclusively CaSR mediated transient peaks. Using the CaSR calcimimetics, calcilytics and W7 displayed significant changes to the CaSR mediated oscillatory patterns in both the cells. An overall change in oscillation distribution was determined with the use of CaSR allosteric agonist (cinacalcet) and antagonist (NPS-2143) as well as W7, an inhibitor of CaM, a CaSR regulating protein. Use of all three drugs displayed significant changes to the CaSR mediated oscillatory

patterns, start and end of oscillation, number of responding cells as well as oscillation frequency in the HEK293 cells. We showed for the first time that W7 is able to rescue partially the cinacalcet overactivation, or that cinacalcet can rescue the W7 inhibition. These results (1) validated the oscillation and transient peaks in C cells were at least partially CaSR mediated, (2) provides direct evidence of tissue and species-specific CaSR mediated signaling and (3) provides a hint towards biased signaling in C cells. (4) Our findings also provide an important insight in the modulation of intracellular Ca^{2+} signaling through regulation of CaSR activation by using CaSR agonist in C cells. This (4) provides an exciting platform in changing intracellular Ca^{2+} in C cells and indirectly controlling its Ca^{2+} dependent molecular functions, possibly for therapeutic purposes.

The investigation of the molecular cause of the above-mentioned differential signaling could be due to the presence of about six-fold lower expression in both 6-23 and TT cells as compared to stably wild type CaSR transfected HEK293 cells (5001) or transiently transfected HEK293 cells. We were able to show a variable pattern in the monomer and dimer forms of CaSR in C cells. Additionally, the effect in the trafficking of CaSR to the plasma membrane may affect the sensitivity of the CaSR. Further, RT-PCR method was used to characterize the CaSR in 6-23 but due to low transcript, the sequencing was partial. However, we showed for the first time that 6-23 contained CaSR with isoform I with 10 amino acid insertion in its 6^{th} exon. The full sequencing by RNAseq may provide us with valuable information on CaSR in C cells.

Similar to chapter III, chapter IV investigates the differential CaSR mediated $G\alpha_q$ associated $Ca^{2+}{}_i$ response, such as the intracellular calcium oscillation and IP_1 which were missing in PC3. Additionally, $ERK_{1/2}$ was perturbed as compared to the wild type CaSR in HEK293 cells. Even using the agonists could not rescue the CaSR mediated intracellular Ca^{2+} response. Overexpression of wild type CaSR in these cells cannot rescue these signaling indicating that PC3

may lack the $G\alpha_q$ and other necessary regulators required for the oscillation signaling. In order to explain these differences, PC3 cells and CaSR in these cells were studied at molecular levels. We noted CaSR in PC3 occurs as a monomer in non-reducing condition and has a lower molecular weight with 110 kDa, indicating incapability to form a dimer and presence of a variant with a splice-variant or lower glycosylation. PC3, on the contrary, is able to generate a dimer when artificially transfected. Immunostaining showed that most CaSR occurs within the cell as compared to functional plasma membrane CaSR. Next, using RT-PCR we showed that a full CaSR with all seven exons are present. These results support that the CaSR in PC3 is present in the immature stage.

To understand the PC3 cells better, we carried the global proteomics to understand shed light into the changes we observed. We note that global proteome is highly differential between the HEK293 cells and PC3 cells where the observation of CaSR through MS is null and general proteome increased in PC3 cells. The gene ontology of proteins in Ca^{2+} and EGTA conditions vary in PC3 where the citric acid cycle and trans-Golgi related proteins are upregulated in Ca^{2+}. The proteomics is the integrative way to understand the biomarkers for prostate cancer but proper controls such as the normal prostate and prostate cancer at various states could be used for the comparison. Our results and methods will contribute to the future work to understand PC3 cells and CaSR in PC3 cells, as well as other pathological cells.

The previous study in our laboratory has indicated the involvement of CaSR in PC3 colonization in bones by preventing cell apoptosis of cancer cells, inhibiting invasion, and promoting mesenchymal-epithelial transition. My work in-vivo in collaboration with Dr. Wu showed a significant decrease in tumor growth when PC3 cells with CaSR knockdown and control knockdown are injected in mouse tibia in the presence of zoledronic acid. This result proves the

essential role of Ca^{2+} in prostate cancer proliferation in the bone. My work provides fundamental information of PC3 cell line as well as the role and molecular function of CaSR in PC3 cells. Further work is required to obtain decisive pathways and mechanisms in this context.

In Chapter V we demonstrate that the expression of hCx26 has been improved with the use of C43(DE3)pLysS. Purification with 3.5% empigen has been found optimal for the intact hCx26 from bacterial. However, further optimization needs to be sought to improve the yield as well as purity and longer stability of hCx26 for additional biophysical interrogation. This intensive optimization will allow the future investigator to obtain higher expression of hCx26 and to solely focus on purification and characterization. This method could be used for other full membrane expression as well. Using Tb^{3+} titration and Tb^{3+}/Ca^{2+} competition, we have determined that K_d of hCx26 for Tb^{3+} as 0.6 μM and K_d for Ca^{2+} as 36 mM. It has been established that the C-terminus of Cx26 does not interact with the CaM using BRET. Other constructs need to be cloned and various combinations between Cx26- /CaM- and Rluc/ Venus needs to be studied using BRET to study the interactions in live cell.

7 PUBLICATIONS AND MANUSCRIPTS IN PROGRESS

- **R. Gorkhali et al.** "Global effect of extracellular calcium ion on calcium-sensing receptor interactome". 2019. (In working version)
- **R. Gorkhali**, X. Tan, J. Yang. "Calcium-sensing receptor". Book chapter. *Encyclopedia of signaling molecules.* 2017.
- M. Kirberger, **R. Gorkhali**, M. Salarian, J. Yang. "CaM". Book Chapter. *Encyclopedia of signaling molecules.* 2017.
- F. Reddish, C. Miller, **R. Gorkhali,** J. Yang. "Monitoring ER/SR calcium release with the targeted Ca^{2+} sensor CatchER". *J Vis Exp.* 2017.
- F. Reddish, C. Miller, **R. Gorkhali**, Yang J. J. "Calcium Dynamics Mediated by the endoplasmic/Sarcoplasmic Reticulum and Related diseases". *Int J Mol Sci.* 2017. 18 (5).
- **R. Gorkhali,** K. Huang, M. Kirberger, J. Yang. "Defining potential roles of Pb^{2+} in neurotoxicity from a calciomics approach". *Metallomics*. 2016. 8: 563-578.
- C. Zhang, T. Zhang, J. Zou, C. Miller, **R. Gorkhali**, J. Yang, K. Huang, E. Brown, K. Moremen, J. Hu, J. Yang. "Structural basis for regulation of human calcium-sensing receptor by magnesium ions and an unexpected tryptophan derivative co-agonist". *Science Advances*. 2016. 2:1-9.
- C. Zhang, C. Miller**, R. Gorkhali**, J. Zou, K. Huang, E. Brown, J. Yang. "Molecular Basis of the Extracellular Ligand Mediated Signaling by Calcium-sensing Receptor." *Front Physiol*. 2016. 7: 441.

8 REFERENCES

1. Diaz-Soto, G., et al., *The Calcium-Sensing Receptor in Health and Disease.* Int Rev Cell Mol Biol, 2016. **327**: p. 321-369.
2. Tennakoon, S., A. Aggarwal, and E. Kallay, *The calcium-sensing receptor and the hallmarks of cancer.* Biochim Biophys Acta, 2016. **1863**(6 Pt B): p. 1398-407.
3. Huang, Y., et al., *Calmodulin regulates Ca2+-sensing receptor-mediated Ca2+ signaling and its cell surface expression.* J Biol Chem, 2010. **285**(46): p. 35919-31.
4. Gorkhali, R., X. Tan, and J.J. Yang, *Calcium Sensing Receptor (CASR).* Encyclopedia of Signaling Molecules, 2018: p. 662-668.
5. Hannan, F.M., et al., *The calcium-sensing receptor in physiology and in calcitropic and noncalcitropic diseases.* Nature Reviews Endocrinology, 2019. **15**(1): p. 33-51.
6. Raue, F. and H. Scherubl, *Extracellular calcium sensitivity and voltage-dependent calcium channels in C cells.* Endocr Rev, 1995. **16**(6): p. 752-64.
7. Terrillon, S. and M. Bouvier, *Roles of G-protein-coupled receptor dimerization.* EMBO Rep, 2004. **5**(1): p. 30-4.
8. Zhang, C., et al., *Molecular Basis of the Extracellular Ligands Mediated Signaling by the Calcium Sensing Receptor.* Front Physiol, 2016. **7**: p. 441.
9. Muller, D.J., et al., *Conformational changes in surface structures of isolated connexin 26 gap junctions.* EMBO J, 2002. **21**(14): p. 3598-607.
10. Marie, P.J., *The calcium-sensing receptor in bone cells: a potential therapeutic target in osteoporosis.* Bone, 2010. **46**(3): p. 571-6.
11. Wagner, C., *Function of connexins in the renal circulation.* Kidney Int, 2008. **73**(5): p. 547-55.
12. Fajtova, V.T., S.J. Quinn, and E.M. Brown, *Cytosolic calcium responses of single rMTC 44-2 cells to stimulation with external calcium and potassium.* Am J Physiol, 1991. **261**(1 Pt 1): p. E151-8.
13. Haller-Brem, S., et al., *Role of cytosolic free calcium concentration in the secretion of calcitonin gene-related peptide and calcitonin from medullary thyroid carcinoma cells.* Endocrinology, 1987. **121**(4): p. 1272-7.
14. Grant, M.P., et al., *Agonist-driven maturation and plasma membrane insertion of calcium-sensing receptors dynamically control signal amplitude.* Sci Signal, 2011. **4**(200): p. ra78.
15. Lai-Cheong, J.E., K. Arita, and J.A. McGrath, *Genetic diseases of junctions.* J Invest Dermatol, 2007. **127**(12): p. 2713-25.

16. Desai, A.J., et al., *Role of receptor activity modifying protein 1 in function of the calcium sensing receptor in the human TT thyroid carcinoma cell line.* PLoS One, 2014. **9**(1): p. e85237.

17. Peacock, M., *Calcium metabolism in health and disease.* Clin J Am Soc Nephrol, 2010. **5 Suppl 1**: p. S23-30.

18. Thimm, J., et al., *Calcium-dependent open/closed conformations and interfacial energy maps of reconstituted hemichannels.* J Biol Chem, 2005. **280**(11): p. 10646-54.

19. Wang, L., et al., *Nanosized particles in bone and dissolution insensitivity of bone mineral.* Biointerphases, 2006. **1**(3): p. 106-11.

20. Campbell, A.K., *Calcium as an intracellular regulator.* Proc Nutr Soc, 1990. **49**(1): p. 51-6.

21. Bootman, M.D., et al., *Calcium signalling--an overview.* Semin Cell Dev Biol, 2001. **12**(1): p. 3-10.

22. Robertson, W.G. and R.W. Marshall, *Calcium measurements in serum and plasma--total and ionized.* CRC Crit Rev Clin Lab Sci, 1979. **11**(3): p. 271-304.

23. Clapham, D.E., *Calcium signaling.* Cell, 2007. **131**(6): p. 1047-58.

24. Strynadka, N.C. and M.N. James, *Crystal structures of the helix-loop-helix calcium-binding proteins.* Annu Rev Biochem, 1989. **58**: p. 951-98.

25. Bazydlo, L.A.L., M. Needham, and N.S. Harris, *Calcium, Magnesium, and Phosphate.* Labmedicine, 2014. **45**(1): p. E44-E50.

26. Cates, M.S., M.L. Teodoro, and G.N. Phillips, Jr., *Molecular mechanisms of calcium and magnesium binding to parvalbumin.* Biophys J, 2002. **82**(3): p. 1133-46.

27. Dudev, M. and C. Lim, *Discovering structural motifs using a structural alphabet: Application to magnesium-binding sites.* Bmc Bioinformatics, 2007. **8**.

28. Dudev, T., J.A. Cowan, and C. Lim, *Competitive binding in magnesium coordination chemistry: Water versus ligands of biological interest.* Journal of the American Chemical Society, 1999. **121**(33): p. 7665-7673.

29. Falke, J.J., et al., *Molecular tuning of ion binding to calcium signaling proteins.* Q Rev Biophys, 1994. **27**(3): p. 219-90.

30. Brown, E.M., et al., *Cloning and characterization of an extracellular Ca(2+)-sensing receptor from bovine parathyroid.* Nature, 1993. **366**(6455): p. 575-80.

31. Hendy, G.N. and L. Canaff, *Calcium-Sensing Receptor Gene: Regulation of Expression.* Front Physiol, 2016. **7**: p. 394.

32. Smajilovic, S., et al., *The calcium-sensing receptor and calcimimetics in blood pressure modulation.* Br J Pharmacol, 2011. **164**(3): p. 884-93.

33. Breitwieser, G.E., *Pharmacoperones and the calcium sensing receptor: exogenous and endogenous regulators.* Pharmacol Res, 2014. **83**: p. 30-7.

34. Heilbrunn, L.V., *An outline of general physiology*. 1937, Philadelphia, London,: W.B. Saunders Company. 3 p. l., 11-608 p.

35. Potts, J.T. and T.J. Gardella, *Progress, paradox, and potential: parathyroid hormone research over five decades.* Ann N Y Acad Sci, 2007. **1117**: p. 196-208.

36. Jurutka, P.W., et al., *Molecular nature of the vitamin D receptor and its role in regulation of gene expression.* Rev Endocr Metab Disord, 2001. **2**(2): p. 203-16.

37. Quinn, S.J., et al., *The Ca2+-sensing receptor: a target for polyamines.* Am J Physiol, 1997. **273**(4 Pt 1): p. C1315-23.

38. Hofer, A.M. and E.M. Brown, *Extracellular calcium sensing and signalling.* Nat Rev Mol Cell Biol, 2003. **4**(7): p. 530-8.

39. Conigrave, A.D. and D.T. Ward, *Calcium-sensing receptor (CaSR): pharmacological properties and signaling pathways.* Best Pract Res Clin Endocrinol Metab, 2013. **27**(3): p. 315-31.

40. Quinn, S.J., M. Bai, and E.M. Brown, *pH Sensing by the calcium-sensing receptor.* J Biol Chem, 2004. **279**(36): p. 37241-9.

41. Saidak, Z., et al., *Agonists and allosteric modulators of the calcium-sensing receptor and their therapeutic applications.* Mol Pharmacol, 2009. **76**(6): p. 1131-44.

42. Handlogten, M.E., et al., *Extracellular Ca(2+)-sensing receptor is a promiscuous divalent cation sensor that responds to lead.* Am J Physiol Renal Physiol, 2000. **279**(6): p. F1083-91.

43. Spurney, R.F., et al., *Aluminum is a weak agonist for the calcium-sensing receptor.* Kidney Int, 1999. **55**(5): p. 1750-8.

44. Gorkhali, R., et al., *Defining potential roles of Pb(2+) in neurotoxicity from a calciomics approach.* Metallomics, 2016. **8**(6): p. 563-78.

45. McGehee, D.S., et al., *Mechanism of extracellular Ca2+ receptor-stimulated hormone release from sheep thyroid parafollicular cells.* J Physiol, 1997. **502 (Pt 1)**: p. 31-44.

46. Brown, E.M., *Extracellular Ca2+ sensing, regulation of parathyroid cell function, and role of Ca2+ and other ions as extracellular (first) messengers.* Physiol Rev, 1991. **71**(2): p. 371-411.

47. Brown, E.M., et al., *Neomycin mimics the effects of high extracellular calcium concentrations on parathyroid function in dispersed bovine parathyroid cells.* Endocrinology, 1991. **128**(6): p. 3047-54.

48. Katz, C.L., et al., *Structure-function relationships for the effects of various aminoglycoside antibiotics on dispersed bovine parathyroid cells.* Endocrinology, 1992. **131**(2): p. 903-10.

49. Ward, D.T., S.J. McLarnon, and D. Riccardi, *Aminoglycosides increase intracellular calcium levels and ERK activity in proximal tubular OK cells expressing the extracellular calcium-sensing receptor.* J Am Soc Nephrol, 2002. **13**(6): p. 1481-9.

50. Pace, A.J., L. Gama, and G.E. Breitwieser, *Dimerization of the calcium-sensing receptor occurs within the extracellular domain and is eliminated by Cys --> Ser mutations at Cys101 and Cys236.* J Biol Chem, 1999. **274**(17): p. 11629-34.

51. Magno, A.L., B.K. Ward, and T. Ratajczak, *The calcium-sensing receptor: a molecular perspective.* Endocr Rev, 2011. **32**(1): p. 3-30.

52. Brennan, S.C. and A.D. Conigrave, *Regulation of cellular signal transduction pathways by the extracellular calcium-sensing receptor.* Curr Pharm Biotechnol, 2009. **10**(3): p. 270-81.

53. Chang, W. and D. Shoback, *Extracellular Ca2+-sensing receptors--an overview.* Cell Calcium, 2004. **35**(3): p. 183-96.

54. Breitwieser, G.E., *Calcium sensing receptors and calcium oscillations: calcium as a first messenger.* Curr Top Dev Biol, 2006. **73**: p. 85-114.

55. Huang, C. and R.T. Miller, *The calcium-sensing receptor and its interacting proteins.* J Cell Mol Med, 2007. **11**(5): p. 923-34.

56. Wellendorph, P. and H. Brauner-Osborne, *Molecular basis for amino acid sensing by family C G-protein-coupled receptors.* Br J Pharmacol, 2009. **156**(6): p. 869-84.

57. Cheng, S.X., J.P. Geibel, and S.C. Hebert, *Extracellular polyamines regulate fluid secretion in rat colonic crypts via the extracellular calcium-sensing receptor.* Gastroenterology, 2004. **126**(1): p. 148-58.

58. Tu, C.L., et al., *The role of the calcium-sensing receptor in epidermal differentiation.* Cell Calcium, 2004. **35**(3): p. 265-73.

59. Mathias, R.S., et al., *Identification of the calcium-sensing receptor in the developing tooth organ.* J Bone Miner Res, 2001. **16**(12): p. 2238-44.

60. Hinson, T.K., et al., *Identification of putative transmembrane receptor sequences homologous to the calcium-sensing G-protein-coupled receptor.* Genomics, 1997. **45**(2): p. 279-89.

61. Cheng, I., et al., *Identification and localization of the extracellular calcium-sensing receptor in human breast.* J Clin Endocrinol Metab, 1998. **83**(2): p. 703-7.

62. Cima, R.R., et al., *Identification and functional assay of an extracellular calcium-sensing receptor in Necturus gastric mucosa.* Am J Physiol, 1997. **273**(5 Pt 1): p. G1051-60.

63. Buchan, A.M., et al., *Mechanism of action of the calcium-sensing receptor in human antral gastrin cells.* Gastroenterology, 2001. **120**(5): p. 1128-39.

64. Lundgren, S., et al., *A protein involved in calcium sensing of the human parathyroid and placental cytotrophoblast cells belongs to the LDL-receptor protein superfamily.* Exp Cell Res, 1994. **212**(2): p. 344-50.

65. Brown, E.M., *Physiology and pathophysiology of the extracellular calcium-sensing receptor.* Am J Med, 1999. **106**(2): p. 238-53.

66. Brown, E.M. and R.J. MacLeod, *Extracellular calcium sensing and extracellular calcium signaling.* Physiol Rev, 2001. **81**(1): p. 239-297.

67. Chattopadhyay, N., et al., *Extracellular calcium-sensing receptor induces cellular proliferation and activation of a nonselective cation channel in U373 human astrocytoma cells.* Brain Res, 1999. **851**(1-2): p. 116-24.

68. Hebert, S.C., *Extracellular calcium-sensing receptor: implications for calcium and magnesium handling in the kidney.* Kidney Int, 1996. **50**(6): p. 2129-39.

69. Hofer, A.M., et al., *The extracellular calcium-sensing receptor and cell-cell signaling in epithelia.* Cell Calcium, 2004. **35**(3): p. 297-306.

70. Fudge, N.J. and C.S. Kovacs, *Physiological studies in heterozygous calcium sensing receptor (CaSR) gene-ablated mice confirm that the CaSR regulates calcitonin release in vivo.* BMC Physiol, 2004. **4**(1): p. 5.

71. Kovacs, C.S., et al., *Regulation of murine fetal-placental calcium metabolism by the calcium-sensing receptor*. J Clin Invest, 1998. **101**(12): p. 2812-20.

72. Rey, O., et al., *Amino acid-stimulated Ca2+ oscillations produced by the Ca2+-sensing receptor are mediated by a phospholipase C/inositol 1,4,5-trisphosphate-independent pathway that requires G12, Rho, filamin-A, and the actin cytoskeleton.* J Biol Chem, 2005. **280**(24): p. 22875-82.

73. Evron, T., T.L. Daigle, and M.G. Caron, *GRK2: multiple roles beyond G protein-coupled receptor desensitization.* Trends Pharmacol Sci, 2012. **33**(3): p. 154-64.

74. Zhang, C., et al., *Role of Ca2+ and L-Phe in regulating functional cooperativity of disease-associated "toggle" calcium-sensing receptor mutations.* PLoS One, 2014. **9**(11): p. e113622.

75. Loretz, C.A., *Extracellular calcium-sensing receptors in fishes.* Comp Biochem Physiol A Mol Integr Physiol, 2008. **149**(3): p. 225-45.

76. Herberger, A.L. and C.A. Loretz, *Vertebrate extracellular calcium-sensing receptor evolution: selection in relation to life history and habitat.* Comp Biochem Physiol Part D Genomics Proteomics, 2013. **8**(1): p. 86-94.

77. Huang, Y., et al., *Multiple Ca(2+)-binding sites in the extracellular domain of the Ca(2+)-sensing receptor corresponding to cooperative Ca(2+) response.* Biochemistry, 2009. **48**(2): p. 388-98.

78. Geng, Y., et al., *Structural mechanism of ligand activation in human calcium-sensing receptor.* Elife, 2016. **5**.

79. Bai, M., et al., *Expression and characterization of inactivating and activating mutations in the human Ca2+o-sensing receptor.* J Biol Chem, 1996. **271**(32): p. 19537-45.

80. Bai, M., S. Trivedi, and E.M. Brown, *Dimerization of the extracellular calcium-sensing receptor (CaR) on the cell surface of CaR-transfected HEK293 cells.* J Biol Chem, 1998. **273**(36): p. 23605-10.

81. Hendy, G.N., V. Guarnieri, and L. Canaff, *Calcium-sensing receptor and associated diseases.* Prog Mol Biol Transl Sci, 2009. **89**: p. 31-95.

82. Ward, B.K., et al., *The role of the calcium-sensing receptor in human disease.* Clin Biochem, 2012. **45**(12): p. 943-53.

83. Hannan, F.M., et al., *Identification of 70 calcium-sensing receptor mutations in hyper- and hypo-calcaemic patients: evidence for clustering of extracellular domain mutations at calcium-binding sites.* Hum Mol Genet, 2012. **21**(12): p. 2768-78.

84. Jeong, S., et al., *Genetic polymorphisms of CASR and cancer risk: evidence from meta-analysis and HuGE review.* Onco Targets Ther, 2016. **9**: p. 655-69.

85. Hizaki, K., et al., *Epigenetic inactivation of calcium-sensing receptor in colorectal carcinogenesis.* Mod Pathol, 2011. **24**(6): p. 876-84.

86. Chakravarti, B., et al., *Calcium-sensing receptor in cancer: good cop or bad cop?* Endocrine, 2009. **35**(3): p. 271-84.

87. Clines, G.A., *Mechanisms and treatment of hypercalcemia of malignancy.* Curr Opin Endocrinol Diabetes Obes, 2011. **18**(6): p. 339-46.

88. Mundy, G.R., *Metastasis to bone: causes, consequences and therapeutic opportunities.* Nat Rev Cancer, 2002. **2**(8): p. 584-93.

89. Paget, S., *The distribution of secondary growths in cancer of the breast. 1889.* Cancer Metastasis Rev, 1989. **8**(2): p. 98-101.

90. Feng, J., et al., *Prostate cancer metastatic to bone has higher expression of the calcium-sensing receptor (CaSR) than primary prostate cancer.* Receptors Clin Investig, 2014. **1**(6).

91. Liao, J., et al., *Extracellular calcium as a candidate mediator of prostate cancer skeletal metastasis.* Cancer Res, 2006. **66**(18): p. 9065-73.

92. Joeckel, E., et al., *High calcium concentration in bones promotes bone metastasis in renal cell carcinomas expressing calcium-sensing receptor.* Mol Cancer, 2014. **13**: p. 42.

93. McNeil, L., et al., *Functional calcium-sensing receptor expression in ovarian surface epithelial cells.* Am J Obstet Gynecol, 1998. **178**(2): p. 305-13.

94. Hobson, S.A., et al., *Activation of the MAP kinase cascade by exogenous calcium-sensing receptor.* Mol Cell Endocrinol, 2003. **200**(1-2): p. 189-98.

95. Asadi, F., et al., *Effect of parathyroid hormone related protein, and dihydrotestosterone on proliferation and ornithine decarboxylase mRNA in human prostate cancer cell lines.* Int Urol Nephrol, 2001. **33**(3): p. 417-22.

96. Yano, S., et al., *Calcium-sensing receptor activation stimulates parathyroid hormone-related protein secretion in prostate cancer cells: role of epidermal growth factor receptor transactivation.* Bone, 2004. **35**(3): p. 664-72.

97. Ongkeko, W.M., et al., *Parathyroid hormone related-protein promotes epithelial-to-mesenchymal transition in prostate cancer.* PLoS One, 2014. **9**(1): p. e85803.

98. Huang, C., S. Liu, and R.T. Miller, *Role of p115RhoGEF in the regulation of extracellular Ca(2+)-induced choline kinase activation and prostate cancer cell proliferation.* Int J Cancer, 2011. **128**(12): p. 2833-42.

99. Angel, T.E., et al., *Mass spectrometry-based proteomics: existing capabilities and future directions.* Chem Soc Rev, 2012. **41**(10): p. 3912-28.

100. Nielsen, M.S., et al., *Gap junctions.* Compr Physiol, 2012. **2**(3): p. 1981-2035.

101. Beyer, E.C. and V.M. Berthoud, *Gap junction gene and protein families: Connexins, innexins, and pannexins.* Biochim Biophys Acta Biomembr, 2018. **1860**(1): p. 5-8.

102. Oshima, A., et al., *Three-dimensional structure of a human connexin26 gap junction channel reveals a plug in the vestibule.* Proc Natl Acad Sci U S A, 2007. **104**(24): p. 10034-9.

103. Maeda, S., *[Structure and function of human gap junction channel]*. Tanpakushitsu Kakusan Koso, 2009. **54**(13): p. 1760-6.

104. Gerido, D.A. and T.W. White, *Connexin disorders of the ear, skin, and lens.* Biochim Biophys Acta, 2004. **1662**(1-2): p. 159-70.

105. Kalra, J., et al., *Cx26 inhibits breast MDA-MB-435 cell tumorigenic properties by a gap junctional intercellular communication-independent mechanism.* Carcinogenesis, 2006. **27**(12): p. 2528-37.

106. Li, X., et al., *Connexin 26 is down-regulated by KDM5B in the progression of bladder cancer.* Int J Mol Sci, 2013. **14**(4): p. 7866-79.

107. Oshima, A., et al., *Asymmetric configurations and N-terminal rearrangements in connexin26 gap junction channels.* J Mol Biol, 2011. **405**(3): p. 724-35.

108. Maeda, S., et al., *Structure of the connexin 26 gap junction channel at 3.5 A resolution.* Nature, 2009. **458**(7238): p. 597-602.

109. Tu, C.L., W. Chang, and D.D. Bikle, *The role of the calcium sensing receptor in regulating intracellular calcium handling in human epidermal keratinocytes.* J Invest Dermatol, 2007. **127**(5): p. 1074-83.

110. Putney, J.W., Jr., et al., *Mechanisms of capacitative calcium entry.* J Cell Sci, 2001. **114**(Pt 12): p. 2223-9.

111. Gama, L. and G.E. Breitwieser, *A carboxyl-terminal domain controls the cooperativity for extracellular Ca2+ activation of the human calcium sensing receptor. A study with receptor-green fluorescent protein fusions.* J Biol Chem, 1998. **273**(45): p. 29712-8.

112. Breitwieser, G.E., S.U. Miedlich, and M. Zhang, *Calcium sensing receptors as integrators of multiple metabolic signals.* Cell Calcium, 2004. **35**(3): p. 209-16.

113. Tfelt-Hansen, J. and E.M. Brown, *The calcium-sensing receptor in normal physiology and pathophysiology: a review.* Crit Rev Clin Lab Sci, 2005. **42**(1): p. 35-70.

114. Brown, E.M., *Four-parameter model of the sigmoidal relationship between parathyroid hormone release and extracellular calcium concentration in normal and abnormal parathyroid tissue.* J Clin Endocrinol Metab, 1983. **56**(3): p. 572-81.

115. Breitwieser, G.E., *The calcium sensing receptor life cycle: trafficking, cell surface expression, and degradation.* Best Pract Res Clin Endocrinol Metab, 2013. **27**(3): p. 303-13.

116. Breitwieser, G.E., *Minireview: the intimate link between calcium sensing receptor trafficking and signaling: implications for disorders of calcium homeostasis.* Mol Endocrinol, 2012. **26**(9): p. 1482-95.

117. Huang, Y., et al., *Calcium-sensing receptor ubiquitination and degradation mediated by the E3 ubiquitin ligase dorfin.* J Biol Chem, 2006. **281**(17): p. 11610-7.

118. Goldner, W., *Cancer-Related Hypercalcemia.* J Oncol Pract, 2016. **12**(5): p. 426-32.

119. Stewart, A.F., *Clinical practice. Hypercalcemia associated with cancer.* N Engl J Med, 2005. **352**(4): p. 373-9.

120. Jick, S., et al., *Prevalence of hypercalcemia of malignancy among cancer patients in the UK: analysis of the Clinical Practice Research Datalink database.* Cancer Epidemiol, 2015. **39**(6): p. 901-7.

121. Murray, R.M., et al., *Hypocalcemic and normocalcemic hyperparathyroidism in patients with advanced prostatic cancer.* J Clin Endocrinol Metab, 2001. **86**(9): p. 4133-8.

122. Tucci, M., et al., *Prognostic significance of disordered calcium metabolism in hormone-refractory prostate cancer patients with metastatic bone disease.* Prostate Cancer Prostatic Dis, 2009. **12**(1): p. 94-9.

123. Body, J.J., D. Niepel, and G. Tonini, *Hypercalcaemia and hypocalcaemia: finding the balance.* Support Care Cancer, 2017. **25**(5): p. 1639-1649.

124. Smith, B.M., et al., *Mice lacking Gpr37 exhibit decreased expression of the myelin-associated glycoprotein MAG and increased susceptibility to demyelination.* Neuroscience, 2017. **358**: p. 49-57.

125. Seyfried, N.T., et al., *A Multi-network Approach Identifies Protein-Specific Co-expression in Asymptomatic and Symptomatic Alzheimer's Disease.* Cell Syst, 2017. **4**(1): p. 60-72 e4.

126. Cox, J., et al., *Andromeda: a peptide search engine integrated into the MaxQuant environment.* J Proteome Res, 2011. **10**(4): p. 1794-805.

127. Luber, C.A., et al., *Quantitative proteomics reveals subset-specific viral recognition in dendritic cells.* Immunity, 2010. **32**(2): p. 279-89.

128. Yang, P., et al., *Improving X!Tandem on peptide identification from mass spectrometry by self-boosted Percolator.* IEEE/ACM Trans Comput Biol Bioinform, 2012. **9**(5): p. 1273-80.

129. MacLean, B., et al., *Skyline: an open source document editor for creating and analyzing targeted proteomics experiments.* Bioinformatics, 2010. **26**(7): p. 966-8.

130. Tyanova, S., et al., *The Perseus computational platform for comprehensive analysis of (prote)omics data.* Nat Methods, 2016. **13**(9): p. 731-40.

131. Huang, D.W., B.T. Sherman, and R.A. Lempicki, *Systematic and integrative analysis of large gene lists using DAVID bioinformatics resources.* Nature Protocols, 2009. **4**(1): p. 44-57.

132. Han, J., et al., *The Identification of Novel Protein-Protein Interactions in Liver that Affect Glucagon Receptor Activity.* PLoS One, 2015. **10**(6): p. e0129226.

133. Daulat, A.M., et al., *Purification and identification of G protein-coupled receptor protein complexes under native conditions.* Mol Cell Proteomics, 2007. **6**(5): p. 835-44.

134. Arthur, J.M., et al., *Specific coupling of a cation-sensing receptor to G protein alpha-subunits in MDCK cells.* Am J Physiol, 1997. **273**(1 Pt 2): p. F129-35.

135. Arulpragasam, A., et al., *The adaptor protein 14-3-3 binds to the calcium-sensing receptor and attenuates receptor-mediated Rho kinase signalling.* Biochem J, 2012. **441**(3): p. 995-1006.

136. Stepanchick, A. and G.E. Breitwieser, *The cargo receptor p24A facilitates calcium sensing receptor maturation and stabilization in the early secretory pathway.* Biochem Biophys Res Commun, 2010. **395**(1): p. 136-40.

137. Dessauer, C.W., M. Chen-Goodspeed, and J. Chen, *Mechanism of Galpha i-mediated inhibition of type V adenylyl cyclase.* J Biol Chem, 2002. **277**(32): p. 28823-9.

138. Saikia, M., et al., *Genome-wide identification and quantitative analysis of cleaved tRNA fragments induced by cellular stress.* J Biol Chem, 2012. **287**(51): p. 42708-25.

139. Li, X., et al., *G protein beta2 subunit-derived peptides for inhibition and induction of G protein pathways. Examination of voltage-gated Ca2+ and G protein inwardly rectifying K+ channels.* J Biol Chem, 2005. **280**(25): p. 23945-59.

140. Wu, H.C., et al., *G protein beta2 subunit antisense oligonucleotides inhibit cell proliferation and disorganize microtubule and mitotic spindle organization.* J Cell Biochem, 2001. **83**(1): p. 136-46.

141. Zha, Z., et al., *A Non-Canonical Function of Gbeta as a Subunit of E3 Ligase in Targeting GRK2 Ubiquitylation.* Mol Cell, 2015. **58**(5): p. 794-803.

142. Fu, H., R.R. Subramanian, and S.C. Masters, *14-3-3 proteins: structure, function, and regulation.* Annu Rev Pharmacol Toxicol, 2000. **40**: p. 617-47.

143. Aitken, A., *14-3-3 proteins: a historic overview.* Semin Cancer Biol, 2006. **16**(3): p. 162-72.

144. Deng, Q., et al., *Vesicle-Associated Membrane Protein-Associated Protein A Is Involved in Androgen Receptor Trafficking in Mouse Sertoli Cells.* Int J Endocrinol, 2018. **2018**: p. 4537214.

145. Zerial, M. and H. McBride, *Rab proteins as membrane organizers.* Nat Rev Mol Cell Biol, 2001. **2**(2): p. 107-17.

146. Zhuang, X., et al., *Rab1 small GTP-binding protein regulates cell surface trafficking of the human calcium-sensing receptor.* Endocrinology, 2010. **151**(11): p. 5114-23.

147. Lim, W.K., K.C. Kanelakis, and R.R. Neubig, *Regulation of G protein signaling by the 70kDa heat shock protein.* Cell Signal, 2013. **25**(2): p. 389-96.

148. Alawieh, A., et al., *A Rich-Club Organization in Brain Ischemia Protein Interaction Network.* Sci Rep, 2015. **5**: p. 13513.

149. Tsukahara, F., T. Yoshioka, and T. Muraki, *Molecular and functional characterization of HSC54, a novel variant of human heat-shock cognate protein 70.* Mol Pharmacol, 2000. **58**(6): p. 1257-63.

150. Jakobsson, M.E., et al., *Identification and characterization of a novel human methyltransferase modulating Hsp70 protein function through lysine methylation.* J Biol Chem, 2013. **288**(39): p. 27752-63.

151. Chen, B., et al., *The HSP90 family of genes in the human genome: insights into their divergence and evolution.* Genomics, 2005. **86**(6): p. 627-37.

152. Pozzan, T., et al., *Molecular and cellular physiology of intracellular calcium stores.* Physiol Rev, 1994. **74**(3): p. 595-636.

153. Berridge, M.J., *The endoplasmic reticulum: a multifunctional signaling organelle.* Cell Calcium, 2002. **32**(5-6): p. 235-49.

154. Raffaello, A., et al., *Calcium at the Center of Cell Signaling: Interplay between Endoplasmic Reticulum, Mitochondria, and Lysosomes.* Trends Biochem Sci, 2016. **41**(12): p. 1035-1049.

155. Ranieri, M., et al., *Excessive signal transduction of gain-of-function variants of the calcium-sensing receptor (CaSR) are associated with increased ER to cytosol calcium gradient.* PLoS One, 2013. **8**(11): p. e79113.

156. Wang, Q.C., et al., *TMCO1 Is an ER Ca(2+) Load-Activated Ca(2+) Channel.* Cell, 2016. **165**(6): p. 1454-1466.

157. Paul, I. and M.K. Ghosh, *The E3 ligase CHIP: insights into its structure and regulation.* Biomed Res Int, 2014. **2014**: p. 918183.

158. Zhou, Y., S. Xue, and J.J. Yang, *Calciomics: integrative studies of Ca2+-binding proteins and their interactomes in biological systems.* Metallomics, 2013. **5**(1): p. 29-42.

159. Trinkle-Mulcahy, L., et al., *Identifying specific protein interaction partners using quantitative mass spectrometry and bead proteomes.* J Cell Biol, 2008. **183**(2): p. 223-39.

160. Ashby, M.C. and A.V. Tepikin, *ER calcium and the functions of intracellular organelles.* Semin Cell Dev Biol, 2001. **12**(1): p. 11-7.

161. Corbett, E.F., et al., *Ca2+ regulation of interactions between endoplasmic reticulum chaperones.* J Biol Chem, 1999. **274**(10): p. 6203-11.

162. Araki, K. and K. Nagata, *Protein folding and quality control in the ER.* Cold Spring Harb Perspect Biol, 2011. **3**(11): p. a007526.

163. Ye, R., et al., *Grp78 heterozygosity promotes adaptive unfolded protein response and attenuates diet-induced obesity and insulin resistance.* Diabetes, 2010. **59**(1): p. 6-16.

164. Carreras-Sureda, A., P. Pihan, and C. Hetz, *Calcium signaling at the endoplasmic reticulum: fine-tuning stress responses.* Cell Calcium, 2018. **70**: p. 24-31.

165. Oliver, J.D., et al., *Interaction of the thiol-dependent reductase ERp57 with nascent glycoproteins.* Science, 1997. **275**(5296): p. 86-8.

166. Wyles, J.P., C.R. McMaster, and N.D. Ridgway, *Vesicle-associated membrane protein-associated protein-A (VAP-A) interacts with the oxysterol-binding protein to modify export from the endoplasmic reticulum.* J Biol Chem, 2002. **277**(33): p. 29908-18.

167. Martinez, O. and B. Goud, *Rab proteins.* Biochim Biophys Acta, 1998. **1404**(1-2): p. 101-12.

168. White, J., et al., *Rab6 coordinates a novel Golgi to ER retrograde transport pathway in live cells.* J Cell Biol, 1999. **147**(4): p. 743-60.

169. Stepanchick, A., et al., *Calcium sensing receptor mutations implicated in pancreatitis and idiopathic epilepsy syndrome disrupt an arginine-rich retention motif.* Cell Physiol Biochem, 2010. **26**(3): p. 363-74.

170. Skieterska, K., P. Rondou, and K. Van Craenenbroeck, *Regulation of G Protein-Coupled Receptors by Ubiquitination.* Int J Mol Sci, 2017. **18**(5).

171. Mukherjee, R., et al., *Calcium dependent regulation of protein ubiquitination - Interplay between E3 ligases and calcium binding proteins.* Biochim Biophys Acta Mol Cell Res, 2017. **1864**(7): p. 1227-1235.

172. Bucci, C., et al., *The small GTPase rab5 functions as a regulatory factor in the early endocytic pathway.* Cell, 1992. **70**(5): p. 715-28.

173. Nielsen, E., et al., *Rab5 regulates motility of early endosomes on microtubules.* Nat Cell Biol, 1999. **1**(6): p. 376-82.

174. Bem, D., et al., *Loss-of-function mutations in RAB18 cause Warburg micro syndrome.* Am J Hum Genet, 2011. **88**(4): p. 499-507.

175. Meimaridou, E., S.B. Gooljar, and J.P. Chapple, *From hatching to dispatching: the multiple cellular roles of the Hsp70 molecular chaperone machinery.* J Mol Endocrinol, 2009. **42**(1): p. 1-9.

176. Lu, F.H., et al., *Calcium-sensing receptors regulate cardiomyocyte Ca2+ signaling via the sarcoplasmic reticulum-mitochondrion interface during hypoxia/reoxygenation.* J Biomed Sci, 2010. **17**: p. 50.

177. Bootman, M.D., et al., *Control of inositol 1,4,5-trisphosphate-induced Ca2+ release by cytosolic Ca2+.* Biochem J, 1995. **306 (Pt 2)**: p. 445-51.

178. Dong, C., et al., *Regulation of G protein-coupled receptor export trafficking.* Biochim Biophys Acta, 2007. **1768**(4): p. 853-70.

179. Achour, L., et al., *An escort for GPCRs: implications for regulation of receptor density at the cell surface.* Trends Pharmacol Sci, 2008. **29**(10): p. 528-35.

180. Bouschet, T., S. Martin, and J.M. Henley, *Regulation of calcium-sensing-receptor trafficking and cell-surface expression by GPCRs and RAMPs.* Trends Pharmacol Sci, 2008. **29**(12): p. 633-9.

181. Rands, E., et al., *Mutational analysis of beta-adrenergic receptor glycosylation.* J Biol Chem, 1990. **265**(18): p. 10759-64.

182. Saunders, C. and L.E. Limbird, *Disruption of microtubules reveals two independent apical targeting mechanisms for G-protein-coupled receptors in polarized renal epithelial cells.* J Biol Chem, 1997. **272**(30): p. 19035-45.

183. Duvernay, M.T., et al., *Alpha2B-adrenergic receptor interaction with tubulin controls its transport from the endoplasmic reticulum to the cell surface.* J Biol Chem, 2011. **286**(16): p. 14080-9.

184. Dong, C. and G. Wu, *Regulation of anterograde transport of alpha2-adrenergic receptors by the N termini at multiple intracellular compartments.* J Biol Chem, 2006. **281**(50): p. 38543-54.

185. Zhang, X., et al., *Di-acidic motifs in the membrane-distal C termini modulate the transport of angiotensin II receptors from the endoplasmic reticulum to the cell surface.* J Biol Chem, 2011. **286**(23): p. 20525-35.

186. Hoxhaj, G., K. Dissanayake, and C. MacKintosh, *Effect of IRS4 levels on PI 3-kinase signalling.* PLoS One, 2013. **8**(9): p. e73327.

187. Lavin, D.P., M.F. White, and D.P. Brazil, *IRS proteins and diabetic complications.* Diabetologia, 2016. **59**(11): p. 2280-2291.

188. Cai, S., et al., *Effect of mulberry leaf (Folium Mori) on insulin resistance via IRS-1/PI3K/Glut-4 signalling pathway in type 2 diabetes mellitus rats.* Pharm Biol, 2016. **54**(11): p. 2685-2691.

189. Rufinatscha, K., et al., *Dipeptidyl peptidase-4 impairs insulin signaling and promotes lipid accumulation in hepatocytes.* Biochem Biophys Res Commun, 2017. **485**(2): p. 366-371.

190. Lu, C.C., et al., *Insulin induction instigates cell proliferation and metastasis in human colorectal cancer cells.* Int J Oncol, 2017. **50**(2): p. 736-744.

191. Jiao, B., et al., *Insulin receptor substrate-4 interacts with ubiquitin-specific protease 18 to activate the Jak/STAT signaling pathway.* Oncotarget, 2017. **8**(62): p. 105923-105935.

192. Zhen, Y., et al., *Nuclear import of exogenous FGF1 requires the ER-protein LRRC59 and the importins Kpnalpha1 and Kpnbeta1*. Traffic, 2012. **13**(5): p. 650-64.

193. Enz, R., *Metabotropic glutamate receptors and interacting proteins: evolving drug targets.* Curr Drug Targets, 2012. **13**(1): p. 145-56.

194. Wang, H.G., et al., *Ca2+-induced apoptosis through calcineurin dephosphorylation of BAD.* Science, 1999. **284**(5412): p. 339-43.

195. Mekahli, D., et al., *Endoplasmic-reticulum calcium depletion and disease.* Cold Spring Harb Perspect Biol, 2011. **3**(6).

196. Streb, H., et al., *Release of Ca2+ from a nonmitochondrial intracellular store in pancreatic acinar cells by inositol-1,4,5-trisphosphate.* Nature, 1983. **306**(5938): p. 67-9.

197. Putney, J.W., Jr., *A model for receptor-regulated calcium entry.* Cell Calcium, 1986. **7**(1): p. 1-12.

198. Master, S.R. and B. Burns, *Cancer, Medullary Thyroid*, in *StatPearls*. 2018: Treasure Island (FL).

199. Ding, H., et al., *Localization of CaSR antagonists in CaSR-expressing medullary thyroid cancer.* J Clin Endocrinol Metab, 2013. **98**(11): p. E1722-9.

200. Chau, N.G. and R.I. Haddad, *Vandetanib for the treatment of medullary thyroid cancer.* Clin Cancer Res, 2013. **19**(3): p. 524-9.

201. Cabanillas, M.E., et al., *Challenges associated with tyrosine kinase inhibitor therapy for metastatic thyroid cancer.* J Thyroid Res, 2011. **2011**: p. 985780.

202. Lombardi, G., et al., *The roles of parathyroid hormone in bone remodeling: prospects for novel therapeutics.* J Endocrinol Invest, 2011. **34**(7 Suppl): p. 18-22.

203. Hsu, Y.J., et al., *Calcitonin-stimulated renal Ca2+ reabsorption occurs independently of TRPV5.* Nephrol Dial Transplant, 2010. **25**(5): p. 1428-35.

204. Jaeger, P., et al., *Evidence that calcitonin stimulates 1,25-dihydroxyvitamin D production and intestinal absorption of calcium in vivo.* J Clin Invest, 1986. **78**(2): p. 456-61.

205. Wongsurawat, N. and H.J. Armbrecht, *Calcitonin stimulates 1,25-dihydroxyvitamin D production in diabetic rat kidney.* Metabolism, 1991. **40**(1): p. 22-5.

206. Hurley, D.L., et al., *Axial and appendicular bone mineral density in patients with long-term deficiency or excess of calcitonin.* N Engl J Med, 1987. **317**(9): p. 537-41.

207. Riccardi, D. and E.M. Brown, *Physiology and pathophysiology of the calcium-sensing receptor in the kidney.* Am J Physiol Renal Physiol, 2010. **298**(3): p. F485-99.

208. Gagel, R.F., et al., *Establishment of a calcitonin-producing rat medullary thyroid carcinoma cell line. II. Secretory studies of the tumor and cells in culture.* Endocrinology, 1980. **107**(2): p. 516-23.

209. Gagel, R.F., et al., *Somatostatin production by a human medullary thyroid carcinoma cell line.* Endocrinology, 1986. **118**(4): p. 1643-51.

210. Mehrke, G., et al., *The Ca(++)-channel blocker Ro 40-5967 blocks differently T-type and L-type Ca++ channels.* J Pharmacol Exp Ther, 1994. **271**(3): p. 1483-8.

211. Scherubl, H., G. Schultz, and J. Hescheler, *A slowly inactivating calcium current works as a calcium sensor in calcitonin-secreting cells.* FEBS Lett, 1990. **273**(1-2): p. 51-4.

212. Freichel, M., et al., *Expression of a calcium-sensing receptor in a human medullary thyroid carcinoma cell line and its contribution to calcitonin secretion.* Endocrinology, 1996. **137**(9): p. 3842-8.

213. Eckert, R.W., et al., *Rhythmic oscillations of cytosolic free calcium in rat C-cells.* Mol Cell Endocrinol, 1989. **64**(2): p. 267-70.

214. Thomsen, A.R., et al., *Strontium is a biased agonist of the calcium-sensing receptor in rat medullary thyroid carcinoma 6-23 cells.* J Pharmacol Exp Ther, 2012. **343**(3): p. 638-49.

215. Yamashita, N. and S. Hagiwara, *Membrane depolarization and intracellular Ca2+ increase caused by high external Ca2+ in a rat calcitonin-secreting cell line.* J Physiol, 1990. **431**: p. 243-67.

216. Rasmussen, H., *The calcium messenger system (1).* N Engl J Med, 1986. **314**(17): p. 1094-101.

217. Fried, R.M. and A.H. Tashjian, Jr., *Actions of rat growth hormone-releasing factor and norepinephrine on cytosolic free calcium and inositol trisphosphate in rat C-cells.* J Bone Miner Res, 1987. **2**(6): p. 579-85.

218. Kretsinger, R.H. and C.E. Nockolds, *Carp muscle calcium-binding protein. II. Structure determination and general description.* J. Biol. Chem., 1973. **248**(9): p. 3313-26.

219. Maximciuc, A.A., et al., *Complex of calmodulin with a ryanodine receptor target reveals a novel, flexible binding mode.* Structure, 2006. **14**(10): p. 1547-56.

220. Merrill, M.A., et al., *Displacement of alpha-actinin from the NMDA receptor NR1 C0 domain By Ca2+/calmodulin promotes CaMKII binding.* Biochemistry, 2007. **46**(29): p. 8485-97.

221. Suh, Y.H., et al., *Regulation of metabotropic glutamate receptor 7 (mGluR7) internalization and surface expression by Ser/Thr protein phosphatase 1.* J Biol Chem, 2013. **288**(24): p. 17544-51.

222. Hammerland, L.G., et al., *Allosteric activation of the Ca2+ receptor expressed in Xenopus laevis oocytes by NPS 467 or NPS 568.* Mol Pharmacol, 1998. **53**(6): p. 1083-8.

223. Kessler, A., et al., *N2-benzyl-N1-(1-(1-naphthyl)ethyl)-3-phenylpropane-1,2-diamines and conformationally restrained indole analogues: development of calindol as a new calcimimetic acting at the calcium sensing receptor.* Bioorg Med Chem Lett, 2004. **14**(12): p. 3345-9.

224. Goodman, W.G., *Calcimimetic agents and secondary hyperparathyroidism: treatment and prevention.* Nephrol Dial Transplant, 2002. **17**(2): p. 204-7.

225. Chonchol, M., et al., *A randomized, double-blind, placebo-controlled study to assess the efficacy and safety of cinacalcet HCl in participants with CKD not receiving dialysis.* Am J Kidney Dis, 2009. **53**(2): p. 197-207.

226. Abdulnour-Nakhoul, S., et al., *Cytoskeletal changes induced by allosteric modulators of calcium-sensing receptor in esophageal epithelial cells.* Physiol Rep, 2015. **3**(11).

227. Li, H., et al., *The calcimimetic R-568 induces apoptotic cell death in prostate cancer cells.* J Exp Clin Cancer Res, 2009. **28**: p. 100.

228. Mine, Y. and H. Zhang, *Anti-inflammatory Effects of Poly-L-lysine in Intestinal Mucosal System Mediated by Calcium-Sensing Receptor Activation.* J Agric Food Chem, 2015. **63**(48): p. 10437-47.

229. Leach, K., et al., *Engendering biased signalling from the calcium-sensing receptor for the pharmacotherapy of diverse disorders.* Br J Pharmacol, 2014. **171**(5): p. 1142-55.

230. Nakamura, A., et al., *Loss-of-function and gain-of-function mutations of calcium-sensing receptor: functional analysis and the effect of allosteric modulators NPS R-568 and NPS 2143.* J Clin Endocrinol Metab, 2013. **98**(10): p. E1692-701.

231. Huang, Y. and G.E. Breitwieser, *Rescue of calcium-sensing receptor mutants by allosteric modulators reveals a conformational checkpoint in receptor biogenesis.* J Biol Chem, 2007. **282**(13): p. 9517-25.

232. Chuang, T.T., L. Paolucci, and A. De Blasi, *Inhibition of G protein-coupled receptor kinase subtypes by Ca2+/calmodulin.* J Biol Chem, 1996. **271**(45): p. 28691-6.

233. Dvorak, M.M., et al., *Physiological changes in extracellular calcium concentration directly control osteoblast function in the absence of calciotropic hormones.* Proc Natl Acad Sci U S A, 2004. **101**(14): p. 5140-5.

234. Huang, Y., et al., *Identification and dissection of Ca(2+)-binding sites in the extracellular domain of Ca(2+)-sensing receptor.* J Biol Chem, 2007. **282**(26): p. 19000-10.

235. Zhang, X., et al., *A synthetic antibody fragment targeting nicastrin affects assembly and trafficking of gamma-secretase.* J Biol Chem, 2014. **289**(50): p. 34851-61.

236. Dupre, D.J., et al., *The role of Gbetagamma subunits in the organization, assembly, and function of GPCR signaling complexes.* Annu Rev Pharmacol Toxicol, 2009. **49**: p. 31-56.

237. Ritter, S.L. and R.A. Hall, *Fine-tuning of GPCR activity by receptor-interacting proteins.* Nat Rev Mol Cell Biol, 2009. **10**(12): p. 819-30.

238. Lagerstrom, M.C. and H.B. Schioth, *Structural diversity of G protein-coupled receptors and significance for drug discovery.* Nat Rev Drug Discov, 2008. **7**(4): p. 339-57.

239. Sokolina, K., et al., *Systematic protein-protein interaction mapping for clinically relevant human GPCRs.* Mol Syst Biol, 2017. **13**(3): p. 918.

240. Yap, K.L., et al., *Calmodulin target database.* J Struct Funct Genomics, 2000. **1**(1): p. 8-14.

241. Hannan, F.M., V.N. Babinsky, and R.V. Thakker, *Disorders of the calcium-sensing receptor and partner proteins: insights into the molecular basis of calcium homeostasis.* J Mol Endocrinol, 2016. **57**(3): p. R127-42.

242. Breuksch, I., M. Weinert, and W. Brenner, *The role of extracellular calcium in bone metastasis.* J Bone Oncol, 2016. **5**(3): p. 143-145.

243. Saidak, Z., R. Mentaverri, and E.M. Brown, *The role of the calcium-sensing receptor in the development and progression of cancer.* Endocr Rev, 2009. **30**(2): p. 178-95.

244. Rodriguez, F.D., E. Bardaji, and J.R. Traynor, *Differential-Effects of Mg2+ and Other Divalent-Cations on the Binding of Tritiated Opioid Ligands.* Journal of Neurochemistry, 1992. **59**(2): p. 467-472.

245. Williams, L.T., D. Mullikin, and R.J. Lefkowitz, *Magnesium dependence of agonist binding to adenylate cyclase-coupled hormone receptors.* J Biol Chem, 1978. **253**(9): p. 2984-9.

246. Sibley, D.R. and I. Creese, *Regulation of ligand binding to pituitary D-2 dopaminergic receptors. Effects of divalent cations and functional group modification.* J Biol Chem, 1983. **258**(8): p. 4957-65.

247. Zhang, C., et al., *Structural basis for regulation of human calcium-sensing receptor by magnesium ions and an unexpected tryptophan derivative co-agonist.* Sci Adv, 2016. **2**(5): p. e1600241.

248. Conigrave, A.D., S.J. Quinn, and E.M. Brown, *L-amino acid sensing by the extracellular Ca2+-sensing receptor.* Proc Natl Acad Sci U S A, 2000. **97**(9): p. 4814-9.

249. Zhang, Z., et al., *L-phenylalanine and NPS R-467 synergistically potentiate the function of the extracellular calcium-sensing receptor through distinct sites.* J Biol Chem, 2002. **277**(37): p. 33736-41.

250. Mun, H.C., et al., *A double mutation in the extracellular Ca2+-sensing receptor's venus flytrap domain that selectively disables L-amino acid sensing.* J Biol Chem, 2005. **280**(32): p. 29067-72.

251. Kerr, D.I. and J. Ong, *Potentiation of metabotropic GABAB receptors by L-amino acids and dipeptides in rat neocortex.* Eur J Pharmacol, 2003. **468**(2): p. 103-8.

252. Nemeth, E.F., et al., *Calcimimetics with potent and selective activity on the parathyroid calcium receptor.* Proc Natl Acad Sci U S A, 1998. **95**(7): p. 4040-5.

253. Masters, J.R., et al., *Short tandem repeat profiling provides an international reference standard for human cell lines.* Proc Natl Acad Sci U S A, 2001. **98**(14): p. 8012-7.

254. Chatterjee, R., *Cell biology. Cases of mistaken identity.* Science, 2007. **315**(5814): p. 928-31.

255. MacLeod, R.A., et al., *Widespread intraspecies cross-contamination of human tumor cell lines arising at source.* Int J Cancer, 1999. **83**(4): p. 555-63.

256. Sweeney, C.J., et al., *Chemohormonal Therapy in Metastatic Hormone-Sensitive Prostate Cancer.* N Engl J Med, 2015. **373**(8): p. 737-46.

257. Imbriaco, M., et al., *A new parameter for measuring metastatic bone involvement by prostate cancer: the Bone Scan Index.* Clin Cancer Res, 1998. **4**(7): p. 1765-72.

258. Roodman, G.D., *Mechanisms of bone metastasis.* N Engl J Med, 2004. **350**(16): p. 1655-64.

259. Sanders, J.L., et al., *Ca(2+)-sensing receptor expression and PTHrP secretion in PC-3 human prostate cancer cells.* Am J Physiol Endocrinol Metab, 2001. **281**(6): p. E1267-74.

260. Roderick, H.L. and S.J. Cook, *Ca2+ signalling checkpoints in cancer: remodelling Ca2+ for cancer cell proliferation and survival.* Nat Rev Cancer, 2008. **8**(5): p. 361-75.

261. Prevarskaya, N., R. Skryma, and Y. Shuba, *Calcium in tumour metastasis: new roles for known actors.* Nat Rev Cancer, 2011. **11**(8): p. 609-18.

262. Mahalingam, D., et al., *Mipsagargin, a novel thapsigargin-based PSMA-activated prodrug: results of a first-in-man phase I clinical trial in patients with refractory, advanced or metastatic solid tumours.* Br J Cancer, 2016. **114**(9): p. 986-94.

263. Kuchay, S., et al., *PTEN counteracts FBXL2 to promote IP3R3- and Ca(2+)-mediated apoptosis limiting tumour growth.* Nature, 2017. **546**(7659): p. 554-558.

264. Silver, I.A., R.J. Murrills, and D.J. Etherington, *Microelectrode studies on the acid microenvironment beneath adherent macrophages and osteoclasts.* Exp Cell Res, 1988. **175**(2): p. 266-76.

265. Schwartz, G.G., *Prostate cancer, serum parathyroid hormone, and the progression of skeletal metastases.* Cancer Epidemiol Biomarkers Prev, 2008. **17**(3): p. 478-83.

266. Riccardi, D., S.C. Brennan, and W. Chang, *The extracellular calcium-sensing receptor, CaSR, in fetal development.* Best Pract Res Clin Endocrinol Metab, 2013. **27**(3): p. 443-53.

267. Cheng, Z., et al., *Sex and age modify biochemical and skeletal manifestations of chronic hyperparathyroidism by altering target organ responses to Ca2+ and parathyroid hormone in mice.* J Bone Miner Res, 2013. **28**(5): p. 1087-100.

268. Al-Dujaili, S.A., et al., *Calcium Sensing Receptor Function Supports Osteoblast Survival and Acts as a Co-Factor in PTH Anabolic Actions in Bone.* J Cell Biochem, 2016. **117**(7): p. 1556-67.

269. Henderson, J., et al., *Dysregulation of parathyroid hormone-like peptide expression and secretion in a keratinocyte model of tumor progression.* Cancer Res, 1991. **51**(24): p. 6521-8.

270. Kremer, R., et al., *Parathyroid-hormone-related peptide in hematologic malignancies.* Am J Med, 1996. **100**(4): p. 406-11.

271. Merryman, J.I., et al., *Regulation of parathyroid hormone-related protein production by a squamous carcinoma cell line in vitro.* Lab Invest, 1993. **69**(3): p. 347-54.

272. Hellman, P., et al., *Regulation of proliferation in JEG-3 cells by a 500-kDa Ca2+ sensor and parathyroid hormone-related protein.* Arch Biochem Biophys, 1993. **307**(2): p. 379-85.

273. Rizzoli, R., et al., *Regulation of parathyroid hormone-related protein production in a human lung squamous cell carcinoma line.* J Endocrinol, 1994. **143**(2): p. 333-41.

274. Dhanasekaran, S.M., et al., *Delineation of prognostic biomarkers in prostate cancer.* Nature, 2001. **412**(6849): p. 822-6.

275. Aljameeli, A., et al., *Calcitonin Receptor-Zonula Occludens-1 Interaction Is Critical for Calcitonin-Stimulated Prostate Cancer Metastasis.* PLoS One, 2016. **11**(3): p. e0150090.

276. Thomas, S. and G. Shah, *Calcitonin induces apoptosis resistance in prostate cancer cell lines against cytotoxic drugs via the Akt/survivin pathway.* Cancer Biol Ther, 2005. **4**(11): p. 1226-33.

277. Shah, G.V., et al., *Calcitonin promotes in vivo metastasis of prostate cancer cells by altering cell signaling, adhesion, and inflammatory pathways.* Endocr Relat Cancer, 2008. **15**(4): p. 953-64.

278. Ritchie, C.K., et al., *Effects of the calciotrophic peptides calcitonin and parathyroid hormone on prostate cancer growth and chemotaxis.* Prostate, 1997. **30**(3): p. 183-7.

279. Tai, S., et al., *PC3 is a cell line characteristic of prostatic small cell carcinoma.* Prostate, 2011. **71**(15): p. 1668-79.

280. Tetu, B., et al., *Small cell carcinoma of the prostate. Part I. A clinicopathologic study of 20 cases.* Cancer, 1987. **59**(10): p. 1803-9.

281. Oesterling, J.E., C.G. Hauzeur, and G.M. Farrow, *Small cell anaplastic carcinoma of the prostate: a clinical, pathological and immunohistological study of 27 patients.* J Urol, 1992. **147**(3 Pt 2): p. 804-7.

282. Yao, J.L., et al., *Small cell carcinoma of the prostate: an immunohistochemical study.* Am J Surg Pathol, 2006. **30**(6): p. 705-12.

283. Wang, W. and J.I. Epstein, *Small cell carcinoma of the prostate. A morphologic and immunohistochemical study of 95 cases.* Am J Surg Pathol, 2008. **32**(1): p. 65-71.

284. Kaighn, M.E., et al., *Establishment and characterization of a human prostatic carcinoma cell line (PC-3).* Invest Urol, 1979. **17**(1): p. 16-23.

285. Horoszewicz, J.S., et al., *The LNCaP cell line--a new model for studies on human prostatic carcinoma.* Prog Clin Biol Res, 1980. **37**: p. 115-32.

286. Horoszewicz, J.S., et al., *LNCaP model of human prostatic carcinoma.* Cancer Res, 1983. **43**(4): p. 1809-18.

287. Barry, M.J., *Clinical practice. Prostate-specific-antigen testing for early diagnosis of prostate cancer.* N Engl J Med, 2001. **344**(18): p. 1373-7.

288. Terada, N., et al., *Prognostic and predictive biomarkers in prostate cancer: latest evidence and clinical implications.* Ther Adv Med Oncol, 2017. **9**(8): p. 565-573.

289. Wyatt, A.W., et al., *Genomic Alterations in Cell-Free DNA and Enzalutamide Resistance in Castration-Resistant Prostate Cancer.* JAMA Oncol, 2016. **2**(12): p. 1598-1606.

290. Robinson, D., et al., *Integrative Clinical Genomics of Advanced Prostate Cancer.* Cell, 2015. **162**(2): p. 454.

291. Bradbury, R.A., et al., *Expression of the parathyroid Ca(2+)-sensing receptor in cytotrophoblasts from human term placenta.* J Endocrinol, 1998. **156**(3): p. 425-30.

292. Oda, Y., et al., *The calcium sensing receptor and its alternatively spliced form in keratinocyte differentiation.* J Biol Chem, 1998. **273**(36): p. 23344-52.

293. Blakeley, P., et al., *Investigating protein isoforms via proteomics: a feasibility study.* Proteomics, 2010. **10**(6): p. 1127-40.

294. Pan, Q., et al., *Deep surveying of alternative splicing complexity in the human transcriptome by high-throughput sequencing.* Nat Genet, 2008. **40**(12): p. 1413-5.

295. Graveley, B.R., *Alternative splicing: increasing diversity in the proteomic world.* Trends Genet, 2001. **17**(2): p. 100-7.

296. Jiao, Y., et al., *Developmentally regulated alternative splicing of densin modulates protein-protein interaction and subcellular localization.* J Neurochem, 2008. **105**(5): p. 1746-60.

297. Passetti, F., C.G. Ferreira, and F.F. Costa, *The impact of microRNAs and alternative splicing in pharmacogenomics.* Pharmacogenomics J, 2009. **9**(1): p. 1-13.

298. Zikherman, J. and A. Weiss, *Alternative splicing of CD45: the tip of the iceberg.* Immunity, 2008. **29**(6): p. 839-41.

299. Resch, A., et al., *Assessing the impact of alternative splicing on domain interactions in the human proteome.* J Proteome Res, 2004. **3**(1): p. 76-83.

300. Burkard, T.R., et al., *Initial characterization of the human central proteome.* BMC Syst Biol, 2011. **5**: p. 17.

301. Geiger, T., et al., *Comparative proteomic analysis of eleven common cell lines reveals ubiquitous but varying expression of most proteins.* Mol Cell Proteomics, 2012. **11**(3): p. M111 014050.

302. Geiger, T., et al., *Proteomic portrait of human breast cancer progression identifies novel prognostic markers.* Cancer Res, 2012. **72**(9): p. 2428-39.

303. El-Haibi, C.P., et al., *Differential G protein subunit expression by prostate cancer cells and their interaction with CXCR5.* Mol Cancer, 2013. **12**: p. 64.

304. Wu, H.C., et al., *Derivation of androgen-independent human LNCaP prostatic cancer cell sublines: role of bone stromal cells.* Int J Cancer, 1994. **57**(3): p. 406-12.

305. Thalmann, G.N., et al., *Androgen-independent cancer progression and bone metastasis in the LNCaP model of human prostate cancer.* Cancer Res, 1994. **54**(10): p. 2577-81.

306. Flanagan, A.M. and T.J. Chambers, *Inhibition of bone resorption by bisphosphonates: interactions between bisphosphonates, osteoclasts, and bone.* Calcif Tissue Int, 1991. **49**(6): p. 407-15.

307. Rodan, G.A., *Mechanisms of action of bisphosphonates.* Annu Rev Pharmacol Toxicol, 1998. **38**: p. 375-88.

308. Rogers, M.J., D.J. Watts, and R.G. Russell, *Overview of bisphosphonates.* Cancer, 1997. **80**(8 Suppl): p. 1652-60.

309. Major, P.P. and R.E. Coleman, *Zoledronic acid in the treatment of hypercalcemia of malignancy: results of the international clinical development program.* Semin Oncol, 2001. **28**(2 Suppl 6): p. 17-24.

310. Corey, E., et al., *Zoledronic acid exhibits inhibitory effects on osteoblastic and osteolytic metastases of prostate cancer.* Clin Cancer Res, 2003. **9**(1): p. 295-306.

311. Shao, Y., et al., *Metabolomics and transcriptomics profiles reveal the dysregulation of the tricarboxylic acid cycle and related mechanisms in prostate cancer.* Int J Cancer, 2018. **143**(2): p. 396-407.

312. Liu, Y., L.S. Zuckier, and N.V. Ghesani, *Dominant uptake of fatty acid over glucose by prostate cells: a potential new diagnostic and therapeutic approach.* Anticancer Res, 2010. **30**(2): p. 369-74.

313. Zha, S., et al., *Peroxisomal branched chain fatty acid beta-oxidation pathway is upregulated in prostate cancer.* Prostate, 2005. **63**(4): p. 316-23.

314. Chappell, R.L., et al., *Histidine suppresses zinc modulation of connexin hemichannels.* Biol Bull, 2004. **207**(3): p. 188-90.

315. Ebihara, L., X. Liu, and J.D. Pal, *Effect of external magnesium and calcium on human connexin46 hemichannels.* Biophys J, 2003. **84**(1): p. 277-86.

316. Sun, Z., D.Q. Zhang, and D.G. McMahon, *Zinc modulation of hemi-gap-junction channel currents in retinal horizontal cells.* J Neurophysiol, 2009. **101**(4): p. 1774-80.

317. Peracchia, C., *Chemical gating of gap junction channels; roles of calcium, pH and calmodulin.* Biochim Biophys Acta, 2004. **1662**(1-2): p. 61-80.

318. Dodd, R., et al., *Calmodulin association with connexin32-derived peptides suggests trans-domain interaction in chemical gating of gap junction channels.* J Biol Chem, 2008. **283**(40): p. 26911-20.

319. Reichow, S.L., et al., *Allosteric mechanism of water-channel gating by Ca2+-calmodulin.* Nat Struct Mol Biol, 2013. **20**(9): p. 1085-92.

320. Bhattacharya, S., C.G. Bunick, and W.J. Chazin, *Target selectivity in EF-hand calcium binding proteins.* Biochim Biophys Acta, 2004. **1742**(1-3): p. 69-79.

321. Jiang, J., et al., *Site-specific modification of calmodulin Ca(2)(+) affinity tunes the skeletal muscle ryanodine receptor activation profile.* Biochem J, 2010. **432**(1): p. 89-99.

322. VanScyoc, W.S. and M.A. Shea, *Phenylalanine fluorescence studies of calcium binding to N-domain fragments of Paramecium calmodulin mutants show increased calcium affinity correlates with increased disorder.* Protein Sci, 2001. **10**(9): p. 1758-68.

323. Kirberger, M., et al., *Metal toxicity and opportunistic binding of Pb(2+) in proteins.* J Inorg Biochem, 2013. **125**: p. 40-9.

324. Wang, X. and J.A. Putkey, *PEP-19 modulates calcium binding to calmodulin by electrostatic steering.* Nat Commun, 2016. **7**: p. 13583.

325. Zou, J., et al., *Gap junction regulation by calmodulin.* FEBS Lett, 2014. **588**(8): p. 1430-8.

326. Ikura, M. and J.B. Ames, *Genetic polymorphism and protein conformational plasticity in the calmodulin superfamily: two ways to promote multifunctionality.* Proc Natl Acad Sci U S A, 2006. **103**(5): p. 1159-64.

327. Zou, J., et al., *Direct visualization of interaction between calmodulin and connexin45.* Biochem J, 2017. **474**(24): p. 4035-4051.

328. Rosano, G.L. and E.A. Ceccarelli, *Recombinant protein expression in microbial systems.* Front Microbiol, 2014. **5**: p. 341.

329. Khan, K.H., *Gene expression in Mammalian cells and its applications.* Adv Pharm Bull, 2013. **3**(2): p. 257-63.

330. Lakowicz, J.R., *Principles of frequency-domain fluorescence spectroscopy and applications to cell membranes.* Subcell Biochem, 1988. **13**: p. 89-126.